Quantification of Carbon Emissions and Savings in Smart Grids

A thesis submitted to Brunel University London for the degree of Doctor of Philosophy

Eng Tseng Lau

2016

College of Engineering, Design and Physical Sciences
Brunel University London

Abstract

In this research, carbon emissions and carbon savings in the smart grid are modelled and quantified. Carbon emissions are defined as the product of the activity (energy) and the corresponding carbon factor. The carbon savings are estimated as the difference between the conventional and improved energy usage multiplied by the corresponding carbon factor. An adaptive seasonal model based on the hyperbolic tangent function (HTF) is developed to define seasonal and daily trends of electricity demand and the resultant carbon emissions. A stochastic model describing profiles of energy usage and carbon emissions for groups of consumers is developed. The flexibility of the HTF for modelling cycles of energy consumption is demonstrated and discussed with several case studies. The analytical description to determine electricity grid carbon intensity in the UK is derived, using the available fuel mix data from the Elexon portal. The uncertain realisation of energy data is forecasted and assimilated using the ensemble Kalman filter (EnKF). The numerical optimisation of carbon emissions and savings in the smart grid is further performed using the ensemble-based Closed-loop Production Optimisation Scheme (EnOpt). The EnOpt involves the optimisation of fuel costs and carbon emissions (maximisation of carbon savings) in the smart grid subject to the operational control constraints. The software codes for the based on the application of EnKF and EnOpt are developed, and the optimisation of energy, cost and emissions is performed. The numerical simulation shows the ability of EnKF in forecasting and assimilating the energy data, and the robustness of the EnOpt in optimising costs and carbon savings. The proposed approach addresses the complexity and diversity of the power grid and may be implemented at the level of the transmission operator in collaboration with the operational wholesale electricity market and distribution network operators. The final stage of work includes the quantification of carbon emissions and savings in demand response (DR) programmes. DR programmes

such as Short Term Operating Reserve (STOR), Triad, Fast Reserve, Frequency Control by Demand Management (FCDM) and smart meter roll-out are included, with various types of smart interventions. The DR programmes are modelled with appropriate configurations and assumptions in power plants used in the energy industry. This enables the comparison of emissions between the business-as-usual (BAU) and the smart solutions applied, thus deriving the carbon savings. Several case studies involving the modelling and analysing DR programmes are successfully performed. Thus, the thesis represents novel analytical and numerical techniques applied in the fast-growing UK market of smart energy solutions.

Acknowledgements

I would like to express my sincere appreciation and gratitude to my supervisors, Dr. Qing-Ping Yang, Dr. Valerie Livina, Prof.Gareth Taylor and Prof. Alistair Forbes for providing valuable guidance and support during my research project. Without them this thesis cannot be realised. I am also deeply thankful to Dr. Livina and Dr. Yang for their unconditional support, for being always available (including weekends) whenever I needed their guidance and advices to further develop my ideas. With their knowledge, commitment, attitude and kindness I gained a lot of confidence in developing this thesis.

I would like to express my appreciation for the industrial partners in fulfilling my thesis work even though their contributions are kept in the condition of anonymity. Overall, their feedback, guidance and valuable suggestions are highly recognised.

I want to express my gratitude to the Mathematics, Modelling and Simulation group from National Physical Laboratory, Teddington, UK for their scientific support contributed to the research methodology. I also enjoyed the companionship of student fellows at National Physical Laboratory throughout my PhD study.

My appreciation to the Brunel University and National Physical Laboratory for sponsoring this research and providing excellent research facilities in order to fulfil my research project.

I also would like to thank all my friends from Brunel University and my friends in Malaysia during my research in the UK.

My heartiest gratitude and appreciation to my wife for her sacrifices, unconditional love, perseverance and motivation.

I want to thank my parents, my brother and sisters, and my big family tree for all their encouragement and support.

Finally, thanks to everyone who put their faith in me.

Contents

List of figures

List of tables

Nomenclature

Acronyms

BMRS	Balancing mechanism reporting system
CCGT	Combined cycle gas turbine
CCS	Carbon capture and storage
CHP	Combined heat and power
DECC	Department of Energy and Climate Change
DR	Demand response
DSM	Demand side management
EAC	Estimated annual consumption
ED	Economic despatch
EnKF	Ensemble Kalman filter
EnOpt	Ensemble-based close-loop production optimisation
FCDM	Frequency control by demand management
HH	Half hourly
IHEM	In-home electricity monitor
LB	Lower boundary
LCA	Life cycle assessment
LCT	Low carbon technology
NHH	Non half-hourly
OCGT	Open cycle gas turbine
OLR	Overall load reduction
PC	Profile class
PS	Pumped storage
PV	Photo-voltaic
STOR	Short term operating reserve
TD	Transmission and distribution losses
TNUoS	Transmission network use of system
ToU	Time of use
UB	Upper boundary

List of publications

Journals

[1] E. T. Lau, Q. Yang, A. B. Forbes, P. Wright, and V. N. Livina, "Modelling carbon emissions in electric systems," *Energy Conversion and Management*, vol. 80, no. 59, pp. 573–581, Apr. 2014.

[2] E. T. Lau, Q. Yang, L. Stokes, G. A. Taylor, A. B. Forbes, P. Clarkson, P. S. Wright, and V. N. Livina, "Carbon savings in the UK demand side response programmes," *Applied Energy*, vol. 159, no. 1, pp. 478–489, Aug. 2015.

[3] E. T. Lau, Q. Yang, A. B. Forbes, and V. N. Livina, "Application of Ensemble Kalman filter in forecasting the electricity grid carbon factor," *International Journal of Electrical Energy*, vol. 3, no. 4, pp. 209–212, Dec. 2015.

Conferences

[1] E. T. Lau, Q. Yang, G. A. Taylor, A. B. Forbes, P. Wright, and V. N. Livina, "Optimisation of carbon emissions in smart grids," in *Proceedings of the 49th International Universities' Power Engineering Conference, UPEC*, IEEE, Sep. 2015, pp. 1–4.

[2] E. T. Lau, Q. Yang, G. A. Taylor, L. Stokes, A. B. Forbes, P. Wright, and V. N. Livina, "The UK electricity demand side response: Carbon savings analysis," in *Proceedings of the 12th International Conference on European Energy Market, EEM*, doi: 10.1109/EEM.2015.7216719, IEEE, Sep. 2015, pp. 1–4.

Reports

[1] E. T. Lau and V. N. Livina, "Assessment of carbon savings of the British Telecommunications (BT) participation in the Triad programme of the National Grid (NG)," National Physical Laboratory, Tech. Rep., Sep. 2015.

[2] E. T. Lau and V. N. Livina, "Carbon savings of demand side reponse of a UK energy aggregator," National Physical Laboratory, Tech. Rep., Sep. 2015, [Online]. Available: `http://www.npl.co.uk/content/ConPublication/6739`.

Unpublished

[1] E. T. Lau, Q. Yang, G. A. Taylor, A. B. Forbes, P. Wright, and V. N. Livina, "Optimisation of costs and carbon savings in relation to the economic despatch problem associated with power system operation," unpublished. Submitted to *Electric Power Systems Research*, 2015.

Chapter 1

Introduction

1.1 Background of the research

The UK national energy system experiences large and increasing loads on the infrastructure, as well as uncertainty in energy consumption due to: variable heating in colder seasons; the addition of intermittent green generators; insufficient storage facilities. Additionally, the legislation on the 2050 low carbon economy requires the reduction of emissions by 80 % below 1990 levels, with 40 % reduced emissions by 2030 and 60 % by 2040 (DG Clima, 2016). The legislation by DG Clima (2016) requires the participation from all sectors with feasibility and affordability in the transition of low carbon. According to E.ON UK (2016), the needs to concentrate the carbon reduction targets, as well as their affordability, and maintain the security of energy supply are the "energy trilemma" problem. This is because the need to optimise the one element of the energy trilemma problem may lead to the rise of other issues. For instance, the renewable energy that does not guarantee the security of energy supply due to its intermittency.

Therefore, various low carbon energy plans are implemented, with rising need to quantify their environmental impact as well as to avoid upgrade of infrastructure. One of the modelling framework that addresses this is the UK MARKAL-Macro developed by Strachan and Kannan (2008). The model predicts the aggregated energy demand response and technological change through the 2007 UK Energy White Paper policy framework. It provides the quantification of cost-economical implications due to the long-term decarbonisation strategies.

In general, the task in quantifying the carbon emissions and savings ranges from the energy generation at power plants to the end household consumer in order to meet the national need for sustainability. electrical energy. A good balance between traditional and renewable electricity is critical not only for keeping the electricity financial costs down but also for environmental benefits. Hence, studying dynamical changes of electricity consumption and generation are important in quantifying the carbon impacts. Moreover, there is also a need to quantify and report the environmental impact under the requirements of the Greenhouse gases (GHG) conversion and reporting. The papers by Hill et al. (2014, 2013) describe how the amount of direct and indirect emissions used in a company's assets (fuel combustion vehicles, purchased electricity, scientific and research development in laboratories, logistics and supply chains, as well as waste). Such GHG reporting allows the company to evaluate the consequences of the activities and seek actions to mitigate the GHG impacts. The emission due to carbon dioxide from the GHG protocol is selected for quantification of emissions and savings in this research. Carbon emissions are reported in grams of carbon dioxide (CO_2) equivalent for a given period (Carbon Trust, 2012; Wiedmann and Minx, 2008).

Furthermore, the recent rollout of smart meters across Europe provided new ways of monitoring energy networks and real-time management and control of the power grid efficiently. Smart meters permit dual way communications between households and energy suppliers, with further feedback on demand and requirements for energy generation. However, according to Depuru et al. (2011), several issues that may threaten the smart meter system are: 1) high investment cost; 2) lack of proper infrastructure for integrating smart meters with the existing technology; 3) increased complexity in the smart meter system due to huge volume of smart meter installations; 4) increased complexity due to large amount of data transfer between smart meters and servers in the base station.

Therefore, new modelling frameworks have to address the expansion of the system and growing complexity of the system. New mathematical and software solutions have to be introduced for better control and optimisations of the power grid. The real-time price-based demand response management was applied by Chen et al. (2012) in a system with smart meters to minimise the expected daily electricity payment while controlling the uncertainties in electricity tariffs. The existing economically-based models with optimisation, however, either show the absence of taking into account carbon emissions, or

take them as a minor parameter in the power grid. This leads to the huge gaps or trade-offs between the cost and the carbon impact.

Therefore, a modelling approach is proposed that focusses on quantification of carbon emissions that are produced due to electrical consumption and generation, and further optimises carbon savings. The approach is based on the energy data forecast and assimilation by the ensemble Kalman Filter (EnKF) combined with the optimisation using ensemble-based closed-loop production optimisation scheme (EnOpt) algorithm. The framework integrates the electrical data from consumers and generators assimilated by the EnKF. On the other hand, the model allows the optimisation of social welfare (consumption and generation of energy) subject to operational control constraints and they are optimised using EnOpt representing the smart grid system.

In addition to the numerical optimisation of the power grid, due to the possibility of postponing large-scale upgrades of the network infrastructure, the ancillary service balancing the power grid has been established. The demand response (DR) programmes are studied and modelled for reduction of energy usage and costs (Mazinani and Zaeefi, 2013; Palensky and Dietrich, 2011). The assessment of carbon emissions in DR programmes besides the cost benefit evaluation is very important for the identification of the preferable directions of the future sustainability. While DR programmes are claimed to ensure the grid stability, it is also important to acknowledge that they may achieve carbon emissions that may be counter-intuitive when one compares conventional solution and smart interventions. At particular operational stages, balancing energy demands may require the highest 'peaking load' of the power plants that is highly polluting. Surprisingly, the similarly polluting replacement solutions may produce carbon savings. Additionally, there is a misperception about green energy generation. The deployment of green generation is widely known to promote carbon savings. However in reality this cannot be always true due to the intermittency of green generation (for instance, wind farms). This may cause a sudden large deviation of the energy supply due to green generation shortage. Therefore conventional polluting plants will still have to be in standby-mode for several hours before being capable of generating electricity. Such additional standby-mode and generation of plants may introduce additional costs and emissions.

In this work, apart from numerical optimisation of the power grid, the quantification of carbon emissions and savings under various DR programmes with smart solutions has

been performed. The assessment of DR programmes is based on the novel framework modelling operational profiles of reserve power stations. The novelty of the present study is the focus on short-term DR interventions, which become widely used in the UK energy market because of the rapid response to peak demands. DR programmes such as the Short Term Operating Reserve (STOR), Triad, Fast Reserve, Frequency Control by Demand Management (FCDM), and Irish smart metering pilot project of Demand Side Management (DSM) have been accessed in this research. The analysed data was provided by the UK industrial partners. The proposed approach combines accurate modelling of the operational cycle of the power plants with assessment of smart interventions.

The overall energy trilemma diagram that corresponds to the research is presented in Fig. 1.1. The main focus of this research is to quantify the carbon emissions and savings across the smart grid. Hence, the other two aspects – the energy cost reduction and improved security of generation due to generation intermittencies, are considered as the secondary in this context.

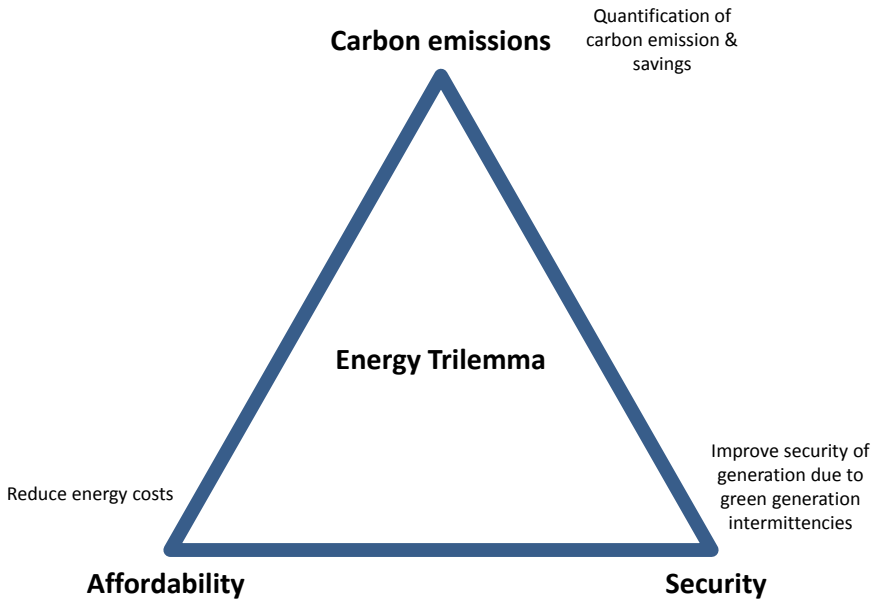

Figure 1.1: The energy trilemma.

1.2 Overview of the research

This PhD project was sponsored by Brunel University London and National Physical Laboratory (NPL). The NPL project code was "115947_NMS/IRD2012.12 Verification of Carbon Saving for Smart Infrastructure", of total duration of three years. The research was carried out at both Brunel University London and National Physical Laboratory (NPL) to ensure the full coverage of research facilities and supervisions.

1.3 Aim and objectives

1.3.1 Research aim

The research focuses on the wide assessment of carbon emissions and savings, taking into account both the smart grid optimisation problems and smart interventions of DR programmes. The aim of this research is the development of sound methodology for the quantification of carbon emissions and savings under smart grids.

1.3.2 Research objectives

Objective 1. To obtain the electricity data and define the model variables depending on the input data: real power input data or based on proxies in seasonal based modelling of energy consumption data.

Objective 2. To quantify the carbon emissions and savings in the power grid that allow the unified conversion of energy into carbon dioxide equivalent.

Objective 3. To quantify the uncertainties in power grids.

Objective 4. To perform numerical optimisation of a smart grid using closed-loop based optimal control.

Objective 5. To quantify the carbon emissions and savings under DR programmes in the UK.

1.4 Scope of the research

In order to develop the methodology for the reduction of carbon emissions and maximisation of carbon savings, research objectives as outlined in Section 1.3.2 are established.

The Objective 1 acquires the electricity data and defines the model variables depending on the input. This can be achieved through finding the most suitable method in modelling and forecasting of the electrical data based on the literature review of numerous methodologies. Further, the real power input data is required, whether from the public domain or from energy companies.

The Objective 2 quantifies the carbon emissions and savings. The thorough review of carbon dioxide and other Greenhouse gases (GHG) is performed. Such quantification allows the unified conversion of energy into carbon dioxide equivalent.

The Objective 3 deals with uncertainties quantification in the power grid. The uncertainties in the power grid will be identified and the approach to quantify the uncertainties will be proposed through review of uncertainty estimation from peer-review journals.

The Objective 4 deals with the numerical optimisation in the power grid. Several numerical optimisation techniques in the power grid are reviewed. A suitable optimal control for the smart grid will be established based on reviews of optimisation techniques.

The Objective 5 deals with the quantification of carbon emissions and savings under DR services in the UK. The DR services in the UK as well as the smart interventions involved in the DR services are pointed out. This further allows mathematical modelling of DR services with current smart interventions in providing rapid response demands in the UK.

1.5 Significance and novelty of the research

This research provides information on the current issues of the power grid, particularly on the carbon impact due to energy generation and consumption. This would raise the awareness of the electricity providers and users to counteract the environmental impact of the energy industry.

Further, this research also reviews costs and environmental impact of the power grid. In principle, the optimisation of costs and emissions in the smart grid may be implemented

at the level of the transmission operator such as the UK National Grid in collaboration with the operational wholesale electricity market and distribution network operators.

The DR modelling framework is beneficial to household consumers, the transmission operator, the energy suppliers and distribution network operators. Such framework allows an optimal operating strategy for better demand management in ensuring environmental sustainability for the future.

The study can provide baseline information on the current the carbon impact across the power grid (generation and consumption).

1.6 Structure of the thesis

The thesis is organised as follows: **Chapter 2** provides the literature review that corresponds to the research aim and objectives. **Chapter 3** presents the methodology for carbon savings estimation. **Chapter 4** presents the results along with the general discussion. Finally, **Chapter 5** concludes, presents the research contributions and suggestions for future research and improvement.

Chapter 2

Modelling of power grids

2.1 Modelling background review

Numerous paradigms have been proposed for modelling and forecasting energy consumption/demand data. Dordonnat et al. (2008) presented a periodic Gaussian time series model for short-term forecasting of electricity based on stochastic time-varying processes with various parametric trends (including seasons, short-term dynamics, weather effects and non-linear function for heating effects). They used Fourier series as the daily cycle base function and further established a multiple-equation linear time-varying regression model that reproduced the hourly electricity load forecasting. Svoboda and Brčák (2013) applied the least-square regression method to determine the relationship of a set of variables proportionate to electrical consumption in Czech Republic households. Shang (2012) applied principal component analysis to predict very short-term (in minutes) electricity demand. They further applied the univariate time series forecasting method and regression techniques (Shang, 2012). However, this method did not reproduce trends (daily, weekly and yearly).

Dordonnat et al. (2008) reported that if the variance matrices in the regression model became substantially large, multiple parameters or variables must be introduced with high degree of unknowns and consequently various assumptions and restrictions were required. Brossat (2013) stressed the sophistication, efficiency and high specifications of Fourier series, except for the difficulties in fitting many parameters into the model. According to McLoughlin et al. (2013), the use of Fourier series in modelling the electrical

load was applicable when electricity demand was stable, but the performance was relatively poor in response to sudden changes in demands.

Autoregressive Integrated Moving Average (ARIMA) models have been implemented in forecasting electricity demand due to fewer assumptions needed. ARIMA models are often associated with seasonality for better prediction of future demand. The stochastic modelling of monthly inflows into a reservoir system using an ARIMA model based on 25 years of data by Mohan and Vedula (1995) showed that ARIMA models were applicable in long-term forecasting (in the condition that the prior knowledge or historical records of seasonal profile must be available). Contreras et al. (2003) applied the ARIMA model in predicting the next-day electricity price by analysing time series and load forecasting (past and present) in Spain and California. Based on quantitative analysis using an ARIMA model, Jia et al. (2010) reported that ARIMA provided the accuracy and the quality in the prediction of results and the predicted environmental footprints might help in better energy planning for ensuring sustainability. Jia et al. (2010) asserted that the ARIMA is much more flexible than the Autoregressive (AR), Moving Average (MA), and Autoregressive Moving Average (ARMA) models. A comparison of ARIMA forecasting and heuristic modelling by Wang et al. (2011) showed that ARIMA models are more accurate than heuristic models.

However, the benefits of ARIMA models were contested by several other findings. Sumer et al. (2009) concluded that the regression model with seasonal latent variables provided more successful results in forecasting electricity demand than the ARIMA and Seasonal Integrated Moving Average (SARIMA) due to the capability of the regression model to reproduce seasonal fluctuations. The possible difficulty in interpreting results based on economic point of view also contributed the drawback of the ARIMA model (Dordonnat et al., 2008; Mečiarová, 2007). In forecasting aggregated diffusion models, ARIMA models tended to provide inaccurate results for long-term predictions (Christodoulos et al., 2010).

A large number of Artificial Neural Networks (ANNs) have been proposed to handle seasonal variations which offer numbers of advantages such as the ability to detect nonlinear relationships, interactions between variables and the availability of multiple training algorithms (Tu, 1996). However, several potential drawbacks of ANNs are also prevalent. Hippert et al. (2001) highlighted the two main drawbacks of ANNs: (a) forecast

ANNs might be over-parameterised with large number of components (neurons) resulting in huge amount of parameters that are hard to be estimated in a small data set; (b) results generated using ANNs were not always adequate and realistic. Similarly, Kourtis et al. (2011) stated that over-fitting (over-parameterised) problem might be in such the way that the close approximation in reaching high accuracy would eventually turn into noise approximations (small data set). They further stated that the noise resulted in poor generalisation of data and thus provided poor predictions. Modelling of seasonal and trend time series by Zhang and Qi (2005) demonstrated that ANNs were not capable of reproducing seasonal trends accurately unless the raw data was pre-processed (deseasonalising and detrending) along with an adequate neural forecaster. Zhang and Qi (2005) further emphasized that without pre-processed data, ANNs could perform worse than ARIMA models.

In power grids, ANNs can be classified as a 'black box approach', where coefficients of variables do not represent temporal and magnitude components of the electrical load profile (McLoughlin et al., 2013; McMenamin and Monforte, 1998; Tu, 1996). Other ANNs issues raised by Maier and Dandy (2000) were: (i) possible lack of appropriate model inputs; (ii) low availability of data and pre-processing data in the backpropagation algorithm; and (iii) inadequate process of choosing the stopping criteria and optimising the system. These factors could affect accuracies of seasonal trends. Kourtis et al. (2011) advocated that ANNs suffered from non-linear optimization problem where the search for multiple local optimum for the objective function using gradient-based approach might happen, as only one local optimum is required.

On the other hand, several recent studies, particularly in the energy field, showed the usability of ANNs in providing promising results. The earlier review of ANNs by Kalogirou (2000) showed that ANNs were applicable in modelling various energy-related networks (heating, ventilations, power generation systems and load forecasting). The recent analysis of variance (ANOVA) approach with combinations of ANNs and regression model demonstrated accurate forecasting of the annual electricity consumption (Azadeh et al., 2008). The statistical test performed by Schellong (2011) showed that using the backpropagation technique with "momentum term" and "flat spot elimination" as a learning rule, together with measured consumption in the previous week, forecasted results would be more accurate. A comparative study by Jebaraj et al. (2011) demonstrated that

ANNs provided better results in forecasting coal consumption.

Generally, the suitability of a model is highly dependent on the speciality and adaptability of a particular application. Moreover, the suitability also depends on the accuracy in the choice of parameters, variables and the input data to be evaluated. Still, there is a need for a model that is capable of reproducing realistic behaviour of electricity data, as well as being computationally light, requiring a reasonably small number of parameters and providing adequate flexibility in fitting diverse types of data profiles. To this end, the hyperbolic tangent function (HTF) can be applied in fitting the model of seasonal trends. It is one of the most common sigmoid transfer functions in forecasting trajectories of dynamical systems in many fields.

2.1.1 Hyperbolic tangent function application

The hyperbolic functions can be defined on arcs of a hyperbola, that exhibits the unit circle in the ordinary trigonometry (Dattoli, 2010). The HTF is applied in filtration design (Basokur, 1998), as the hidden layer for the configuration of the ANNs (Basam et al., 2012; Catalão et al., 2011; Jammazi and Aloui, 2012; Liu, 2012; Rahmani and Jamshidnezhad, 2013), forecasting energy related demands (Catalão et al., 2011; Colorado et al., 2011; Zarenezhad and Aminian, 2011) and rainfalls (Hung et al., 2009). HTF is defined as follows:

$$\tanh(\mathrm{y}) = \frac{\sinh(\mathrm{y})}{\cosh(\mathrm{y})} = \frac{e^{\mathrm{y}} - e^{-\mathrm{y}}}{e^{\mathrm{y}} + e^{-\mathrm{y}}} = \frac{e^{2\mathrm{y}} - 1}{e^{2\mathrm{y}} + 1}. \tag{2.1}$$

Blickle et al. (1998) presented a general description and analytical formula of the HTF distribution family. A number of distribution functions: log-normal, Rosin-Rammler and beta distribution analysed by Blickle et al. (1998) were well approximated by HTF, thus providing a very convenient method in quantitative comparison of measurement data. Basokur (1998) designed a low band-pass filter using the combination of HTF and the Fourier Transforms in the frequency domain. He concluded that the inclusion of the HTF in the filter design led to easier control of the slope and the suppression of the ripples (oscillations) of a function. The analysis performed by Mohanta and Mishra (2009) showed that the HTF was the most suitable function in fitting coal preparation distribution curves. Jammazi and Aloui (2012) asserted that HTF was the most stable and presented

convergences between the actual and predicted signals, thus realising the goodness of fits. Schellong (2011) also recommended the use of HTF along with logistics and limited sine function in training neurons in ANN for adequate forecasting of the heat and power demand in Germany.

In terms of forecasting, Hung et al. (2009) concluded that the ANNs model fitted with HTF provided the best forecast of rainfalls in Bangkok, Thailand, for days ahead. A similar result of forecasting by Jammazi and Aloui (2012) that used HTF as an activation function in ANNs. They showed that 19 months of forecasting were close to the real anticipated future price of crude oil.

The distribution of HTF is symmetrical at the origin (the inflection point), but some model does not always present symmetric cases. According to Balabin et al. (2008), the HTF in multi-layer perceptron did not work well in the calibration model based on gasoline Near Infrared Spectroscopy (NIR).

As the aim is to build a model representing energy consumption and demand, a realistic seasonal trend of power consumption is needed for further state estimation of energy consumption for derivation of carbon emissions. Henceforth, HTF is chosen as the basis of a stochastic model of seasonal trends in energy consumption. The main reason of selecting HTF for this purpose is because it has few parameters, relatively simple and high flexibility in fitting the distribution curves.

2.2 Carbon emissions, factors and savings of power grids

2.2.1 Carbon emissions

There are numerous definitions and concepts of carbon footprints (emissions) varying from general to scientific literature (Wiedmann and Minx, 2008; Wright et al., 2011). Several definitions of the carbon footprint are adopted to avoid numerous definitions of the carbon footprint without a clear consensus.

According to POSTnote 268 (2006), the carbon footprint is the total amount of emitted greenhouse gases (GHG) over a complete life cycle of a process or product. Carbon Trust (2012) defined the carbon footprint as the total GHG emissions resultant (direct or indirect) from a human being, organisation, product or event. Wiedmann and Minx (2008) proposed a clear definition of carbon footprint: they stated that it is a measure of the total emissions of carbon dioxide that is directly and indirectly caused by an activity or the accumulated life stages of a product. The activity and product from the definition by Wiedmann and Minx (2008) encompassed individuals, communities, governments, organisations, processes, industry retailers, goods, and services.

Overall, the carbon footprint targeted to justify the total quantity of GHG emitted over the full life cycle of an activity and a product (POSTnote 383, 2011). In agreement with Carbon Trust (2012), the carbon footprint incorporates six of the Kyoto Protocol GHGs: carbon dioxide, methane, nitrous oxide, hydrofluorocarbons, perfluorocarbons and sulphur hexafluoride. Among GHG gases, carbon dioxide (CO_2) is the most important and practical GHG (Carbon Trust, 2012; POSTnote 383, 2011; Wiedmann and Minx, 2008). For other GHG, the Carbon Trust (2012) provided a solution for the conversion of them into carbon dioxide. Hill et al. (2013) from the UK Department of Energy and Climate Change (DECC) presented the methodology for the conversion factor that enables the calculation of GHG emissions. The final methodology for the calculation GHG emissions is reported by Hill et al. (2014). POSTnote 383 (2011) provided a shortened statement of the way that one of the GHG, methane (CH_4), can be quantified into carbon dioxide equivalent, by calculating the emissions relative to carbon dioxide within the specified scale (by default, 100 years). The main reason for long scale duration of prediction is the need for projections of smaller amount of other GHG due to insufficient

availability of data (Wiedmann and Minx, 2008). However, due to rapid technological changes, the distribution of all GHG is subject to change. Wright et al. (2011) proposed that the carbon footprint measurement should include carbon dioxide and methane due to technological changes.

In the energy industry, the majority of GHGs are produced by power stations operating on fossil fuels, and even green generators have carbon footprint, which are derived using the Life Cycle Assessment (LCA) methodology (Convenant of Mayors, 2010). POST-note 268 (2006) illustrated the four phases of the LCA: 1) goal and scope; 2) inventory analysis – the carbon footprint is categorised here ; 3) impact assessment; 4) interpretation/improvement.

The measurement unit for carbon footprint is expressed as g, kg or tonne of CO_2 equivalent for a given time period (Carbon Trust, 2012; Wiedmann and Minx, 2008). In this paper, the carbon dioxide is selected as the main GHG for the assessment of carbon footprint. In subsequent sections the carbon footprint is termed as 'carbon emissions'.

2.2.2 Carbon factors

The carbon factor (emission factor or intensity) is reported in grams (or kilograms) of carbon dioxide CO_2 equivalent per unit of energy (kWh) during time period (Bowyer et al., 2012). Since generated energy is given in kWh and carbon factor in $kgCO_2$/kWh, carbon emissions can be estimated as CO_2 equivalent for a given time period.

The UK carbon factor is calculated by the Ricardo-AEA (2015), with quality assurance performed by the Department for Environmental Food (DEFRA) and the Department of Energy and Climate Change (DECC). Results are reported annually in the website (DEFRA, 2015). The latest data are available in the form of Microsoft Excel spreadsheets on the website (DEFRA, 2015), where statistics are currently stored for the years 2002 to 2015 inclusive.

Carbon factors for fuel generators in the UK can also be found in the post-notes of the Parliamentary Office of Science and Technology (POSTnote 268, 2006; POSTnote 383, 2011, see) and Carbon Trust. The UK real-time and historical energy demand data is provided by Balancing Mechanism Reporting System (BMRS) and Elexon portal that is used by the National Grid (BMRS, 2015; Elexon, 2015). BMRS reports the power

flows of the electric transmission system in the UK and also provides aggregated fuel mix data from different power stations. As reported by Killip (2005), different fuels have different compositions and require different operating mechanisms in order to provide the right amount of electricity. The knowledge of the fuel types used determine the amount of emitted carbon dioxide per unit of energy delivered (Killip, 2005). This allows one to estimate the nationwide carbon emissions generated by clusters of power stations using the same fuel to produce electricity: coal, gas, nuclear sources and renewables.

Electricity grid carbon factor can be calculated using the fuel mix data (BMRS, 2015; Elexon, 2015), with estimation of uncertainties due to standard errors of generation carbon factor for each fuel. For example, there may be intermittent generation of green energy on the background of conventional non-green power stations, at times of high or unpredictable demand more polluting power plants are employed to provide reserves in supplying sufficient energy to customers, thus resulting in fluctuations of carbon emissions. The web-site (Realtimecarbon, 2013) illustrated plots of the monitored variations of the grid carbon factor due to the effect of fuel mix, but without quantifying the uncertainties. Carbon emissions corresponding to the fuel mix may change due to the variation of the national fuel mix, as well as of proportion of net imported electricity (Hill et al., 2014).

2.2.3 Carbon savings

Carbon savings are determined as the difference between carbon emissions in a conventional business-as-usual (BAU) scenario and carbon emissions of an improved scenario. The improved emissions come from interventions from technologies, processes, services, optimised networks and avoided energy use. Similar approach is used in the quantification of carbon savings in Jenkins (2008); Jenkins et al. (2009); Lin et al. (2011b); ODPM (2006). The Office of the Deputy Prime Minister (ODPM, 2006) defined carbon savings as the difference between the carbon emissions improved using the micro combined-heat and power and the BAU carbon emissions of using boilers. Jenkins (2008) applied BAU as the baseline for energy use and the intervention technique as the improved scenarios in order to calculate carbon savings in a UK supermarket. The later paper by Jenkins et al. (2009) asserted that carbon savings could be determined based on the difference between

the carbon factor of a gas plant (improved) and a conventional electricity grid (BAU). Lin et al. (2011b) computed carbon savings through the avoided carbon emissions based on conservations of green energy considered (reduction of air conditioning and use of trees for cooling) in Beijing, China. Healy (2012) applied the formula from the ODPM and derived a new expression of carbon savings from combined heat and power.

In summary, the term 'carbon savings' in this paper is the difference between the BAU and improved carbon emissions. The BAU scenario implies the use of existing conventional infrastructure and plants. In contrast, the improved emissions are based on the modification or changes on the BAU method or, independently a completely new infrastructure to replace the BAU method.

2.3 Uncertainties in power grids

The complexity of a power network requires flexibility of participating nodes, with consumers and generators connecting and disconnecting from the grid depending on conditions and demand. Due to the intermittency of green generation, there is a need to balance the power output using the non-green generation.

Measurements of energy generation according to fuel types have been reported at 5 and 30 minute resolution. Due to the changing dynamics of energy generation, the short-term forecast and assimilation of energy generation incorporating the uncertainty estimation is necessary. This is where the ensemble Kalman filter (EnKF) plays a useful role.

The green generators are known to be intermittent. For instance, the uncertainty of the wind generation which cannot be fully abated by wind forecasts alters the current infrastructure of the network and energy production of plants and generators (Abrell and Kunz, 2014). Therefore the contribution of green generation to the grid is highly uncertain, and non-green generators have to provide back-up for the green generators. In case of high green generation, this creates excess of generated energy, which currently cannot be stored due to limited available energy storage. Experimental storage solutions are being developed but not employed at the level of National Grid yet. Thus, the green energy excess can be dumped in the system due to the infrastructural constraints. Such constraints are defined by nationwide energy demand and network capacity. Abrell and Kunz (2014) incorporated minimum and maximum amount of energy generation as the constraint for the electricity market model. The paper by Zhu et al. (2015) summarised that general constraints in electric power system included resource availability, balancing of networks (supply and demand), carbon emissions permits, and permits in network reinforcements. These reviews outline the uncertainties of the modelled power grid, which should be embedded with modelling constraints (energy capacity and demand) in the power grid. It is critically important to satisfy the energy constraints while ensuring sufficient, safe and stable energy supply according to consumers' demand and generators' capacity (Dai et al., 2012).

Several methodologies have been developed to address uncertainties in power grids. One can express the uncertainties using levels of fuzziness (fuzzy programming), or the

Monte Carlo sampling techniques, for instance, the Stochastic Approximation (SA) and Sample Average Approximation (SAA). Li et al. (2010) applied a multistage interval-stochastic integer linear programming method in modelling electric power grids under uncertainties. This method was initially used as the uncertainty estimation for water resources management by Li et al. (2008). Lin et al. (2011a) developed a dynamic optimisation model for energy system planning under uncertainty through the integration of interval-parameter, fuzzy and mixed integer programming techniques within a network energy system. Abrell and Kunz (2014) applied stochastic programming technique in lowering the start-up costs of flexible generation plants operating at part-load level conditions that provided balancing of wind outputs. Chen et al. (2010b) developed a two-stage inexact programming method for estimation of carbon emissions under uncertainty. Zhu et al. (2013) further extended the methodology from Chen et al. (2010b); Li et al. (2010) by developing a full-infinite interval-stochastic mixed-integer programming (FIMP) for modelling carbon emissions to address uncertainties (for instance, constraints of energy demand and supply balance). Recently, Zhu et al. (2015) further transformed the FIMP model into risk-explicit mixed-integer full-infinite programming (RMFP) model for quantification of uncertainties. Examples of uncertainties included by them are various electricity-generation activities with uncertain event durations and plants used, and errors in estimating the model parameters.

However, the accuracy of fuzzy strategies is low. Albertos and Sala (1998) argued that fuzzy strategy did not work well in scenarios where high levels of precisions and accuracies are required. Nemirovski et al. (2009) stated that the multidimensional expectation integral of the objective function could not be computed with high accuracy. As the scenario of national energy generation and demand require high accuracy and precise estimations, the fuzzy programming is not suitable to forecast the uncertain realisations of energy generation and consumption.

2.3.1 Ensemble Kalman Filter (EnKF)

The EnKF is applied to forecast the uncertain realisations of the energy consumption and generation. EnKF was first introduced by Evensen (1994) and further developed and applied in multiple publications in various branches of science (see Evensen (1994, 2003)

and references therein).

The EnKF was originated from the Kalman filter (KF), which was frequently used in linear models. An alternative approach was proposed that addressed the non-linear model problems by using the Extended Kalman filter (EKF). The EKF was based on the Jacobian technique of linearizing the non-linear models (Jensen, 2007). However, both KF and EKF had limitations. John and Mandel (2008); Mandel (2009); Reichle et al. (2002); Smith (2007) stressed that while the KF had proven optimality in linear models, the main drawback was that the KF was not feasible in the computation, storage and maintenance of the covariance matrix for high-dimensional systems. For EKF, Jensen (2007) stated that the EKF was not suitable for large scale non-linear problems.

The limitations in both KF and EKF have led to the establishment of EnKF (Almendral-Vazquez and Syversveen, 2006; Altaf et al., 2014; Evensen, 2003; Jensen, 2007; Nævdal et al., 2003). EnKF is a recursive filter based on a Monte-Carlo approach for generation of an ensemble of model representations. An ensemble is a system representation based on a random sampling of the system distribution (Evensen, 1994). The 'true' state of the model is approximated by the ensemble mean, or in other words, the mean of the member of the ensemble (Almendral-Vazquez and Syversveen, 2006). The covariance matrix in EnKF is predicted (forecast) and analysed by using statistics of the ensemble (Jensen, 2007). EnKF is suitable for sequential data assimilation in high-dimensional nonlinear systems. Even a few ensemble members have the ability to demonstrate the large-scale covariance behaviour of the system (John and Mandel, 2008). John and Mandel (2008) clarified that the eigenvalues of covariance matrix in EnKF decay rapidly and has the ability to generate large scale behaviour of the covariance.

According to Gillijins et al. (2006); Nævdal et al. (2003), the EnKF comprises two main steps, where the first step involves the forecast, followed by the analysis step. The input data for the forecast step was eventually the previous updated description of the model after assimilating a new set of measurements attained from the analysis step (Nævdal et al., 2003). During the forecast step, the model simulator for each of the model realisations was operated (Nævdal et al., 2003). As reported by Evensen (2003); Gillijins et al. (2006), since the 'true' state of a model is not always known, the ensemble of model states is approximated in the state space by forecasting the ensemble mean as the best estimate of the state based on the spread of the ensemble members. The spread of

the ensemble members around the ensemble mean is the error variance between the finest and actual approximation (Almendral-Vazquez and Syversveen, 2006; Evensen, 2003; Gillijins et al., 2006).

The analysis step, on the other hand, comprises the assimilation of measurement sets, where the EnKF performed the parallel data assimilation cycles to update model states and/or parameters for the input to the next forecast step (Altaf et al., 2014; Gillijins et al., 2006; Nævdal et al., 2003). Evensen (2003) asserted that at the analysis step, the new perturbed observations by each set of measurements were represented by another ensemble, where the mean defined the actual measurement and the ensemble variance was based on the measurement errors. Altaf et al. (2014) also clarified that the ensemble representation of perturbed observations according to each measurement set was generated with the sample mean and covariance as the measurement state and error covariance matrix. Therefore, it is at the analysing step, the model states and/or parameters are assimilated and updated using the EnKF updating formula, not at the forecast step. Altaf et al. (2014) further suggested that the data assimilation methods were able to enhance model simulations and predictions by constraining outputs with available realisations of observations.

Almendral-Vazquez and Syversveen (2006) provided a very useful example of EnKF simulation. The example started with a problem in finding a real state given a nonlinear characteristic of the model dynamics. The simulation began with a set or ensemble of model states, and each realisation of the model state through the model dynamics was evaluated that allowed the formation of a new ensemble in the forecast step. The new ensemble was termed as the *priori* ensemble, which was the ensemble of model representations to access the required statistics. In the next analysing (updating) step, based on all the members in the ensemble, an ensemble of observation (also termed as the perturbed observations) from a measurement sets was simulated, using the mean as the 'true' observations. Each of the *priori* ensemble member was then updated using the EnKF updating formula to reflect the simulated observations, which was termed as the *posteriori* ensemble. The process was then forwarded as the input to the next forecast step and the whole process was repeated in finding the convergence of simulated observations.

Formulation of the EnKF is widely available (see Almendral-Vazquez and Syversveen, 2006; Chen et al., 2009; Evensen, 2003; Jensen, 2007; Mandel, 2009; Nævdal et al., 2003). EnKF has been used for assimilation of the real-time production data (Begum,

2009; Chen et al., 2009). EnKF is able to provide both the estimate of a model and the corresponding uncertainties, by keeping track of the whole ensemble (Chen et al., 2009; Jahangiri, 2012). Nævdal et al. (2003) applied 100 ensembles in their simulation in atmospheric data assimilation, and the method was performing sufficiently well.

However, there are some cases when the EnKF can underperform. The earlier hydrological data assimilation by Reichle et al. (2002) showed that the EnKF provided poor forecast for 100 ensemble members, but the estimations derived by the filter were favourable when the 500 members of ensemble size were used. Altaf et al. (2014) asserted that the EnKF application required larger ensemble sizes in providing much-alike accuracy for forecasts of storms. The large ensemble size may provide better estimation for a particular application but may still create other type of problems. Houtemaker et al. (2014) stated that a large size of ensemble will increase the array sizes for computations and will exceed available memory amounts and finally, which may lead to a software crash.

As EnKF may suffer from large computational effects (due to high ensemble sizes), Houtemaker et al. (2014) suggested that the most obvious remedy would be employing high-performance computational clusters. Therefore, it is possible to use EnKF to estimate uncertainties in ensemble simulation of a power grid based on propagations by the whole ensemble of data. Additionally, the performance of EnKF is highly dependent on the prior knowledge of the considered model to be predicted using EnKF.

2.4 Optimisations in power grids

In a power grid, the grid operator aims to appropriately tune power flow with minimal system losses (Crow, 2009). However, the tuning of parameters in randomised manner without optimal planned strategy may increase the power operating costs, and also the environmental effects due to unnecessary firing-up of power plants. Instead of randomly tuning the parameters without proper arrangements and strategies, the optimisation of parameters through a selected objective function is required (Crow, 2009; Zhu, 2009). The objective function is formulated to minimise operational resources such as generating costs, reservoir production level, as well as system losses. The most common objective function is the minimisation of generating costs (Crow, 2009; Hetzer et al., 2008; Huang et al., 2012; Rau, 2009; Zhu, 2009).

2.4.1 Economic despatch (ED) problem

With the increasing need to optimise power generation, ED models were introduced. As stated by Zhu (2009), the aim of ED is to minimise the operating cost of power generators by optimising the power output in each generators (thermal units) subject to specific constraints. The ED problem is composed of the characteristics of input-output sets in a thermal-based power generating unit (Zhu, 2009). The input set is the fuel consumption function whereas the output set is the operating cost function. The unit of the generator fuel consumption function is Megawatt per hour (MW/h). The operating cost function has the unit of £ per hour (£/h). Zhu (2009) further added that examples of thermal generating units are steam turbines, boilers and generators. The gas turbine can be also categorised as one of the thermal generating units due to the combustion processes involved in the gas turbine and also the steam raised by the gas turbine. The ED minimisation problem is subject to minimum and maximum operating capacity of thermal units. Such operational constraints on the minimum and maximum load limitations are required in maintaining the fuel combustion stability of thermal units (Zhu, 2009).

The basic ED problem can be extended to the case with security constraints, emissions estimation and renewable generation. The security-of-supply constraint is an important element, when the ordinary ED model is constrained by the network security other than

minimum and maximum generating capacity of power generators. The security-of-supply constraints include power balance and line overload prevention (Huang et al., 2012). The emissions function is added to ED to become the economic emission dispatch (EED) model. However, such addition may introduce trade-offs between costs and emissions. The priority of optimising costs rather than emissions may increase emissions in the smart grid. Rajasomashekar and Aravindhababu (2012); Ramanathan (1994) presented a methodology that includes emissions constraints by applying the weighted sum technique to translate the multi-objective function (costs and emissions) into a single objective function. The multi-objective problem is represented as a single objective function by assigning different weights. Rajasomashekar and Aravindhababu (2012) further enhance the objective function through normalising the fuel cost and emission components to provide the equal significance in the objective function. Huang et al. (2012) applied analytical hierarchy process approach to determine weighting factor to convert the multi-objective function into a single objective function. Similarly, Senthil and Manikandan (2010); Subramanian and Ganesan (2010) converted a multi-objective function to a single optimisation problem using the price penalty factor approach.

In addition to the security and emission constraints, the ED problem can be further integrated with renewable energy. Notably renewable energy such as wind is widely applied into both ED and EED problem. Hetzer et al. (2008) integrated the overestimation and underestimation of available wind energy into the ED model as a factor. In their model, a linear cost function was assumed for the wind energy. On the other hand, Li et al. (2014b) introduced the mean-variance multi-objective ED problem (due to the difficulty in obtaining the weights) for generators in integration with the wind energy. Besides the wind energy, Khan et al. (2015) presented a combined EED model developed for a system consisting of several photo voltaic (PV) fleets and thermal units.

ElDesouky (2013) introduced Dynamic Economic Emission Dispatch (DEED) model incorporating the security-of-supply constraints, emissions and renewable energy (wind and photovoltaic) and thermal units. The multi-objective model was converted into single objective by pre-multiplying each objective with a user-specified weight (weighted sum method). The simulation results demonstrated the effectiveness of the DEED model for optimal and secure power system operations. Niu and Wei (2013) presented a novel approach of the social, environment and ED model for thermal and wind power systems.

The Karush-Kuhn-Tucker (KKT) method was used to convert multi-objective function into a single objective function and also to eliminate the need for using weights. The optimisation results in Niu and Wei (2013) demonstrated the effectiveness to enhance the security of a power grid and also to decrease the costs and emissions.

In summary, the ordinary ED problem must be integrated with other factors, such as the emissions and renewable generation. This is to decrease the trade-offs among those factors and also to maintain the required stability of power grids, the social and the environmental aspects (Niu and Wei, 2013). The conventional (BAU) generation is to be evaluated and optimised along with integration of the renewable energy, network security and emissions minimisation. The formulation of the ED model for the smart grid will be established in the Methodology section.

2.4.2 Power grid optimisation applications

Wei et al. (2014) proposed the bi-level (the government and the grid operator) economical optimisation model that determines the optimal tax rate among power generating units, balances carbon emissions and profits of the energy sectors. Chen et al. (2013) developed an inexact optimisation method for supporting the carbon emissions management in the energy system, by employing interval-parameter programming within a robust optimisation framework. The optimisation scenarios generate alternative decisions to mitigate carbon emissions within the economic context. Similar strategy was proposed in Gharaie et al. (2013), by presenting a mathematic model based on mixed-integer non-linear programming to mitigate carbon emissions in process industries. Process units are based on the integrations between large fleets of heat exchangers and the area utility system. The model presented optimised carbon emissions with suitable mitigation and investment options for emissions reduction target. The optimisation results demonstrate the importance of carbon trading in the process economics that aided the emission reductions. The work by Gharaie et al. (2013) had the similar objective with Zhu et al. (2013, 2015). Zhu et al. (2013, 2015) mainly addressed the uncertainty in carbon emission trading and the later involves the risk analysis for planning the carbon emission trading for Beijing. Most interestingly, Cui et al. (2012) presented a bi-level robust model that combined consumers and utility companies to optimise social welfare by incorporating a feedback system that acted

as a global controller. They also used a feedback system that acted as a global controller to manage the whole system integration between the consumers and utility companies. The dynamic pricing model function constructed allowed all participants (consumers and utility companies) to alter the choices of power consumption pattern.

However, the environmental impact of a power grid is still evaluated at a very crude level. In the context of real-time control operations, the carbon reduction target is mostly pre-conditioned by the needs of positive economic impacts (profitable investments subject to operational constraints). The rapid assessment of costs and environmental impact in the power grid is extremely important, as the later evaluation of energy data solely does not guarantee minimisation of the emission and security level across the power grid. For instance, due to rapid technological changes, the lack of continuous real-time assessment of environmental and network security effects may contribute the high amount of unnecessary emissions and costs, and thus fail to sustain the power grid for the future. Henceforth, an efficient optimisation model is needed that does not only guarantee the profitable economical return of investment in the ED problem, but also reduces the nationwide emissions while adhering to operational constraints. As the objective of this research is to perform numerical optimisation of smart grids, a mathematical model based on optimisation methods is required that minimises costs and carbon emissions. Furthermore, due to the needs to optimise the total costs associated with generation, as well as carbon emissions, under security-of-supply constraints, a feedback system is required. For instance, in line with Cui et al. (2012), generating units (non-renewable and renewable) should have the optimal amount of energy generation corresponding to demand which are controlled by the system operator using the EMS software. Based on this, a universal feedback system controller must be established that optimises the power grid in the real time.

2.4.3 The open and closed-loop control

There are two distinct types of controls: the open-loop and the closed-loop feedback control. The open-loop is a non-feedback control that allows signals flow unidirectional and the final output of a grid depends on the pre-set value of the system input (Roth et al., 2014). That is to say, the inaccuracy of the output parameters will not alter the pre-set

value of the system input. Conversely, in the closed-loop feedback control, the behaviour of the system output depends on the controlled system input. Therefore, the system output is controlled by the condition of the system input through the concept of feedback control. The feedback control is a fundamental control of power grids, where the information about state variables obtained from a measurement or estimation is fed back to the system as a reference point through a controller with the intention of achieving the desired output (Capolei et al., 2013; Roth et al., 2014).

The closed-loop feedback control, compared to the open-loop control, is more flexible in achieving the required level of system behaviour with high robustness and reliability (Dong and Petersen, 2010; Roth et al., 2014). For instance, when there is a fluctuation (changing dynamics) from the system output, the feedback control allows the unstable trend of system output to be stabilised continuously. This is achieved by continuously obtaining the controlled variables that tune the system until the desired output is achieved. In contrast, in the case where there is strong repeatability and consistency of the system output, the open-loop control is more favourable than the closed-loop control. In the application of smart well reservoir engineering field, Capolei et al. (2013); Chen et al. (2009) fully asserted that the closed-loop feedback based optimal control technologies permitted higher oil recovery than the open-loop control (reactive based strategy). Back to the concept of the smart grid, the energy demand is highly uncertain and fluctuating (due to the impact of seasonal, climate and variety of behavioural usage among consumers). Due to such unavoidable circumstances, a highly responsive integrated closed-loop based smart grid model is compulsory in actively engaging the unexpected trends of the system output.

2.4.4 Ensemble-based closed-loop production optimisation (EnOpt)

In order to fully focus on quantifying the cost and carbon saving with rapid and continuous model updating in the smart grid, the EnOpt is applied in order to develop optimal operating strategies in the ED problem. The closed-loop feedback concept is the essential operating mechanism in the EnOpt model, which is, a production optimisation model that combines the EnKF and optimisation, and was initially developed for the smart well technologies in the oil industry (Chen et al., 2009). EnKF forecasts and assimilates system state with respect to the historical production data. Such data assimilation aims to

minimise the mismatch between the model predictions and the production data (Chen et al., 2009). The production optimisation model of the EnOpt plays an important role in searching for the optimal control parameters in order to improve the operating plans that maximise the net present value (NPV). The maximised NPV in EnOpt is achieved by adjusting the production rate from individual well constraints through inflow control valves in the smart well reservoir management (Asadolladi et al., 2014; Capolei et al., 2013; Chen et al., 2010a, 2009; Dehdari et al., 2012; Fonseca, 2011; Forouzantar et al., 2013; Hasan et al., 2013; Jafroodi and Zhang, 2011; Jahangiri, 2012; Nwaozo, 2006; Petvipusit, 2011; Zabalza-Mezghani et al., 2004). Li et al. (2014a) asserted that the production optimisation technique maximised cumulative productions of land fill gas by providing solution of optimal controls.

The EnOpt estimates the expectation of the objective function based on assimilated data along with optimised control constraints (Chen et al., 2009; Jahangiri, 2012; Nwaozo, 2006). At the end of the EnOpt simulation, the best control settings are the optimal control variables that minimise the objective function (Chen et al., 2009; Jahangiri, 2012; Nwaozo, 2006). The flow of EnKF and EnOpt is presented in Fig. 2.1.

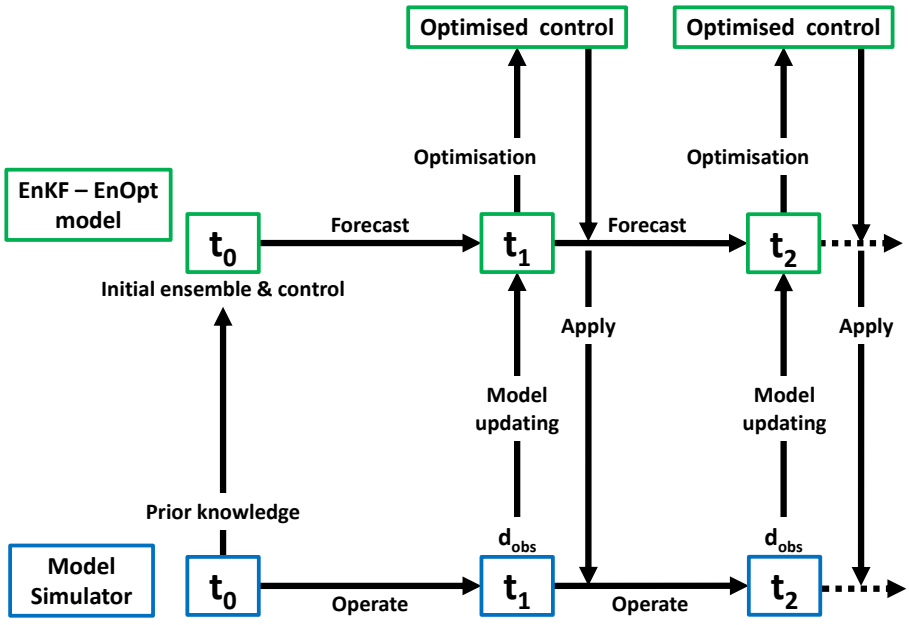

Figure 2.1: EnKF and EnOpt flow diagram. Adapted from Chen et al. (2009); Nævdal et al. (2006).

The EnKF and EnOpt flow is based on the earlier model adopted by Chen et al. (2009);

Nævdal et al. (2006). The following explanation of the EnKF and EnOpt flow diagram in Fig. 2.1 is adopted based on the earlier explanation by Chen et al. (2009); Nævdal et al. (2006). Firstly, a 'true' model simulator is developed based on available prior knowledge and historical records. When an observation data is available (the model prediction through the model simulator), the new ensemble is created which represents the perturbed from the model prediction. Then, in the EnKF and EnOpt model, the EnKF algorithm is initially applied for the data assimilation process. The model is then optimised using EnOpt based on the ensemble updates from the EnKF. The process is repeated in the next time steps.

The model is highly affected by parameterised noises such as process and measurement noises (Nævdal et al., 2006). Nævdal et al. (2006) stated that it was more convenient to use a synthetic model representation rather than real system model due to the difficulty in conducting a simulation from a complex, high-dimensional model. This is where the EnKF plays the useful role in data assimilation of state updates based on the 'true' synthetic model. Therefore, the perturbation of energy data based on the forecast (prediction) technique from a model simulator is developed and further updated using EnKF. The resultant EnKF propagation of state updates are to be further applied and optimised in EnOpt. The optimised control based on EnOpt is integrated into the model simulator that allows the model state forecast and updates in the next time step.

2.4.4.1 Optimisation techniques

Numerous optimisation techniques have been proposed that are widely used in oil and gas engineering. Most well-known methods are gradient-based or gradient-free (non-gradient-based) methods (Dehdari et al., 2012; Li et al., 2014a). Gradient-based optimisations are commonly used to find the gradient of an objective function that converge to local minimum and maximum (Chen et al., 2010a, 2009; Dehdari et al., 2012; Forouzantar et al., 2013; Nwaozo, 2006). The notable gradient based approaches are the steepest ascent or descent, and sequential quadratic programming (SQP) approach. Dehdari et al. (2012) provided a good review and example on gradient based approaches in a case study for the comparison of optimisation techniques in reservoir management.

The steepest ascent or descent in the gradient-based approach is a popular technique in reservoir management field in maximising the economical objective function (NPV). Ac-

cording to Chen et al. (2009); Dehdari et al. (2012), as steepest ascent or descent methods are unconstrained optimisation algorithms, at each step iteration, the updated control parameters that lie outside the feasible region must be truncated according to the constraints in the optimisation problem. The main advantage of this technique is the relatively inexpensive computations due to the neglected constraints in the gradient (Chen et al., 2009; Dehdari et al., 2012; Li et al., 2014a).

In contrast, when constraints are considered, the SQP approach is used. According to Dehdari et al. (2012), the non-linear constrained optimisation problem is mapped to the environment of quadratic optimisation. During the iteration step, only a quadratic optimisation is solved, eliminating the need in solving a non-linear optimisation problem. In the end result, optimised parameters can be found. They further asserted that the SQP method was the first selection of gradient-based method, as higher NPV could be obtained compared with steepest ascent or descent approach. However, Dehdari et al. (2012), along with Li et al. (2014a) agreed that SQP with constrained optimisation method suffered from high computational cost due to the additional constraints. Furthermore, the SQP applied to solve constrained production optimisation based on a case study in Brugge field by Dehdari (2012) showed that the computational costs of the optimisation is still much higher than those of the gradient method, although sources of inefficiency in the optimisation are mitigated. In the smart grid, the low computational cost, high efficiencies and the prompt (almost instant) operating strategies are required in responding to high amount of uncertainties in energy demand and intermittency in power generation. Without meeting these requirements the stability of the smart grid is not guaranteed, and this may cause massive power failure throughout the country.

In contrast, non-gradient-based methods are stochastic methods that include genetic algorithms, particle swarm, simulated annealing and pattern search methods (Dehdari et al., 2012; Hou et al., 2015; Li et al., 2014a). The computational efficiency of gradient-based methods are higher compared with non-gradient approaches, but the method suffers from the difficulty in transforming from one simulator to the another (Hou et al., 2015). Additionally, the ad-hoc constraints of gradient-based approach forbids higher NPV values (Dehdari et al., 2012). The gradient-free approaches are independent of numerical simulators but require more simulations to find the optimum (Hou et al., 2015).

2.4.5 Summary of the EnOpt

This research mainly focuses on using the gradient-based approach for the EnOpt simulation. The steepest descent gradient-based approach is selected for the simulation of EnOpt that allows instant operating solutions in determining the optimal generation in the smart grid. The updated model simulator in the EnKF is selected as the description of the system state in the smart grid. In the EnOpt production optimisation process, the control variable seeks to minimise the cost or carbon emission based on the updated simulator model assimilated by the EnKF. Such process is repeated for the next time step until the end of model simulation. The model can be implemented in real time and the operating strategy and management are stored (Chen et al., 2009). Overall, when new datasets are available in the next time step, the process is repeated and the states of the model are updated through the assimilation of data (Capolei et al., 2013). The updated states will be used in the optimisation (EnOpt) for obtaining of optimal trajectories based on the modified control variables (Capolei et al., 2013).

2.5 Demand Response (DR) programmes

The UK energy infrastructure is currently experiencing volatility in demand and load (variable heating in colder seasons and addition of green generators under the limitation of storage facilities). One of the solutions is the implementation of the energy efficient technologies and programme. Admitting that overall reductions in energy usage and costs are presumed 'slightly evident', the positive impact of towards the environment is still concealed. The review on carbon footprint collection and analysis by Brewer (2009); Robin (2011) noted that the full emphasis on energy efficiency did not guarantee the reduction of carbon emissions. Brewer (2009) further clarified that the improvement of energy efficiency might create the rebound effect, either as a good reduction in emissions or counterproductive as additional emissions. Overall, the concept of energy efficiency does not necessary lead to reduction of carbon emissions but may reduce costs of generation and energy despatch. The reduction of carbon emissions is therefore not the highest priority in the context of energy generation.

In order to alleviate energy efficiency problem and the possibility to postpone large-scale upgrades of the network infrastructure, Robin (2011) suggested several solutions such as cutting energy usage through incentive-based regulation, real-time smart metering and rethinking behaviour. Additionally, large attention is paid to novel energy storage as the crucial solution in providing reliable balancing of renewable energy outputs (Kousksou et al., 2014; Michael et al., 2013). Kousksou et al. (2014); Michael et al. (2013) outlined possible benefits of using energy storage: 1) to meet short-term and random fluctuations in demand that would eliminate the need to adjust the frequency deviation by BAU plants; 2) to eliminate the need for part-loaded BAU plants which would be in 'stand-by mode' to meet contingencies in demand and renewable energy; 3) to store the energy generated overnight during off-peak electricity prices.

However, the storage solutions cannot be fully realised without a precise control mechanism. Michael et al. (2013) clarified that the energy storage could be viewed as energy savings technology rather than cost savings by additionally implementing control mechanisms. This has further led to the initial establishment of storage technologies with controls, as well as the balancing services that were named as the DR programme.

2.5.1 DR programme – background study

According to Gast et al. (2014), energy storage could be either real (batteries or reservoirs) or virtual. DR is defined as alterations in electric usage by consumers from the BAU consumption patterns in response to alterations in the price of electricity, or the incentive-based schemes designed to force the lower electricity usage during high wholesale market prices or system stresses (U.S. DoE, 2006). The DR does not concentrate on power production side, rather DR acts as the balancing services in balancing the energy across the grid. While there are numerous practices in optimising energy generation and consumption, DR programmes are the most notable mechanism in reducing energy usage and cost effectiveness (Mazinani and Zaeefi, 2013; Palensky and Dietrich, 2011). Wang et al. (2010) studied the role of DR in providing the load reduction, off-peak storage and pricing signals in mitigating electricity shortage in China. Gast et al. (2014) studied the impact of DR on the electricity markets by incorporating two-stage market model with dynamic aspects of generation, demand and DR. Magnago et al. (2015) also evaluated the impact of electricity prices through DR modelling by using mixed integer programming unit commitment model as the market operation network and day-ahead market model regime. Both evaluation by Gast et al. (2014); Magnago et al. (2015) proved that DR provided a better social welfare due to the capability to lessen the pressure on electricity prices. Boait et al. (2013) proposed a novel DR-based scheme that allowed an aggregator to strengthen the relationship between consumers and the electricity market. A signal was provided to a "smart home" control unit that managed electrical usage to address the consumer's needs and preferences. The signal was 'shaped' to inform the consumer about the best time to use their appliances. A similar concept was elaborated in the paper by Marwan et al. (2014), where a DR model was developed that aided the electrical consumers in managing air-conditioning during peak electricity demand. Consumers who participated the DR programme as indicated by Marwan et al. (2014) were exposed to the fluctuations of the market prices. The DR model was simulated through numerical optimisation in finding the set of air-conditioning temperatures that satisfied the constraints and provided minimum energy costs. Logenthiran et al. (2014) successfully applied a load-shifting algorithm to induce the changes in consumption patterns, taking into account the multi-agent system based simulation of consumers (residential, commercial and indus-

trial). Stözer et al. (2015) used a novel DR approach to analyse the load-shifting potential in the residential and commercial sectors in Germany. The most recent paper by Ceseña et al. (2015) presented comprehensive techno-economic DR methodologies focusing on small (below 100 kW) residential and commercial end-users.

In summary, DR programmes are established to deter the reinforcement of network infrastructure through demand shifts, reduced consumption and additional storage options (back-up generation). DR services available at National Grid are the Short Term Operating Reserve (STOR), Fast Reserve, Frequency Control by Demand Management (FCDM) and Triad, with interventions or contracts through back-up generation, storage and demand reduction (National Grid, 2013b; Ward et al., 2012; Warren, 2014). The term 'interventions' in the remaining Chapters are further named as "smart interventions" that implies the improved solutions based on modified BAU method, or the completely new infrastructures (replacement of BAU methods) that promotes carbon savings.

However, the implementation of the DR is still at low level. Main barriers are insufficient marketing strategies, uncertainties in the value of DR, poor understanding of DR and low awareness of DR in promoting energy and cost savings (Nolan and O'Malley, 2015; Strbac, 2008; Wang et al., 2010). According to Palensky and Dietrich (2011); Strbac (2008), specific challenges of the DR implementation are the lack of interoperability and stability of algorithms, high competition with traditional approaches, increased complexity of the system operation and inappropriate market incentives. Case studies of DR in 15 companies were investigated by Lindberg et al. (2014) who showed very low implementation of DR in Sweden due to the complexity in reaching a reliable production after power plants were in 'parking' phase. They further clarified that the complication in contracts for electricity due to expensive and fixed price contributed to the barriers to DR implementation. Additionally, although DR programmes are widely promoted for their cost-effectiveness and greater energy system efficiency (see Atzeni et al., 2013; Drysdale et al., 2015; Logenthiran et al., 2012; Neves et al., 2015; Shen et al., 2014), only a few attempt to quantify related carbon emissions in DR programmes have been made. Cooper et al. (2014) analysed the impact of heat pumps and micro-cogenerations participating in DR programmes. The results suggested that DR programmes enabled large deployment of heat pumps and caused significant reduction in carbon emissions. It is important to note that this study was technology-specific and small-scale. The assessment of carbon

emissions in DR programmes is indeed very important in the context of environmental impact and identification of the preferable directions of development of technologies. While DR programmes maintains the stability of the grid, it is also necessary to remember that carbon emissions may be counter-intuitive when one compares BAU and smart interventions. At particular operational stages, balancing of energy demand may require 'peaking' of power plants, which may be highly polluting. However, the replacement solutions, which may have high carbon footprints, may still lead to carbon savings. Additionally, the use of green generation does not assure the stability and reduction of carbon emissions due to its intermittency.

In this work, the quantification of carbon emissions and savings under various DR programmes is implemented. The novel framework of carbon savings quantification includes modelling of operational profiles of reserve power stations. DR programmes including STOR, Triad, Fast Reserve, FCDM, and use of tariffs (demand reduction) in the Irish smart metering programme are modelled. Such DR services integrate electrical energy data with corresponding smart interventions, which in turn enable assessment of carbon emissions and the associated savings. The novelty of this research is the focus on short-term DR smart interventions, which become wider used in the UK energy market because of the need to respond to peak demands. While the operational cycles of the common industrial power plants (BAU plants) are well known, the adequate modelling of the carbon emissions for comparison with DR smart interventions has not been performed before.

2.5.2 Overview of DR programmes

2.5.2.1 Short Term Operating Reserve (STOR)

The STOR programme allows the transmission system operator, such as National Grid, to balance the power output by providing temporary reserve services during the time of demand stress, including sudden generation losses, unpredictable changes in demand and intermittent renewable energy generation (Hall, 2014; National Grid, 2013c, 2014c). National Grid allocates and utilises a number of reserve resources to cope with demand stress, either through generation or demand reduction (National Grid, 2013c, 2014c). National Grid provides tendering and bidding contracts for the STOR participants by allocating a number of reserve resources, where biddings can be accepted or rejected

entirely. The STOR is tendered twice a year and reservations are tendered at different availability periods (total of six availability windows in STOR terms) in competitive tender rounds (Hall, 2014; National Grid, 2013c, 2014c).

There are two main STOR schemes: Balancing mechanism (BM) and Non-Balancing Mechanism (Non-BM) (National Grid, 2013c, 2014c). BM participants provide large amount of energy generation and can be directly linked to the UK Transmission System. On the other hand, the Non-BM participants are represented by smaller providers connected to the lower voltage distribution networks. Both categories are often referred to as 'demand side providers'.

A STOR provider supplies National Grid with sufficient operating reserve for at least two hours (ideally within two to four hours) in real time, and a large proportion of generating units are made available within 20 minutes. The minimum load reserving capacity that a STOR provider must supply is 3 MW in the form of generation or demand reduction (Hall, 2014; National Grid, 2015c; Ward et al., 2012).

However, it may happen that some participants who wish to join the STOR have insufficient amount of generation to meet the minimum STOR contract. This happens particularly to small-to-medium enterprises (for instance, small supermarket chains). In order to overcome the limitations, there are several companies known as Aggregators that merge the smaller loads from participating companies (supermarkets, schools, universities and hospitals) into STOR units that are 3 MW or greater in achieving minimum requirement for the STOR supply. A Non-BM aggregator plays an important role in this case by combining (aggregating) smaller loads into STOR units of $\geq$ 3 MW and further submits the aggregated energy volume to National Grid. The aggregated volumes contribute to the overall proportion of STOR tendered for the particular availability window and presented to National Grid (National Grid, 2013c). Fig. 2.2 shows an example of fuel type composition of Non-BM STOR providers extracted from National Grid (2013c).

STOR contracts typically vary in different seasons. For instance, a total of 2809 MW of STOR contracts were accepted for season 8.3 (18/08/2014–22/09/2014) and 3444 MW for season 8.5 (27/10/2014–02/02/2015) (National Grid, 2013c, 2014c). When National Grid signals a STOR provider to supply the necessary reserve services, a STOR provider will apply their own interventions to operate during the STOR event such as the standby generation, load reduction, combined heat and power (CHP) generation. This should

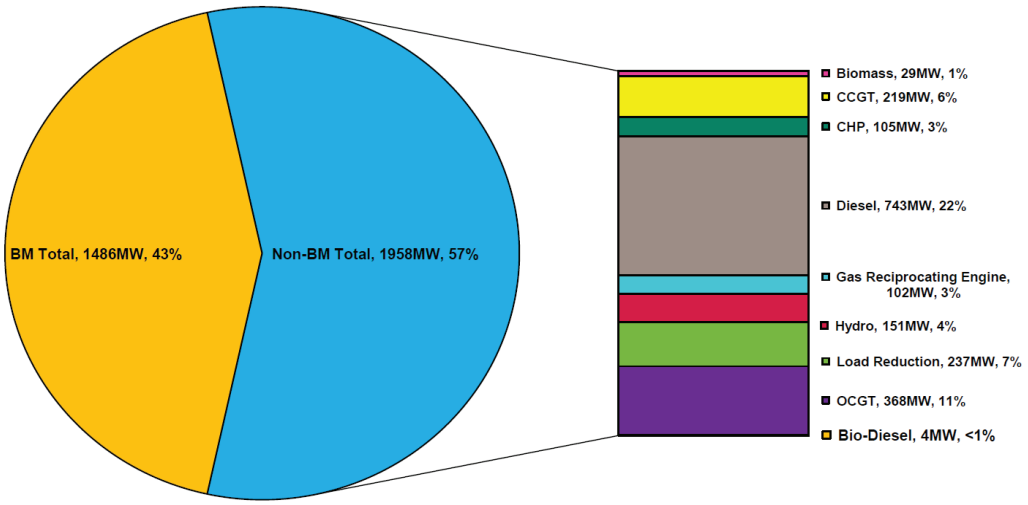

Figure 2.2: Fuel type composition of Non-BM STOR providers. Adapted from National Grid (2013c).

be done within the STOR timescales once the STOR triggering instruction is relayed by National Grid.

2.5.2.2 Triad

The Triad programme comprises three settlement periods of maximum energy demand within one financial year in winter, which takes place between November and February. The Triad programme occurs during the evening peak period. The three settlements of the maximum energy demand result in Triad charges, which are levied to electrical consumers by National Grid. The Triad charges are determined through the first half-hourly (HH) system peak demand, and the other two HHs of the next highest demand, which have to be different from the system peak demand and isolated from each other by at least ten clear days (Flexitricity, 2010). The average of the three highest demand periods is used to calculate the Transmission Network Use of System (TNUoS) charges according to different zonal tariffs in the UK (EDF Energy, 2013; Flexitricity, 2013). Unlike other energy balancing services available at National Grid, Triad charges are calculated when the Triad season is over, for the licensed suppliers of National Grid (Flexitricity, 2010; Ward et al., 2012). According to Ward et al. (2012), the minimum load for reserving is 1 MW. The Triad participants subscribe for the Triad programme by forecasting the potential peak demand during the active periods. Triad warnings (or Triad avoidance/management) are sent to consumers that avoid using electricity from the main grid. From 10 to 40 Triad

warnings can be issued annually, depending on the nature of forecasts by participating companies. Overall, the Triad programme aims to decrease demand in the national network during the winter season in order to boost the deferred network reinforcement plans and in that way keep down the TNUoS charges (Ward et al., 2012).

According to Flexitricity (2015), Triad is one of the profit-making DR revenue programme. During the Triad period, generators (used for replacement of energy supply) will usually operate for an hour at winter peaks from 5pm to 6pm (Ward et al., 2012) – instead of drawing from the UK energy grid operated by reserve power plants controlled by National Grid that are switched off if the Triad programme is running. It is cheaper to use in-house diesel generators for energy generation than purchase it from the UK energy grid. This is only due to the reduction in TNUoS charges as the result of hitting all three Triad peaks.

2.5.2.3 Fast Reserve

Similar to the STOR programme, the Fast Reserve is another type of DR service that provides rapid and reliable delivery of active power through a range of demand changes, from generation to demand reduction, following acceptance of an electronic despatch instruction from National Grid (Hall, 2014; National Grid, 2013a). Fast Reserve service is highly important in accommodation of the very rapid changes in demand. For instance, TV pick-ups, boiling water and watching a live event (sport event) at the same time. Fast Reserve service can be triggered at any time of the year, and can be announced on daily basis (Ward et al., 2012). Fast Reserve is procured by National Grid through a monthly contracted process, with each contract containing technical information of power plants by the Fast Reserve provider (Hall, 2014; National Grid, 2013a).

In order to participate in the Fast Reserve service, a typical provider must be capable of despatching power delivery within two minutes following the instruction by National Grid, with the requirement of minimum run up and run down rates of 25 MW/minute (Hall, 2014; National Grid, 2013a; Ward et al., 2012). This is not the same as the STOR programme that allows operation within 20 minutes of capability in despatching power. Documentation by (Hall, 2014; National Grid, 2013a; Ward et al., 2012) stated that supply of energy for Fast Reserve should be sustainable for at least 15 minutes. Similarly to STOR, a Fast Reserve provider should supply a minimum of 50 MW, or can be aggregated by

merging smaller units to achieve the total volume of minimum 50 MW (National Grid, 2013a). Pump-based storage for electrical generation is the most common technology in the Fast Reserve service.

2.5.2.4 Frequency control by demand management (FCDM)

The FCDM automatically maintains the frequency of the grid through demand interruptions among consumers in supporting the management of low frequency (National Grid, 2015b; Ward et al., 2012). When the frequency falls below a threshold value, for instance, $\leq$ 49.8Hz, relays are triggered at providers' sites that 'trip' the demand automatically (Ward et al., 2012). The FCDM is introduced in managing large frequency deviations due to the failure of large generation and incorrect frequency. The service provides route to market for demand side providers and non-dynamic responses (National Grid, 2015b). The event frequency for FCDM may occur at any time of the day with approximately ten to thirty times per annum (National Grid, 2015b; Ward et al., 2012).

According to National Grid (2015b), the FCDM providers will be prepared for demand to be interrupted for at least 30 minutes with at least 3 MW of demand reduction. Similar to STOR, smaller loads can be aggregated in contributing the amount of 3 MW or greater. The FCDM provider must be capable of providing response in the form of demand reduction within 2 seconds (primary and high frequency response), 30 seconds (secondary response) and 2-10 seconds (non-dynamic response).

2.5.2.5 Smart Meter pilot project: the Irish case study of demand reduction

The Irish smart meter pilot project is considered here as an example of behavioural demand reduction in the DR programme. The project explores the impact of smart meter roll-out on the consumer behavioural response with over 5000 participants (CER11080a, 2011). The considered smart intervention is the time-of-use (ToU) tariffs in combination with demand side management (DSM) stimuli. The smart metering trial aims to discover the willingness of consumers to shift the electrical usage to low peak tariff rates. The energy data is recorded every 30 minutes (in kWh). According to CER11080a (2011), the trial begins with the establishment of benchmarking level of electricity usage (01/07/2009–31/12/2009) and later testing of various ToU tariffs with DSM stimuli

(01/01/2010–31/12/2010). At the end of the benchmark state, consumers in the trials are divided into two groups: consumers with ToU tariffs and DSM stimuli smart intervention (test group) and the BAU consumers (BAU group). The main finding of this trial is that there is overall reduction of electricity usage by 2.5 % and peak usage by 8.8 %. The ToU tariffs from CER11080a (2011) are shown in Table 2.1. Four different ToU tariffs are established for the behavioural trial programme.

Table 2.1: Residential ToU bands and tariffs.

Time band	Morning-afternoon rate	Peak rate	Night rate	Midnight-morning rate
	8am-5pm	5pm-7pm	7pm-11pm	11pm-8am
Tariff A (cents per kWh)	14.0	20.0	14.0	12.0
Tariff B (cents per kWh)	13.5	26.0	13.5	11.0
Tariff C (cents per kWh)	13.0	32.0	13.0	10.0
Tariff D (cents per kWh)	12.5	38.0	12.5	9.0

The ToU tariffs are combined with specific DSM initiatives:

1) Monthly detailed energy bill (MO);

2) Bi-monthly detailed energy bill (BI);

3) In-home electricity monitor (IHEM);

4) Overall load reduction incentive (OLR).

The BAU group performed non-controlled energy usage and this was to be compared with the test group with smart interventions.

2.5.3 Summary of the DR programmes

Details of the DR programmes from Sections 2.5.2.1 to 2.5.2.5 are shown in Table 2.2:

Table 2.2: Summary of DR programmes.

Service	**STOR**	**Triad**	**Fast Reserve**	**FCDM**	**Irish smart grid**
Notice period	Within 20 minutes	Nature of forecast (day ahead or short	Within 2 minutes	2 seconds	Almost instant
Duration	At least 2 hours	1 hour	At least 15 minutes	at least 30 minutes	2 hours during the peak period (5-7 pm)
Minimum load	3 MW	1 MW	50 MW	3 MW	Arbitrary based on desired load
Time of occurence	Morning & evening peaks, within 6 availability windows	November-February (5-6pm)	Anytime when there are rapid changes in demand	Anytime when low frequency is detected	Anytime when the ToU tariff rate is high

Chapter 3

Methodology

The overall flow of the research methodology is illustrated in Fig. 3.1:

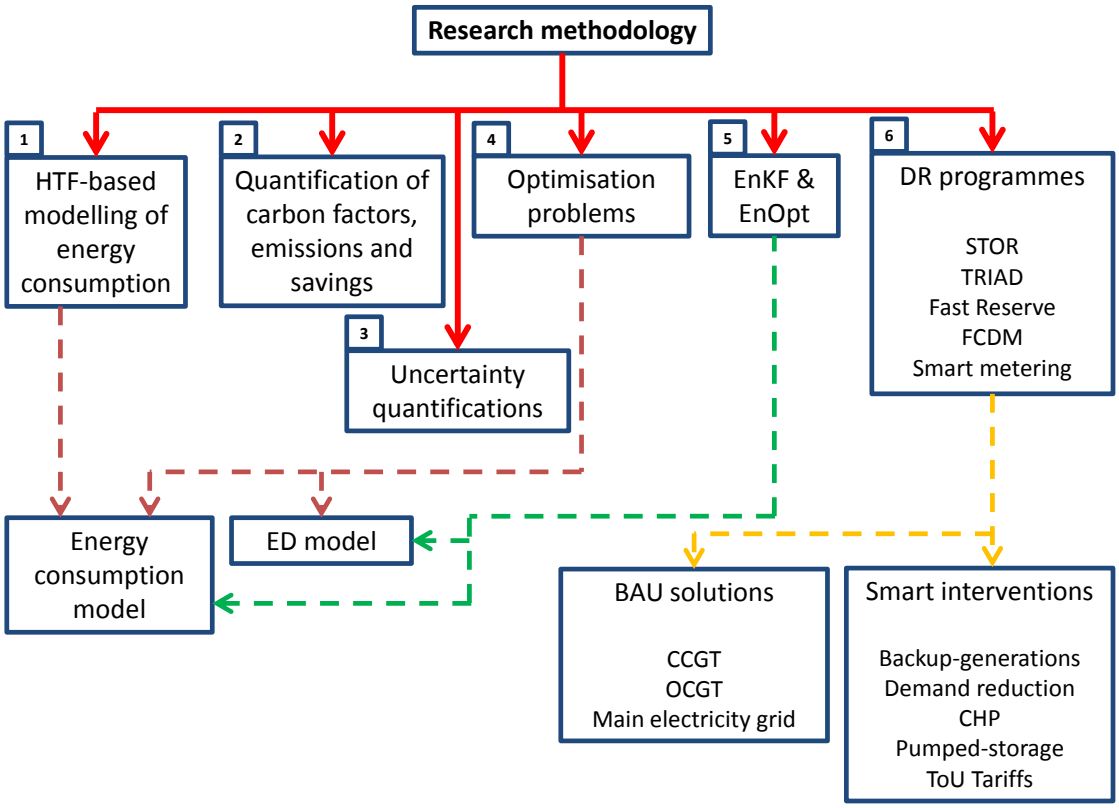

Figure 3.1: Research methodology.

The research methodology begins with a schematic diagram representing an electric system. The profile trend of the electricity consumption is developed stochastically using the asymmetric HTF-based function. The next step involves the methodology in quantifications and estimations of carbon factors, emissions and savings. Uncertainty quan-

tification formulas in this thesis are presented in the next action. Then, two optimisation problems based on the perspectives of energy consumption and the ED model are formulated. The EnKF and EnOpt algorithm are further adopted and applied in the optimisation problems. The final methodology includes the modelling of DR programmes with corresponding to different operational profiles of BAU solutions and smart interventions.

3.1 Electric system

A schematic representation of an electric system network that includes generation, transmission, distribution and consumption of electricity is shown in Fig. 3.2. In the first stage, the electricity is generated from various sources of power plant providers, either from green or non-green sources. In the next stage, the transmission lines transfer the generated electricity over a long distance with high voltages. In the distribution stage, using stepped-down transformers high voltages in transmission lines are reduced to lower voltages at substations. Finally, the stepped-down nominal voltages from substations are delivered to the end industrial and household consumers.

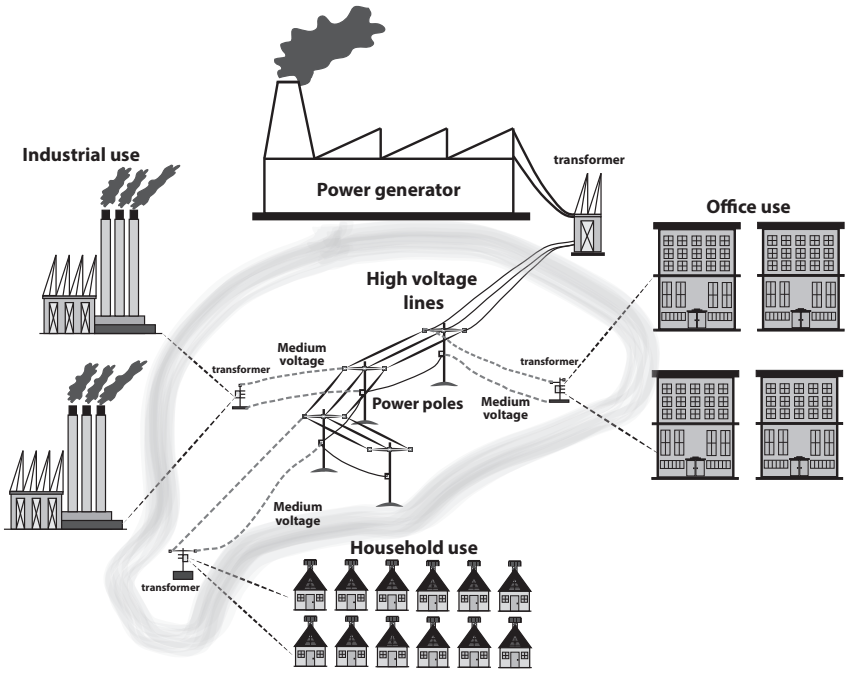

Figure 3.2: Schematic of the electric system.

3.2 Stochastic modelling of electricity consumption

The energy consumption/demand data from industrial and electrical consumers is recorded at longer time scale and sampled discretely, as the amount of power per time unit (Wh). According to the specification of smart meters, the metering data are recorded every 30 minutes – it has still being decided at which time interval these data will be stored by the energy providers in industrial databases.

As electricity consumption changes with time and has various influencing factors (in particular weather-related change of consumers' behaviour), the generated time series of the electricity data should have diurnal, $D(t)$, and annual, $A(t)$, periodicities. The state representation of the consumed electricity signal can be generally expressed in terms of the hypothetical periodical function as follows:

$$P_i(t) = A\left(\frac{t}{T_1}\right) + D_i\left(\frac{t}{T_2}\right) + \varepsilon_i, \tag{3.1}$$

where $P_i(t)$ is the true state of electrical consumption at time t, $A(t)$ is the annual cycle function, $D_i(t)$ is the diurnal cycle function, T_1 is the annual periodicity that is 365 days, T_2 is the diurnal periodicity that is 24 hours, t is the time variable sampled at hourly rate, ε_i is the signal noise, i represents a group of consumers at a particular substation.

In the electrical grid, the signal may combine the following sources of noises: (i) thermal noise; (ii) harmonic generation noise; (iii) transient noise; and (iv) frequency deviation. It is assumed that the stochastic component ε includes all of these noises combined.

Two main types of periodicities, $A(t)$ and $D_i(t)$, are adopted to describe trends of the energy consumption. Trend $A(t)$ is modelled and developed deterministically based on four seasons, when the level of the electricity consumption generally change because of heating, air conditioning, holiday periods, and other factors (Dordonnat et al., 2008; Young, 2013).

Using an asymmetric HTF-based function, the seasonal trend $A(t)$ can be represented as:

$$A(t) = C_1 + \sum_{k=1}^{K}\left(C_2\ \left(\tanh\frac{t-a_k}{L_A}\right)\right), \tag{3.2}$$

where t denotes the time index, $t = 1, 2, .., T_1$ with T_1 as the annual periodicity of 365 days,

C_1 is the scaling constant, C_2 is the adjustment constant of a particular HTF term, a_k is time parameter (hours), L_A represents the width and the slope of the HTF, k is the time index of the number of data subsets to be modelled by a single HTF function – those are later 'stitched' together by using appropriate parameters to obtain a smooth curve. K is the total time index of the number of data subsets.

$D_i(t)$ similarly models the trend of the electricity consumption during the period of every 24 hours. The $D_i(t)$ profiles are developed based on four main category of electricity consumers (connected to a certain substation): (i) working family; (ii) pensioner; (iii) daytime office; and (iv) one-day-shift industria.

The analytical expression of $D_i(t)$ is similar to $A(t)$ that uses asymmetric HTFs:

$$D_i(t) = C_{1,i} + \sum_{k=1}^{K} \left(C_{2,i} \left(\tanh \frac{t_b - b_k}{L_{D_i}} \right) \right),$$

$$t_b = \begin{cases} 0 & \text{if } t = p_b \\ t_b + 1 & \text{otherwise} \end{cases} \tag{3.3}$$

$$p_b = \begin{cases} p_b + T_2 & \text{if } t = p_b \end{cases}$$

t denotes the time index ($t = 1, 2, .., T_1$) for the entire periodicity to be simulated together with $A(t)$, t_b is the time index for the diurnal cycle at every $t_b = 1, 2, ..., T_2$, $T_2 = 24$ hours presents the diurnal periodicity from Eq. (3.1), $C_{1,i}$ is the scaling constant, b_k is the particular time interval (hours), L_{D_i} is the width of the HTF, k is the index of the number of data subset, K is the total time index of the number of data subsets, $C_{2,i}$ is the adjustment constant of a particular HTF term (if necessary; otherwise $C_{2,i} = 1$), i indexes the consumers. The p_b is the accumulator for the diurnal cycle trend of $D_i(t)$ with $p_b = 24, 48, 96, ..., 8760$ (in hourly scale).

The working algorithm of Eq. (3.3) is explained. Initially, p_b is set to 0 with $T_2 = 24$ in order to obtain the accumulated p_b for the first time step ($k = 1$) with $t_b = 1, 2, 3, ..., 24$ to form a complete diurnal cycle at $p_b = 24$. When $t_b = 24$, a complete diurnal profile of the energy consumption is formed. In the next time step ($k = 2$), t_b is reset to 0 with

$p_b = 48$ that is used to develop the next diurnal profile. The process is repeated until the end of the elapsed time.

Both $A(t)$ and $D_i(t)$ in Eqs. (3.2) and (3.3) form the dynamic model trends of the energy consumption, as defined in Eq. (3.1). Additionally, both units of $A(t)$ and $D_i(t)$ are not limited to single unit (hours) but can be in seconds, minutes or HH scale. For later simulation of $A(t)$ and $D_i(t)$, units are converted into HH scale equivalent to represent the energy consumption data recording that is compatible with smart meters. The profiled energy consumption data is further applied in the optimisation problem of the energy consumption.

3.3 Estimations of carbon factors, carbon emissions and savings

Carbon factors have units of kilograms of carbon dioxide equivalent (eqCO_2) per unit of energy (kWh). This unit describes the GHG involved as having the same global warming potential as the corresponding amount of CO_2. In the energy industry, the majority of GHG gases are produced by power stations operating on fossil fuels, and even green generators have carbon factors, which are derived using the LCA methodology (Convenant of Mayors, 2010). Carbon emissions ($\mathscr{E}$) are estimated with units kilogramCO_2 (kgCO_2), tonneCO_2 (tCO_2), kilotonneCO_2 (ktCO_2) or MegatonneCO_2 (MtCO_2),

$$\mathscr{E} = \sum_{s=1}^{S} \sum_{n=1}^{N} P_n(s) C_n(s) \Delta t(s), \tag{3.4}$$

where $C_n(s)$ are the carbon factors (kgCO_2/kW); $P_n(s)$ is the instantaneous power generated and delivered to consumers (kW) using the dynamical model (Eq. (3.1)) at time step s; $\Delta t(s)$ is the time step with HH step size at s = 1 (30 minutes), s = 2 (60 minutes), ..., , S; n is the sample number of the entities of power generated or consumed; N is the total number of samples.

Carbon emissions $\mathscr{E}$ from Eq. (3.4) resulting from energy generation and consumption are calculated as:

$$\mathscr{E} = \sum_{t=1}^{T} \sum_{n=1}^{N} E_n(t) C_n(t), \tag{3.5}$$

where $C_n(t)$ is the carbon factors (kgCO_2/kWh); $E_n(t)$ is either the amount of energy generation or the consumption (kWh) at time step t; t is the time step with HH step size at t = 1 (30 minutes), t = 2 (60 minutes), ..., T; n is the sample number of the entities of energy generated or consumed; N is the total number of samples.

The Eq. (3.5) quantifies general carbon emissions. It should be noted that the notation in Eq. (3.5) will be modified according to different scenarios applied. The detailed calculation of $\mathscr{E}$ based on different scenarios are explained in later sections.

Carbon savings S are determined as the difference between the business-as-usual (BAU) $\mathscr{E}_{\mathrm{BAU}}$ and the improved $\mathscr{E}_{\mathrm{I}}$ carbon emissions:

$$S = \mathscr{E}_{\mathrm{BAU}} - \mathscr{E}_{\mathrm{I}}. \tag{3.6}$$

Both $\mathscr{E}_{\mathrm{BAU}}$ and $\mathscr{E}_{\mathrm{I}}$ are obtained based on either real energy data or the model simulator. The $\mathscr{E}_{\mathrm{I}}$ is determined according to two scenarios: 1) The optimised costs and carbon emissions in the smart grid; 2) Carbon savings in smart interventions in DR programmes. However, because in some cases the carbon emissions from the improved solutions exceed emissions compared to the BAU solution, obtained carbon savings values may be negative, which indicate that actual savings are not achieved; such interventions introduce additional emissions.

The optimisation of costs and carbon savings is achieved by implementing algorithms that seek to minimise both the costs and carbon emissions throughout the assimilation of the recorded energy data. Therefore, it is crucial for the implementation of the proposed methodology to obtain high resolution data from broad groups of electricity consumers (working family, pensioner, daytime office, and one-day-shift industrial) apart from energy generation data.

On the other hand, smart interventions are employed under various DR programmes for ensuring that energy generation and demand in the power grid are well-balanced. Smart interventions are the improved solutions based on modified BAU method, or the completely new infrastructures that promote carbon savings. Therefore, smart interventions in DR programmes are employed in order to maintain the security of supply in power grids. DR programmes may create revenue and rewarding opportunities for participating companies and consumers However, there is lack of assessment of the environmental im-

pact due to the DR interventions.

The Eq. (3.6) demonstrates the general approach in quantifying S. Different notations for the subscript in $\mathscr{E}_I$ are used later in this paper due to improved emissions from various sources of interventions. The detailed methodology of quantifying S based on different scenarios and case studies are explained in later sections and chapters.

3.3.1 Estimation of electricity grid carbon factor

Consumers and retailers who draw electricity from the grid indirectly produce carbon emissions. The electricity grid carbon factor in this paper is estimated based on the fuel mix (green and non-green sources) during the energy generation. Consumers in the same area that use energy from the same grid segment (regardless of type) will contribute carbon emissions depending on the amount of energy used.

To derive dynamically varying electricity grid carbon factor, carbon factors of main electricity generators are used with known uncertainties. Monte Carlo method is applied with uniformly distributed data drawn from uncertainty intervals corresponding to the fuels (coal, oil, nuclear, wind, hydro and gas), as described in POSTnote 268 (2006); POSTnote 383 (2011) to quantify the uncertainties for the electricity grid carbon factor. The uniform distribution ensures the equal probability of sample data being selected.

The UK real-time and historical energy generation and demand data are provided by Balancing Mechanism Reporting System (BMRS) that is used by the National Grid (BMRS, 2015). BMRS reports the power flows of the electric transmission system in the UK and also provides aggregated fuel mix data from different power stations. The fuel generation data from BMRS and the Elexon portal are used to estimate the resultant electricity grid carbon factor generated by clusters of green and non-green types of power stations. The dynamical formula of the electricity grid carbon factor from Lau et al. (2014) is as follows:

$$G(t) = \frac{\sum_{m=1}^{N_m} \left(F_m \cdot E_m^g(t)\right)}{\sum_{m=1}^{N_m} E_m^g(t)}, \tag{3.7}$$

where $E_m^g(t)$ denotes the energy generation data; F_m denotes the carbon factors for fuels m; m denotes the fuel types; N_m is the total number of fuels used in energy generation.

In the estimation of $G(t)$ in Eq. (3.7), the effect of transmission and distribution (TD) losses are excluded. The values of corresponding F_m are listed in Table 3.1.

Table 3.1: Carbon factors ($kgCO_2/kWh$) for different fuel types. Adapted from Carbon Trust (2013); DEFRA (2015); Hill et al. (2014, 2013); POSTnote 268 (2006); POSTnote 383 (2011).

Types of Fuel	Fuel Code	Carbon factors ($kgCO_2/kWh$)
Coal	COAL	0.788-0.899
Nuclear	NUCLEAR	0.020-0.026
Oil	OIL	0.600-0.699
Wind	WIND	0.020-0.094
Hydro	NPSHYD	0.002-0.013
Combined Cycle Gas Turbine	CCGT	0.367-0.487
Open Cycle Gas Turbine	OCGT	0.466-0.586

3.4 Uncertainty quantifications

According to the 'Guide to the expression of uncertainty in measurement (GUM)' methodology (JCGM_100:2008, 2008), when the standard uncertainty (denoted as σ with corresponding index) of the measurement is obtained from the values of other quantities, they are combined into standard uncertainty σ_c, which is calculated as the square root of the sum of variances corresponding to different measurements assuring the input quantities are independent. The documentation by JCGM_100:2008 (2008) further states that the combined uncertainty and its components are expressed in the format of standard deviations.

Thus, the combined standard uncertainty σ_c is obtained as

$$\sigma_c = \sqrt{\sum_{i=1}^{N_i} \sigma_i^2}, \tag{3.8}$$

where σ_i can be referred as the standard error of carbon emissions, savings, costs, fuel mix factor from a particular event.

The estimated value (x_c) will be expressed with the combination of uncertainties ($x_c \pm k\sigma_c$). The k denotes the coverage factor and the determination of k is based on the level of confidence interval required (JCGM_100:2008, 2008). In this work, it is assumed that $k = 2$ that allows the 95 % confidence level of interval.

Particular simulations may require percentage increase along with the percentage uncertainty based on the two distinct BAU and improved solution. For better explanation, the percentage increase is further denoted as percentage improvement. The percentage improvement is calculated as the difference (reduction) between the two values (BAU and improved solution) divided by the BAU value in terms of percentage. Alternatively, if tabulated values are negative, the percentage decrease is obtained. In other words, the BAU solution provides better operating strategies than the improved solution.

The percentage uncertainty along the percentage improvement is calculated as:

$$\text{Percentage Uncertainty} = \frac{\text{Absolute Uncertainty}}{\text{Measured Value}} \times 100 \tag{3.9}$$

3.5 Optimisation problems in smart grids

This section formulates optimisation problem later used in the EnOpt algorithm. The section is divided into two parts, where the first problem involves optimisations of carbon emissions and savings in the perspective of consumers. The second problem is based on the optimisation of costs based on the ED problem subject to security-of-supply constraints, the integration of emissions and the renewable energy.

3.5.1 The optimisation problem in energy consumption

From Eq. (3.5), the BAU carbon emissions $\mathscr{E}_{\text{BAU}}$ are calculated as:

$$\mathscr{E}_{\text{BAU}} = \sum_{i=1}^{N_i} \sum_{t=1}^{N_t} E_i^c(t) G(t), \tag{3.10}$$

where E_i^c denotes energy consumption, $G(t)$ is the variable electricity grid carbon factor (Eq. (3.7)), t is the time index, i indexes the consumers, N_t is the total number of time steps, N_i is the total number of consumers.

Similarity, the optimised carbon emissions $\mathscr{E}_{\text{O}}$ along with optimised control constraints based on EnOpt algorithm is calculated as:

$$\mathscr{E}_{\text{O}} = \sum_{i=1}^{N_i} \sum_{t=1}^{N_t} E_i^c(\mathbf{x}, t) G(t), \tag{3.11}$$

where **x** denotes the vector of control variables to be optimised. The explanation of **x** is postponed to Section 3.7.1.

The profile of E_i^c used is based on the earlier developed HTF-based modelling of energy consumption from Eq. (3.1). It is further assumed that consumers in the same area that use energy from the same grid segment (regardless of type) will contribute carbon emissions depending on the amount of energy used. In this case, the variable electricity grid carbon factor $G(t)$ applies to all types of consumers in this work. From Eqs. (3.10) and (3.11), carbon savings S are calculated as:

$$S = \mathscr{E}_{\mathrm{BAU}} - \mathscr{E}_{\mathrm{O}}, \tag{3.12}$$

where the subscript O defines the optimised emissions.

3.5.1.1 Constraints

The optimisation constraints include maximum and minimum allowable energy consumption for all consumers. The constraints can be determined using the input data that is derived from the previously modelled HTF-based energy profiles.

The second constraint limits the sum of energy consumption for all consumers to be equal or smaller than the aggregated sum of energy demand for all consumers. As the energy demand is highly proportional to the amount of energy generation, the aggregated summation of energy consumption for all consumers should correspond to the energy generation. For simplicity, amount of energy generation is typically not a constraint for the optimisation in this problem, but rather the amount of energy generation is used as the representation for proportional parts of fuel-mix energy generation. It is assumed that the amount of green power generation is above 10 % of non-green power generation.

In general form, the constraints are formulated as follows:

$$\begin{aligned} E_i^{\min} &\leq E_i^c \leq E_i^{\max}, \\ \mathbf{E}^c &\geq \sum_{i=1}^{N_i} E_i^c. \end{aligned} \tag{3.13}$$

The $E_i^{\min}$ is the minimum allowable energy consumption, $E_i^{\max}$ is the maximum allowable energy consumption corresponds to ith consumer, $\mathbf{E}^c$ reflects the aggregated sum of

energy demand for all consumers.

As described, the resultant energy generation is a sum of aggregated energy demand among consumers (with additional safe energy usage), the proportion of green and non-green energy generation can be determined using the following formula:

$$\begin{aligned} E_m^{g\prime} &\approx \mathbf{E}^c, \\ E_m^g &= U_{\text{safe}} E_m^{g\prime}, \\ E_m^{\text{green}} &\approx U_{\text{percent}} E_m^g, \\ E_m^{\text{non-green}} &\approx E_m^g (1 - U_{\text{percent}}), \end{aligned} \tag{3.14}$$

where $E_m^{g\prime}$ is the energy generation (kWh) which is proportional to the energy demand $\mathbf{E}^c$, E_m^g denotes the energy (kWh) generated with fuel m, E_m^{green} is the amount of green energy generated(kWh), $E_m^{\text{non-green}}$ is the non-green energy generated (kWh), U_{safe} is the proportional amount of safe energy usage, U_{percent} is the proportional balance of green and non-green energy generation.

3.5.1.2 Objective function

Eq. (3.11) is the primary objective function for the EnOpt simulation. Upon the end of EnOpt simulation, the values of $\mathscr{E}_O$ represent the expectation of optimised carbon emissions $\mathscr{E}_O$ in Eqs. (3.11) and (3.12).

3.5.1.3 Consumers and generators

The earlier Eq. (3.1) is used as the model simulator to forecast the input energy data that can be represented as the energy consumption (E_i^c) for groups of consumers. The E_i^c is assigned into Eqs. (3.10) and (3.11) in tabulating the respective $\mathscr{E}_{\text{BAU}}$ and $\mathscr{E}_{\text{O}}$.

The profile of the energy generation E_m^g in this problem is determined based on the aggregated sum of energy demand of consumers ($\mathbf{E}^c$). It is widely known that green generation is intermittent. With assistance of non-green generator that balances the output of the green generation, this results in much alike trend of resultant energy generation with the aggregated energy demand profile. Therefore, such implementation would require some kind of storage with green generators, otherwise the non-green generator would have to fluctuate in accordance with intermittency of the green generator, which is not

feasible.

3.5.1.4 Mathematical formulation of optimisation problem

The optimisation model is summarised as:

$$\begin{aligned} \underset{x}{\text{minimise}} \quad & \mathscr{E}_{\mathrm{O}} = \sum_{i=1}^{N_i} \sum_{t=1}^{N_t} E_i^c(\mathbf{x},t) \cdot G(t) \\ \text{subject to} \quad & E_i^{\min} \leq E_i^c \leq E_i^{\max} \\ & \mathbf{E}^c \geq \sum_{i=1}^{N_i} E_i^c \\ & E_i^c \geq 0, \forall i \text{ and } t \in N, \end{aligned} \tag{3.15}$$

where N denotes the integers.

3.5.2 The ED optimisation problem

The optimisation problem of costs and carbon emissions based on the ED problem of generating units is considered. This is due to the present environmental policies that require reduction of polluting generation and also balance of the power output of the renewable energy due to its intermittency. Henceforth, this has changed the overall regulation of the BAU power generation system. An operator also intends to balance the trade-offs between costs and emissions of thermal generating units. Such optimisation is important in order to prevent minimisation of costs without emissions concerns, and vice versa. Before formulating the objective function, it is necessary to know the principles of the fuel cost and the emission function.

3.5.2.1 Fuel cost function

According to Zhu (2009), examples of thermal generating units are steam turbines, boilers and diesel generators. Additionally, a gas turbine is also categorised as one of the thermal units due to the combustion processes.

The fuel cost function is commonly described as a quadratic form of the active energy output (Huang et al., 2012; Rajasomashekar and Aravindhababu, 2012; Ramanathan,

1994; Senthil and Manikandan, 2010; Subramanian and Ganesan, 2010).

$$\mathscr{C}_i(E_{i,t}) = a_i + b_i E_{i,t} + c_i E_{i,t}^2, \tag{3.16}$$

where a, b and c are the cost coefficients of the generating unit i, $E_{i,t}$ is the amount of energy generation from the ith generator at time t. The unit of the fuel cost function C is £/HH.

3.5.2.2 Emission function

The emission function of the ED model is also commonly described in the quadratic form (Huang et al., 2012; Rajasomashekar and Aravindhababu, 2012; Ramanathan, 1994; Senthil and Manikandan, 2010; Subramanian and Ganesan, 2010), which is similar to Eq. (3.16)

$$\mathscr{E}_i(E_{i,t}) = d_i + e_i E_{i,t} + f_i E_{i,t}^2, \tag{3.17}$$

where d, e and f are the emissions coefficients of the generating unit i, E is the amount of generation from the ith generator at time t. The unit of the emission function $\mathscr{E}$ is $ktCO_2$/HH.

3.5.2.3 Renewable function

The wind energy is used in this work as the renewable energy that integrates with the ED model. As suggested by Geetha et al. (2015); Hetzer et al. (2008), the linear cost of generating the wind energy model is as follows:

$$\mathscr{C}_{\mathrm{W},i}(W_{i,t}) = d_i^{\mathrm{W}} W_{i,t}, \tag{3.18}$$

where d_i^{W} is the coefficient of wind generation at ith wind generator at time t, $W_{i,t}$ is the active energy generation of ith wind generator at time t.

As well known, the wind energy output is always subject to high intermittency. According to ElDesouky (2013); Geetha et al. (2015); Hetzer et al. (2008), the distribution of the wind speed converted from the rotation of the wind to the energy output follows closely the Weibull distribution. This generally provides a handy guideline for the ED modelling, as in actual field the wind distribution is largely uncertain due to varieties of

geographic and climate locations. The Eq. (3.18) is now subject to the nonlinearity of the wind power output and is re-formulated as

$$\mathscr{C}_{\mathrm{W},i}(W_{i,t}) = d_i^{\mathrm{W}} f^{\mathrm{W}}(W_{i,t}) W_{i,t}. \tag{3.19}$$

The cost of wind generation is now with the additional Weibull probability distribution function (PDF) term of the of wind power $f^{\mathrm{W}}(W_{i,t})$. Derivation of the $f^{\mathrm{W}}(W_{i,t})$ is described by ElDesouky (2013); Hetzer et al. (2008). Since the documentation by DECC (2013) provided the levelised electricity generation cost ranges for wind generation, the direct cost coefficient data d_i^{W} can be generated. Using the Monte-Carlo method, random sampling of d_i^{W} based on the data provided by DECC (2013) is implemented in order to compute the standard mean of d_i^{W}. Additionally, the d_i^{W} are obtained dynamically in different periods (on- and off-peak periods). d_i^{W} is profiled based on the bid-offer spread of the electricity market imbalance volume. Therefore, the detailed formulation of $f^{\mathrm{W}}(W_{i,t})$ is not necessary in this work. This results in simplified sampling of wind energy by using Eq. (3.18) as the main wind cost function instead of using Eq. (3.19). The cost function of the wind generation from Eq. (3.18) is therefore reformulated as:

$$\mathscr{C}_{\mathrm{W},i}(W_{i,t}) = d_{i,t}^{\mathrm{W}} W_{i,t}. \tag{3.20}$$

3.5.2.4 Objective function

The Eq. (3.11) is the primary objective function for optimisation of carbon emissions. However, as the main interest is to optimise the costs, the objective function is not directly expressed in terms of carbon emissions, but rather will be expressed as the cost equivalent objective function.

The multiple objective functions from Eqs. (3.16), (3.17) and (3.20) are converted into a single objective function, incorporating the maximum price penalty factor $h_{\max}$ in the emission function following Geetha et al. (2015); Khan et al. (2015); Senthil and Manikandan (2010); Subramanian and Ganesan (2010). The weighted sum strategy is not applied in this case due to the nature of complexity in tabulating the weight values. By following Khan et al. (2015); Senthil and Manikandan (2010); Subramanian and Ganesan

(2010), the objective function of the ED problem becomes:

$$\begin{aligned}\mathscr{C} = &\sum_{i=1}^{NG}\sum_{t=1}^{N_t}\left(a_i + b_i E_{i,t} + c_i E_{i,t}^2\right) + h_{\max,i}\sum_{i=1}^{NE}\sum_{t=1}^{N_t}\left(d_i + e_i E_{i,t} + f_i E_{i,t}^2\right) \\ &+ \sum_{i=1}^{NW}\sum_{t=1}^{N_t} d_{i,t}^{\mathrm{W}} W_{i,t},\end{aligned} \tag{3.21}$$

where the first term refers to fuel costs (Eq. (3.16)), the second term is the emission function (Eq. (3.17)), the final term is the wind function (Eq. (3.20)). The NG is the total number of thermal units, NE is the total number of generating units that contribute carbon emissions, NW is the total number of wind generators.

The Eq. (3.21) presents the total fuel, emissions and wind costs of production to deliver the amount of E and W at time t and ith generator. The Eq. (3.21) can be simplified as:

$$\mathscr{C} = \sum_{i=1}^{NG}\sum_{t=1}^{N_t}\mathscr{C}_i(E_{i,t}) + h_{\max,i}\sum_{i=1}^{NE}\sum_{t=1}^{N_t}\mathscr{E}(E_{i,t}) + \sum_{i=1}^{NW}\sum_{t=1}^{N_t}\mathscr{C}_{\mathrm{W},i}(W_{i,t}), \tag{3.22}$$

The maximum price penalty factor $h_{\max,i}$ is calculated as the ratio of the maximum of the fuel cost to the maximum emissions at the energy output:

$$h_{\max,i} = \frac{\mathscr{C}_{\max,i}}{\mathscr{E}_{\max,i}}. \tag{3.23}$$

Similar to the wind function, using to the publicly available fuel and emission cost data from DECC (2013), cost coefficients $a - f$ in Eq. (3.21) are not computed and can be omitted. The available data from DECC (2013) allows one to estimate the direct profile trends of fuel and emission costs. This eliminates the need to compute the cost coefficients corresponding to individual generators. Eq. (3.22) is further simplified taking into account the BAU costs as follows:

$$\mathscr{C}_{\mathrm{BAU}} = \sum_{i=1}^{NG}\sum_{t=1}^{N_t} d_{i,t}^{\mathrm{G}} E_{i,t} + h_{\max,i}\sum_{i=1}^{NE}\sum_{t=1}^{N_t} d_{i,t}^{\mathscr{E}} E_{i,t} + \sum_{i=1}^{NW}\sum_{t=1}^{N_t} d_{i,t}^{\mathrm{W}} W_{i,t}, \tag{3.24}$$

where $d_{i,t}^{\mathrm{G}}$ and $d_{i,t}^{\mathscr{E}}$ are the coefficients of fuel and emission costs corresponding to ith generating units at time t.

Similarly, the optimised cost of generation based on the integration of control vector $\mathbf{x}$

corresponding to ith generating units for the EnOpt algorithm is calculated as:

$$\mathscr{C}_{\mathrm{O}} = \sum_{i=1}^{NG}\sum_{t=1}^{N_t} d_{\mathrm{G}i,t}E_{i,\mathbf{x},t} + h_{\max,i}\sum_{i=1}^{NE}\sum_{t=1}^{N_t} d_{i,t}^{\mathscr{E}}E_{i,\mathbf{x},t} + \sum_{i=1}^{NW}\sum_{t=1}^{N_t} d_{i,t}^{\mathrm{W}}W_{i,t}. \tag{3.25}$$

As mentioned, DECC (2013) provides documentation with levelised electricity generation cost ranges where the direct cost coefficient data ($d_{i,t}^{\mathrm{G}}, d_{i,t}^{\mathscr{E}}$ and $d_{i,t}^{\mathrm{W}}$) can be obtained. Using the Monte-Carlo simulations, random sampling of cost coefficients based on the data provided by DECC (2013) is implemented in order to compute the standard mean of cost coefficients. The bid-offer price data is available in the portal maintained by Elexon (2015). Documentation (Elexon, 2014; Investopedia Staff, 2014) provides detailed explanation of bid and offer price, and also determination of net market imbalance volume and price. A bid price is the price that a party pays for decrease in generation or increase in demand (in MWh) and an offer price is the price that a party is paid for increase in generation or decrease in demand (in MWh) (Elexon, 2014). Spreads are determined by liquidity, as well as supply and demand for a specific security. The bid-offer price spread is generally a measure of liquidity (trading activities). According to Investopedia Staff (2014), the high liquidity (high bid price) will have very low spreads due to no major imbalance between supply and demand. On the other hand, if there is a significant imbalance and low liquidity, the bid-ask spread will significantly expand.

The bid-offer price spread ratio is calculated as:

$$\mathrm{bid\_offer}_{i,t} = \frac{\mathrm{offer\_price}_{i,t} - \mathrm{bid\_price}_{i,t}}{\mathrm{offer\_price}_{i,t}}, \tag{3.26}$$

where i refers to the thermal units and wind generators at time t.

Using Eq. (3.26), the updated cost coefficient for the ED problem can be calculated as:

$$\begin{aligned} d_{i,t}^{\mathrm{G}} &= d_{i,t}^{\mathrm{G}\prime}(1+\mathrm{bid\_offer}_{i,t}),\\ d_{i,t}^{\mathscr{E}} &= d_{i,t}^{\mathscr{E}\prime}(1+\mathrm{bid\_offer}_{i,t}),\\ d_{i,t}^{\mathrm{W}} &= d_{i,t}^{\mathrm{W}\prime}(1+\mathrm{bid\_offer}_{i,t}), \end{aligned} \tag{3.27}$$

where $d_{i,t}^{\mathrm{G}\prime}, d_{i,t}^{\mathscr{E}\prime}$ and $d_{i,t}^{\mathrm{W}\prime}$ are standard means of prior cost coefficients resulting from the Monte-Carlo simulation of the levelised electricity generation costs from the data (DECC, 2013).

Based on Eq. (3.25), as wind generation is uncertain, other conventional generators (thermal units and hydro) are used primarily to balance the wind output. The integration of conventional generators with the wind energy ensures sufficient amount of energy output that satisfies energy demand. The wind energy is generally assumed to be uncontrollable in adjusting the required load factor. Hence, there is no associated control vector in the wind function. In the context of EnKF, the wind energy can be used for short-term forecast, which is possible by using HH wind generation data from the portal (BMRS, 2015; Elexon, 2015). On the other hand, the wind energy in EnOpt will be simulated as BAU solution, and other generators will be used to balance the wind output.

The total costs savings due to the EnOpt simulation are calculated as:

$$\mathscr{C}_{\mathrm{S}} = \mathscr{C}_{\mathrm{BAU}} - \mathscr{C}_{\mathrm{O}}. \tag{3.28}$$

Similarly, the Eq. (3.12) can be used to determine the amount of carbon savings by using the second term of the cost function in Eqs. (3.24) and (3.25).

3.5.2.5 Constraints

The optimisation is subject to the generation capacity constraints, energy balance constraints, and the actual wind energy generation limits:

$$\begin{aligned} & E_{\min,i} \leq E_{i,\mathrm{x}} \leq E_{\max,i}, \\ & \sum_{i=1}^{NG} E_{i,\mathrm{x}} + \sum_{i=1}^{NW} (W_i) - E_{\mathrm{L}} - E_{\mathrm{D}} = 0, \\ & 0 \leq W_i \leq W_{\max,i}, \end{aligned} \tag{3.29}$$

where E_{L} refers to energy losses during the TD process, E_{D} is the total energy demand, NG is the total number of thermal units, NW is the total number of wind generator.

According to BMRS (2015), as it is the normal routine to have breakdowns during energy generation by fuel type, any fuel type with negative values in the dataset is capped to zero of total positive generation in order to meet the energy demand. Additionally, as there is no minimum operating energy limit for wind generation, the minimum amount of wind generation is set as zero (Geetha et al., 2015). According to Ramanathan (1994), the emissions constraint is not needed to be computed as the optimality condition can be

achieved by imposing the constraint of the energy balance and generator limits.

3.5.2.6 Mathematical formulation of the ED problem

The optimisation for the ED model is summarised as:

$$\begin{aligned}
\underset{\mathbf{x}}{\text{minimise}} \quad & \mathscr{C}_{\mathrm{O}} = \sum_{i=1}^{NG}\sum_{t=1}^{N_t} d_{i,t}^{\mathrm{G}} E_{i,\mathbf{x},t} + h_{\max,i}\sum_{i=1}^{NE}\sum_{t=1}^{N_t} d_{i,t}^{\mathscr{E}} E_{i,\mathbf{x},t} + \sum_{i=1}^{NW}\sum_{t=1}^{N_t} d_{i,t}^{\mathrm{W}} W_{i,t}, \\
\text{subject to} \quad & E_{\min,i} \leq E_{i,\mathbf{x}} \leq E_{\max,i} \\
& \sum_{i=1}^{NG} E_{i,\mathbf{x}} + \sum_{i=1}^{NW} (W_i) - E_{\mathrm{L}} - E_{\mathrm{D}} = 0 \\
& 0 \leq W_i \leq W_{\max,i}, \forall i \text{ and } t \in N,
\end{aligned} \tag{3.30}$$

where N is integer.

3.6 EnKF method

As described by Nævdal et al. (2003), EnKF provides short-term forecast and uses realisations of a model state and state updates that is acquired through the combination of 'true' model and predicted ensemble estimates. Through EnKF, the model state is forecast and assimilated based on the ensemble propagated with the Kalman update.

EnKF is widely used in high dimensional systems in coping with the limitation of the standard KF and EKF as the covariance matrix in EnKF is forecast and analysed by using statistics of an ensemble (Jensen, 2007). In this research EnKF formulations by Almendral-Vazquez and Syversveen (2006); Evensen (2003); Gillijins et al. (2006); Jensen (2007) are followed, with key equations and parameters outlined. The formulation of EnKF provides the foundation for the energy data forecast and assimilation in Section 3.6.2.

3.6.1 EnKF general formulation

As described in Section 2.3.1, EnKF consists the two important steps, forecast and analysis. In the forecast step, as the 'true' state is not always available, new ensemble is created based on the realisations in each of the model state through the model dynamics

(simulator).

$$y_j^p = y^p + w_j, \tag{3.31}$$

where j indexes the ensemble member, y^p is the state vector of the model simulator, y_j^p is the resultant new formation of a set of ensemble through the prediction of the model state y^p at ensemble member j, w_j is the model process noise. The superscript p denotes the *priori* state vector. As in line with Almendral-Vazquez and Syversveen (2006), the initial ensemble members of y^p are sampled from a normal distribution with the zero mean and standard deviation.

The spread of the ensemble members are further represented into a matrix Y^P to denote the collection of the *priori* ensemble:

$$Y^p = \left[y_1^p,\ y_2^p,\ ...,\ y_j^p,\ ...,\ y_{N_e}^p \right], \tag{3.32}$$

where N_e is the total number of ensemble member.

The *priori* error covariance C_p based on Y^p is computed as follows:

$$C_p = \frac{A_{\text{prior}} {A_{\text{prior}}}^T}{N_e - 1}, \tag{3.33}$$

where

$$A_{\text{prior}} = Y^p - \overline{Y^p} = Y^p (I - \mathbf{1}_{N_e}). \tag{3.34}$$

The $\mathbf{1}_N$ is the matrix where each element is equal to $1/N_e$, the N_e is the total number of ensemble. The $\overline{Y^p}$ indicates the ensemble mean and is calculated as:

$$\overline{Y^p} = \frac{1}{N_e} \sum_{j=1}^{N_e} y_j^p. \tag{3.35}$$

As in line with Evensen (2003); Gillijins et al. (2006) the forecast ensemble mean will be characterised as the best forecast estimation of the state. The distribution of the ensemble member around the mean is the error between the best estimation and the 'true' state.

On the other hand, during the analysis step, new observations from the measurement sets are represented by another ensemble. In order to obtain consistent error propagation using the EnKF, the observations have to be considered as random variables (Nævdal

et al., 2003). This is accomplished by using the actual measurement (or whenever measurements are available) as the reference and the random measurement noise added to the measurement to obtain the perturbed observations (Evensen, 2003; Jensen, 2007; Nævdal et al., 2003). In general, the d in the EnKF that serves as the reference measurement of the model prediction is perturbed using ensemble representations, this later forms another set of ensemble of perturbed observations denoted by $d_{\text{obs},j}$. Therefore, given a model prediction set d, the perturbed observations for each member of the ensemble $d_{\text{obs},j}$ are generated randomly as:

$$d_{\text{obs},j} = d + v_j, \tag{3.36}$$

where v_j is the measurement noise at jth ensemble member.

Additionally, d is used to reflect the actual measurements resulting from the model prediction. Values of $d_{\text{obs},j}$ are collected into matrix D_{obs} that denotes the realisations of perturbed observations based on model predictions d:

$$D_{\text{obs}} = \left[d_{\text{obs},1},\ d_{\text{obs},2},\ \ldots,\ d_{\text{obs},j},\ \ldots,\ d_{\text{obs},N_e} \right], \tag{3.37}$$

where N_e is the total number of ensemble member.

Both Y^p in Eq. (3.32) and D_{obs} in Eq. (3.37) are perturbed with model error: the process noise w with zero mean and covariance Q for Y^p and similarly, the measurement noise v with zero mean and covariance R for D_{obs}, i.e. values w and v are assumed to be drawn from Gaussian distributions as $w \sim N(0,Q)$ and $v \sim N(0,R)$. The measurement error is very important in the EnKF, because without it the system may be over-specified and no solutions resulting from EnKF propagations obtained (Jensen, 2007). On the other hand, the addition of model error is used to describe the model uncertainty in the EnKF and the adjustment of the model noises are varied depending on the degree of nonlinearities in a problem (Jensen, 2007).

With the computed Y^P and D_{obs}, each of the ensemble members in Y^P is assimilated and updated using the EnKF updating formula to reflect the simulated observations. The Kalman gain K is computed and the updated ensemble estimates Y^u (*posteriori*) based on Y^p are obtained as follows:

$$Y^u = Y^p + K(D_{\text{obs}} - HY^p), \tag{3.38}$$

where H is the measurement operator relating the predicted state to D_{obs} allowing for measurement errors v_j (Evensen, 2003) and only consists of 0's and 1's as its components (Jahangiri, 2012; Nwaozo, 2006). The D_{obs} also corresponds to HY^p. The formula for calculating K is provided as follows:

$$K = \frac{C_p H^T}{HC_p H^T + R}. \tag{3.39}$$

In general, K serves as the weighing matrix to update all ensemble members. The R is the measurement covariance error. Since R is a covariance matrix and is always positive definite, the update can be implemented using Cholesky decomposition. The product $C_p H^T$ is the cross-covariance between state variables and predicted observations, $HC_p H^T$ is the auto-covariance of the predicted observations.

Finally, the *posteriori* covariance update C^u is computed in the following way:

$$C_u = \frac{A_{\text{post}} {A_{\text{post}}}^T}{N_e - 1}, \tag{3.40}$$

where

$$A_{\text{post}} = Y^u - \overline{Y^u} = Y^u(I - \mathbf{1}_{N_e}), \tag{3.41}$$

and Y^u is the *posteriori* ensemble. The $\overline{Y^u}$ indicates the ensemble mean and is calculated as:

$$\overline{Y^u} = \frac{1}{N_e} \sum_{j=1}^{N_e} y_j^u. \tag{3.42}$$

The model states and parameters are updated at the analysis step, not at the forecast step. During the assimilation process, all the members in the ensemble Y^p and D_{obs} are assimilated using the EnKF updating formula from Eq. (3.38), taking the mean of the perturbed observations as the actual observation. Each of the Y^p ensemble member is updated to obtain Y^u. The process is repeated in computing the convergence of EnKF propagations of Y^u and the actual observations. The difference between the Y^u and the actual observation is the EnKF propagation error. A summary of the EnKF algorithm following Jensen (2007) is presented in Table 3.2.

Table 3.2: EnKF algorithm.

Forecast step:	
$w,\ v$	compute input noises
$y_j^p = y^p + w_j$	create initial ensemble
$Y_p = \left[y_1^p,\ ...,\ y_j^p,\ ...,\ y_{N_e}^p\right]$	collect ensembles into Y_p
$C_p = \frac{A_{\text{prior}} {A_{\text{prior}}}^T}{N_e - 1}$	compute *priori* covariance ensemble
Analysis step:	
$d_{\text{obs},j} = d + v_j$	compute measurement state
$D_{\text{obs}} = \left[d_{\text{obs},1},\ ...,\ d_{\text{obs},j},\ ...,\ d_{\text{obs},N_e}\right]$	collect ensembles into D_{obs}
$K = C_p H^T \left(H C_p H^T + R\right)^{-1}$	compute Kalman gain
$Y^u = Y^p + K\left(D_{\text{obs}} - H Y^p\right)$	compute *posteriori* state ensemble
$C_u = \frac{A_{\text{post}} {A_{\text{post}}}^T}{N_e - 1}$	compute *posteriori* covariance ensemble

3.6.2 Application of EnKF

This section shows the EnKF application using the formulated EnKF algorithm in Section 3.6.1 in short-term forecast and updating of energy data based on two optimisation problems of: 1) energy consumption using the dynamical model developed in Section 3.5.1: 2) cost based on the ED problems subject to network security constraints, the integration of emissions and the wind energy from Section 3.5.2.

In EnKF, the main aim is to estimate the *posteriori* ensemble based on realisations of available energy data (consumption and generation). Before proceeding to EnKF the initialisation is needed by providing the model and input parameters for computation of *priori* ensemble.

3.6.2.1 EnKF application to energy consumption

As the 'true' state of energy consumption is not always available, new ensemble is created using Eq. (3.31). It is based on realisation in each of the model state through the model dynamics Eq. (3.1). The step involving the realisation of model states is explained below.

In the application of energy consumption, the variable of interest includes consumers' energy consumption patterns and profiles, as well as measurements, based on prior knowledge and records are normally added to the components of state vector y^p. Instead of adding complex components to y^p, for simplicity the component of y^p is augmented with

HTF-based model of forecast (predicted) energy consumption:

$$y^p = \begin{bmatrix} m \\ d \end{bmatrix}. \tag{3.43}$$

In the simulation experiment, m is the model parameters of $P_i(t)$ from the dynamical model Eq. (3.1). $P_i(t)$ is converted into energy consumption equivalent (E_i^c). It is the resultant periodicities ($A(t)$ and $D_i(t)$) that allows the model prediction (d) of energy consumption data. Generally, Eq. (3.43) forms and predicts the energy demand profile. For simplicity, the parameters of HTF-periodic component for m remain constant throughout the data simulation except the model process noise. This results in similar energy usage pattern from groups of consumers but with varied energy usages. The d is the model prediction of the energy consumption and is denoted as the actual measurement relating to the m parameter. The component d in vector y^p changes with the simulation at every time step. Parameters m and d are perturbed with model errors as mentioned in Section 3.6.1 in order to generate new sets of ensemble members.

The component of y^p can be further rewritten as:

$$y^p = \left[P_1, P_2, \ ..., \ P_i, \ E_1^c, \ E_2^c, \ ..., \ E_i^c\right]^T. \tag{3.44}$$

The P_i in the component m refers to the HTF-based model of energy consumption profiles (Eq. (3.1)). The component of d is the predicted energy consumption measurement data E_i^c. Using Eqs. (3.31) and (3.44) new sets of *priori* ensemble y_j^p are created. Collections of forecasts y_j^p are stored in matrix in Eq. (3.32). The augmented Eq. (3.32) becomes

$$Y^p = \left[y_1^p, y_2^p, \ ..., \ y_j^p, \ ..., \ y_{N_e}^p\right]^T, \tag{3.45}$$

where $j = 1, 2, ..., N_e$ indexes the ensemble member and N_e is the total number of ensemble members.

Eq. (3.45) with N_e simulation runs can be further extrapolated as:

$$Y^p = \left(\begin{array}{cccc} P_{1,1} & P_{1,2} & \cdots & P_{1,j} \\ P_{2,1} & P_{2,2} & \cdots & P_{2,j} \\ \vdots & \vdots & \ddots & \vdots \\ P_{i,1} & P_{i,2} & \cdots & P_{i,j} \\ \hline E^c_{1,1} & E^c_{1,2} & \cdots & E^c_{1,j} \\ E^c_{2,1} & E^c_{2,2} & \cdots & E^c_{2,j} \\ \vdots & \vdots & \ddots & \vdots \\ E^c_{i,1} & E^c_{i,2} & \cdots & ,E^c_{i,j} \end{array}\right) \begin{array}{l} \left.\begin{array}{l} \\ \\ \\ \\ \end{array}\right\} m \\ \\ \left.\begin{array}{l} \\ \\ \\ \\ \end{array}\right\} d \end{array}, \tag{3.46}$$

where $i = 1,2,...,N_i$ indexes the consumer and $j = 1,2,...,N_e$ indexes the ensemble member. The N_i is the total number of consumers and N_e is the total number of ensemble members.

Given the actual measurement set d (also the model prediction), the perturbed observations are created that form another new ensemble $d_{\text{obs},j}$ (Eq. (3.36)).

The *priori* ensemble member y^p_j will be assimilated using the EnKF algorithm in order to obtain the updated *posteriori* ensemble y^u_j using Eq. (3.38). A similar equation from Eq. (3.38) that further extends the *posteriori* update (y^u_j) in every jth ensemble member is formulated as follow:

$$y^u_j = y^p_j + C_p H^T (HC_p H^T + R)^{-1} (d_{\text{obs},j} - Hy^p_j), \tag{3.47}$$

where d corresponds to Hy^p_j.

Eq. (3.47) is therefore the extension of Eq. (3.38) that shows the updating step in every jth ensemble member.

Another way of expressing the *priori* covariance C_p from Eq. (3.33) is formulated as follows:

$$C_p \approx \frac{1}{N_e - 1} (Y^p - \overline{Y^p})(Y^p - \overline{Y^p})^T. \tag{3.48}$$

Similarly, the *posteriori* covariance C_u from Eq. (3.40) is formulated as:

$$C_u \approx \frac{1}{N_e - 1} (Y^u - \overline{Y^u})(Y^u - \overline{Y^u})^T. \tag{3.49}$$

Additionally, Eq. (3.50) shows the alternative approach to express the covariance C in both cases C_p and C_u.

$$C \approx \begin{pmatrix} P_{1,1} & P_{1,2} & \cdots & P_{1,a} \\ P_{2,1} & P_{2,2} & \cdots & P_{2,a} \\ \vdots & \vdots & \ddots & \vdots \\ P_{a,1} & P_{a,2} & \cdots & ,P_{a,a} \end{pmatrix}, \tag{3.50}$$

where $a = 1, 2, ..., N_a$ is the number of model states.

Eq. (3.50) is particularly convenient for direct observations of the measurement error when the sizes of ensembles and state vectors are small. In contrast, computation or storing results of Eq. (3.50) at every time step can be computationally expensive and slow when sizes of ensembles and state vectors are large. Therefore, careful considerations of presenting C are required, that depend on the complexity of the system and model dimensions.

3.6.2.2 EnKF applications to energy generation in the ED model

In the ED problem, the variables of interest include the power grid properties such as transformer settings, capacity of generators, energy profiles and data which are normally added to the components of state vector y^p in Eq. (3.43). In this case, the parameter m in Eq. (3.43) is the real historical energy data representing the thermal units and wind generators from the portal (BMRS, 2015; Elexon, 2015). This results in model prediction d of the energy generation data for thermal units and wind generators. As parameters of m are adopted from the portal (BMRS, 2015; Elexon, 2015), they remain constant throughout the data assimilation. On the other hand, the d is the model prediction (actual measurement) of energy generation $E_{i,t}$ from real parameters m. The component d in vector y changes with data assimilation, incorporating the model errors in addition to m at every time step.

Similarly, the components of y^p are perturbed with model errors in order to generate new sets of ensemble members. The components of y^p from Eq. (3.43) are as follows:

$$y^p = \Big[m_1,\ m_2,\ ...,\ m_i,\ E_1, E_2,\ ...,\ E_i,\ W_1,\ W_2,\ ...,\ W_i\Big]^T. \tag{3.51}$$

The m_i components refer to real parameters of the thermal units and wind generators

from the portal (BMRS, 2015; Elexon, 2015). The components of d consist of: 1) the predicted energy generation data for thermal units $E_1, E_2, \ldots, E_i$; 2) the predicted wind energy generation $W_1, W_2, \ldots, W_i$.

Using Eqs. (3.31), (3.32) and (3.51) new sets of *priori* ensemble y_j^p are created. Collections of forecasts y_j^p are stored in matrix in Eq. (3.32). The augmented Eq. (3.32) with N_e realisations is as follows:

$$Y^p = \begin{pmatrix} m_{1,1} & m_{1,2} & \cdots & m_{1,j} \\ m_{2,1} & m_{2,2} & \cdots & m_{2,j} \\ \vdots & \vdots & \ddots & \vdots \\ m_{i,1} & m_{i,2} & \cdots & m_{i,j} \\ \hline E_{1,1} & E_{1,2} & \cdots & E_{1,j} \\ E_{2,1} & E_{2,2} & \cdots & E_{2,j} \\ \vdots & \vdots & \ddots & \vdots \\ E_{i,1} & P_{i,2} & \cdots & E_{i,j} \\ \hline W_{1,1} & W_{1,2} & \cdots & W_{1,j} \\ W_{2,1} & W_{2,2} & \cdots & W_{2,j} \\ \vdots & \vdots & \ddots & \vdots \\ W_{i,1} & W_{i,2} & \cdots & ,W_{i,j} \end{pmatrix} \begin{matrix} \left.\begin{matrix} \\ \\ \\ \\ \end{matrix}\right\} m \\ \left.\begin{matrix} \\ \\ \\ \\ \end{matrix}\right\} d \end{matrix} . \tag{3.52}$$

The $i = 1, 2, ..., N_i$ indexes the thermal units and wind generators, $j = 1, 2, ..., N_e$ indexes the ensemble members.

The perturbed observations given a new measurement set d, are created that form another set of ensemble $d_{\text{obs},j}$ using the perturbed observation formula (Eq. (3.36)). Similar with the EnKF application to energy consumption in Section 3.6.2.1, the y_j^p is assimilated in the EnKF algorithm in order to obtain the new updated *posteriori* ensemble y_j^u using Eqs. (3.47) to (3.49).

3.7 EnOpt method

EnOpt is applied for optimising the objective function, which describes costs and carbon emissions, based on the propagated *posteriori* (y_j^u) ensemble from EnKF. Ensembles of y_j^u are denoted as Y^u in matrix form. The EnOpt approaches of Chen et al. (2009); Jafroodi

and Zhang (2011); Jahangiri (2012); Nwaozo (2006) are followed. Such formulation of EnOpt provides the foundation for optimisation problems of carbon savings.

3.7.1 EnOpt general formulation

The control vector $\mathbf{x}$ is introduced that integrates the energy data modelled at different control steps. The components of $\mathbf{x}$ contain:

1. the energy consumption/demand output that minimises the carbon emissions subject to constraints as outlined in Eq. (3.15);

2. the energy generation output of thermal units that minimise costs and carbon emissions within the imposed constraints for the ED optimisation problem (Eq. (3.30)).

The control vector $\mathbf{x}$ is as follows:

$$\mathbf{x} = \kappa \cdot \Big[x_1,\ x_2,\ \ldots,\ x_i,\ x_{N_x} \Big]. \tag{3.53}$$

where i indexes the component of $\mathbf{x}$, κ is the smoothing coefficient, N_x is the total number of control variables. For the case of consumers in Eq. (3.15), N_x is the product of the number of consumers and the control steps. Conversely, for the case of Eq. (3.30), N_x is determined as the product of the number of thermal units and the control steps.

The objective function (Eq. (3.11)) is used in EnOpt to optimise the expectation of carbon emissions of consumers and is estimated as:

$$\mathscr{E}(\mathbf{x}, Y^u) = \sum_{t=1}^{N_t} Y^u(\mathbf{x}, t) G(t), \tag{3.54}$$

where Y^u denotes the *posteriori* ensemble estimates through the EnKF propagation from Eqs. (3.38) and (3.47), $\mathbf{x}$ is the control vector to be optimised.

Eq. (3.25) is used as the primary objective function of the ED model. Simulations obtained in the EnKF are further used in the EnOpt optimisation module to optimise energy generation:

$$\mathscr{C}(\mathbf{x}, Y^u_{\mathrm{G}}) = \sum_{t=1}^{N_t} d_{\mathrm{G}}(t) Y^u_{\mathrm{G}}(\mathbf{x}, t) + h_{\max} \sum_{t=1}^{N_t} d_{\mathscr{E}}(t) Y^u_{\mathrm{G}}(\mathbf{x}, t) + \sum_{t=1}^{N_t} d_{\mathrm{W}}(t) Y^u_{\mathrm{W}}(t), \tag{3.55}$$

where Y_{G}^{u} is the *posteriori* ensemble estimates of thermal generating units and Y_{W}^{u} is the *posteriori* ensemble estimates of wind generators. Both Y_{G}^{u} and Y_{W}^{u} are based on the resultant EnKF propagation using Eqs. (3.38) and (3.47).

It should be noted that the control vector $\mathbf{x}$ in Eqs. (3.54) and (3.55) is not the identical control vector used in both carbon emissions and ED costs optimisation model. Rather it is a presentation of how the $\mathbf{x}$ integrates with the state estimates resultant from the EnKF propagation. The dimension of $\mathbf{x}$ and also its control steps correspond to different scenarios will be explained explicitly in the Results section.

Since EnOpt is based on realisations of y_j^u with N_e simulation runs, the augmented objective functions from Eqs. (3.54) and (3.55) can be denoted as

$$\mathscr{E}_Y(\mathbf{x}) = \frac{1}{N_e}\sum_{j=1}^{N_e}\mathscr{E}(\mathbf{x}_j, y_j^u), \tag{3.56}$$

and also

$$\mathscr{C}_Y(\mathbf{x}) = \frac{1}{N_e}\sum_{j=1}^{N_e}\mathscr{C}(\mathbf{x}_j, y_j^u). \tag{3.57}$$

N_e denotes the total number of ensemble members. $\mathscr{E}(\mathbf{x}_j, y_j^u)$ and $\mathscr{C}(\mathbf{x}_j, y_j^u)$ are based on realisations of y_j^u with N_e simulation runs. The subscript Y indicates that emissions are optimised based on the simulator model updated in the EnKF (Chen et al., 2009). The y_j^u stays constant during the production optimisation process at specific time step while $\mathbf{x}$ is optimised. Therefore $\mathscr{E}_Y(\mathbf{x})$ and $\mathscr{C}_Y(\mathbf{x})$ is expressed as a function of $\mathbf{x}$ only.

The steepest descent method is applied to obtain the optimal $\mathbf{x}$ that minimises $\mathscr{E}_Y(\mathbf{x})$. The steepest descent is performed as follows:

$$\mathbf{x}_{\lambda+1} = \mathbf{x}_\lambda - \frac{1}{\alpha_\lambda} C_{\mathbf{x}} C_{\mathbf{x},\mathscr{E}_Y(\mathbf{x})}, \tag{3.58}$$

where λ denotes the iteration index, α_λ is the tuning parameter that determines the step size, $C_{\mathbf{x}}$ is the convariance matrix of $\mathbf{x}$, $C_{\mathbf{x},\mathscr{E}_Y(\mathbf{x})}$ is the cross-covariance between $\mathbf{x}$ and $\mathscr{C}_Y(\mathbf{x})$ and is formulated as follows:

$$C_{\mathbf{x},\mathscr{E}_Y(\mathbf{x})} \approx \frac{1}{N_e - 1}\sum_{j=1}^{N_e}(\mathbf{x}_{\lambda,j} - \overline{\mathbf{x}_\lambda})(\mathscr{E}(\mathbf{x}_{\lambda,j}, y_j^u) - \overline{\mathscr{E}(\mathbf{x}_\lambda, Y^u)}), \tag{3.59}$$

with

$$\overline{\mathbf{x}_\lambda} = \frac{1}{N_e}\sum_{j=1}^{N_e}\mathbf{x}_{\lambda,j}, \quad \overline{\mathscr{E}(\mathbf{x}_\lambda, Y^u)} = \frac{1}{N_e}\sum_{j=1}^{N_e}\mathscr{E}(\mathbf{x}_{\lambda,j}, y_j^u). \tag{3.60}$$

The same steepest descent method is applied in updating $\mathbf{x}$ in the context of ED problem by using the Eqs. (3.58) to (3.60). In the steepest descent calculations of the ED problem, the notation of $\mathscr{E}$ in Eqs. (3.58) to (3.60) is changed to $\mathscr{C}$.

3.7.2 Implementation of EnKF and EnOpt

In this section, the implementation of EnKF and EnOpt is explained in detail following Chen et al. (2009); Jafroodi and Zhang (2011); Jahangiri (2012). The optimisations problem of carbon savings $\mathscr{E}$ in groups of consumers and the cost $\mathscr{C}$ in the ED problem are illustrated in this section. The following notations are used: $k = 1,2,...,N_k$ is the index for data times, with N_k denoting the total number of data times of EnOpt model; t_k is the time step at data times k in EnOpt model; $Y_k^p, k = 1,2,...,N_k$ is the *priori* ensemble of a dynamical model simulator updated at times t_k; $Y_k^u, k = 1,2,...,N_k$ is the *posteriori* ensemble updated at times t_k; the control vector is denoted by $\mathbf{x}$; λ is the iteration index for EnOpt; $\mathbf{x}_\lambda$ is the control vector at iteration λ; $\mathbf{x}_{\lambda,j}, j = 1,2,...,N_e$ is the realisations of control variables that approximate cross covariance $C_{\mathbf{x},\mathscr{E}_Y(\mathbf{x})}$ and $C_{\mathbf{x},\mathscr{C}_Y(\mathbf{x})}$. In EnOpt, $\mathbf{x}$ is optimised at each λth iteration, whereas y_j^u and Y^u are kept constant at every particular time step t_k (during production optimisation process only).

1. Set $k = 0$. Initialise and generate ensemble Y_0 and $\mathbf{x}$.
2. Run the 'true' synthetic model simulator (Eq. (3.43)), based on prior knowledge, historical records of model specifications or available production data.
3. Propagate Y_k^p and $\mathbf{x}$ from t_k to t_{k+1} through the simulator model (Eq. (3.43)).
4. Apply EnKF to obtain Y^u by updating Y_k using Eq. (3.47). Set $k = k+1$.
5. Start optimisation for the EnOpt at $\lambda = 1$, generate $\mathbf{x}_1$ and $\mathbf{x}_{1,j}, j = 1,2,...,N_e$.
   (a) If $k = 1$, $\mathbf{x}_{1,j}$ is generated in two steps. First, the control mean is sampled from a uniform distribution with lower (LB) and upper bounds (UB). The LB and UB correspond to: 1) minimum and maximum energy consumption; 2)

minimum and maximum thermal capacity constraints. Second, the control mean is further perturbed by adding Gaussian random number with zero mean ($N \sim (0, C_{\mathbf{x}})$). The $\mathbf{x}_1$ is set as $\mathbf{x}_1 = 1/N_e \sum_{j=1}^{N_e} \mathbf{x}_{1,j}$.

(b) If $k \neq 1$ (k is not the first time step), $\mathbf{x}_1$ is set to $\mathbf{x}_1 = x$ in each realisations. The $\mathbf{x}_1$ is the control variable optimised at the previous data assimilation. Gaussian random number with zero mean ($N \sim (0, C_{\mathbf{x}})$) is added to $\mathbf{x}_1$ to form $\mathbf{x}_{1,j}$.

6. If $\lambda \neq 1$, Gaussian random number with zero mean ($N \sim (0, C_{\mathbf{x}})$) is added to form $\mathbf{x}_\lambda$ in each realisations.

7. Run the optimisation model (Eqs. (3.11) and (3.25)) and calculate $\mathscr{E}(\mathbf{x}, Y^u)$ and $\mathscr{C}(\mathbf{x}, Y^u_{\mathrm{G}})$ using Eqs. (3.54) and (3.55), where Y^u_{G} refers to the ensemble representation of Y^u_k.

8. Use Eq. (3.59) to compute $C_{\mathbf{x},\mathscr{E}_Y(\mathbf{x})}$ and $C_{\mathbf{x},\mathscr{C}_Y(\mathbf{x})}$.

9. Compute $\mathbf{x}_{\lambda+1}$ using Eq. (3.58).

10. Evaluate $\mathscr{E}_Y(\mathbf{x}_{\lambda+1})$ using Eq. (3.56) and $\mathscr{C}_Y(\mathbf{x}_{\lambda+1})$ for the ED problem using Eq. (3.57) that require N_e realisations.

11. If $\mathscr{E}_Y(\mathbf{x}_{\lambda+1}) < \mathscr{E}_Y(\mathbf{x}_\lambda)$ and similarly, $\mathscr{C}_Y(\mathbf{x}_{\lambda+1}) < \mathscr{C}_Y(\mathbf{x}_\lambda)$, replace $\mathbf{x}_\lambda$ by $\mathbf{x}_{\lambda+1}$ and let $\lambda = \lambda + 1$; otherwise, keep $\mathbf{x}_\lambda$, increase α_λ and proceed to step (8).

12. If stopping criteria is satisfied, set $\mathbf{x} = \mathbf{x}_\lambda$ and exit the optimisation loop; otherwise, repeat from step (6).

13. Repeat from step (2) until the end of data assimilation t.

Stopping criteria include: (i) a maximum optimisation step $\lambda_{\max}$; (ii) α_λ is not allowed to increase more than twice. According to Dehdari et al. (2012); Petvipusit (2011), in order to calculate α_λ, an initial value based on the variability and scaling of the objective function in varieties of ensembles are assumed. They further added that if the increase of the objective function is relatively insignificant, the α_λ values are increased through an arbitrary multiplier (step size).

$$\alpha_{\lambda+1} = \alpha_\lambda + \alpha_{\text{multiplier}}. \tag{3.61}$$

Petvipusit (2011) further asserted that the initial α_λ is simply determined at the half of standard deviation of the objective function; (iii) the relative increase of the objective function (Eqs. (3.56) and (3.57)) is less than 1 %. The relative increase of the objective function at each iteration is calculated as:

$$\%\Delta_{\lambda,k} = \frac{\text{Actual\_increase}}{\text{Prior}} = \frac{\text{Post}(\mathbf{x}_{\lambda+1,k}) - \text{Prior}(\mathbf{x}_{\lambda,k})}{\text{Prior}(\mathbf{x}_{\lambda,k})} \times 100\,\%, \tag{3.62}$$

where $\text{Post}(\mathbf{x}_{\lambda+1,k})$ refers to the updated objective function value at $\mathbf{x}_{\lambda+1,k}$ and $\text{Prior}(\mathbf{x}_{\lambda,k})$ refers to the objective function value at the previous iteration $\mathbf{x}_{\lambda,k}$.

For a better understanding of the EnKF and EnOpt flow, the EnKF and EnOpt flow diagram is illustrated in Fig. 3.3:

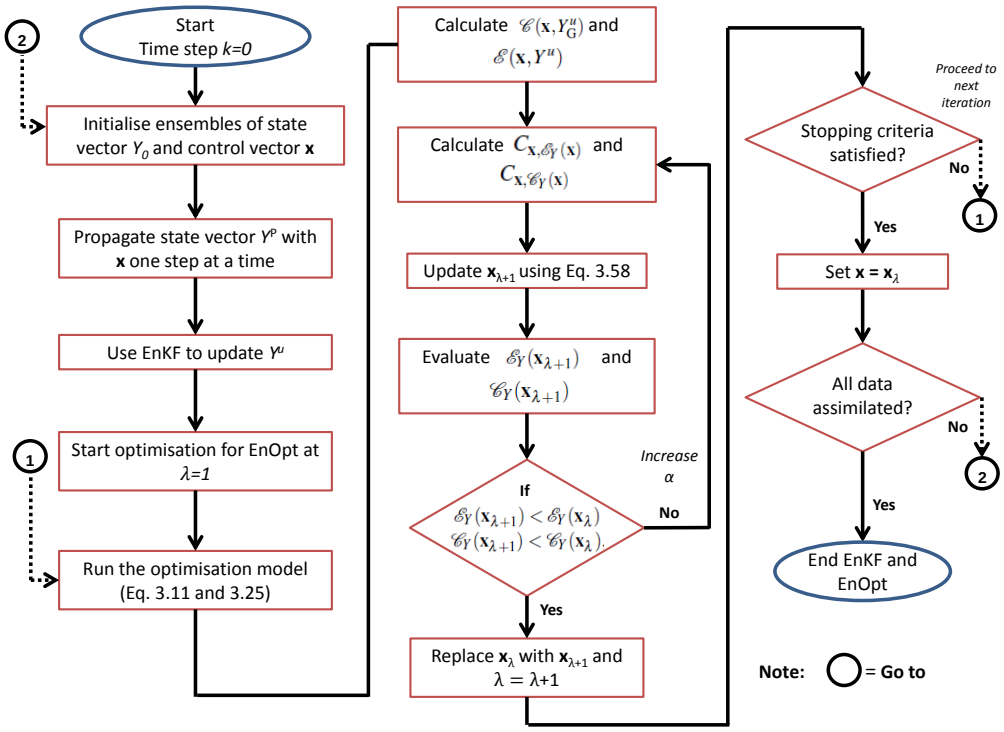

Figure 3.3: The EnKF and EnOpt flow.

The number of ensemble members must be large enough to avoid large errors in Eqs. (3.48) to (3.50) and (3.59) when the size of the ensemble is too small (Chen et al., 2009; Jensen, 2007). Generally, each realisation of the control variable $\mathbf{x}_{\lambda,j}$ is integrated with y_j^u at every time step k. Objective function for EnOpt is computed to further quantify the optimised carbon emissions and costs ($\mathscr{E}_O = \mathscr{E}_Y(\mathbf{x}_\lambda)$ and $\mathscr{C}_O = \mathscr{C}_Y(\mathbf{x}_\lambda)$) in Eqs. (3.56) and (3.57) at the end of simulations. The carbon savings S are computed using Eq. (3.12)

along with the calculation of BAU emissions $\mathscr{E}_{\text{BAU}}$ using Eq. (3.10). Similarly, the optimised cost of generation for the ED model is computed using Eq. (3.28). The BAU cost is calculated using Eq. (3.24). The Eq. (3.12) is also used to determine the amount of carbon savings by using the second term of the cost function (Eqs. (3.24) and (3.25)).

It is also advisable to store optimised $\mathscr{E}_{\text{O}}$ and $\mathscr{C}_{\text{O}}$ at every λth iteration in a matrix form as follows (denoted as matrix Z):

$$\begin{aligned} Z &= \begin{bmatrix} z_1, & z_2, & \cdots, & z_{N_e} \end{bmatrix}, \\ Z_{\mathscr{E}} &= \begin{bmatrix} \mathscr{E}(\mathbf{x}_{\lambda,1}, y_1^u), & \mathscr{E}(\mathbf{x}_{\lambda,2}, y_2^u), & \cdots, & \mathscr{E}(\mathbf{x}_{\lambda,N_e}, y_{N_e}^u) \end{bmatrix} \end{aligned} \tag{3.63}$$

and also

$$Z_{\mathscr{C}} = \begin{bmatrix} \mathscr{C}(\mathbf{x}_{\lambda,1}, y_1^u), & \mathscr{C}(\mathbf{x}_{\lambda,2}, y_2^u), & \cdots, & \mathscr{C}(\mathbf{x}_{\lambda,N_e}, y_{N_e}^u) \end{bmatrix}.$$

The matrix Z illustrates the stored results with N_e simulation runs.

3.8 Profiling the BAU versus smart invervention and modelling the DR programmes

Using Eq. (3.5), the carbon emissions generated due to the interventions from DR, as well as the BAU conventional reserve plants can be obtained. Thus, using Eq. (3.6) carbon savings are estimated as the difference between the BAU solution and the smart intervention in the corresponding DR solutions. As mentioned, Eqs. (3.5) and (3.6) reflect the general formulation of carbon emissions and savings. The carbon assessment formula for the specific DR programme is different and the formulation is made available in each sub-sections of the DR formulations.

Four types of DR programmes are evaluated, namely the STOR, Triad, Fast Reserve, FCDM and the Irish smart metering trial. A short summary for types of BAU and interventions considered in each of the DR programmes is shown in Table 3.3.

In order to determine the amount of carbon emissions produced by plants and generators, it is necessary to study the profiles of BAU plants, taking into account specific time intervals of the DR event. The carbon emissions of BAU plants and smart interventions are compared, with operational assumptions relating to firing up, efficiency, shutdown and

Table 3.3: Types of BAU and interventions in DR programmes.

DR programme	BAU solution	Smart intervention solution
STOR	CCGT OCGT	Backup-generators Demand reduction CHP
Triad	CCGT OCGT	Backup-generators
Fast Reserve	Main UK grid	Hydro-pumped storage
FCDM	Main UK grid	Demand reduction
Demand reduction	Main Irish grid	Irish ToU tariffs in combination with DSM stimuli

corresponding energy generation in DR programmes. Profiles of BAU plants and smart interventions are explained in Sections 3.8.1 and 3.8.2. The methodology of modelling the corresponding DR programmes are explained in Section 3.8.3.

3.8.1 Profiles of BAU plants

3.8.1.1 Combined cycle gas turbine (CCGT) plant – operational profile

A combined cycle gas turbine (CCGT) plant must be warmed up to reach the base load level to operate in stable conditions before it can generate energy (Environmental Agency, 2011). The recommended level of generation by CCGT is above 50 % of the load. It is assumed that CCGT plants will always operate at base-load level to provide the right source of plant margin in order to maintain the security of energy supply (Flexitricity, 2013), and within the same scale of generation. This is because of the need to provide balancing services of electricity supply across the network, in order to mitigate the risks of power station failures, demand rises, and failures of renewable generation due to seasonal variations (Flexitricity, 2013). The 'plant margin' of at least 20 % is strictly needed to avoid power failures. More details on plant margins can be found in the documentations (Flexitricity, 2013; National Grid, 2011).

Due to inflexibility of instantaneous energy generation in responding to unpredictable energy demand, CCGT plants must be operated at base-load level. Before generating energy, CCGT plants need to be in standby mode ('hot standby mode' in this case) awaiting despatching instructions from National Grid. It is common for CCGT plants to undergo complete warm-up process but eventually may or may not be used (Flexitricity, 2013).

During the warm-up period, a conventional CCGT plant burns additional fuel for a few hours throughout the warming up period to full-load before it is capable of generating electricity. For instance, a 380 MW CCGT plant may take 3 hours to reach the full-load condition (Boyle et al., 2003). The long period of warming up is mainly due to the requirement for sequential loading of gas and steam turbine for hours before achieving the base load level (see Boyle et al. (2003); Environmental Agency (2011) for the detailed explanation of warming up of conventional CCGT plants). Since CCGT plants are expected to operate at part-loaded level, the warm-up duration of CCGT plants is assumed to be approximately 35 minutes, excluding the standby period (Riihimaki, 2012). Due to the requirement to sequentially warm up CCGT plants at different part-loading points, such a plant will consume additional fuel and consequently generate carbon emissions. Table 3.4 shows the percentage increase of carbon emissions for CCGT plants at different part-loads. The data in Table 3.4 is originally derived based on the percentage increases of the fuel consumption corresponding to different part-loads by Flexitricity (2013). Martin (2013) further denoted the percentage increases of fuel consumption data from Flexitricity (2013) as the part-loading heat rate. According to Korellis (2014), as the one percent of heat rate is equivalent to one percent of carbon emissions, the percentage increase of fuel consumption or heat rate in this case is expressed as the percentage increase of carbon emissions.

Table 3.4: Percentage increase of carbon emissions at various loads of CCGT plants. Adapted from Flexitricity (2013).

Part load point (%)	Percentage increase of carbon emissions (%)
25	79
50	20
75	10

During the period of operation, CCGT plants will generate the required level of energy when all stages of the warm-up sequence have been completed (except the 'hot-standby' period when awaiting a despatch instruction from National Grid). In this study, a single CCGT plant is assumed to operate at 50 % part-loaded throughout the DR programmes. A group of part-load CCGT plants will generate the required level of energy. As CCGT plants are assumed to operate at 50 % of full load, there will be short term increase of fuel consumption (20 %) and carbon emissions as shown in Table 3.4.

The shutdown time for a CCGT plant is the interval from the initiation of shutdown from the base load (approximately 50 %) to the 'flame-off' signal of the gas turbine (Baling, 2011). CCGT plants have negligible emissions at standstill following the complete shutdown sequence (Baling, 2011). CCGT plants can also 'park' at certain part-load levels instead of complete shutdown (with additional emissions as a result). However, before the flame-off and the complete shutdown of a CCGT plant, the gas turbine rapidly de-loads. During the de-load sequence, the combustion system reverts to start-up mode with an associated short-term increase of carbon emissions (Environmental Agency, 2011). A short-term increase of carbon emissions about 8-10 % is assumed before CCGT plants shut completely after the flame-off phase.

3.8.1.2 Open cycle gas turbine (OCGT) plant – operational profile

In order to cope with increasing uncertainty of the power grid (for instance, wind generation intermittency and variable consumer demand) within short time intervals, National Grid allocates a large number of 'peaking' power plants, particularly, open cycle gas turbine (OCGT) plants for providing standing reserve energy supply (Manchester Centre For Electrical Energy, 2004; National Grid, 2013c). OCGT plant are very flexible in providing standing reserve and often referred as 'peaking plant' due to the shorter duration of start-up time and higher efficiency when operating at various part-loads (Manchester Centre For Electrical Energy, 2004; Wärtsilä, 2012).

Similar to CCGT plants, during the warm-up period OCGT plants are assumed to operate at above 50 % load in order to avoid the increase of emissions (Macak, 2001) and also to operate in a stable state before it can generate energy. There will be short-term increase in fuel consumption at different part-loading points during the start-up sequence, thus increasing the carbon emissions. Table 3.5 shows the percentage increase of carbon emissions for OCGT plants at different part-loads.

The OCGT profile is obtained from Macak (2001). Initially, the emissions corresponding to different part-loads are specified as carbon monoxide (CO) equivalent. To convert from CO to CO_2 the ratio of their atomic weights are considered. The atomic weights of carbon, CO and CO_2 are 12, 28 and 44 atomic mass units respectively. Therefore one tonne of carbon equates to $1 \times 44/12 \approx 3.67$ tCO_2. The ordinary CO emissions at different part-loads analysed by Macak (2001) is further adapted in this study by converting CO

Table 3.5: Percentage increase of carbon emissions at various part-loads of OCGT plants. Adapted from Macak (2001).

Part-load point (%)	Percentage increase of carbon emissions (%)
Idle	100.00
20	35.22
40	17.88
60	7.32
80	5.14
Base-load	6.70

into CO_2 equivalent emissions in terms of percentage scale at different part-loads.

The percentage increase of carbon emissions reduce as load increases (Table 3.5). The method by Macak (2001) is further adapted by considering a nominal 80 MW OCGT unit with dry and low NOx combustors (several units are combined together to provide a required level of STOR/Triad capacity). This configuration is compatible with most of OCGT plants operating in the UK. An OCGT plant has ability to reach full load in 10 – 30 minutes (Macak, 2001; Petzer and Burger, 2007; Riihimaki, 2012). In this work, the duration from start-up to full load for OCGT plants is assumed approximately 30 minutes.

During the period of operation, OCGT plants will generate the required level of energy as soon as the start-up sequence completes. Operating OCGT plants at base-load capacity throughout the DR operations introduce additional 6.7 % increase of fuel consumption and the resultant carbon emissions as shown in Table 3.5.

The shutdown sequence of OCGT plants can be achieved instantly of within 10 minutes (Macak, 2001) . The earlier OCGT profile by Macak (2001) assumed that the emissions during the shutdown sequences are not being taken into account and the assessment of air quality is performed from the start-up sequence to base-load operations only. In this case, it is assumed that there will be a short-term increase of carbon emissions before OCGT plants shut completely.

3.8.2 Profiles of smart interventions

3.8.2.1 Standby diesel generator – operational profile

The standby diesel generation is one of the STOR (National Grid, 2013b) and Triad (Ward et al., 2012) management instruments. Therefore, both STOR and Triad programmes

include the intervention by switching from conventional BAU fuelled production to diesel generators.

Most diesel generators burn no fuel when waiting for peak demand or system failure (Flexitricity, 2013). Diesel generators have the ability to warm up very rapidly within 1-2 minutes (Independent Project Analysis Consulting, Econnect Ltd and Martin Energy, 2006) and shutdown instantly. Due to the rapid response of diesel generators, they are very important in providing flexible reserve and contingency services. This is because most of the power plants are unable to respond to sudden demand peaks, and hence are allowed to operate at base-load level only. However, most of the diesel generators have small size and low efficiency (35 %) with heavily emitting fuel. Multiple diesel generators are required to generate the same amount of energy as one large-scale plant. Given such different operational features of reserve plants and diesel generators, it is necessary to compare the carbon emissions of the two energy generation scenarios in order to quantify possible carbon emissions/savings.

In this work, the carbon emissions resulting from the use of generators (diesel-fuel powered) are compared with reserve BAU plants based on the balancing mechanism controlled by National Grid. The reserve BAU plants are CCGT and OCGT plants.

3.8.2.2 Demand reduction

The intervention through demand reduction (demand turndown) implies switch-off appliances, thus there are no additional emissions caused by the intervention. This demand response results in direct carbon savings due to the reduced volume of the overall energy consumption. The demand reduction is often regarded as the default mechanism in providing electricity in the FCDM programme.

3.8.2.3 Combined heat and power

The combined and and power (CHP) systems generate heat and energy simultaneously in a single process (Hill et al., 2014). They can achieve overall efficiency as high as 80 % (Hill et al., 2014). The amount of carbon savings against all fuels for CHP is available in documentation (DUKES, 2012, 2013). Table 3.6 shows the amount of carbon savings due to installed CHP.

Table 3.6: CHP characteristics in DR. Adapted from DUKES (2012, 2013).

Year	CHP operating hours per annual (hrs)	Carbon savings against all fuels ($kgCO_2$/kWh) (including renewable and non-renewable)
2011	4450	0.339
2012	3807	0.412

The carbon savings given in Table 3.6 are based on estimation of fuel mix and are subject to annual revision (DUKES, 2012, 2013). For every unit of energy produced by a CHP plant, the carbon emissions (and other associated GHG emissions) are less than half of a conventional coal-fired plant. For instance, since the carbon factor for coal per kWh of electricity generated is approximated as 0.80-1.00 kg (DUKES, 2012; Moomaw et al., 2012; Tzimas et al., 2007), the carbon factor for a standard CHP system can be estimated as 0.35–0.45 $kgCO_2$/kWh. Such estimations is similar to the carbon factor values shown in Table 3.6. For a detailed methodology of calculating the fuel and carbon emissions for CHP systems, see the paper by Hedman and Hampson (2011).

3.8.2.4 Hydro-pumped storage – operational profile

Hydro-pumped storage plants are powered by water from an upper reservoir. Each of the conventional power stations may comprise two to four generators/motor pumps. Hydro-pumped storage plants operate in two modes: pumping and generating. During the pumping mode, the pump acts as a 'rechargeable battery' by pumping the water at the foot of a hill to the upper reservoir during the night when electricity tariffs are usually cheap (Scottish Power, 2010). The water is stored in the reservoir and is released as necessary to charge the turbines (generating mode) to meet peak demand. The hydro-pumped storage is often regarded as the default mechanism in providing electricity in the Fast Reserve programme.

The high flexibility of the hydro-pumped storage allows one to achieve the full-load pumping speed within a few minutes. There are restrictions imposed in terms of the maximum number of utilisations (for instance, 300 MWh per operational day for a tendered unit). National Grid (2014a) provided detailed account of maximum utilisation corresponding to tendered units of hydro-pumped storage plants. There are also established restrictions on the total electricity generated by such plants due to the possible environ-

mental effects from waste oils and also oil leakages (Scottish Power, 2010). For instance, Cruachan hydro plant reduced the amount of generated electricity in 2009 to 705 GigaWatts hour (GWh) compared to 885 GWh in 2008.

In this study, the Ffestiniog pumped storage hydroelectricity plant participating in the Fast Reserve programme is selected for assessment of carbon emissions. The general specification of Ffestiniog pumped storage from First Hydro Company (2005, 2009) is given in Table 3.7.

Table 3.7: Specification of the Ffestiniog pumped storage. Adapted from First Hydro Company (2005, 2009).

Number of turbines (units)	4
Number of pumps (units)	4
Total plant capacity	360 MW
Generating capacity (per unit)	90 MW
Pumping capacity (per unit)	75 MW
Cycle efficiency	72-73 %
Total reservoir capacity	1.3 GWh
Duration of achieving full load generation	$\leq$ 5 minutes (from 'standstill') $\geq$ 60 seconds (from 'spinning')

3.8.3 Modelling the DR programmes

In the following sections, modelling of carbon emissions and estimation of carbon savings in the considered DR programmes are explained.

3.8.3.1 STOR

National Grid (2015c,d) reports the STOR market information and tender round results, providing the results of the total accepted power (flexible and committed in MW) within the seasonal span. The contracted capacity is shown in Table 3.8.

The STOR data from Table 3.8 is used to estimate the energy generation and carbon emissions in the STOR programme. Carbon emissions of a Non-BM aggregator are estimated as shown in the earlier illustration in Fig. 2.2. It is assumed that if there is no request of the STOR programme, National Grid would instruct the BAU plants (OCGT and CCGT plants) to provide the entire capacity of STOR. In contrast, if STOR programme is demanded, the aggregator will substitute proportional part of the STOR capacity by

Table 3.8: Contracted STOR period with accepted capacity in 2014 – 2015.

Season	Dates	Accepted MWs
8.1	01/04/14 - 28/04/14	2537
8.2	28/04/14 - 18/08/14	2648
8.3	18/08/14 - 22/09/14	2804
8.4	22/09/14 - 27/10/14	2819
8.5	27/10/14 - 02/02/15	3500
8.6	02/02/15 - 01/04/15	3498

generating the contracted diesel fuelled energy within the availability windows. This further allows for the estimation of carbon emissions and savings from the replacement of the BAU plants (hypothetical, as the plant does not operate during the STOR period) by diesel generators of aggregators at the same scale of generation.

The ratio of the aggregator's diesel-generated capacity to the full STOR capacity of the reserved BAU plants is:

$$k' = \frac{V_a}{V_o}. \tag{3.64}$$

The V_a is the volume provided by the aggregator, V_o is the overall STOR volume contracted to reserved BAU plants.

Through Eq. (3.64), the comparison of the emissions resulting from the reserved BAU plants $\mathscr{E}_B^{ik'}$ and diesel generators $\mathscr{E}_I^k$ can be achieved:

$$\mathscr{E}_B^{ik'} \sim \mathscr{E}_I^k, \tag{3.65}$$

where superscript k indicates the nominal amount of generation, k' is the rescaled energy generated from Eq. (3.64), i indexes the BAU (CCGT and OCGT) plants.

The carbon savings through the intervention by diesel generation are calculated as:

$$S^i_{\text{STOR\_diesel}} = \mathscr{E}_B^{ik'} - \mathscr{E}_I^k = \sum_{t=1}^{N_t} \left(E_B^{ik'}(t) \times C_B^i - E_I^k(t) \times C_D \right), \tag{3.66}$$

where $E_B^{ik'}$ indicates energy generation (kWh) by BAU plants, E_I^k is the energy generation (kWh) resulting from the diesel generators, C_B^i is the carbon factor for BAU plants, C_D is the carbon factor for diesel generators, i indexes the BAU plants, t is the time step, N_t is the total time steps.

For the demand reduction response in STOR programme, in order to compute carbon savings the electricity grid carbon factor $G_{UK}(t)$ is multiplied by the volume reduction for the entire demand turn-down category. The $G_{UK}(t)$ is being calculated individually for the date and time of each event. Such demand response through demand reductions results in carbon savings due to reduced volume of overall energy consumption. The formula for the calculation of carbon savings for the demand reduction response is

$$S_{\text{STOR\_DR}} = \sum_{t=1}^{N_t} E_{\text{reduced,DR}}(t) \times G_{UK}(t) \tag{3.67}$$

where $E_{\text{reduced,DR}}(t)$ is the amount of energy reduced, $G_{UK}(t)$ is the variable UK electricity grid carbon factor, N_t is the total number of time step in the STOR programme.

In the case of the smart intervention by CHP in STOR programme, using the available data from Table 3.6 direct carbon savings in the CHP response can be computed as a result of the reduced volume of overall energy consumption. The formula for the calculation of carbon savings for CHP response is

$$S_{\text{STOR\_CHP}} = \sum_{t=1}^{N_t} E_{\text{reduced,CHP}}(t) \times G_{\text{CHP}}(t) \tag{3.68}$$

where $E_{\text{reduced,CHP}}(t)$ is the amount of energy reduced through the CHP usage, $G_{\text{CHP}}(t)$ is the carbon factor for CHP, N_t is the total number of time step.

3.8.3.2 Triad

There is no standard Triad warning communicated to participants by National Grid as Triad charges are determine by National Grid when the Triad season is over. Therefore, Triad warnings are normally issued based on the forecast mechanism. Hence each period of Triad operation is modelled as one hour. The Triad period can be represented by the unit step function, as shown in Fig. 3.4. When a Triad warning is issued, the instantaneous operation of diesel generators starts.

National Grid would instruct the reserve BAU plants to provide the total capacity if Triad participants do not cut the loads from the main UK energy grid. For simplicity, the capacities of diesel generators are the same scale as the BAU plants during the Triad event by taking 1 GigaWatts (GW) of total generating capacity. This technique implies that

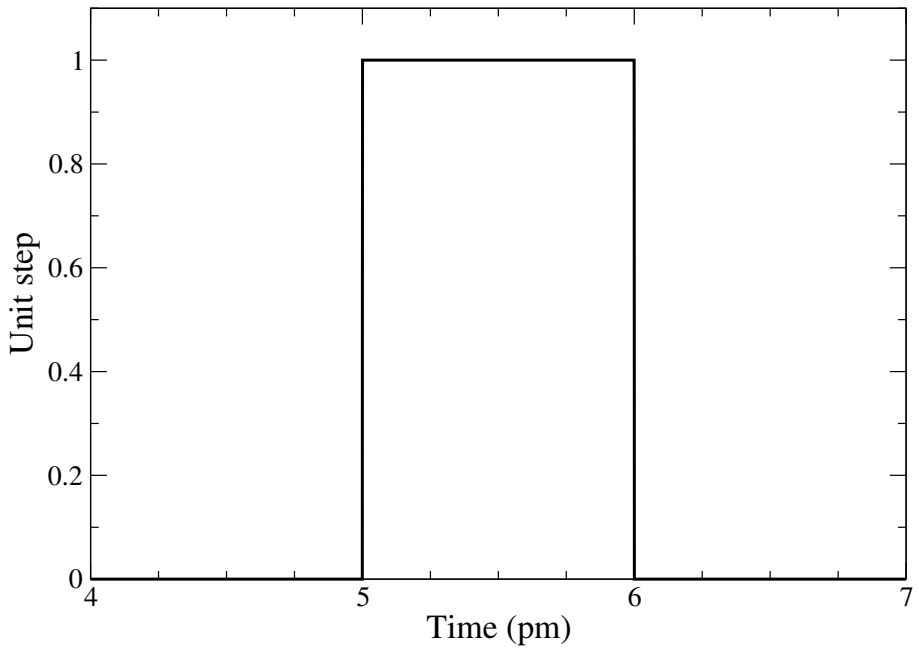

Figure 3.4: Triad event with instant warning, modeled as a unit step.

Triad participants cut loads from the UK energy grid and instead use diesel generators to provide electricity on their sites. This allows estimation of carbon emissions and savings from the replacement of BAU plants by diesel generators at the same scale of generation.

The carbon savings for Triad programme are calculated as follows:

$$S^i_{\text{Triad}} = \mathscr{E}^i_B - \mathscr{E}_I = \sum_{t=1}^{N_t} \left(E^i_B(t) \times C^i_B - E_I(t) \times C_D \right), \tag{3.69}$$

where $\mathscr{E}^i_B$ indicates carbon emissions by reserved BAU plants, $\mathscr{E}_I$ are the carbon emissions resulting from operating diesel $E^i_B(t)$ denotes the energy generated by BAU plants, $E_I(t)$ is the energy generated by diesel generators, C^i_B is the carbon factor for BAU plants, C_D is the carbon factor for diesel generators, i indexes reserved BAU plants, t is the time step, N_t is the total time steps.

3.8.3.3 Fast Reserve

Fast Reserve tenders for the Ffestiniog plant at which the timeline is provided by National Grid (2014a). The tendered results are shown in Table 3.9:

While the Fast Reserve programme can be despatched by the National Grid at any moment, it is presumed that the programme operates daily with maximum demand occurring in both morning and evening. The daily demand data is available publicly in National Grid

Table 3.9: National Grid's accepted tenders for the Fast Reserve programme.

Tendered unit	Tendered period	Tendered Window	
		Monday to Saturday	Sundays
Ffestiniog plant, FFES-2	01/04/13-31/03/14	0700-1230	1600-2230 0900-1300 1700-2230

(2015a). Additionally, the Ffestiniog plant is not always fully utilised in the Fast Reserve event where the Ffestiniog plant is not necessary to provide the full capacity (360 MW) of energy generation. Despatching instruction is only issued by National Grid based on the accepted tendered service period. For that reason, not all generating units are powered at the same instant as some generating units may be allocated for other DR programmes or for BAU mechanism of electricity generation.

In the modelling of Fast Reserve, the Ffestiniog plant fleet number two (FFES-2) is selected for simulation of the Fast Reserve event. Additionally, the reservoir can be refilled when it is partly drained or at times of low peak periods. Utilisation restrictions/constraints are also imposed on the FFES-2. According to National Grid (2014a), the capping for the maximum energy is 250 MWh per day and additionally the maximum of 30 utilisations per day. The FFES-2 refills the reservoir during the night time. The further assumptions include buying energy from the UK grid for FFES-2 based on Economy 7 tariffs. The replenishment of the reservoir will be initiated at 0130 British Summer time or 0030 Greenwich Mean Time. The duration of refilling the reservoir is estimated as

$$N_{t_\alpha} = \frac{C_r}{C_p}, \tag{3.70}$$

where C_r is the capacity of the reservoir (MWh) and C_p is the capacity of the pump (MWh).

Since FFES-2 draws electricity from the UK grid, this results in carbon emissions based on the carbon footprint of electricity grid. In addition, there are still small fractional amount of indirect carbon emissions produced when the FFES-2 is generating electricity. It is mainly due to the rotation of turbines and other transmissions of electricity resulting in energy losses. By using Eq. (3.5) and Eq. (3.7), the carbon emissions resulting from

the FFES-2 are as follows:

$$\mathscr{E}_H = \sum_{t_\alpha=1}^{N_{t_\alpha}} \left(E_H(t_\alpha) \cdot G_{UK}(t_\alpha)\right) + \sum_{t_\beta=1}^{N_{t_\beta}} \left(E_H(t_\beta) \cdot F_H\right), \tag{3.71}$$

where E_H is the amount of energy consumed and generated by FFES-2 (kWh), G_{UK} is the carbon factor of the UK grid, F_H is the carbon factor of FFES-2, t_β is the time index for energy generating mode, t_α is the time index for pumping mode, N_{t_α} is the total pumping duration, N_{t_β} is the total generating duration.

For simplicity, the resultant carbon emissions of the Ffestiniog hydro plant can be computed by considering the same duration and capacity of operation for the remaining fleets (FFES). Emissions $\mathscr{E}'_H$ are calculated as follows:

$$\mathscr{E}'_H = \mathscr{E}_H \times N_H, \tag{3.72}$$

where $\mathscr{E}_H$ are carbon emissions from Eq. (3.71), N_H is the total number of fleets/units in the Ffestiniog hydro plant.

Similar to STOR the programme, it is assumed that National Grid would instruct BAU plants to provide the total capacity for Fast Reserve. The instruction is sent if FFES-2 fails to provide the substitution of grid energy for consumers. Carbon savings of the Fast Reserve resulting from the intervention by hydro-pumped are calculated as:

$$S^i_{\text{Fast\_Reserve}} = \left(\sum_{t_\beta=1}^{N_{t_\beta}} \mathscr{E}^i_B(t_\beta) \right) - \mathscr{E}'_H, \tag{3.73}$$

where $\mathscr{E}^i_B$ is the carbon emissions by reserved BAU plants, $\mathscr{E}'_H$ denotes the overall carbon emissions from Eq. (3.72), i indexes reserved BAU plants, t_β is the time index for energy generating mode, N_{t_β} is the total generating duration.

For a Fast Reserve event, the event duration is assumed to be 15-30 minutes for a normal period (spring-summer) and 15-60 minutes for a critical period (autumn-winter).

3.8.3.4 FCDM

Currently, there is insufficient market information publicly available for FCDM. National Grid (2015b); Ward et al. (2012) stated that the event frequency for FCDM was approximately thirty times per annum. As the demand reduction is the main intervention in the FCDM programme, direct carbon savings are formed due to the volume reduction of energy used. Similar to the demand reduction response in the STOR programme, the electricity grid carbon factor ($G_{UK}(t)$) is being calculated for each event.

Carbon savings for the demand reduction response are as follows:

$$S_{\text{FCDM}} = \sum_{t=1}^{N_t} E_{\text{reduced}}(t) \times G_{UK}(t), \tag{3.74}$$

where $E_{\text{reduced}}(t)$ is the amount of energy reduced, $G_{UK}(t)$ is the variable UK electricity grid carbon factor, N_t is the total number of time steps of the FCDM programme.

3.8.3.5 Irish smart meter project

The electricity consumption data (kWh) of the BAU and test groups of the Irish smart grid is used. The usage of the electrical consumption data allows quantification of the carbon emissions reductions within the two distinct groups. The carbon savings can be estimated as follows:

$$S_{\text{SM}} = \sum_{t=1}^{N_t} (E_B(t) - E_T(t)) \cdot G_{UK}(t), \tag{3.75}$$

where $E_B(t)$ is the electrical consumption by the BAU group (kWh), $E_T(t)$ denotes the electrical consumption by the test group (kWh), G_{UK} is the variable UK electricity grid carbon factor.

Carbon factor $G_{UK}(t)$ is estimated using the datasets from the BMRS and Elexon. The G_{UK} is matched with the timeline trial experiment by the Irish smart grid. This is important, because G_{UK} is affected by various external conditions, such as seasonal and consumer usage patterns. It is assumed that the trend of Irish electricity carbon factor is analogous to the UK carbon factor due to the close proximity to UK and therefore may exhibit similar climate and weather trend with the UK. For this assumption, the UK electricity grid carbon factor can be applied to the case of Irish smart grid.

It is important to monitor and analyse the impact of smart initiatives during the peak

(from 5pm to 7pm daily) and off-peak periods (CER11080a, 2011). The findings in Section 2.5.2.5 presented the results of the percentage energy reduction based on large samples of the BAU and test group with considerations of all smart initiatives. In the present study, due to the need of feasibility in examining all the ToU tariffs in combination of all DSM stimuli, total of 132 trial days from recorded Irish smart grid energy datasets are extracted in order to estimate carbon emissions and savings. The BAU and the test group in every ToU tariffs in combination of DMS stimuli are compared. This allows one to determine the effect of smart interventions due to behavioural changes in response to smart meters roll-out.

Chapter 4

Results

The input elements, models developed that contribute to the output results are presented in Fig. 4.1.

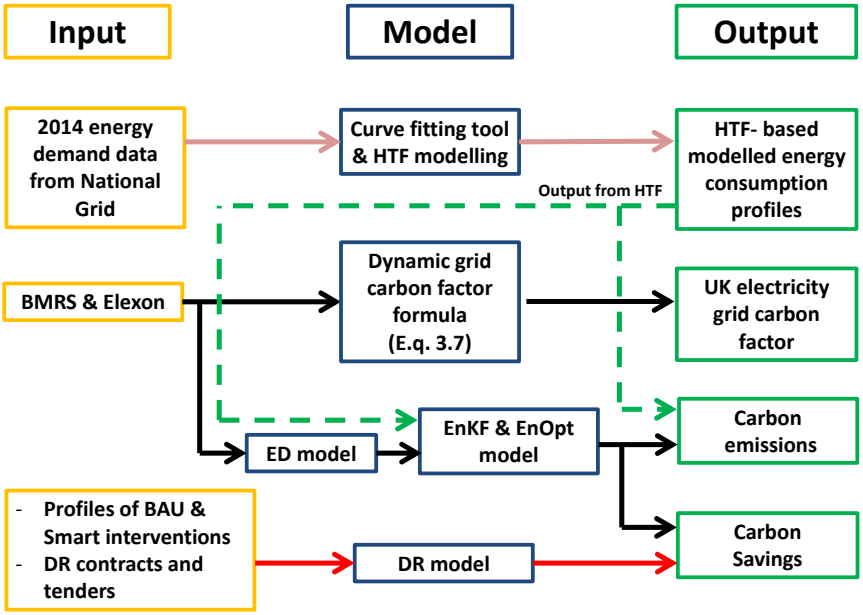

Figure 4.1: Input elements and the models developed that contribute to the output results.

The section begins with the resultant modelled profiles of energy consumption using HTF. Next, the tabulations of carbon emissions based on the energy consumptions and several case studies are presented. Using the publicly available fuel mix data from BMRS and Elexon as the input, the UK electricity grid carbon factor is computed. The later includes the simulation results based on two optimisation problems (energy consumption and the ED model) using the application of EnKF and EnOpt algorithm. The

energy consumption based on HTF modelling is used as the input energy data in the energy consumption optimisation problem and in contrast, the input energy generation data by Elexon and BMRS are adopted in performing the numerical optimisation of the ED problem. The final presents the carbon assessment of DR programmes, as well as the inclusion of several case studies.

4.1 Numerical simulation of energy consumption

This section presents the modelled profiles of energy consumption using HTF and the resultant carbon emissions based on the periodical function $P_i(t)$ (Eqs. (3.1) to (3.3)) for the electricity consumption. Profiles based on four categories of consumers (working family, pensioner, daytime office and one-shift day industrial) are modelled as combinations of $A(t)$ and $D_i(t)$ cycles. The analytical expression of $A(t)$ and $D_i(t)$ based on Eqs. (3.1) to (3.3) are to be further applied for the simulation of the energy consumption E_i^c in the EnKF and EnOpt algorithm.

In order to illustrate parameters of $A(t)$ and $D_i(t)$, the unit for $A(t)$ is shown in daily (days) format, whereas $D_i(t)$ are calculated at hourly resolution. For simulations, units are in HH scale format.

The derived equation for $A(t)$ is as follows:

$$A(t) = C_1 + C_2\left(-\frac{\tanh(t-75)}{L} - \frac{\tanh(t-110)}{L} + \frac{\tanh(t-250)}{L} - \frac{\tanh(t-280)}{L} + \frac{\tanh(t-300)}{L} + \frac{\tanh(t-360)}{L}\right), \tag{4.1}$$

where $C_1 = 4.254$, $C_2 = 0.259$ and $L = 20$ days.

The derived $A(t)$ in Eq. (4.1) is based on the HTF fitting with the 2014 real energy demand data, which is available in the public domain (National Grid, 2015). The real energy demand data is converted to have identical temporal scale with the HTF fitting. The result of the HTF fitting and modelling of annual profile is shown in Table 4.1.

Table 4.1: HTF fitting of the annual consumer profile using the HTF. SSE: Sum of squared errors of prediction; RMSE: Root mean squared error; Coefficients are computed with 95 % confidence interval.

Annual profile	
Function type	HTF
Model	$A(t)$ $(Eq.\ (4.1))$
Coefficients	$C_1 = 4.254(4.193, 4.315)$
	$C_2 = 0.259(0.237, 0.281)$
Goodness of fits	SSE: 31.8
	R-square: 0.602
	Adjusted R-square: 0.601
	RMSE: 0.296

The resulting modelled HTF fitting of the annual profile versus the 2014 real energy demand data is shown in Fig. 4.2.

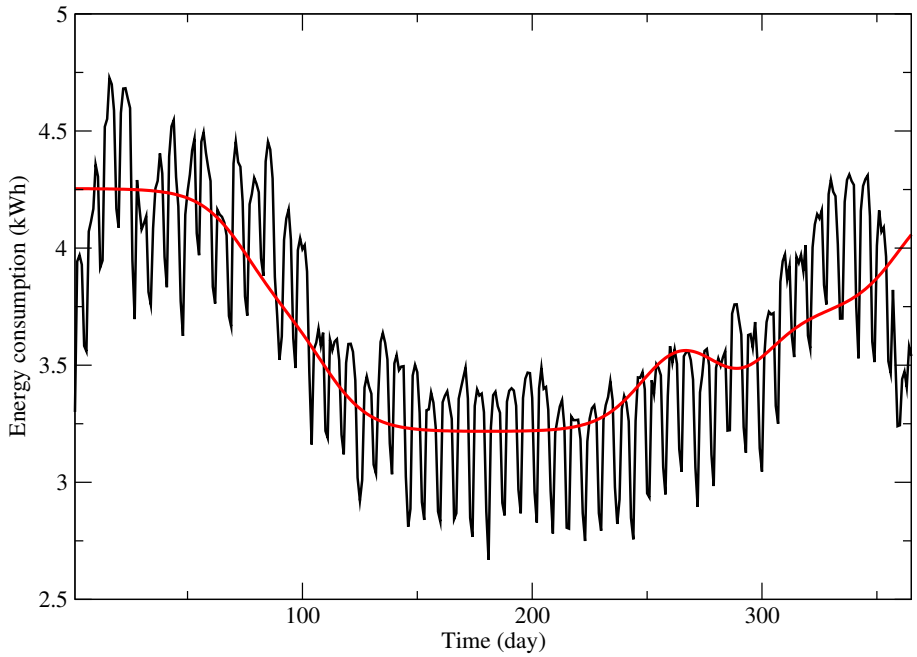

Figure 4.2: Modelled annual cycle profile (HTF-based) compared with the 2014 real energy demand datasets. Red curve: the modelled HTF annual profile, Black curve: 2014 real energy demand data.

Based on Fig. 4.2, the modelled HTF-curve fits relatively well in the distribution of the 2014 real energy demand datasets. Therefore, the HTF-modelled annual profile is applicable in presenting the annual trend that is similar to the real energy demand datasets.

Trend $D_i(t)$ in Eq. (3.1) is modelled according to typical electricity consumption patterns of different consumers with hourly resolution, using Eqs. (4.2) to (4.5):

$$D_1(t) = D_{\text{working\_family}}(t) = C_{1,1} + C_{2,1}\Big(-\tanh(t_b - 0) + \tanh(t_b - 5) - \tanh(t_b - 10) + \tanh(t_b - 16) + \tanh(t_b - 17) - \tanh(t_b - 20) - \tanh(t_b - 22)\Big). \tag{4.2}$$

$$D_2(t) = D_{\text{pensioner}}(t) = C_{1,2} + C_{2,2}\Big(-\tanh(t_b - 0) + \tanh(t_b - 5) - \tanh(t_b - 35)\Big). \tag{4.3}$$

$$D_3(t) = D_{\text{office}}(t) = C_{1,3} + C_{2,3}\Big(-\tanh(t_b - 0) + \tanh(t_b - 10) - \tanh(t_b - 17)\Big). \tag{4.4}$$

$$D_4(t) = D_{\text{industrial}}(t) = C_{1,4} + C_{2,4}\Big(-\tanh(t_b - 0) + \tanh(t_b - 8) + \tanh(t_b - 8) + \tanh(t_b - 12) - \tanh(t_b - 44)\Big). \tag{4.5}$$

The coefficients $C_{1,1}, C_{2,1}, C_{1,2}, C_{2,2}, ..., C_{1,4}, C_{2,4}$ in Eqs. (4.2) to (4.5) are the same as coefficients $C_{1,i}$ and $C_{2,i}$ with i indexes the consumers from Eq. (3.3). Similar to $A(t)$ estimations, the modelled $D_i(t)$ in Eqs. (4.2) to (4.5) is based on the HTF fitting with the 2014 real energy demand data from National Grid (2015). The results of the HTF fitting are shown in Table 4.2.

Table 4.2: HTF fitting of diurnal consumer profiles. SSE: Sum of squared errors of prediction; RMSE: Root mean squared error; Coefficients are computed with 95 % confidence interval.

Diurnal profile	Working family	Pensioner	Office	Industrial
Function type	HTF			
Model	$D_1(t)$ $(Eq.\ (4.2))$	$D_2(t)$ $(Eq.\ (4.3))$	$D_3(t)$ $(Eq.\ (4.4))$	$D_4(t)$ $(Eq.\ (4.5))$
Coefficients	$C_{1,1}$ = 7.62 (-1.62e7, 1.62e7)	$C_{1,2}$ = 7.68 (-1.82e7, 1.82e7)	$C_{1,3}$ = 13.92 (-3.02e7, 3.02e7)	$C_{1,4}$ = 17.68 (-2.23e7, 2.23e7)
	$C_{1,2}$ = 5.806 (4.54, 7.07)	$C_{2,2}$ = 0.73 (0.21, 1.08)	$C_{2,3}$ = 7.15 (5.78, 8.50)	$C_{2,4}$ = 0.62(0.19, 1.06)
Goodness of fits	SSE: 64.69 R-square: 0.95 Adjusted R-square: 0.94 RMSE: 1.27			

The illustrative plot of the HTF fitting of four diurnal profiles is shown in Fig. 4.3. The modeled HTF for four diurnal profiles fitted well with the 2014 real diurnal energy

demand datasets.

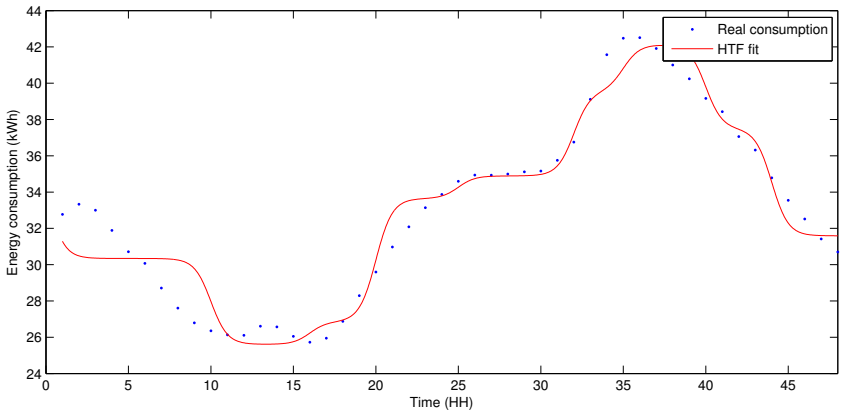

Figure 4.3: Diurnal cycle profile (HTF-based) compared with the 2014 diurnal real energy data.

The $D_i(t)$ plots for the four types of consumers (Eq. (4.2) – Eq. (4.5)) are shown in Fig. 4.4. It is assumed that for a working family the electricity consumption drops during work hours, whereas a pensioner would use heating for longer hours; the daytime office and one-shift day industrial consumption are modelled assuming shifts and heating demands but not 24/7 regime. When an enterprise runs on continuous shifts (operating day and night), their daily energy consumption is more or less constant, and there is no need to model its daily profile continuously (there is still need to model seasonal variability). This is why the continuous diurnal profile modelling is not considered here.

The resultant developed annual trend of energy consumption from Figs. 4.2 and 4.4 (the resultant $A(t)$ and $D_i(t)$) is shown in Fig. 4.5.

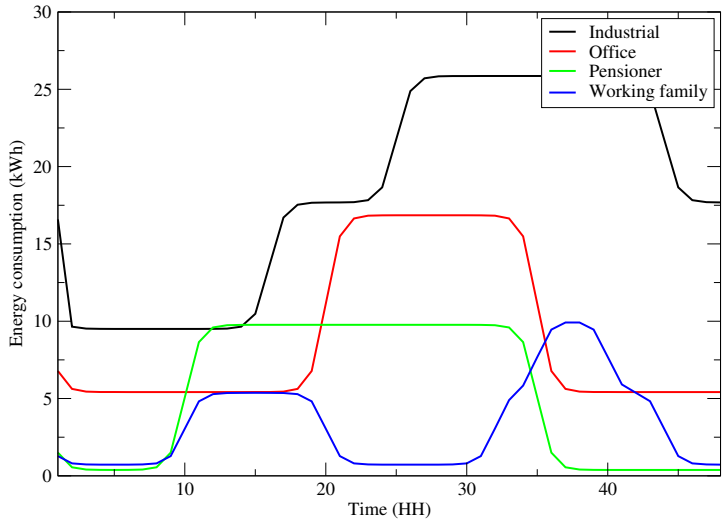

Figure 4.4: Diurnal energy consumption cycles.

A sample of randomly selected energy consumption data (days 200–260th) is shown in Fig. 4.6.

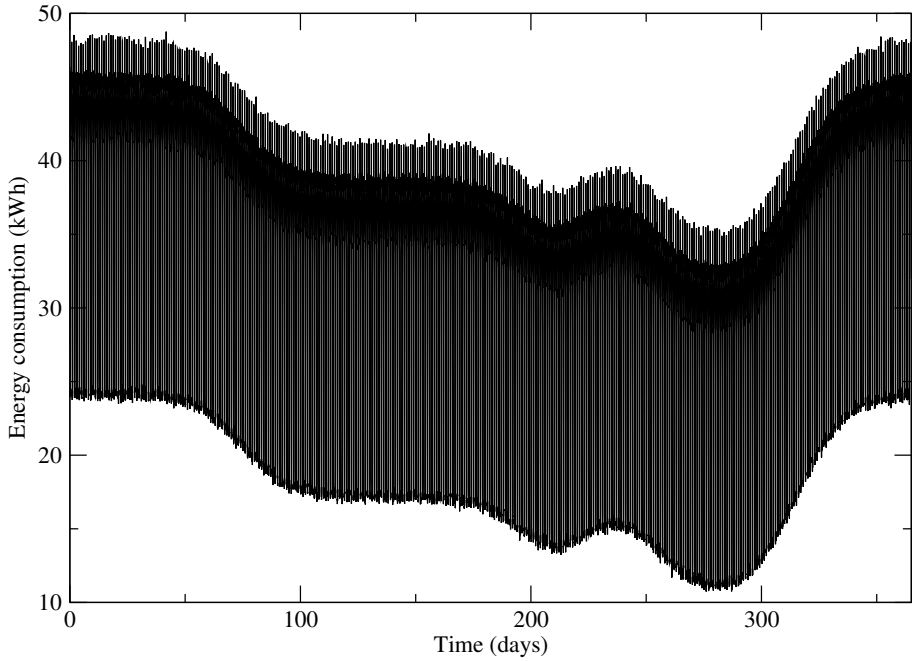

Figure 4.5: Annual trend with daily energy consumption of all consumers.

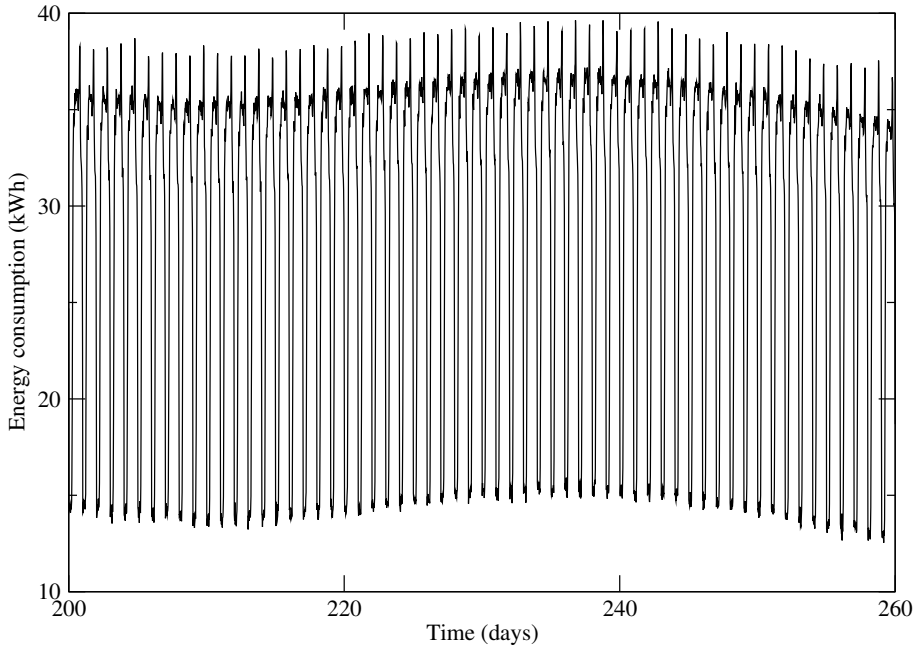

Figure 4.6: Randomly selected datasets of daily energy consumption from day 200th to 260th of all consumers.

4.1.1 Numerical quantification and estimation of carbon emissions

Using Eq. (3.10), the amount of carbon emissions within the HTF-profiled group of consumers are determined. The electricity grid carbon factor $G(t)$ in Eq. (3.10) is estimated using Eq. (3.7). Consumers in the same area that draw energy from the same grid segment will contribute carbon emissions in using the energy from the grid, where the grid has the electricity grid carbon factor.

A weekly plot of carbon emissions based on the four types of consumers is shown in Fig. 4.7.

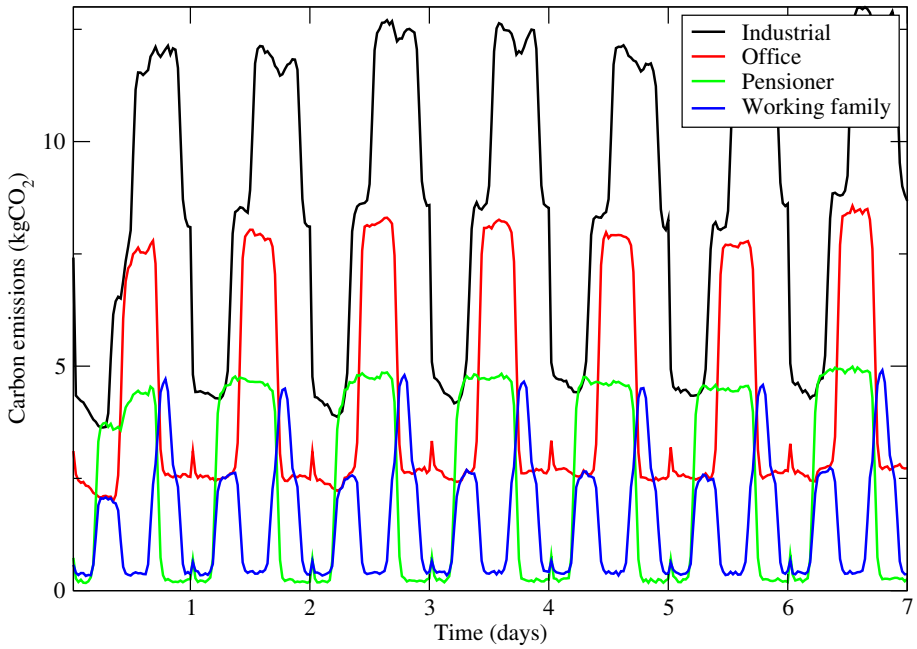

Figure 4.7: Weekly carbon emissions of four types of consumers.

Fig. 4.8 illustrates the cumulative function of carbon emissions corresponding to each type of electricity consumer. Overall, plots from Figs. 4.7 and 4.8 are useful for dynamical estimation of carbon emissions at any moment of the simulations. The one-shift day industrial factory has the highest carbon emissions, followed by daytime office, pensioner and lastly the working family group.

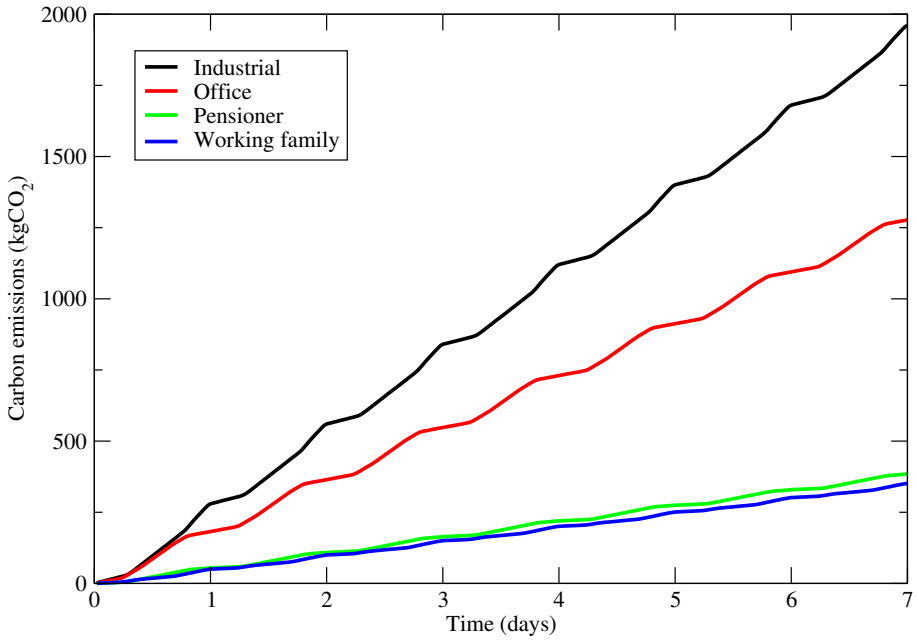

Figure 4.8: Cumulative carbon emissions of four types of electricity consumers.

4.1.2 Case studies

In this section, several real-world case studies are analysed.

4.1.2.1 Case study 1: Photovoltaic energy generation at Brunel University London

This case study implements a dynamic model for calculation of carbon emissions based on the PV electrical data generation obtained at Brunel University (dataset period 01/01/2012 - 31/12/2012). The PV data was recorded at 5-minute intervals. The base function $A(t)$ from the PV data replaces the seasonal trend of the dynamical model.

The PV data of the year 2012 is shown in Fig. 4.9, with top panel showing the temperature recordings, middle panel showing the solar radiation absorbed recordings (energy generated) and the bottom panel showing the computed cumulative plot of carbon emissions. It can be seen that PV generated a large amount of energy during summer, where the maximum amount of solar radiation is absorbed, as expected. It is necessary to stress, however, that this findings occurred during the particular case study. In general, the efficiency of PVs may be different, depending on climate and geographical conditions. A carbon factor of 0.075 $kgCO_2$/kWh representing the carbon factor for solar energy (based on LCA) is used in calculating carbon emissions (POSTnote 268, 2006; POSTnote 383, 2011). The total carbon emissions for the PV generation is approximately 7.20 tCO_2 in

the year 2012, as displayed in the bottom panel of Fig. 4.9.

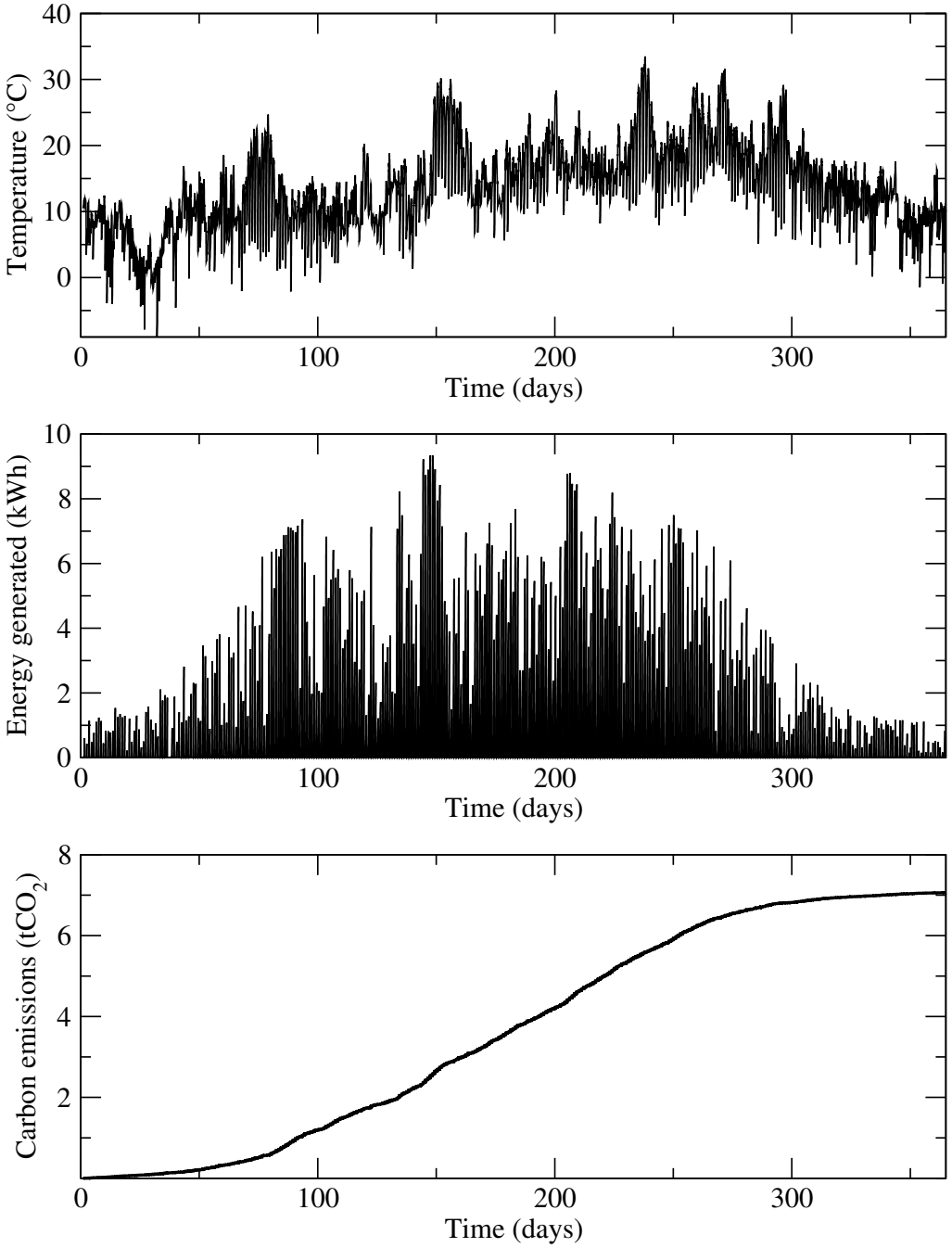

Figure 4.9: PV generation data at Brunel University, year 2012. Top panel: Recorded temperature recording data. Middle panel: Recorded energy generation data. Bottom panel: Computed cumulative carbon emissions.

A weekly plot of recorded PV generation data is shown in Fig. 4.10. Seven peaks of diurnal trends are visible, and they are very close to those given by the $D(t)$ implemented with an HTF function. HTF function may be successfully applied in this case to generate the PV data, providing good energy forecasts.

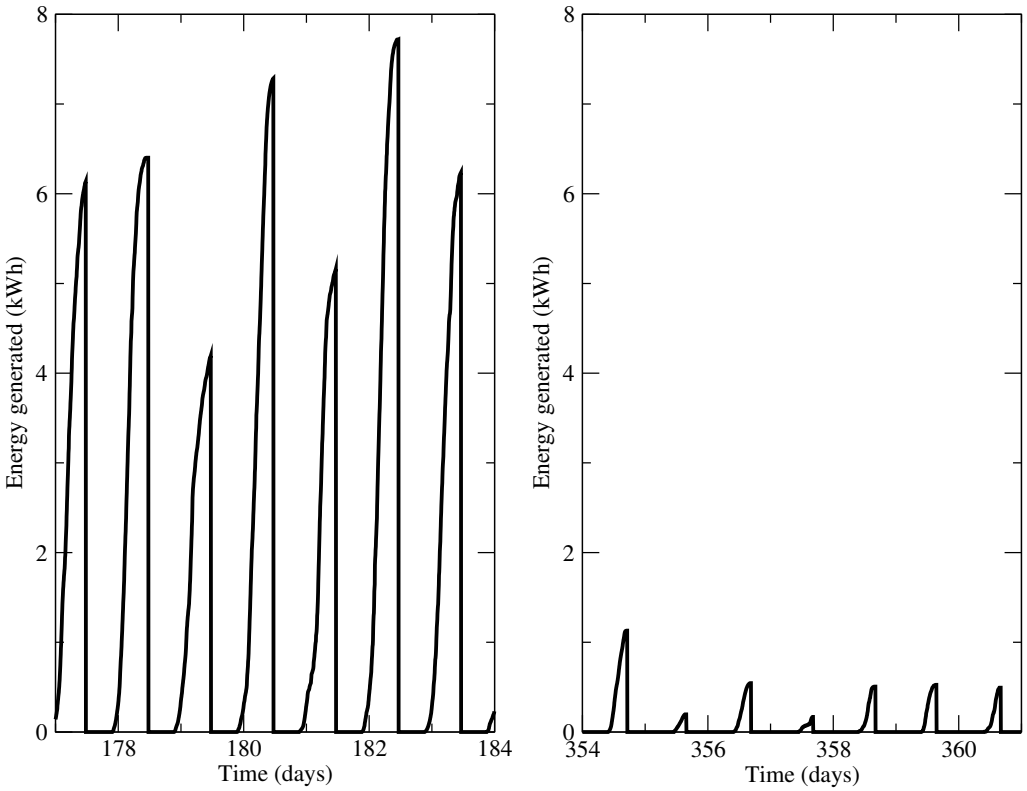

Figure 4.10: Weekly plots of recorded PV energy generation data in 2012. Left panel: summer period (26/06/12–03/07/12). Right panel: winter period (20/12/12–27/12/12)

4.1.2.2 Case study 2: The UK national aggregated data of electricity generation

The UK national data of electricity generation is provided by the National Grid market subsidiary Elexon, which aggregates data according to fuel types of the power stations. This allows one to estimate the nationwide carbon emissions generated by clusters of power stations using the same fuel to produce electricity: coal, gas, nuclear sources, renewables, etc. Four years of five minute data (from 01/01/2008 - 30/09/2012) are considered for further estimatations.

Table 4.3: Carbon emissions calculated for the Elexon datasets of fuel plants, 2008 – 2012.

Types of Energy	Carbon emissions (tCO_2)	Sample size, data points
COAL	6.00×10^6	482,562
CCGT	3.55×10^6	482,562
NUCLEAR	9.05×10^4	482,562
WIND	3.44×10^4	482,560
OIL	1.09×10^4	24,921
HYDRO	2.27×10^3	482,383

The results of carbon emissions for four year data corresponding to a particular energy

source are shown in Fig. 4.11. Due to the low availability of energy data obtained from the oil and OCGT plants, the HTF is difficult to apply to those energy profiles, although most of the other energy plots can be fitted with HTF. Periodic cycle trends in the coal, combined cycle gas turbine, nuclear and hydro plants demonstrate oscillations that can be well fitted with HTF. In contrast, the increasing trend of wind energy generation suggested that an exponential function better fits the distribution of wind plant than HTF. Also, wind energy generation is highly intermittent. Hence, the HTF is not suitable to fit the wind energy distribution.

Fig. 4.11 represents the data in semi-logarithmic plots for convenient comparison of different fuel types of power stations: their production differs by orders of magnitude between fuel types 2008 to 2012. One can see that the main part of electric energy in the UK is produced by gas (CCGT) and coal plants, which also generate most of the carbon emissions. The low carbon emissions of nuclear energy plants are calculated without taking into account the background emissions (like construction of concrete installations): only those directly emitted from this type of fuel are taken into account.

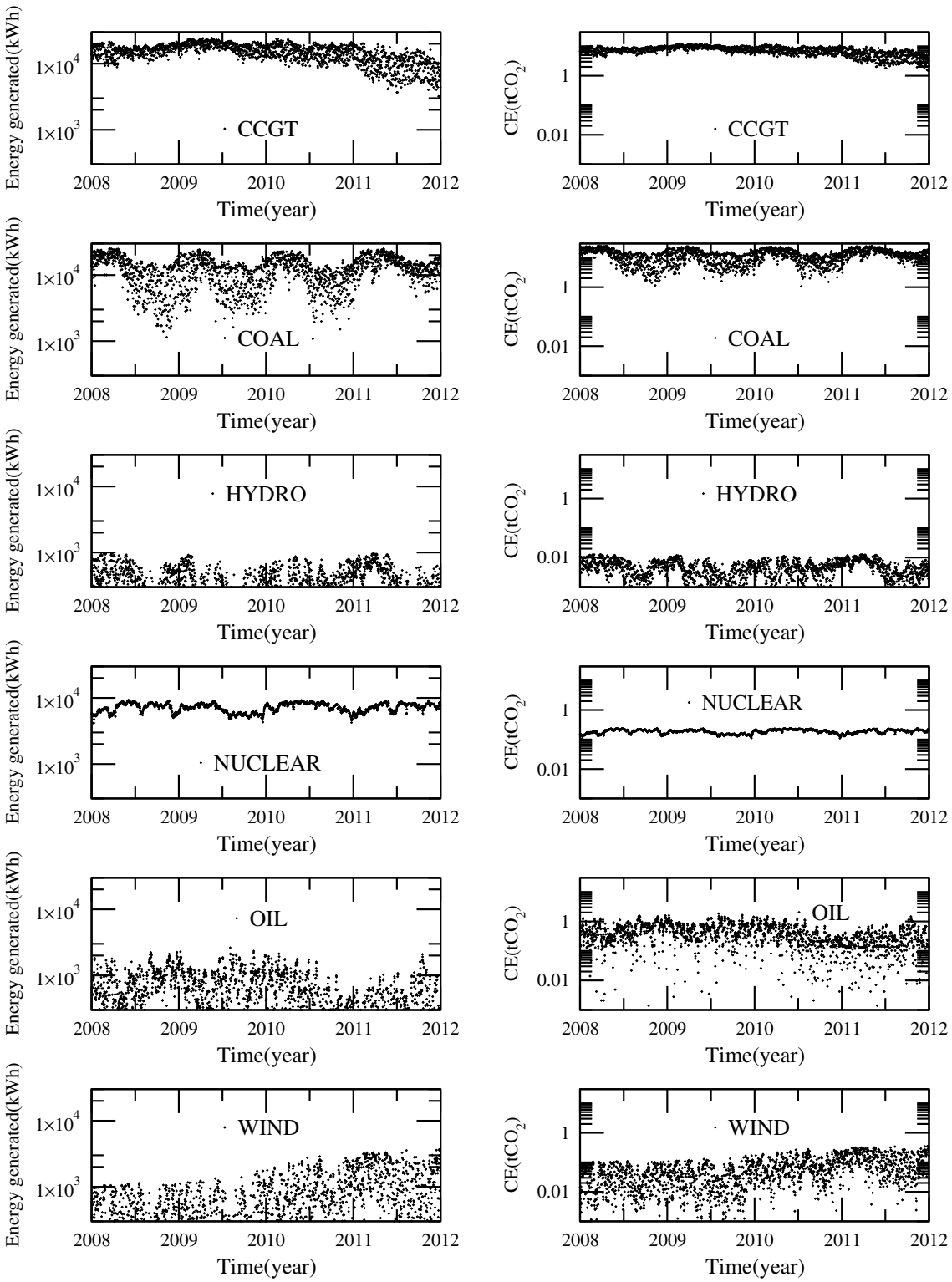

Figure 4.11: Semi-logarithmic plot of carbon emissions (CE) of energy plant from 2008 to 2012.

4.1.2.3 Case study 3: Irish smart grid pilot project

This case study represents the estimation of carbon emissions based on Irish smart grid data. The data was recorded in every 30 minutes (in kWh). 541 days of data in total were considered (dataset period 01/01/2009 - 25/06/2010). Total of 72 samples (53 residents and 19 SMEs) were selected. The example of the data of a resident and a small & medium enterprise (SME) are shown in Fig. 4.12.

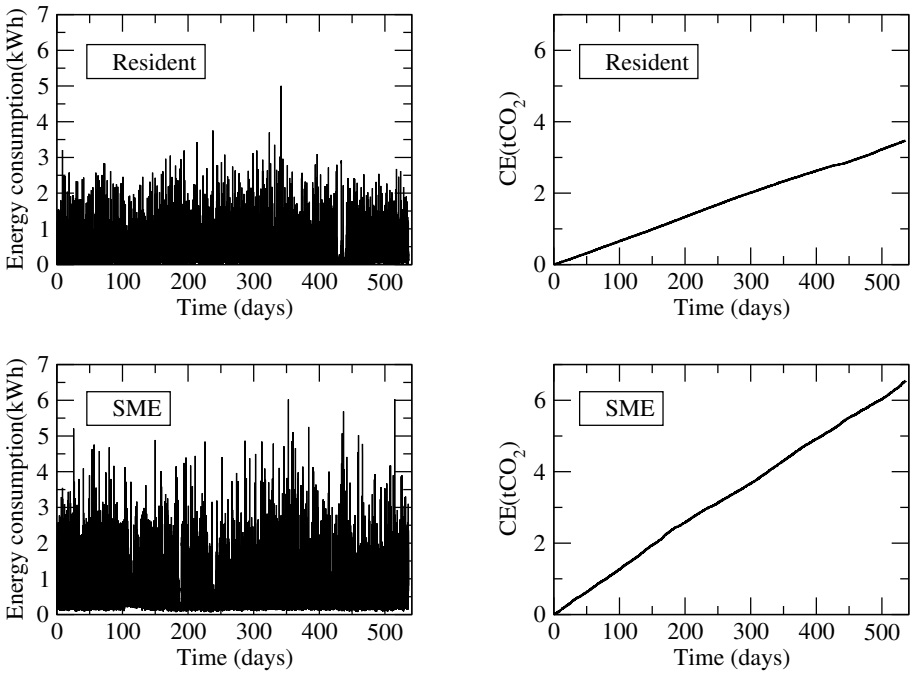

Figure 4.12: Electricity consumed by a resident and an SME. Left panel: energy consumption. Right panel: cumulative carbon emissions (CE).

The cumulative carbon emissions for participating households and SMEs are shown in the right panels of Fig. 4.12. Based on this figure, one can conclude that the amount of carbon emissions by SMEs are higher than for regular residents, with similar gradual dynamics. The electricity consumption, however, does not show clear periodical oscillation trends.

A weekly plot of the resident and a small & medium enterprise (SME) are shown in Fig. 4.13. The plot shows periodic trends of electricity consumption and HTF can be useful to model these data. Even though the overall electricity consumption trends are not similar to $A(t)$, the diurnal trends are very similar to $D_i(t)$ in the dynamic model. This means that the HTF function is useful in generating energy data and predicting the usage of grid electricity in the short-term range (with the addition of model noises to quantify

different electrical usages).

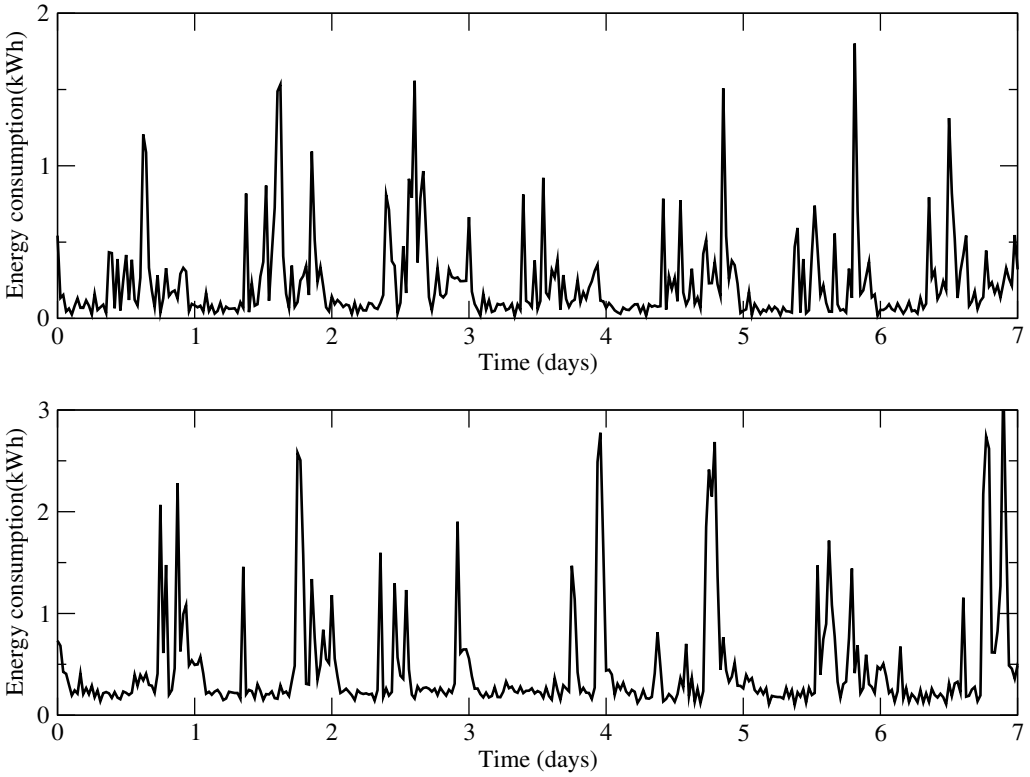

Figure 4.13: Weekly plot of electricity consumed by a resident (top panel) and an SME (bottom panel).

4.1.2.4 Case study 4: The UK's distribution network operator pilot project

The UK's Distribution Network Operator (DNO) case study is considered for calculation of carbon emissions based on a number of substations in the UK. Loads in substations are recorded. The data includes ten minute average values of active and reactive power. For simplicity, only HH values of data are considered in the case study.

For each substation ID data, carbon emissions are computed by the multiplication of the HH electricity grid carbon factor (2012-2013) and HH energy from the substations. Each substation has different start and end date terms of operations (substation failure, idle mode or incomplete records). Therefore, each substation has to be analysed with the electricity grid carbon factor in order to compute the carbon emissions accurately. The monitored data in this case study is summarised in table Table 4.4.

The detailed explanation of profile classes (PC) of consumers is available in the Elexon website (Balancing and Settlement Code, 2008). The estimated annual consumptions

Table 4.4: Parameters of monitored substations data.

Main parameters	Profile Class (PC)
Substation identifier (number)	PC1 – NHH domestic unrestricted (single rate)
Date & time of reading	PC2 – NHH domestic economy 7 (two rate)
Real power average value (kW)	PC3 – NHH non-domestic unrestricted (single rate)
	PC4 – NHH non-domestic non-maximum demand economy 7 type
	PC5 – NHH non-domestic maximum demand (MD) recording capability and with load Factor (LF)$\leq$20 %
	PC6 – NHH non-domestic MD recording capability and with LF 20-30 %
	PC7 – NHH non-domestic MD recording capability and with LF 30-40 %
	PC8 – NHH non-domestic MD recording capability and with LF >40 %
	PC0 – HH metered consumers

(EAC) for all PCs in Table 4.4 are summed (in kWh) and multiplied by the average electricity carbon factor in order to obtain the annual carbon emissions for all PCs. Note that EACs are mainly the non half-hourly (NHH) metered consumers. The measured annual load at substations is compared with the sum of NHH EACs plus the total HH metered customers, as follows:

$$P = \frac{\text{Annual\_Load}}{\text{NHH\_EAC} + \text{total\_HH}} \tag{4.6}$$

All substations are grouped into eight main types according to similarity within types. This allows identification of the highest amount of carbon emissions within types, besides obtaining the clear pattern of grouping by substations. For instance, the 'Type 1' substations are grouped mainly for domestic customers. Note that 'Type 1 – Type 7' are mixed NHH and HH metered consumers. On the other hand, 'Type_HH' refers to HH metered consumers only. Eight groups of electrical consumers according to each profile type are shown in Table 4.5.

Two substations (with IDs 'no.1' and 'no.2', real substation IDs are represented by numbers for anonymity purpose) are analysed, and the overall results are shown in Table 4.6, with 'no.1' having the highest emissions in both energy delivered and the EACs.

Example plots of energy delivered corresponding to substations are shown in Figs. 4.14

Table 4.5: Eight groups of electricity consumers according to each profile type.

Profile type	PCs involved in each type
Type 1	PC1, PC2
Type 2	PC3, PC4
Type 3	PC5, PC6, PC7, PC8
Type 4	PC1, PC2, PC3, PC4
Type 5	PC1, PC2, PC5, PC6, PC7, PC8
Type 6	PC3, PC4, PC5, PC6, PC7, PC8
Type 7	PC1, PC2, PC3, PC4, PC5, PC6, PC7, PC8 (Real Power is delivered by the substation and is used by all PC consumers
Type_HH	HH metered consumers

Table 4.6: The amount of carbon emissions for substation IDs 'no.1' and 'no.2' from 'Type 7' profile.

Profile type	Substation ID	Carbon emissions based on:		
		Energy delivered (tCO_2)	EACs (tCO_2)	Total HH (tCO_2)
Type 7	no.1	409.68	1888.24	0
	no.2	203.33	883.95	0

and 4.15. It is shown that electricity consumption visibly drops around the Christmas breaks. There is also some anomaly in electricity consumption, particularly in Fig. 4.15, which may be due to regime change or maintenance conditions. The dips in load during Christmas from Figs. 4.14 and 4.15 are consistent with the year 2011 – 2014 generation data from the portal (BMRS, 2015; Elexon, 2015). Plots of energy generation data of year 2011 – 2014 are shown in Fig. 4.16.

Overall, the energy delivered shows periodical oscillation trends. Hence, HTF can be applied to model these data assuming that there is no significant change in the trend (abrupt nonlinearities, etc). Using Eq. (4.6), 88 sample of measured data are analysed (full simulation results are available in Appendix A), with the total of EACs and total HH metered data being within $\pm$ 15 % of the measured annual load. Out of 88 samples of substations, 77 samples of substations have performance P within $\pm$ 15 % of the measured annual load Eq. (4.6). This indicates the capability of the DNO in maintaining the loads with respect to the required annual load. The results of the carbon emissions according to each category (real energy generated, EAC and HH) for types 'Type 1 – Type_HH' consumers are presented in Appendix A.

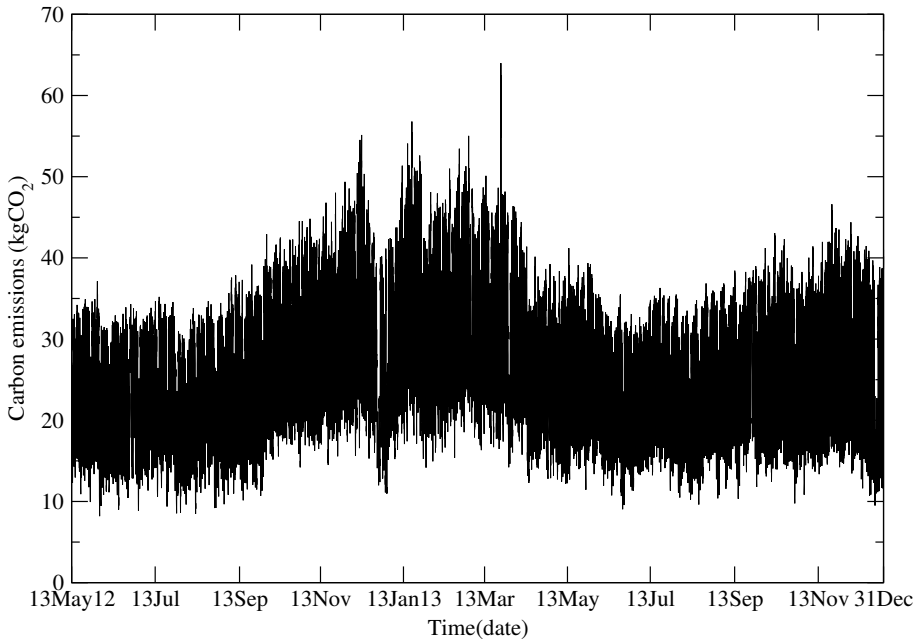

Figure 4.14: Carbon emissions of energy delivered to substation no.1.

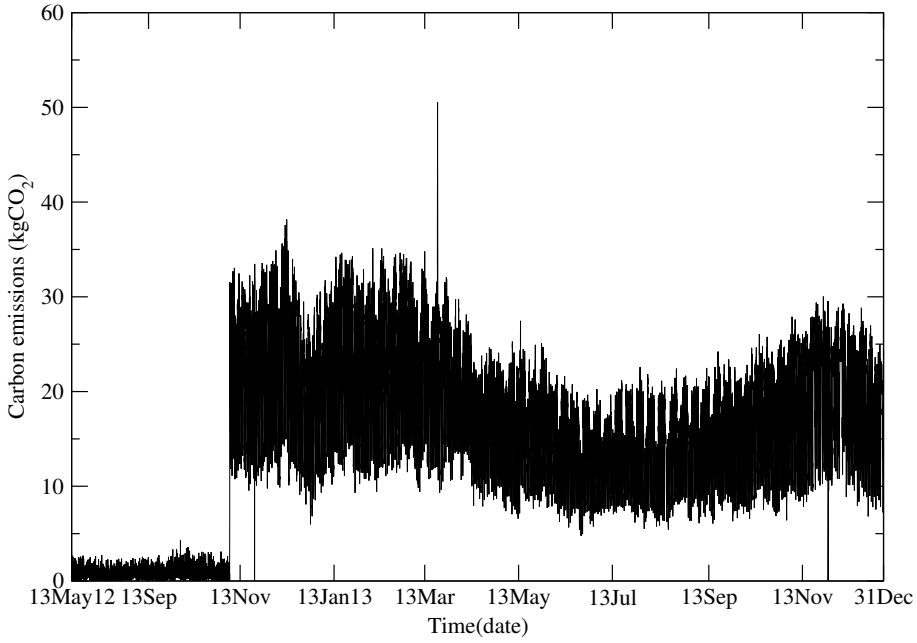

Figure 4.15: Carbon emissions of energy delivered to substation no.2.

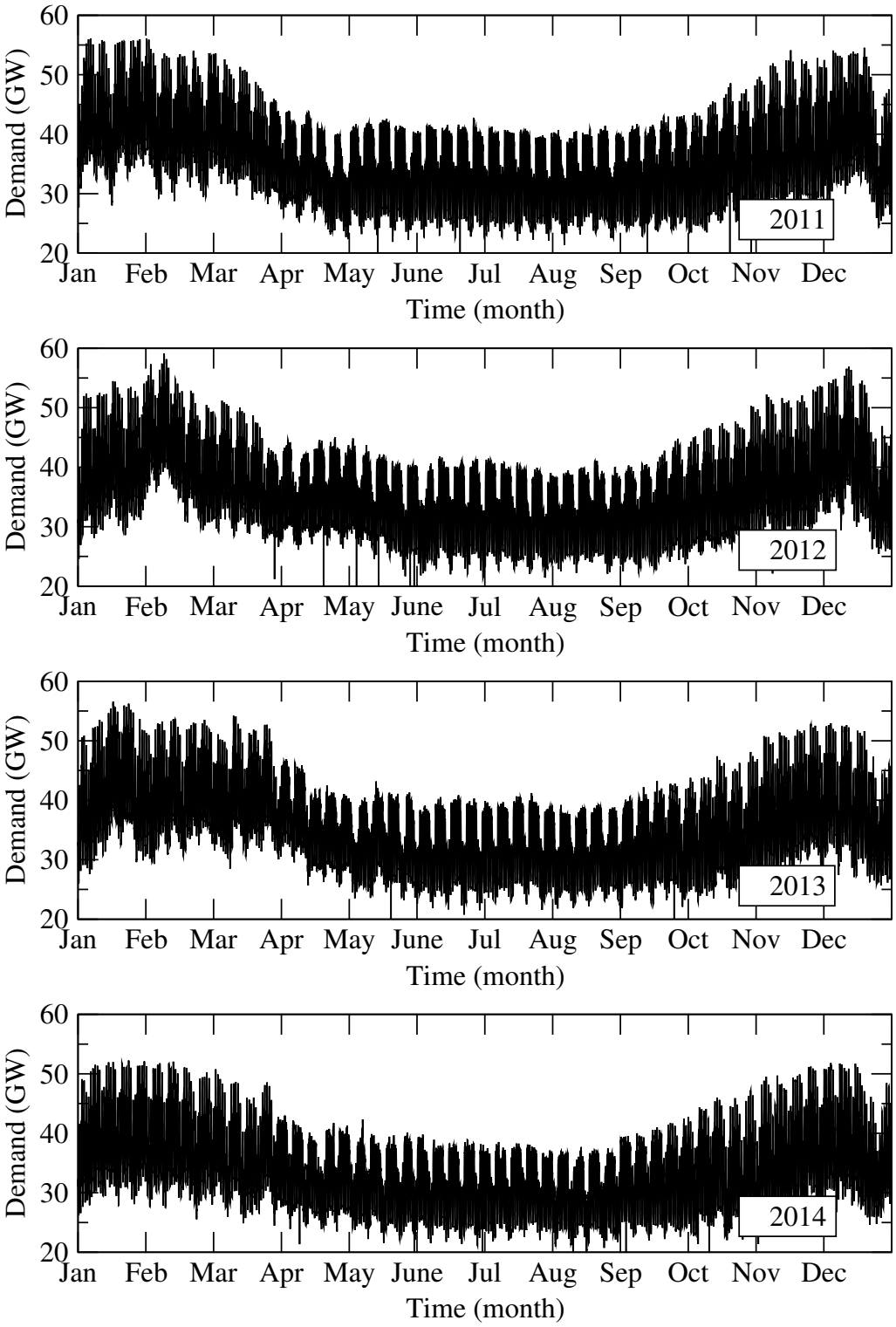

Figure 4.16: Power generation data of the year: 2011 (Top panel); 2012 (Second panel); 2013 (Third panel); 2014 (Bottom panel).

4.2 Numerical estimation of the UK electricity grid carbon factor

The 2014 UK electricity grid carbon factor is estimated using the publicly available data from the portal (BMRS, 2015; Elexon, 2015). Similar to Fig. 4.11, Fig. 4.17 represents the data in semi-logarithmic plots for different fuel types of power stations in 2014, with fuel production varying by orders of magnitude.

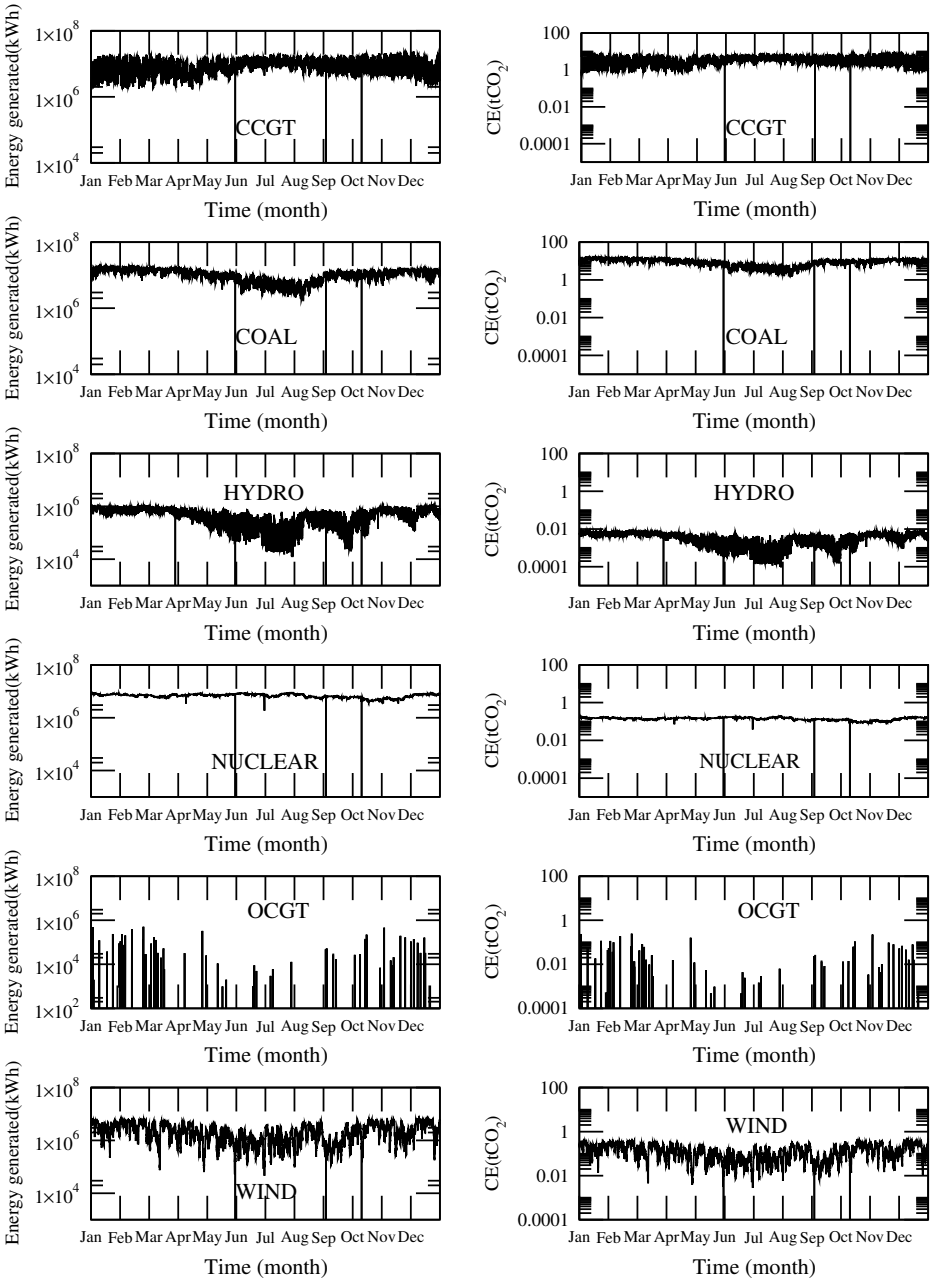

Figure 4.17: Semi-logarithmic plot of carbon emissions (CE) for power plant in 2014.

One can see that the main difference between Fig. 4.11 and Fig. 4.17 is that the OCGT replaces the conventional oil fuel. Additionally, the amount of fuel generations in 2014 are higher than previous years. Moreover, the penetration of wind energy in the UK market is very large in 2014. Hence it can be deduced that there is currently large deployment of wind farms in providing greener energy; the high usage of CCGT plants suggests the need to balance the wind output, in case of the intermittency in wind generation.

By using the available datasets (Fig. 4.17) and using the variable grid carbon factor formula from Eq. (3.7), the electricity grid carbon factor of the year 2014 can be determined. It is shown in Fig. 4.18.

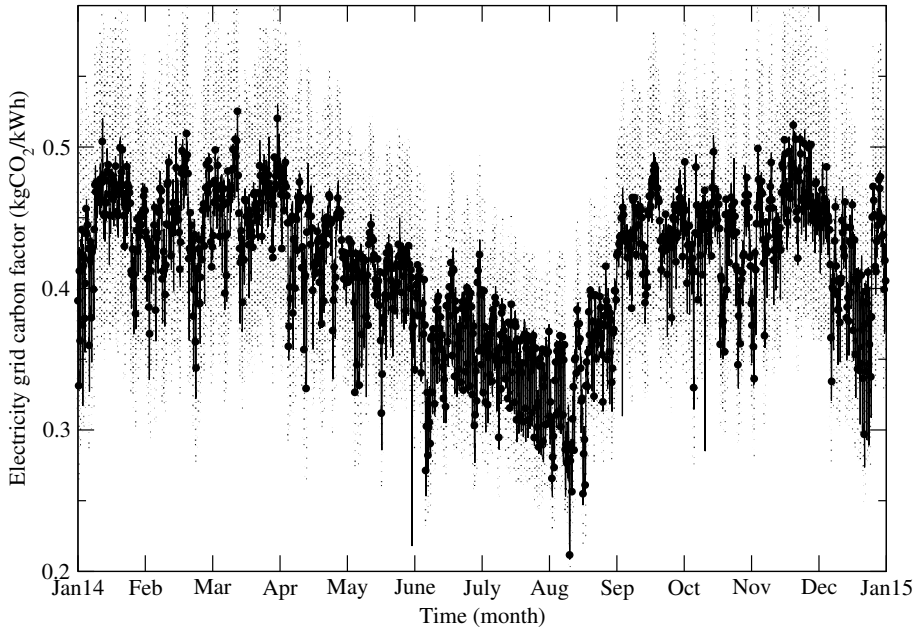

Figure 4.18: Electricity grid carbon factor ($kgCO_2$/kWh) with uncertainties for 2014.

The shaded lines in Fig. 4.18 indicate the uncertainty range based on the fuel mix. One can see that during the summer season, the carbon factor is lower than in the winter period (from December to March). This reflects the fact that more energy is produced during the winter period to satisfy the higher demand (winter heating and lighting), thus increasing carbon emissions. Also, in the winter season, photovoltaic energy generation drops, which reduces the green power contribution in the national energy mix.

The mean value of the average grid carbon factor for 2014 (based on Eq. (3.7)) is determined as 0.416 ± 0.150 $kgCO_2$/kWh. This value is lower than the 2013 electricity grid carbon factor, which is estimated as 0.455 ± 0.180 $kgCO_2$/kWh. One can expect it to decrease in future, when the smart interventions would inevitably make the grid greener.

Table 4.7 shows the carbon emissions for each type of energy source in 2014. One can see that coal contributes the highest amount of carbon emissions in the UK. In contrast, OCGT plants contribute the smallest amount of carbon emissions due to the low usage of this type. OCGT plants are usually expensive in providing electricity as the fuel price per generation is high. However, due to the capability of fast load generation, OCGT plants are often used as peaking plants only in providing reserving or contingency energy.

Additionally, it is also the main interest in tabulating the fuel generation in terms of percentage of fuel mixes. Table 4.8 shows the percentage of fuel mixes of individual fuels in 2013 and 2014. The fuel data is available at the Elexon portal.

Table 4.7: Carbon emissions of different fuel types of generators in 2014.

Types of Energy	Carbon emissions ($ktCO_2$)
COAL	1.62×10^7
CCGT	6.61×10^5
NUCLEAR	2.46×10^3
WIND	2.55×10^3
OCGT	6.20×10^{-3}
HYDRO	6.00×10^{-2}

Table 4.8: Percentage of fuel mixes according to different types of generators in 2013 and 2014.

Types of fuel	Percentage fuel mix (%)	
	Year 2013	Year 2014
Coal	35.80	39.66
CCGT	23.11	24.02
Nuclear	21.48	21.57
Wind	6.95	6.02
OCGT	0.02	0.01
Hydro	1.15	0.89
PS	0.08	0.08
Oil	0	0.01
Interconnector	6.64	5.84
Other	1.34	1.21

Six independent days with percentage fuel mixes are evaluated at every 50th day (days 50, 100, 150, 200, 250 and 300) for years of 2013 and 2014, which are demonstrated in Fig. 4.19 and Fig. 4.20 correspondingly.

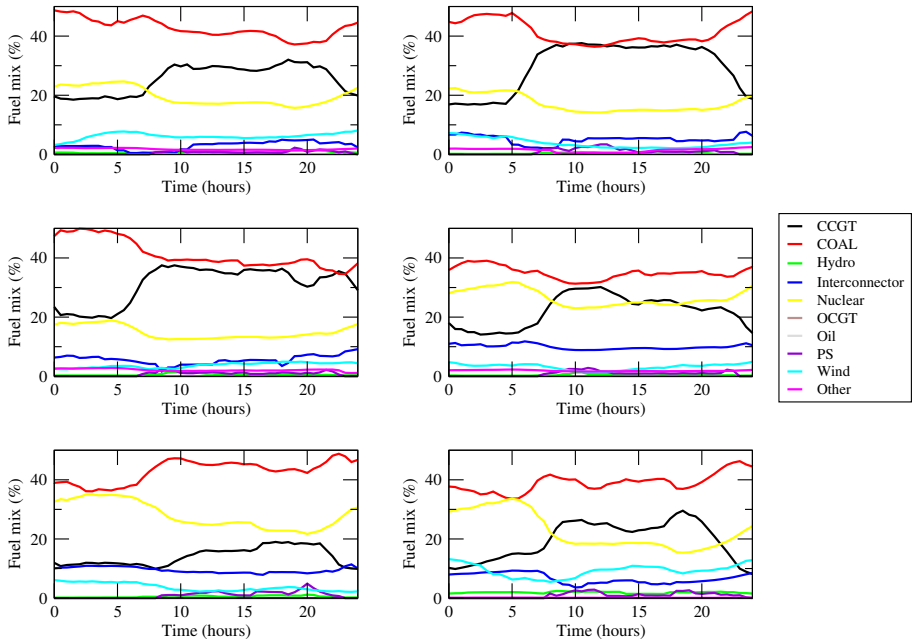

Figure 4.19: Six independent days of the percentage of fuel mixes in 2013. Top left: day 50th, top right: day 100th, middle left: day 150th, middle right, day 200th, bottom left: day 250th, bottom right: day 300th.

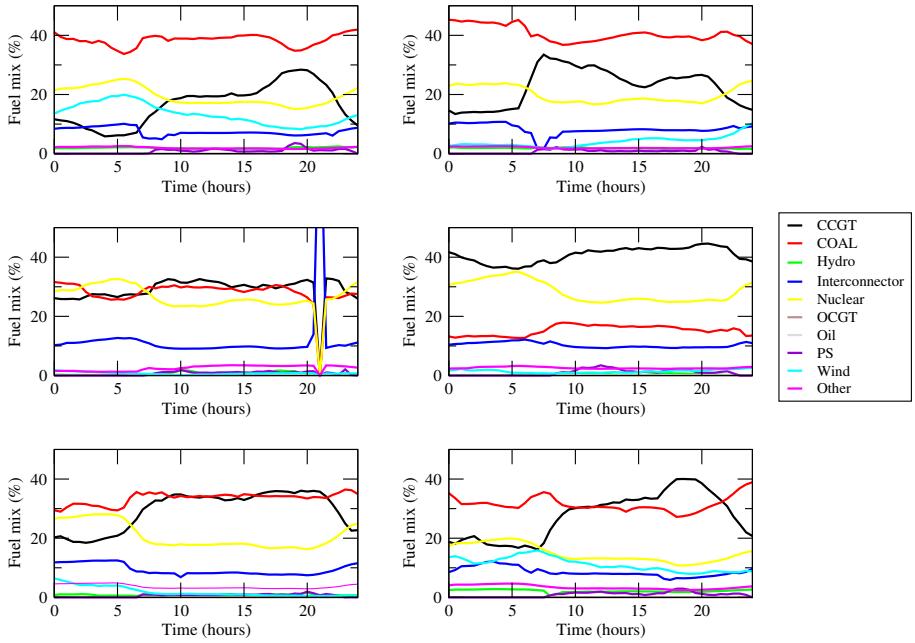

Figure 4.20: Six independent days of the percentage of fuel mixes in 2014. Top left: day 50th, top right: day 100th, middle left: day 150th, middle right, day 200th, bottom left: day 250th, bottom right: day 300th.

Based on Figs. 4.19 and 4.20, the coal and nuclear plant seem to be running base-loaded, and the amount of fuel mix stays relatively constant throughout the day. On the other hand, the CCGT plant provides much of the generation during the daytime and

maintained at low level during the off-peak period (midnight). Similarly, the pumped-storage plant only provides electricity during the daytime and switched-off (no fuel mixes) during the off-peak period. The wind power provides a relatively stable generation throughout the day. The oil plant contributes the lowest amount of generation in both 2013 and 2014. Additionally, the middle left panel (day 150th) of Fig. 4.20 suggests that the UK grid system experienced a problem (in the form of technical fault, system operator failure or security failure). All power plants are not operating at that moment and henceforth the import of power through the interconnector is acquired.

The electricity grid carbon factors for days 50, 100, 150th, 200, 250 and 300 of the years 2013 and 2014 are shown in Table 4.9.

Table 4.9: Electricity grid carbon factors for days 50, 100, 150, 200, 250 and 300 of the years 2013 and 2014.

Day	Electricity grid carbon factor ($kgCO_2/kWh$)	
	Year 2013	Year 2014
50	0.483 ± 0.192	0.429 ± 0.170
100	0.487 ± 0.190	0.467 ± 0.162
150	0.495 ± 0.188	0.395 ± 0.134
200	0.420 ± 0.158	0.331 ± 0.102
250	0.445 ± 0.192	0.445 ± 0.156
300	0.430 ± 0.176	0.421 ± 0.146

The annual percentage fuel mixes from Figs. 4.19 and 4.20 are shown in Fig. 4.21.

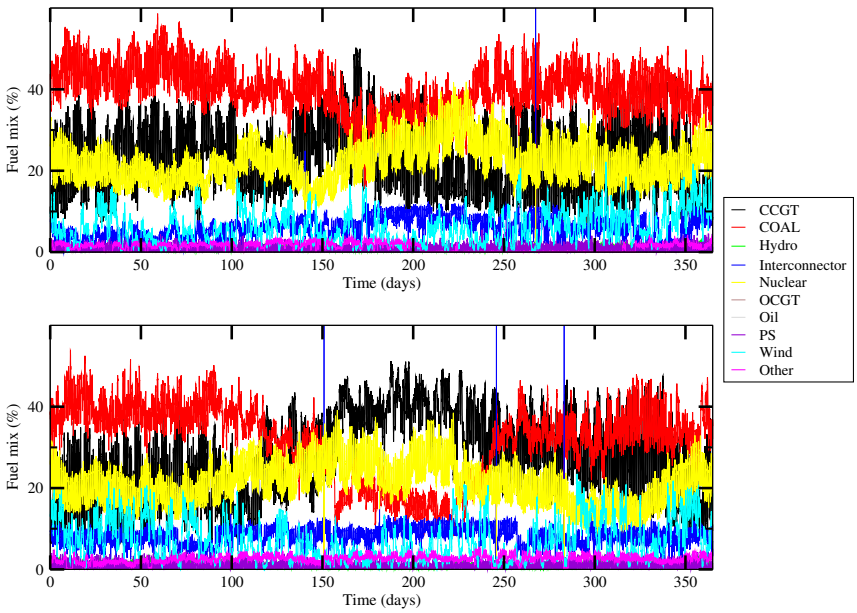

Figure 4.21: The annual percentage fuel mixes. Top panel: 2013, bottom panel: 2014.

4.3 EnKF and EnOpt numerical simulations

In this section, the results of EnKF and EnOpt simulations are presented. The simulation begins with the EnKF that forecasts and performs data assimilation of energy consumption and generation. EnOpt algorithm performs numerical optimisation based on the assimilated energy data through the EnKF algorithm. The two scenarios are developed: a) Optimisation of carbon savings in groups of consumers; b) Optimisation of costs based on the ED problem. EnKF and EnOpt simulations are performed using Matlab.

4.3.1 Energy consumption data assimilation using EnKF and numerical optimisation of carbon savings using EnOpt

4.3.1.1 EnKF simulations

The simulations involve short-term forecasting and assimilation of the energy consumption using EnKF. Four main profiles of electricity consumers (working families, pensioners, daytime offices and one-day-shift industrial estates) with Eq. (4.2) – Eq. (4.5) are considered. Using modelled profile of $A(t)$ from Eq. (4.1), combined HTF functions from Eq. (3.1) are formed with different profiles of $D_i(t)$, with total number of 100 consumers (N_i = 100). Samples of consumers are: 40 working families, 50 pensioners, 5 daytime offices and 5 one-day-shift industrial estates. They are created individually with the addition of model noises in order to reflect forecast energy usages among groups (some variations of energy usages within the same group).

The *priori* ensemble y_j^p is created using Eqs. (3.45) and (3.46), where $j = 1, 2, ..., N_e$ is the ensemble member index and N_e is the total number of ensemble member. The initial ensemble members of y^p are drawn from a normal distribution with the mean and standard deviation $N(0, 20)$. Additionally, the model (process) error w is sampled from $w \sim N(0, 1)$. The measurement error, on the other hand, is sampled from $v \sim N(0, 0.5)$.

In the EnKF, the perturbed observation of energy data $d_{\text{obs},j}$ is based on the model prediction d using Eq. (3.36). Different realisations are created (N_e = 10, 100, 1000) and propagated at every time steps. The ensemble in matrix Y^p (Eqs. (3.45) and (3.46)) is the collection of the *priori* ensemble y_j^p, which is assimilated and updated to form the *posteriori* ensemble (y_j^u) using Eq. (3.47). The y_j^u is further stored in the matrix Y^u. The

ensemble means of the energy consumption with different realisations N_e are computed that allow comparison of the convergence in relation to the actual observations from the model simulator. The actual observations are obtained through the ensemble mean of the perturbed observations $\overline{d_{\text{obs},N_e}}$ at $\overline{d_{\text{obs},10}}, \overline{d_{\text{obs},100}}$ and $\overline{d_{\text{obs},1000}}$.

The diurnal plot with datasets of the actual energy consumption and propagation of Y^u with different ensemble sizes is shown in Fig. 4.22. The figure shows that the larger the ensemble size, the better Y^u estimation converges towards the actual observation of the energy consumption data.

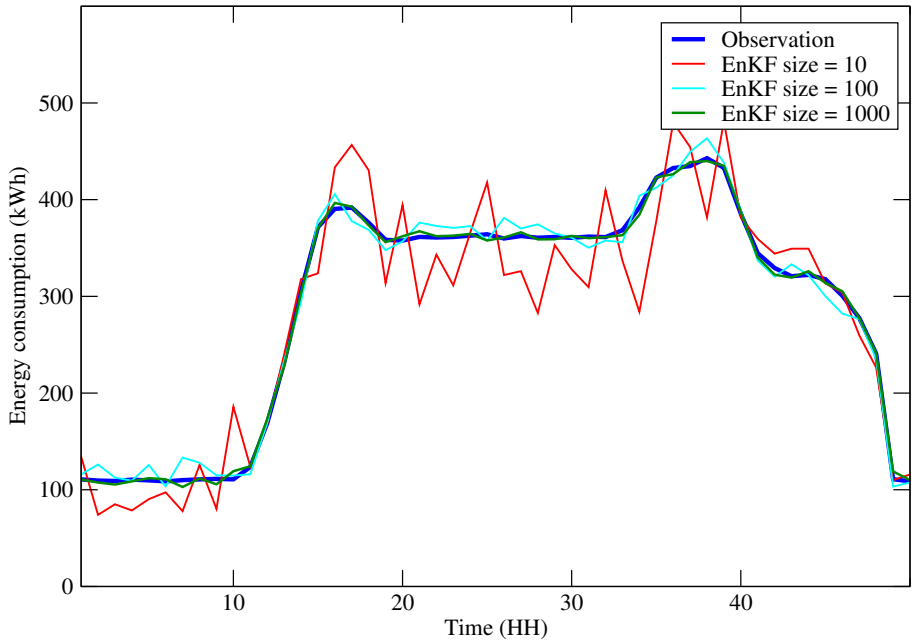

Figure 4.22: Diurnal energy consumption of consumers with different EnKF realisations.

To show the extended one-week plot of actual observation of energy consumption and propagation of Y^u with different ensemble sizes, results are plotted in Fig. 4.23. The figure also reflects that the larger the ensemble size, the better Y^u estimation converges towards the actual energy consumption data.

In order to examine the robustness of EnKF in forecasting the electricity consumption, the sample (a working family) is considered and further evaluated. Similar plots, as in Figs. 4.22 and 4.23, show diurnal and one-week EnKF'ed and observational data of energy consumption for a working family in Figs. 4.24 and 4.25 respectively. The plotted results demonstrate the robustness of EnKF in matching energy consumption with observational data, either in real-time or based on prior knowledge and historical records. However, this can only be accomplished if ensemble sizes are large.

The convergence of EnKF can be also obtained based on the covariance matrix C in Eq. (3.50). An example of the distribution of C is illustrated in Fig. 4.26. Different behaviour of C is due to the different ensemble realisations (N_e = 2, 10, 50, 100). Values of C become stabilised with less oscillations (which indicates smaller model errors) when the ensemble size of the EnKF simulations becomes larger.

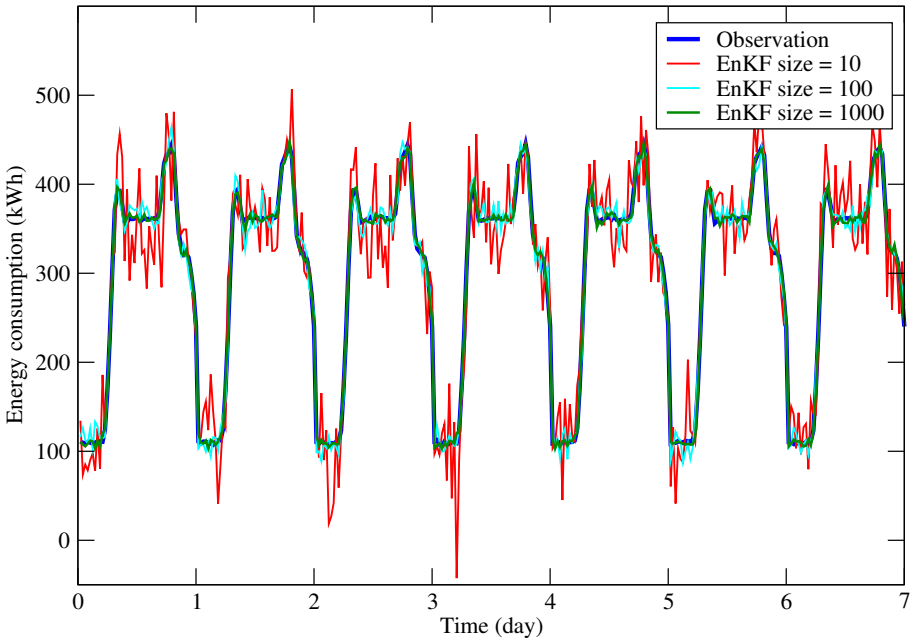

Figure 4.23: One-week energy consumption of consumers with different EnKF realisations.

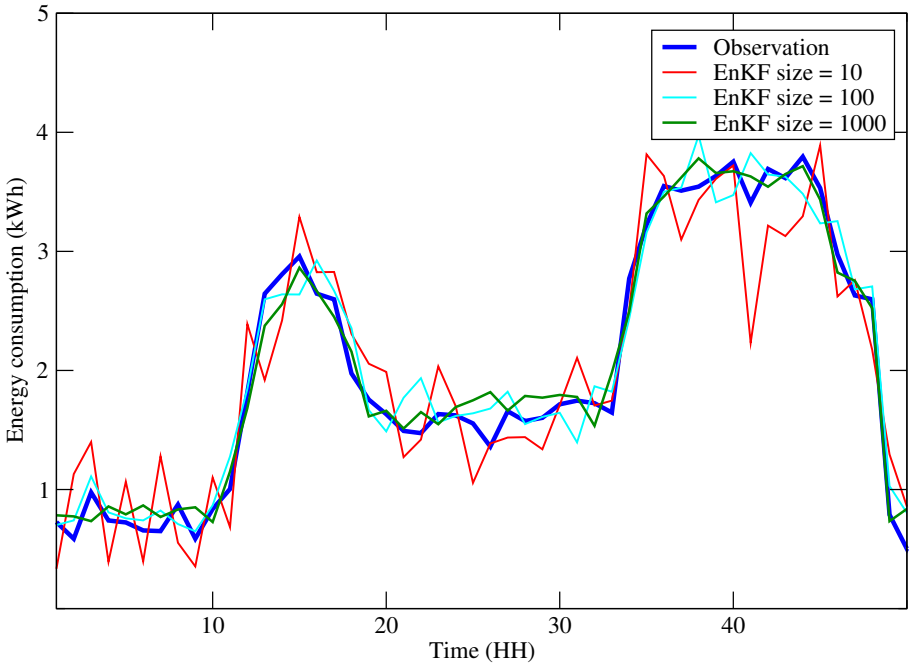

Figure 4.24: Diurnal energy consumption of a working family with different EnKF realisations.

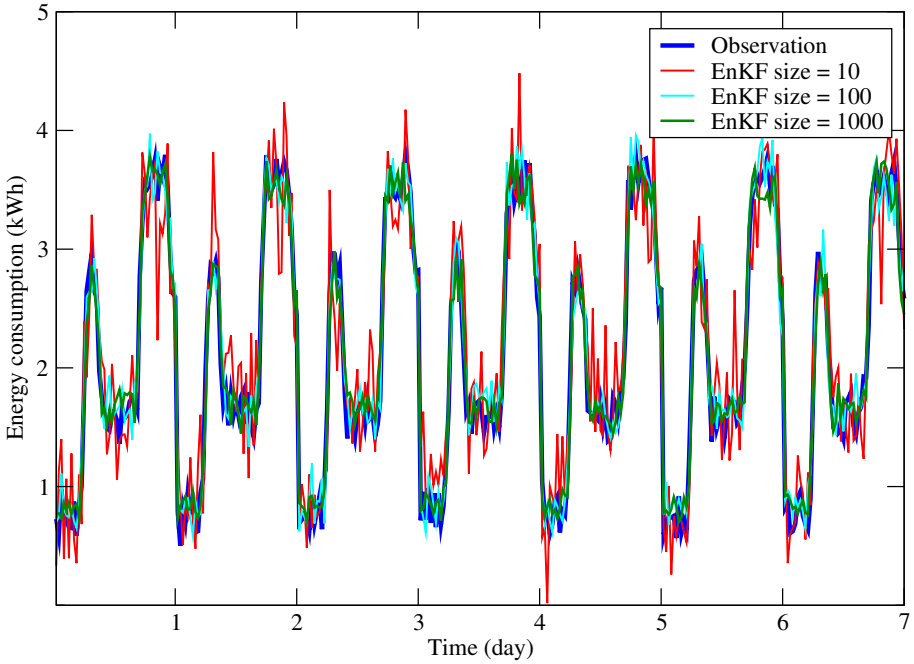

Figure 4.25: One-week energy consumption of a working family with different EnKF realisations.

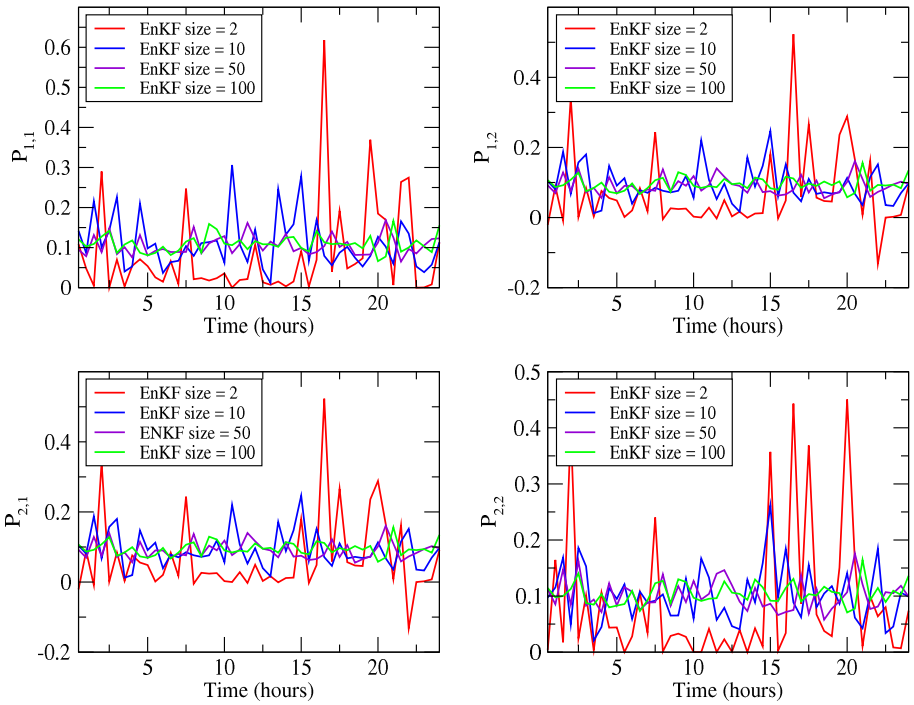

Figure 4.26: Covariance matrices $P_{1,1}$, $P_{1,2}$, $P_{2,1}$ and $P_{2,2}$ (see Eq. (3.50)) for different states of consumers.

4.3.1.2 EnOpt simulations

The matrix Y^u is the stored *posteriori* ensemble (y_j^u) from Eq. (3.47), which is further used in the EnOpt algorithm. Y^u presents the assimilated ensemble estimates that allows the production optimisation to be performed in EnOpt. Y^u stays constant during the EnOpt process at a particular time step. Optimisation of carbon savings is performed using the objective function from Eq. (3.54) along with the optimisation of energy control variables $\mathbf{x}$ in Eq. (3.53)). The optimisation of Eq. (3.54) is subject to control constraints from Eq. (3.13). The initial realisations of control vector $\mathbf{x}$ are generated through the mean of the sampled lower and upper bounds of the energy consumption. The mean of $\mathbf{x}$ is further perturbed with Gaussian random numbers with $N \sim (0, 0.5)$. The components of $\mathbf{x}$ are the energy consumption/demand output to be optimised that integrate with Y^u in regulating the amount of energy consumption. Total number of 100 consumers are considered. The time frame for the optimisation of carbon savings is 24 hours and vector $\mathbf{x}$ is modified in every HH slots. The total number of controls in these EnOpt simulations are $100 \times 48 = 4800$. Total of 50 realisations are used in this numerical example.

As the optimised energy consumption in EnOpt is directly proportional to the amount of energy generation, the sum of energy consumption for all consumers should reflect the energy generation with additional generation capacity in meeting the safe usage regulations. This allows the complete network representation of the EnOpt optimisation model for a smart grid. Energy generation is typically not a constraint for the optimisation problem, but rather a representation of proportional parts of the fuel-mix energy generation. It is assumed that the amount of green power generation should be above 10 % of non-green power generation. In this simulation, a wind farm is selected to represent the green generator and a CCGT plant as the non-green generator. Following Fonseca (2011), the optimisation procedure is allowed to run up to $\lambda_{\max}$ = 500 iterations even though there may be no significant improvement in the objective function $\mathscr{E}_Y(\mathbf{x}_{\lambda+1})$. This allows the relative increase of the EnOpt objective function to stay close to 1 %. Based on Eq. (3.61), the initial tuning parameter α_λ is set to half value of the standard deviation from the objective function (Eq. (3.54)) with the value of the multiplier $\alpha_{\text{multiplier}}$ as 100.

The plot of carbon emissions of BAU $\mathscr{E}_{\text{BAU}}$ and optimised $\mathscr{E}_{\text{O}}$ is shown in Fig. 4.27. It can be seen that the EnOpt model with the control vector $\mathbf{x}$ successfully minimises the car-

bon emissions $\mathscr{E}_{\mathrm{O}}$. The cumulative curves of $\mathscr{E}_{\mathrm{BAU}}$ and $\mathscr{E}_{\mathrm{O}}$ are demonstrated in Fig. 4.28.

As in line with Chen et al. (2009); Dehdari et al. (2012), since the gradient-based method is the unconstrained optimisation algorithm type, the infeasible updated control parameters at every time step will be truncated according to the constraints in the optimisation problem. The updated vector **x** which violates the control constraints in Eq. (3.13) is truncated and the **x** is reallocated proportionally among consumers based on the offset of truncated values.

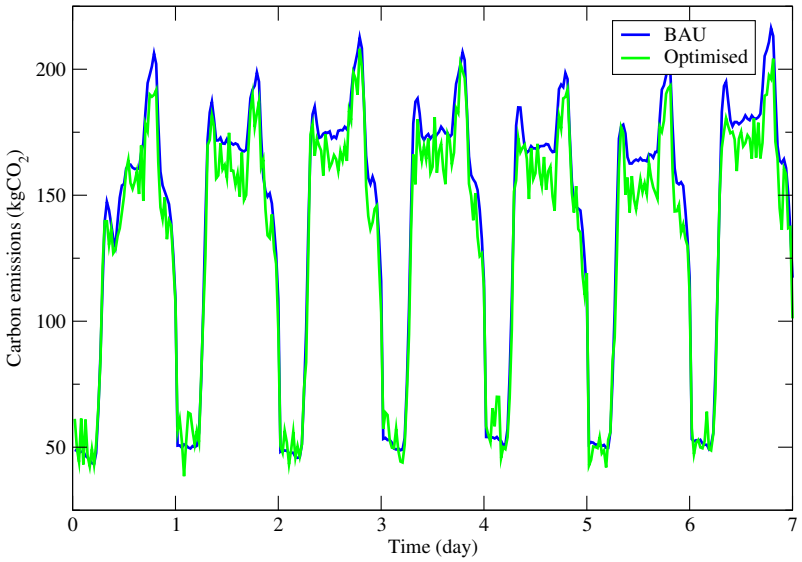

Figure 4.27: BAU versus optimised carbon emissions of consumers at every time step.

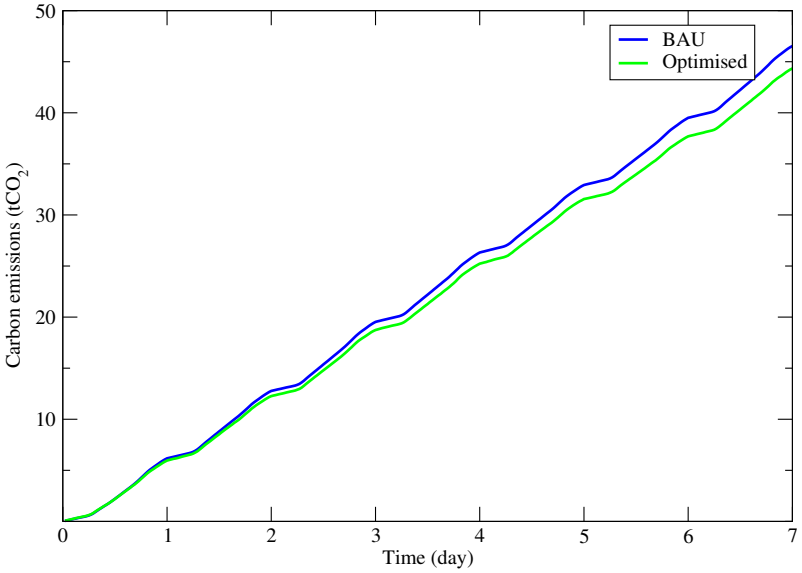

Figure 4.28: Cumulative plot of carbon emissions of consumers ($\mathscr{E}_{\mathrm{BAU}}$ and $\mathscr{E}_{\mathrm{O}}$).

In order to verify the performance of EnOpt, the optimised **x** corresponding to constraints (Eq. (3.13)) are considered. The first constraint involves the maximum $E^{\max}$ (UB) and minimum $E^{\min}$ (LB) allowable energy consumption E_i^c for all consumers. The E_i^c is calculated at the end of EnOpt and the results are shown in Fig. 4.29. This indicates that optimised **x** in EnOpt satisfies the first imposed constraints.

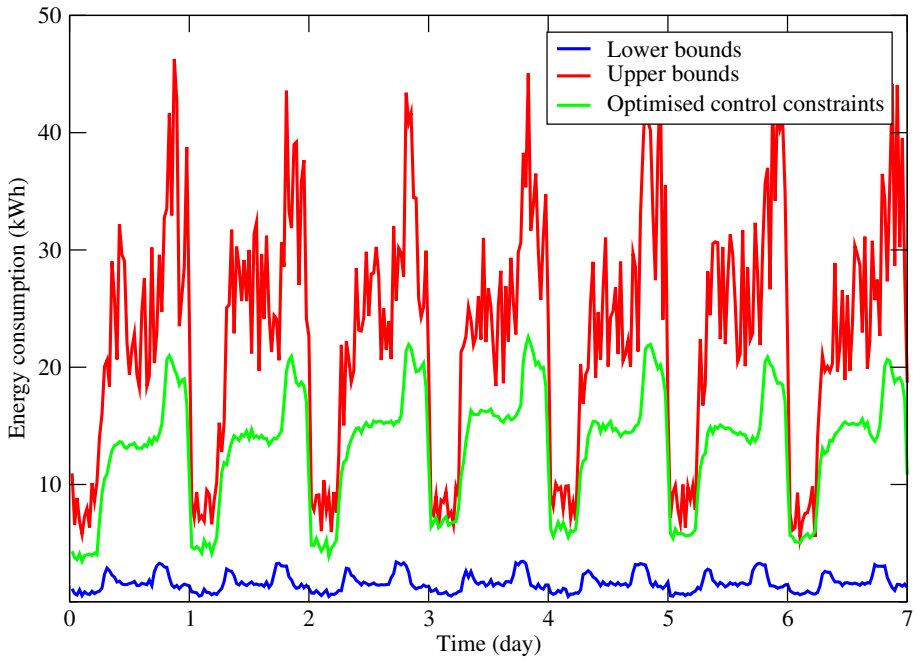

Figure 4.29: Optimised energy consumption of consumers (green curve) located between lower (blue line) and upper (red line) bounds.

The second constraint limits the sum of energy consumption for all consumers ($\sum_{i=1}^{N_i} E_i^c$) to be equal or smaller than the aggregated sum of energy demand for all consumers ($\mathbf{E}^c$). Similar to the calculation method for the first constraint, the E_i^c is calculated at the end of EnOpt. The simulation result is shown in Fig. 4.30, where the optimised energy consumption is smaller than $\mathbf{E}^c$. This indicates that optimised controls in EnOpt satisfy the second imposed constraints.

The energy demand is proportional to the amount of energy generation, and the sum of energy consumption reflects the energy generation. In this example, the wind farm and CCGT plant represent the optimised green and non-green energy generation. The proportion of green and non-green energy generation is determined using Eq. (3.14), by taking the safe energy usage factor ($U_{\text{safe}} = 1.20$) and the proportional green and non-green generation factor ($U_{\text{percent}} = 0.10$). The simulations results are shown in Fig. 4.31 that reflect the generation based on the optimised energy demand.

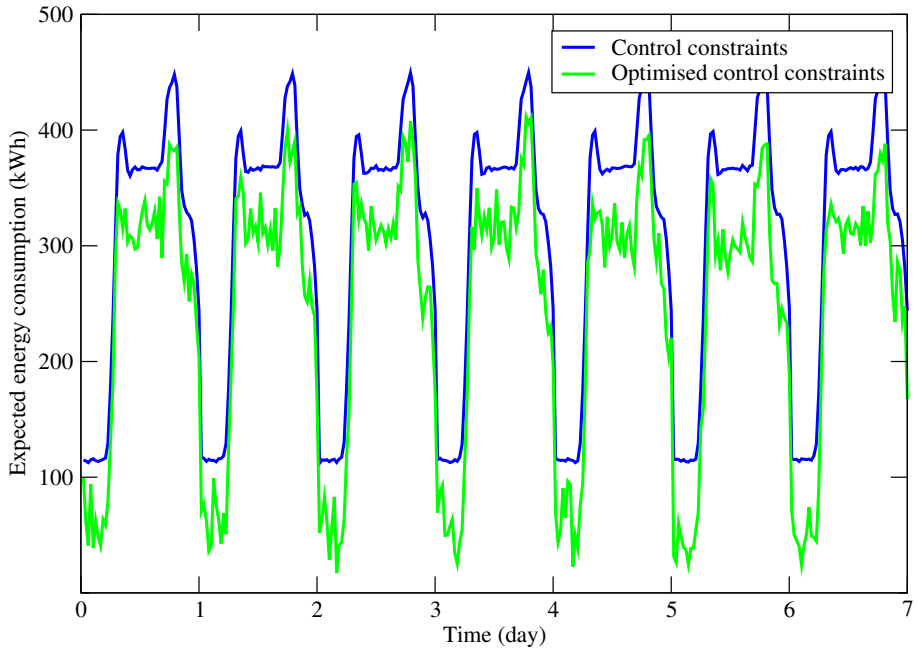

Figure 4.30: Optimised energy consumption of consumers with control constraints corresponding to the sum of energy demand ($\mathbf{E}^c$). Blue line — aggregated sum of energy demand ($\mathbf{E}^c$); green line — optimised energy consumption.

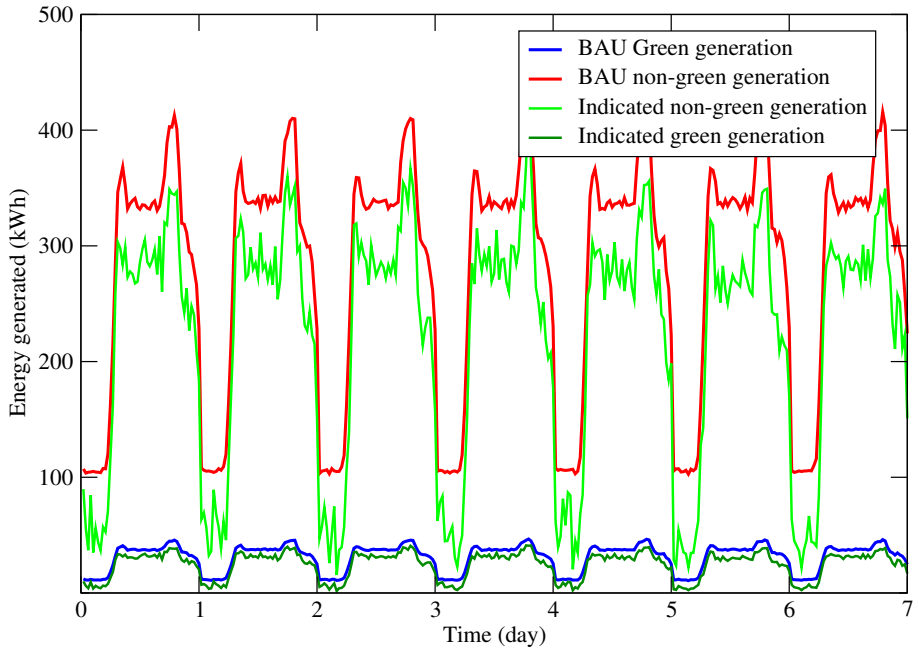

Figure 4.31: Energy generation in BAU versus the green and non-green energy generation. Blue line — BAU green generation; Red line — BAU non-green generation; Light green line — non-green generation; Dark green line — green generation.

The relative increase plots ($\% \, \Delta_{\lambda,k}$) of $\mathscr{E}_Y(\mathbf{x}_\lambda)$ (Eq. (3.56)) corresponding to λth iterations that satisfy the constraints are shown in Fig. 4.32 at time step $t_k = 1$ and in Fig. 4.33 at $t_k = 7$. The clear trend of relative increase of $\mathscr{E}_Y(\mathbf{x}_\lambda)$ can be seen, which converges at

later iterations. There is a possibility that during the EnOpt simulation, the optimised **x** may tend to fluctuate. This happens when no optimal controls are found at a particular iterations, as shown in Figs. 4.32 and 4.33.

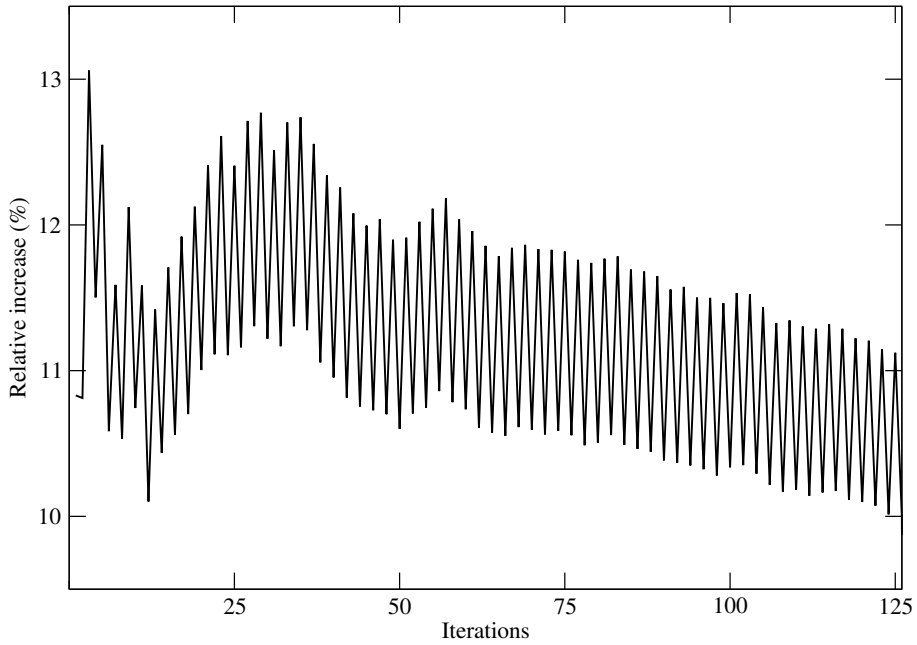

Figure 4.32: The relative increase (%) of the $\mathscr{E}_Y(\mathbf{x}_\lambda)$ corresponding to λth iterations at time step $t_k = 1$ in EnOpt simulations.

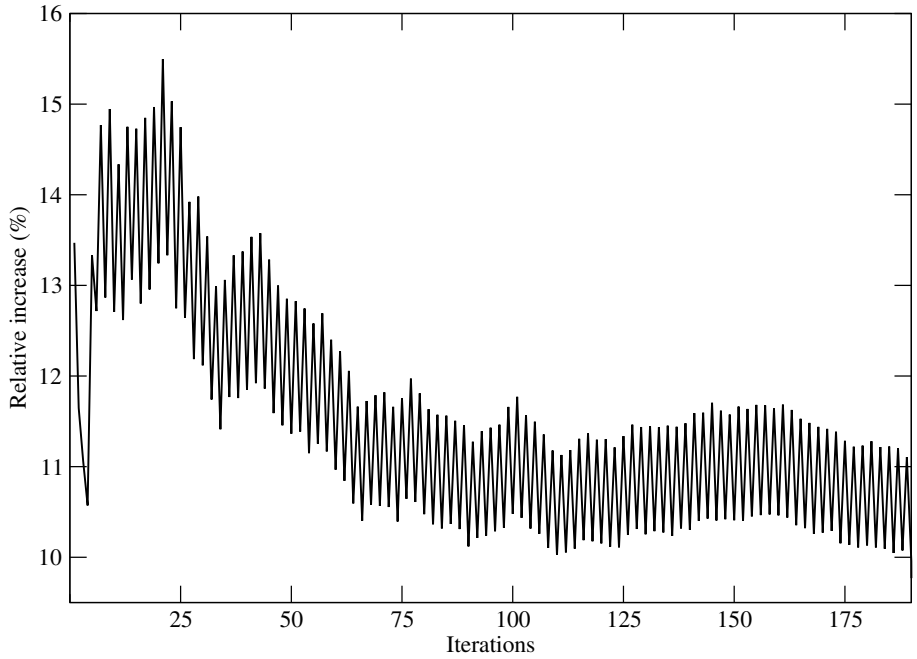

Figure 4.33: The relative increase (%) of the $\mathscr{E}_Y(\mathbf{x}_\lambda)$ corresponding to λth iterations at time step $t_k = 7$ in EnOpt simulations.

On the contrary, there are certain cases when computations of $\mathscr{E}_Y(\mathbf{x}_\lambda)$ do not converge

at $\lambda_{\max}$. Such simulations are shown in Figs. 4.34 and 4.35.

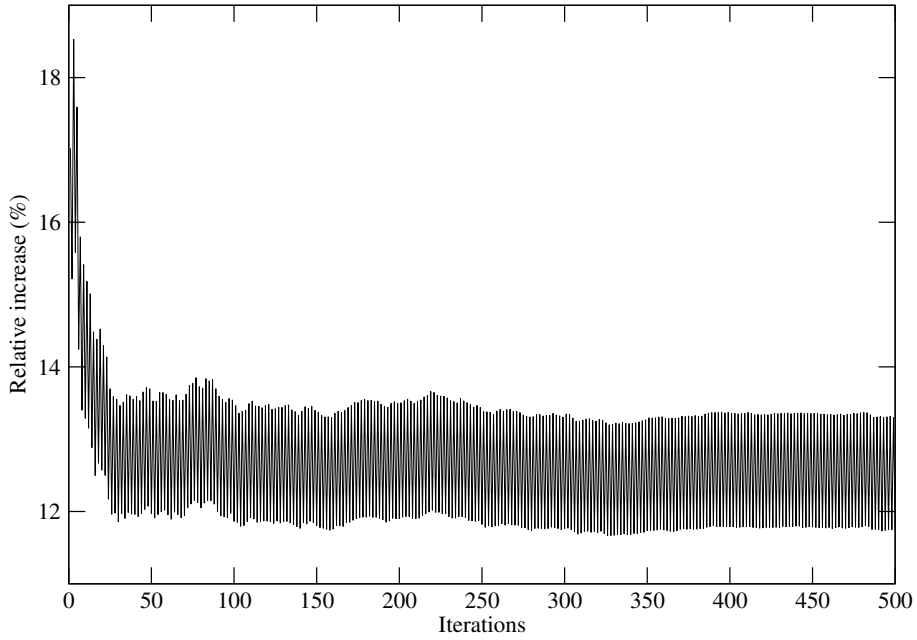

Figure 4.34: The relative increase (%) of the $\mathscr{E}_Y(\mathbf{x}_\lambda)$ corresponding to λth iterations at time step t_k = 40 in EnOpt simulations.

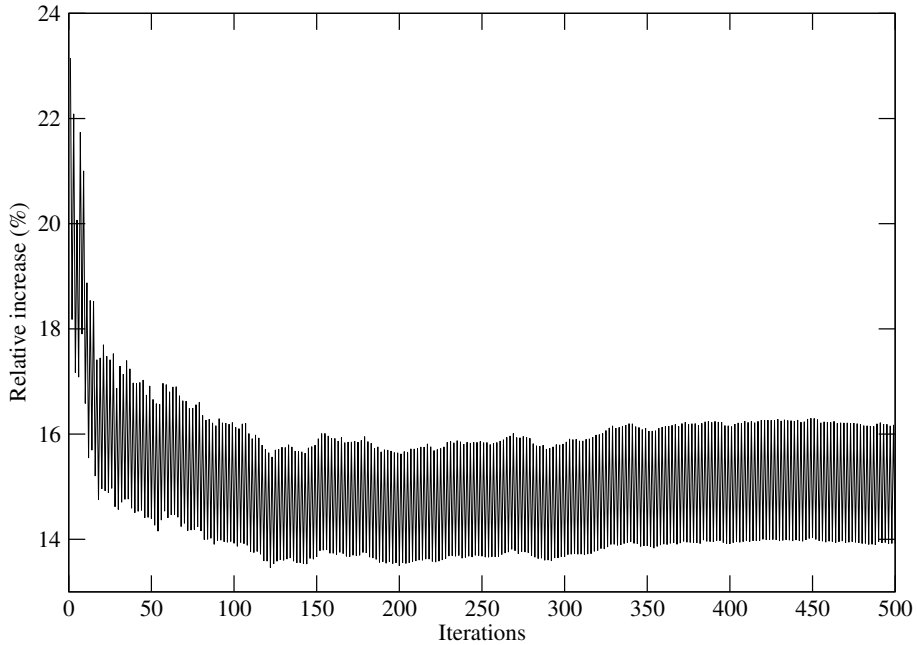

Figure 4.35: The relative increase (%) of the $\mathscr{E}_Y(\mathbf{x}_\lambda)$ corresponding to λth iterations at time step t_k = 144 in EnOpt simulations.

Such cases can happen when the tuning of both α_λ and $\alpha_{\text{multiplier}}$ are not sufficiently accurate in perturbing the small relative increase of $\% \, \Delta_{\lambda,k}$. Furthermore, the prior knowledge in the selection of parameters, or over-parameterisation may impede faster conver-

gence of simulations. Additionally, one can observe that iterations drift closer to a minimum due to almost optimal solution founded, and therefore the steepest descent algorithm shows the 'zig-zag' pattern for a long iteration until a real minimum is achieved. As the steepest descent algorithm points to the maximum direction of change, this makes the slow computation of convergence (improvement) in the steepest descent approach.

The final optimised $\mathscr{E}_Y(\mathbf{x}_\lambda)$ is denoted as $\mathscr{E}_\mathrm{O}$ for estimation of carbon savings S in Eq. (3.12). The overall carbon saving S in Eq. (3.12) for one day of simulation runs are estimated as 0.31 ± 0.02 $\mathrm{tCO_2}$ (percentage improvement 11.20 ± 6.45 %). The value of S obtained based on the numerical simulation of 100 consumers is considered low. One of the reasons for this is that the truncated constraint on gradient-based approach impedes higher objective function obtained (Dehdari et al., 2012). Overall, the converged $\mathscr{E}_Y(\mathbf{x}_\lambda)$ indicates that $\mathbf{x}_\lambda$ is optimised. The $\mathbf{x}_\lambda$ then propagates forward to forecast energy consumption in the next time step.

4.3.2 Energy generation data assimilation using EnKF and numerical optimisation of costs in the ED model using EnOpt

4.3.2.1 EnKF simulations

This section provides the EnKF short-term prediction (forecast) and assimilation based on the historical and real-time HH records of energy generation data by Elexon (2015) and BMRS (2015). Five energy generating thermal units (CCGT, coal, oil, nuclear and OCGT) and one offshore wind generator are considered. The energy data is considered with the addition of model noises in order to forecast the total energy generation among power plants. As mentioned in Section 3.6.2.2, since historical and real-time HH records of energy generation are available in the BMRS and Elexon portal, the state vector y^p (Eq. (3.43)) in this EnKF problem contributes direct model predictions (d) of the energy generation based on the real energy data (m) of thermal units and wind generator. The component of d in y^p are further perturbed with model errors in order to generate new sets of ensemble members. Similarly, the *priori* ensemble y_j^p is created using Eqs. (3.51) and (3.52), where $j = 1, 2, ..., N_e$ indexes the ensemble members. In EnKF, the perturbed observation of energy generation $d_{\mathrm{obs,j}}$ based on d is generated through Eq. (3.36). The initial ensemble members of y^p are drawn from a normal distribution with mean and

standard deviation of $N(0,20)$. Additionally, the model (process) error w is sampled from $w \sim N(0,1)$. The measurement error, on the other hand, is sampled from $v \sim N(0,0.5)$.

Different EnKF realisations are produced (N_e = 10, 100, 1000) and propagated at every time step. The matrix Y^p (Eqs. (3.51) and (3.52)) is the collection of *priori* ensemble y_j^p. The y_j^p is assimilated to reflect the updated *posteriori* ensemble (y_j^u) using Eq. (3.47) and is stored in the matrix Y^u. Ensemble means of $Y_{N_e}^u$ of different realisations N_e are obtained which allow the assessment of convergence of the optimised data to the actual observations. The actual observations are similarly obtained as the mean of the ensemble of the perturbed observations ($\overline{d_{\text{obs},N_e}}$). The assimilation is performed for 48 time steps (24 hours with HH interval).

Daily and weekly plots with datasets of energy generation (thermal units plus wind generators) and the EnKF assimilation of Y^u with different realisations are shown in Figs. 4.36 and 4.37. The figures show that the larger the ensemble size, the better Y^u converges towards the actual observations.

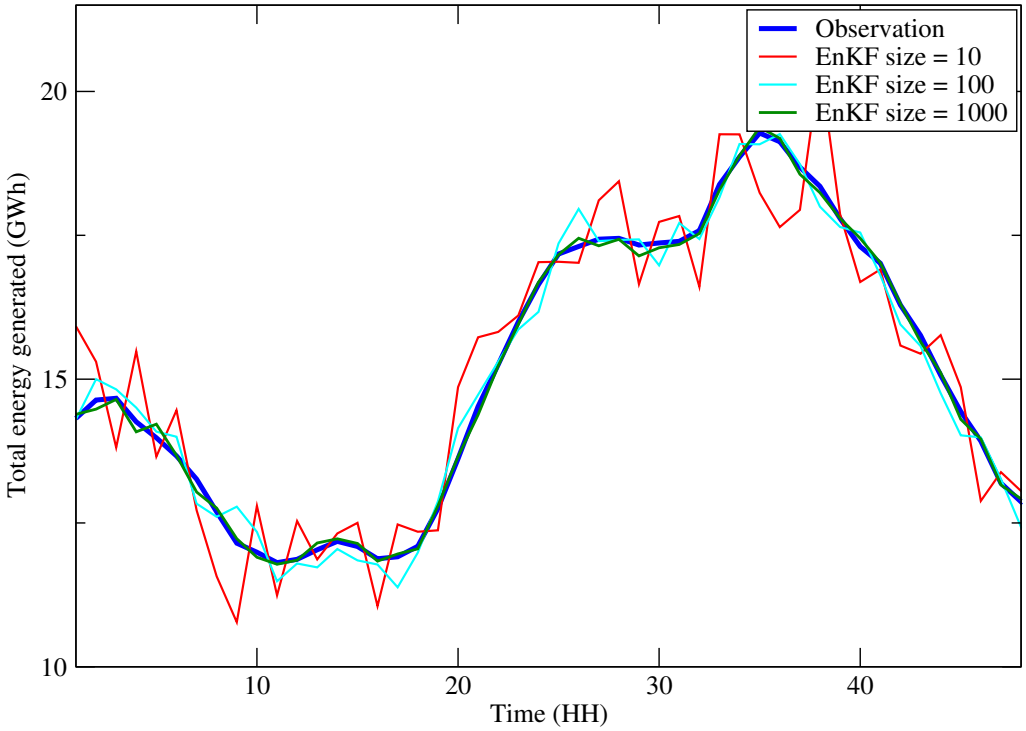

Figure 4.36: Daily energy generation with different EnKF realisations. Generating fleets are thermal units and wind generators.

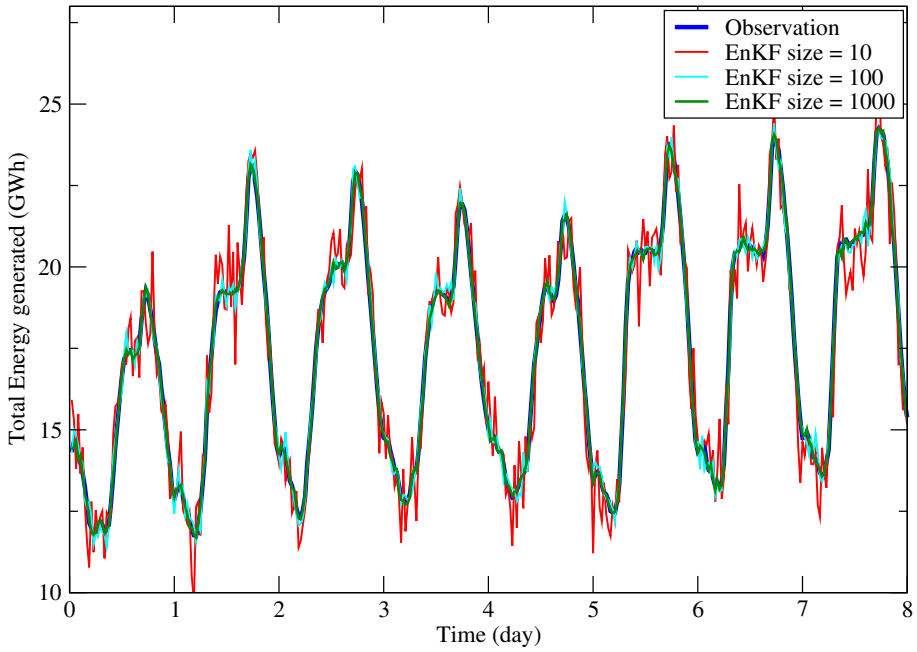

Figure 4.37: Weekly energy generation with different EnKF realisations. Generating fleets are thermal units and wind generators.

Additionally, the EnKF assimilations corresponding to thermal units and wind generators are performed. Different realisations (N_e = 10, 100, 1000) are used in the EnKF assimilation. Fig. 4.38 shows the diurnal EnKF'ed energy generation from thermal units.

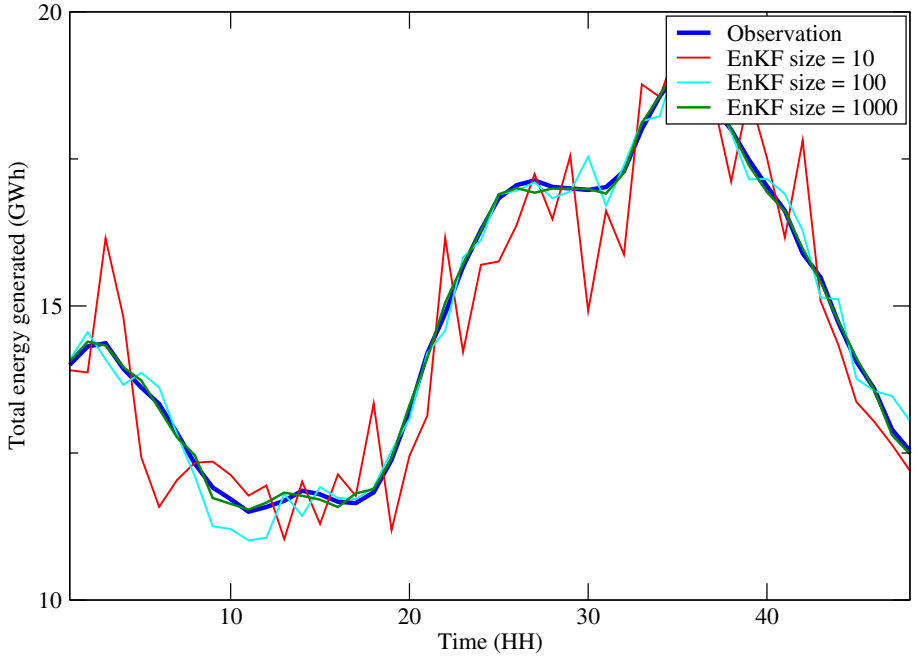

Figure 4.38: Daily energy generation of thermal units with different EnKF realisations.

Similarly, Fig. 4.39 shows the different realisations of the diurnal EnKF'ed energy

generation from wind generators. The small ensemble size (N_e = 10) in Fig. 4.39 results in poor EnKF forecast and assimilation of wind data. Both simulations result in Figs. 4.38 and 4.39 show that the larger the ensemble sizes, the lesser oscillations of the assimilation in EnKF. Consequently, the smaller the EnKF errors relatively to the observations.

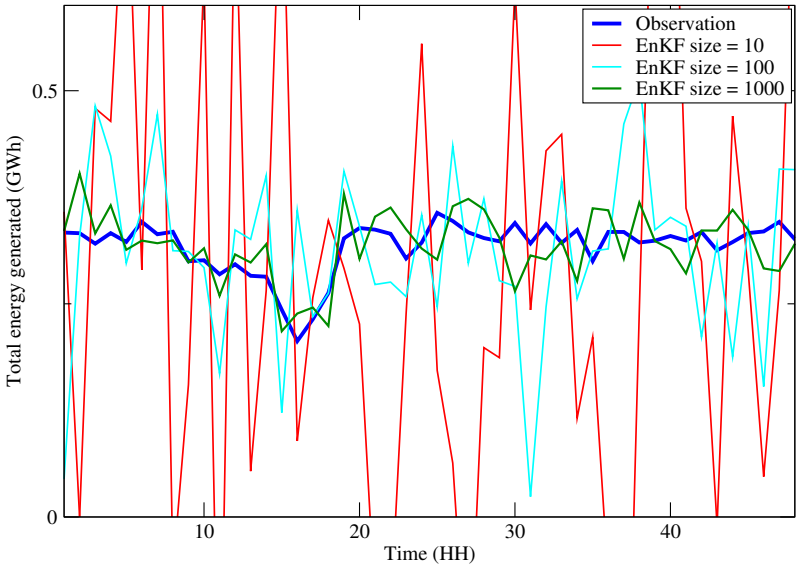

Figure 4.39: Daily wind-based energy generation with different EnKF realisations.

One-week plots from Figs. 4.38 and 4.39 are shown in Figs. 4.40 and 4.41. The simulations demonstrate that EnKF performs well in the assimilation of energy generation data at longer scale without high deviations relatively to actual observations.

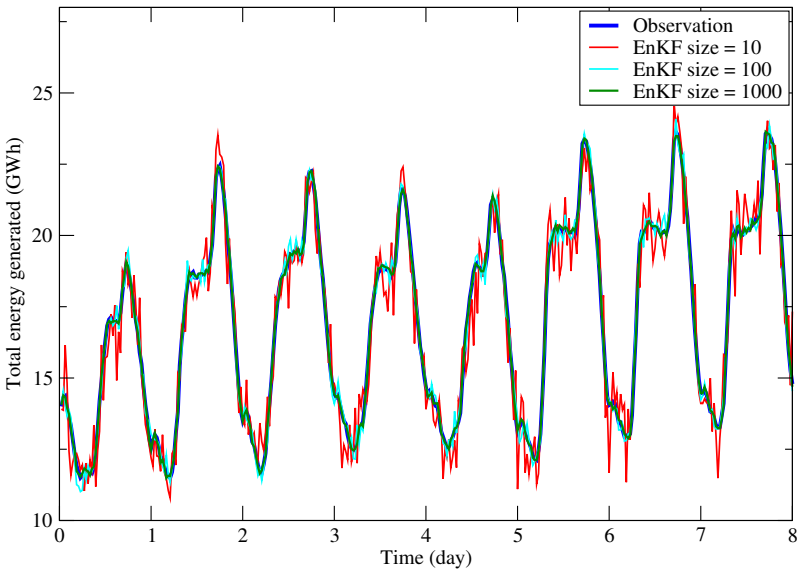

Figure 4.40: One-week energy generation of thermal units with different EnKF realisations.

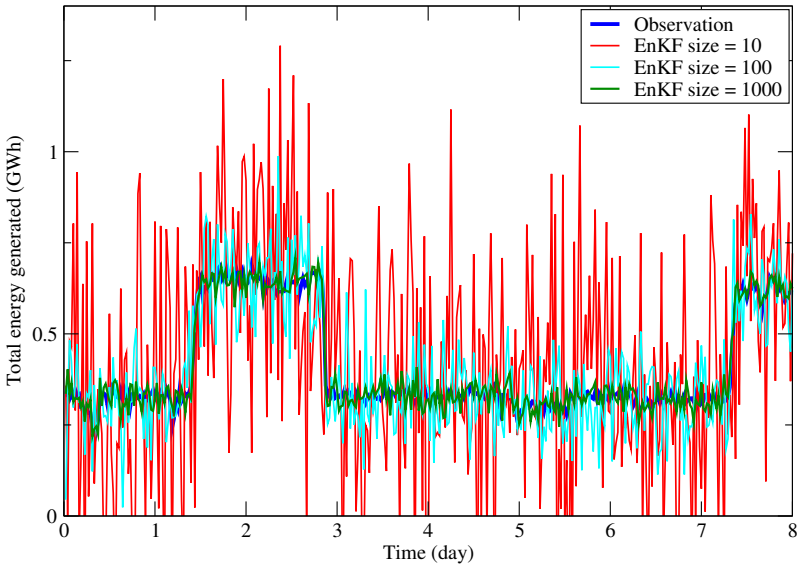

Figure 4.41: One-week wind-based energy generation with different EnKF realisations.

4.3.2.2 EnOpt simulation

The filtered energy Y^u is further used in the EnOpt algorithm in order to optimise energy generation in the ED problem (Eqs. (3.25) and (3.55)) along with optimisation of controls $\mathbf{x}$ in Eq. (3.53)) following the imposed operational constraints in Eq. (3.29). The price penalty factor $h_{\max}$ is introduced that converts the emissions function of the ED problem into the emissions cost function. Additionally, the cost coefficients $d^{\mathrm{G}}_{i,t}, d^{\mathscr{E}}_{i,t}$ and $d^{\mathrm{W}}_{i,t}$ are determined based on the levelised electricity data cost ranges according to fuel types provided by DECC (2013). The cost coefficients of fuel and wind energy generation is shown in Table 4.10. Similarly, the emission cost coefficient are shown in Table 4.11.

Table 4.10: Levelised fuel and wind cost coefficient range. $*$ – assuming gas-oil fired OCGT at 5 % duty.

Generator	Cost (£/MWh)	Cost coefficient
CCGT	$[70...100]$	$d^{\mathrm{G}}_{1,t}$
coal	$[120...135]$	$d^{\mathrm{G}}_{2,t}$
oil*	$[330...400]$	$d^{\mathrm{G}}_{3,t}$
nuclear	$[70...75]$	$d^{\mathrm{G}}_{4,t}$
OCGT	$[110...170]$	$d^{\mathrm{G}}_{5,t}$
wind	$[133...138]$	$d^{\mathrm{W}}_{1,t}$

Using the Monte-Carlo method, the repeated random sampling of cost coefficients ($d^{\mathrm{G}}_{i,t}, d^{\mathscr{E}}_{i,t}$ and $d^{\mathrm{W}}_{i,t}$) based on levelised costs from Tables 4.10 and 4.11 is performed. The

Generator	Emission cost (£/MWh)	Cost coefficient
CCGT	$[18...19]$	$d^{\mathscr{E}}_{1,t}$
coal	$[5...42]$	$d^{\mathscr{E}}_{2,t}$
oil*	$[50...51]$	$d^{\mathscr{E}}_{3,t}$
nuclear	$[0...5]$	$d^{\mathscr{E}}_{4,t}$
OCGT	$[24...26]$	$d^{\mathscr{E}}_{5,t}$

Table 4.11: Levelised emission cost coefficient range. $*$ – assuming gas-oil fired OCGT at 5 % duty.

average HH bid-offer data for thermal units and the wind-generated energy are available in Elexon (2015), and this allows one to compute the bid-offer spread and updated cost coefficients using Eqs. (3.26) and (3.27). The daily average HH bid-offer price spread for fuels and wind energy is shown in Fig. 4.42, which is based on the 2015 February to April bid and offer data provided by Elexon (2015).

Based on Fig. 4.42, the wind is subject to high amount of uncertainty. During the evening peak period, due to high amount of energy demand, there is a high amount of imbalance volume. Therefore, coal and CCGT plant (assuming in 'hot' standby mode) are selected to balance the energy demand and the wind output during the peak demand. Additionally, there are no spreads (no major imbalance) for the nuclear, OCGT and oil plants. The nuclear is a base load type plant and henceforth its generation is strictly required and is not flexible in responding to peak demand. In contrast, the peaking plants such as oil and OCGT plants are often selected to provide energy during peak demand. However, plots of the bid-offer spread show no major imbalances. One of the possible reason is due to the high electricity generation prices that force the peaking plants to switch off (as long as the forecasting of peak demand is highly accurate that does not need to turn on peaking plants).

With the available bid-offer price spread from Fig. 4.42 and the cost coefficient data (Tables 4.10 and 4.11), the updated cost coefficient for the ED problem can be calculated using the formula from Eq. (3.27). The wind energy in this case can be assimilated using EnKF. However, the wind energy is generally uncontrollable. Hence, there is no associated control variable in the wind function. In the context of EnOpt, the wind energy will be simulated as the BAU method, and other generators will be used to balance the wind output. The optimisation of Eq. (3.25) is subject to generator and energy balance

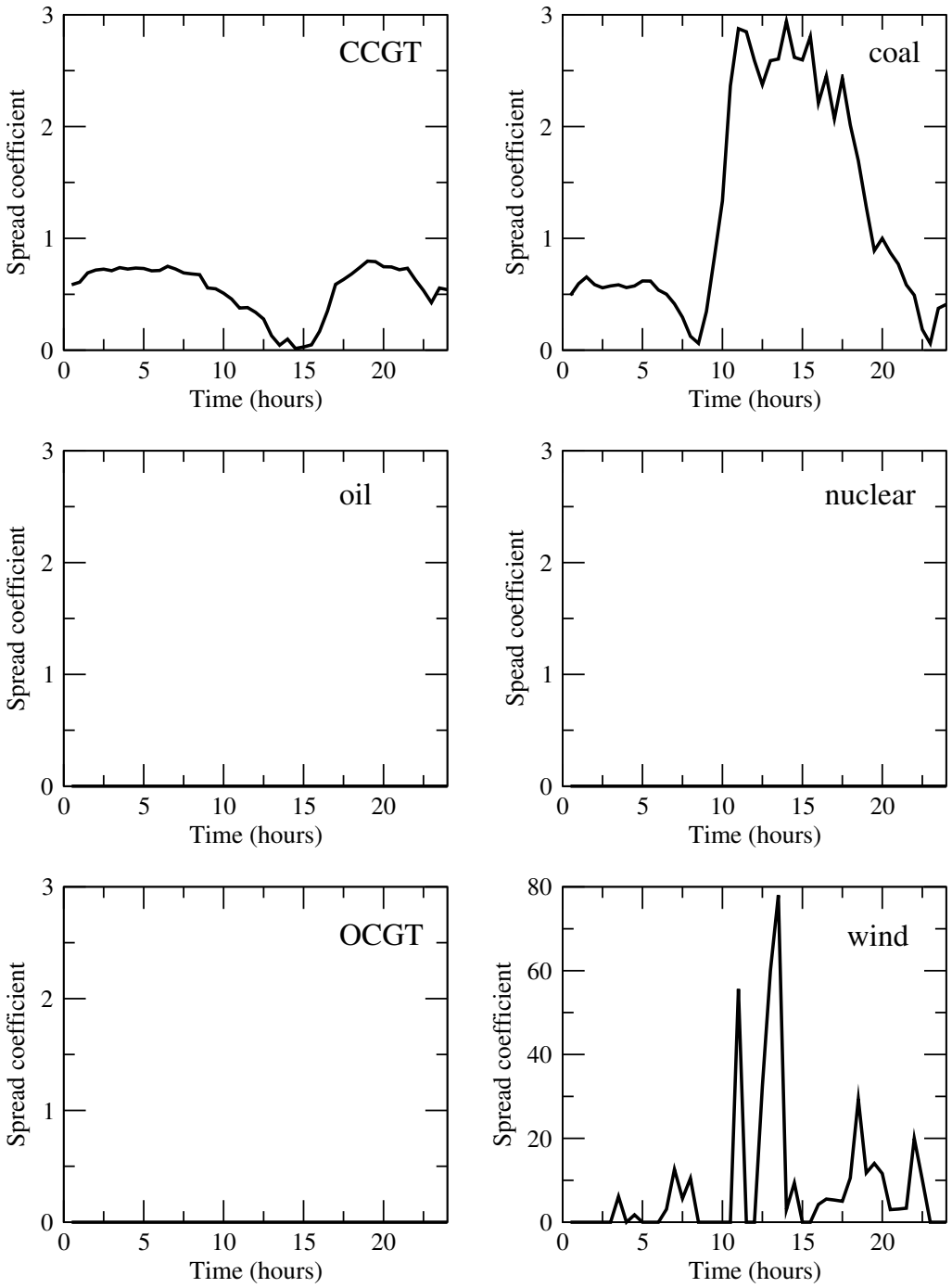

Figure 4.42: The average bid-offer price spread corresponding to different fuels and the wind generation, based on the 2015 February to April bid and offer data. The empty bid-offer spreads (oil, nuclear, OCGT) denote no major imbalances.

constraints from Eq. (3.29).

The initial state of the control vector $\mathbf{x}$ is generated as the mean of the sampled data between lower and upper bounds of generating units. It is further perturbed with Gaussian random numbers $N \sim (0, 0.5)$. Each component of $\mathbf{x}$ consists of energy generation output

value that corresponds to *i*th generating units in Eq. (3.53) which is to be optimised. The $\mathbf{x}$ is further integrated with Y^u that optimises generators.

Total of five thermal units (CCGT, coal, oil, nuclear and OCGT) and one off-shore wind farm generator are considered in the EnOpt simulation. The time frame for the optimisation of costs is 24 hours and the control vector $\mathbf{x}$ is modified in every HH slot. Therefore, the total number of control parameters for the vector $\mathbf{x}$ is $5 \times 48 = 240$, which is the product of the number of the thermal units and the number of the control steps. Total of 100 EnKF realisations are used in this example.

Following Fonseca (2011), the optimisation procedure is allowed to run up to $\lambda_{\max} = 500$ iterations even though there may be no significant improvement in the objective function $\mathscr{C}_Y(\mathbf{x}_{\lambda+1})$. The iterations terminate when the relative increase of the EnOpt objective function is less than 1 %. Based on Eq. (3.61), the initial tuning parameter α_λ is set to half value of the standard deviation from the objective function (Eq. (3.55)) with the value of the multiplier $\alpha_{\text{multiplier}}$ as 100. Constraints as outlined earlier in Eq. (3.29) are summarised in Table 4.12. '0' implies switched-off generation. The TD losses E_{L} account approximately 7.9 % ((DUKES, 2015)).

Table 4.12: Constraints of the ED problem.

Notation	Description	Amount (GWh)
$E_{\text{min},i}$	Minimum allowable thermal generation capacity for	
	$E_{\text{min,CCGT}}$	67.20
	$E_{\text{min,coal}}$	100.80
	$E_{\text{min,oil}}$	0
	$E_{\text{min,nuclear}}$	84
	$E_{\text{min,OCGT}}$	0
$E_{\text{max},i}$	Maximum allowable thermal generation capacity for:	
	$E_{\text{max,CCGT}}$	180
	$E_{\text{max,coal}}$	156
	$E_{\text{max,oil}}$	1.20
	$E_{\text{max,nuclear}}$	7.20
	$E_{\text{max,OCGT}}$	2.40
E_{L}	TD energy losses	2.40
E_{D}	Energy demand	300
$W_{\max}$	Maximum amount of wind generation	36

As the steepest descent method is a type of gradient-based unconstrained optimisation,

the updated vector **x** which violates the control constraints (Eq. (3.29)) is truncated and the new **x** is reallocated proportionally among generators based on the offset of truncated values.

The objective function plot for BAU costs $\mathscr{C}_{\text{BAU}}$ and optimised costs $\mathscr{C}_{\text{O}}$ is shown in Fig. 4.43. It can be seen that the EnOpt model successfully minimises the cost of generation $\mathscr{C}_{\text{O}}$.

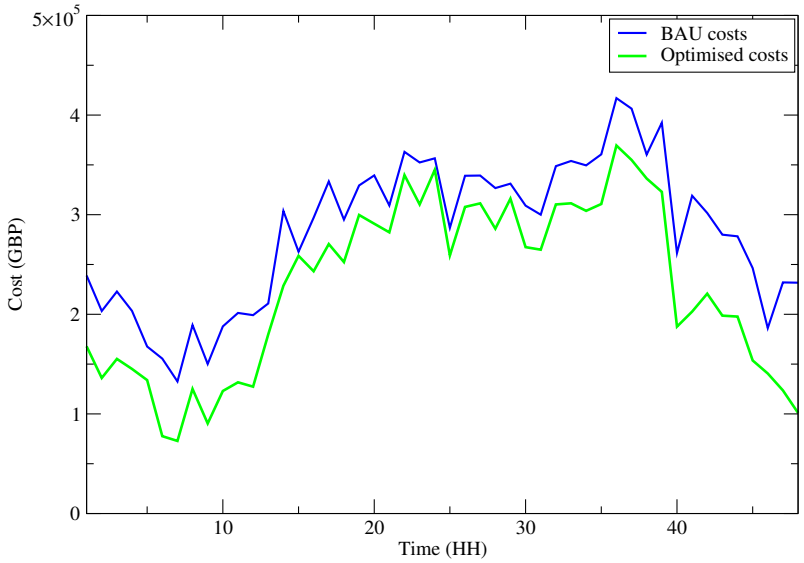

Figure 4.43: Daily plot of the BAU versus optimised costs of the ED problem.

The cumulative curves for the cost of generation for $\mathscr{C}_{\text{BAU}}$ and optimised $\mathscr{C}_{\text{O}}$ in Fig. 4.44.

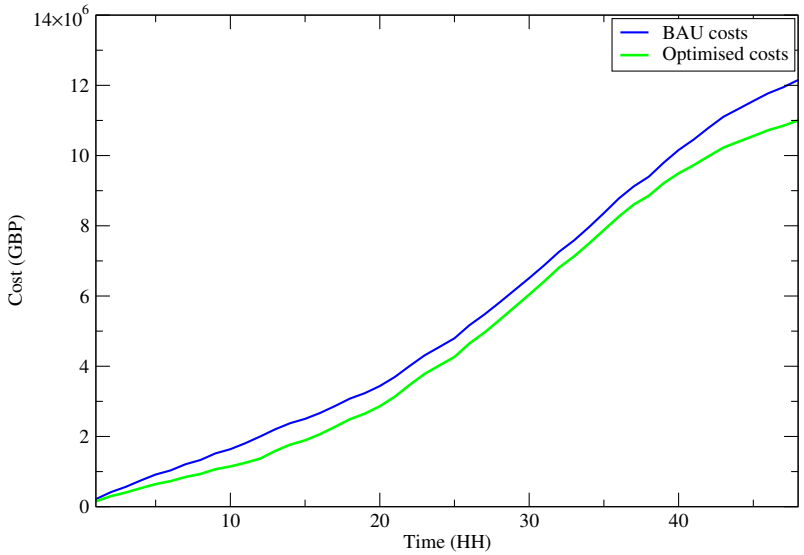

Figure 4.44: Daily cumulative plot of the BAU versus optimised costs of the ED problem.

The total $\mathscr{C}_{BAU}$ within the simulations run from Fig. 4.44 is obtained as £12.16 million, which is comparable with results of Senthil and Manikandan (2010); Subramanian and Ganesan (2010).

The relative increase of the cost savings $\mathscr{C}_{\mathrm{S}}$ based on $\mathscr{C}_{\mathrm{BAU}}$ and $\mathscr{C}_{\mathrm{O}}$ are shown in Fig. 4.45. It can be seen that it is relatively low in the time interval 6am – 8pm. If negative values of relative increase are computed, this means additional costs of generation are required (no cost savings are achieved in this case).

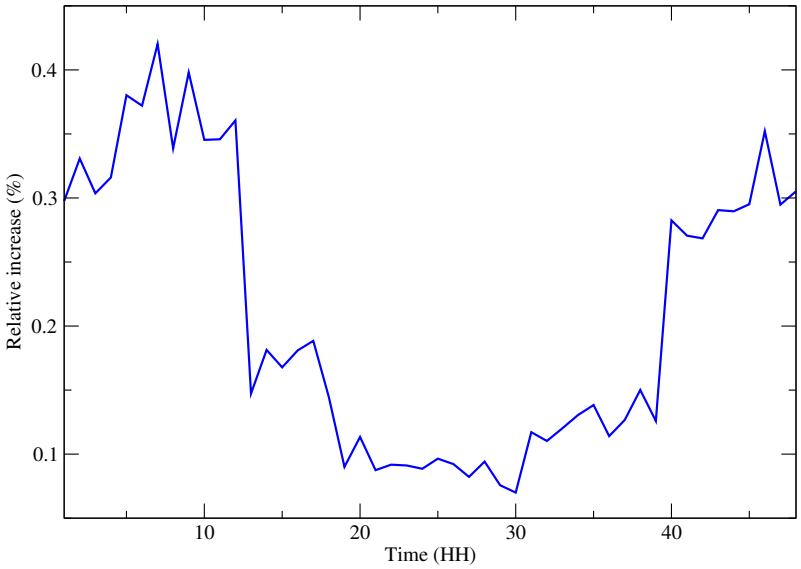

Figure 4.45: The relative increase of cost savings based on difference between BAU and the optimised scenarios.

Besides the optimised costs of generation in the ED problem, it is also of interest to analyse the amount of carbon emissions optimised. The optimised carbon emissions in the ED problem are shown in Fig. 4.46. Due to the regulation of costs in the electricity market, additional carbon emissions are produced in the afternoon. This shows the trade-offs between costs and emissions in the modern electricity market. Thus, the priority of optimising costs may lead to the increase of the emissions. Additionally, the relative increase of carbon savings S based on $\mathscr{E}_{\mathrm{BAU}}$ and $\mathscr{E}_{\mathrm{O}}$ are shown in Fig. 4.47. Negative values of relative increase of emissions are obtained in time interval 5am – 8pm, which means additional carbon emissions are introduced (no carbon savings are achieved).

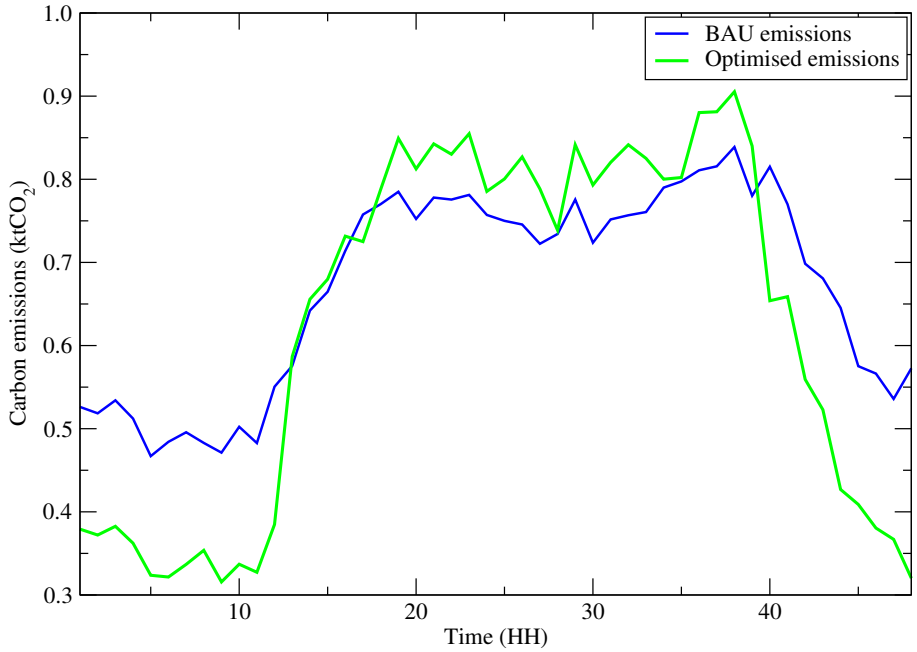

Figure 4.46: Carbon emissions of BAU versus optimised scenarios in the ED problem.

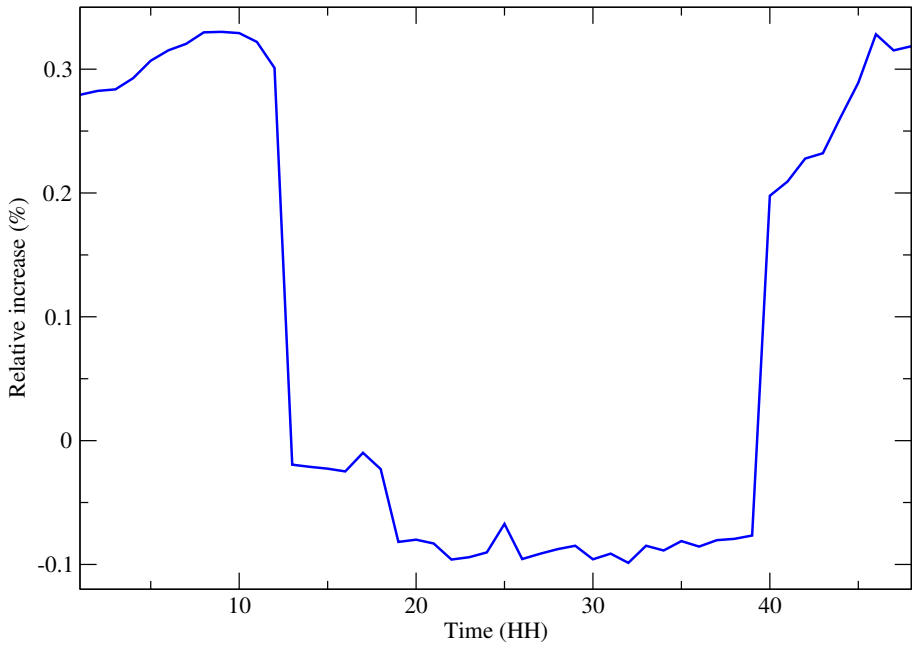

Figure 4.47: The relative increase of carbon savings based on BAU and the optimised scenarios.

The relative increase (% $\Delta_{\lambda,k}$) of the costs $\mathscr{C}_Y(\mathbf{x}_\lambda)$ (Eq. (3.57)) corresponding to λth iterations that satisfies the condition in Table 4.12 is shown in Fig. 4.48. It illustrates the clear trend of relative increase of $\mathscr{C}_Y(\mathbf{x}_\lambda)$, which converges at later iterations. The iterations converge when the relative increase of the objective function is less than 1 %. Henceforth, a solution can be found where the control vector $\mathbf{x}$ is optimised that minimise the objective function (Eq. (3.57)).

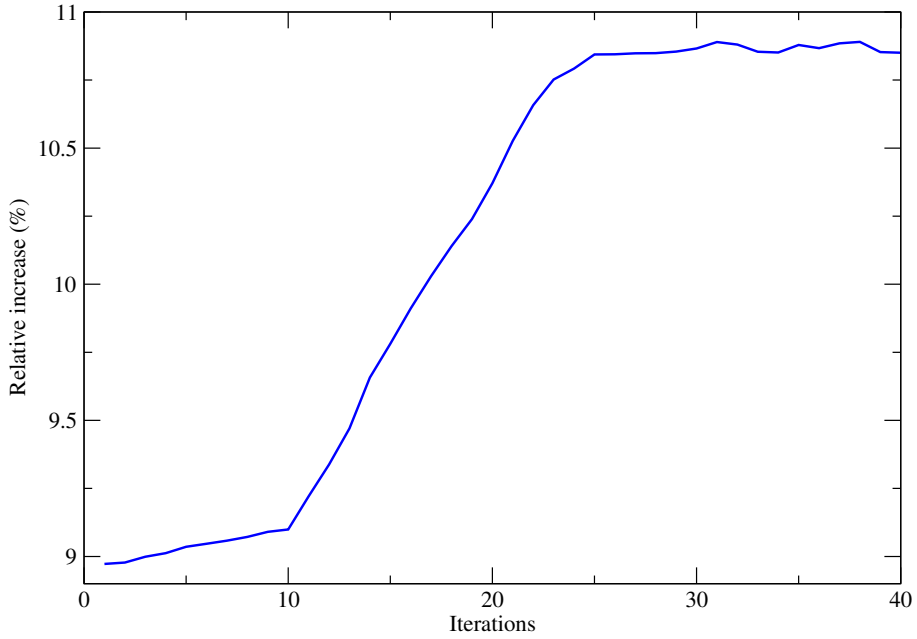

Figure 4.48: The relative increase (% $\Delta_{\lambda,k}$) of the objective function corresponding to λth iterations.

The optimised $\mathscr{C}_O$ at the end of EnOpt simulation is compared with $\mathscr{C}_{BAU}$ (Eq. (3.24)). Cost savings in this ED problem are calculated using Eq. (3.28) and obtained to be equal to £1.15±0.10 million (percentage improvement 9.47±8.69 %). On the other hand, the second term of the Eq. (3.25) is $\mathscr{E}_O$, which is used for estimation of carbon savings S in Eq. (3.6). Due to the truncated constraint of gradient-based approach, this impedes higher objective function. Even though there are no carbon savings during the day time (based on Fig. 4.46), the overall savings S are about and are approximated as 0.81±0.10 $ktCO_2$ (percentage improvement 5.88±12.34 %) in one day of simulations.

Finally, the converged $\mathscr{C}_Y(\mathbf{x}_\lambda)$ indicates that $\mathbf{x}_\lambda$ is optimised. $\mathbf{x}_\lambda$ then propagates forward to regulate the amount of energy generation in the next time step.

4.4 Numerical simulation of DR

To model the DR programmes, Matlab-based simulations of carbon emissions and savings are performed. The input profile data from Section 3.8 is applied to determine the nonlinear relationship between the various load conditions and the corresponding carbon emissions during the warm-up and shutdown periods of BAU plants. Different types of fit based on the available input data are performed using the Matlab 'curve fitting tool'. Three types of data (load factor, carbon emission level, and the resultant carbon emissions) are obtained in each warm-up and shutdown profiles for BAU plants. At the end of the simulations, the carbon emissions for three types of energy sub-profiles (warm-up, operation and shut down) of BAU plants are obtained and further compared with profiles of the smart interventions.

Monte Carlo simulations are performed to randomly sample the carbon factors of gas and diesel fuels, DR periods, and various intervals of parameters for BAU plants, generators, CHP, hydro-pumped storage plants and electricity grid factors across the ranges of the uniformly distributed variables. Simulations of N = 100 random samplings are performed in order to quantify the corresponding uncertainties for the resultant carbon emissions and savings for each operational day. All uncertainties in the present paper are computed as standard uncertainties with the coverage factor ($k = 2$) that allows the computation of 95 % confidence interval. The percentage reduction of overall carbon emissions is also included in the result along with the percentage uncertainty. It is not the scope of this paper to compare the effectiveness of different DR models (due to different projected timelines and trading purposes).

4.4.1 Technological parameters of BAU plants

Table 4.13 shows the parameters of BAU plants and one of the smart interventions, diesel generators participating in the DR programmes. Diesel generators are used to compare with BAU plants, which they substitute. The table provides data to model energy generation and the resulting carbon emissions and savings. Due to different technological cycles of plants and generators and duration of DR programmes, the resultant carbon emissions and savings may vary.

Table 4.13: Parameters of CCGT, OCGT and diesel generators.

Parameters	CCGT	OCGT	Diesel generators
Warm-up duration	35 minutes	30 minutes	1 minute
Shutdown duration	$\leq$ one hour	10 minutes	none
Load condition	Part-load	Full-load	
Standby duration	30 minutes		none
Additional warm-up emissions	Yes, at different part loads		none
Additional operational emissions	15-20 % at base-load	6.70 % operating at nominal load	none
Additional shut down emissions	Yes, at different part loads		none
TD losses	7.7 %		none
Efficiency	52-60 %	35-42 % (Lower heating value)	35 %
Carbon intensity ($kgCO_2$/kWh)	0.365-0.400	0.460-0.480	0.710 (at 35 % efficiency)

4.4.1.1 Modelled profiles of BAU plants

By applying the percentage increases of carbon emissions at different part-loads during the warm-up period for the corresponding CCGT (Table 3.4) and OCGT plants (Table 3.5), and for shutdown profile using the parameters from Table 4.13, the percentage emission increases of the warm-up and shutdown profiles of the CCGT and OCGT plants are created. Tables 4.14 and 4.15 show the models describing the percentage emission increases of the warm-up and shutdown profile for the CCGT and OCGT plants. The x denotes the load factor level across the CCGT and OCGT plants. $f(x)$ is the resultant percentage increases of carbon emissions. The final multiplications of the capacity of CCGT/OCGT, x, the carbon intensity of CCGT/OCGT, $f(x)$ and time elapsed t provide estimation of carbon emissions of the corresponding CCGT and OCGT plants. The detailed warm-up and shut down carbon emission profiles with respect to different load factors and percentage increase of the carbon emissions are shown in Appendix B.

Table 4.14: Model describing the percentage emission increases for the CCGT plant during the warm-up and shut down period. x is the load factor, $f(x)$ is the percentage increase of carbon emissions. SSE: Sum of squared errors of prediction; RMSE: Root mean square error; Coefficients are computed with 95 % confidence interval.

CCGT profile	**Warm-up**	**Shutdown**
Function type	Power exponential	Gaussian
Model	$f(x) = a\exp(bx)$	$f(x) = a\left(\exp\left(\frac{x-b}{c}\right)\right)$
Coefficients	$a = 41430(-45600, 128505)$ $b = -1.946(-2.586, -1.306)$	$a = 102.2(97.1, 107.4)$ $b = 0.2641(0.2551, 0.2731)$ $c = 0.1928(0.1757, 0.21)$
Goodness of fits	SSE: 0.7212 R-square: 0.9997 Adjusted R-square: 0.9995 RMSE: 0.8492	SSE: 1.857 R-square: 0.9998 Adjusted R-square: 0.9995 RMSE: 0.9635

Table 4.15: Model describing the percentage emission increases for the OCGT plant during the warm-up and shut down period. x is the load factor, $f(x)$ is the percentage increase of carbon emissions. SSE: Sum of squared errors of prediction; RMSE: Root mean square error; Coefficients are computed with 95 % confidence interval.

OCGT profile	**Warm-up**	**Shutdown**
Function type	Exponential	
Model	$f(x) = a(\exp(bx)) + c(\exp(dx))$	
Coefficients	$a = 95.10(54.15, 136.10)$ $b = -0.05532(-0.09621, 136.10)$ $c = 4.747(-35.74, 45.24)$ $d = 0.001239(-0.09256, 0.09504)$	$a = 5.273(-2.93, 13.48)$ $b = 3.121(-28.44, 34.68)$ $c = 0.03363(-0.1472, 0.2144)$ $d = 47.42(17.28, 77.56)$
Goodness of fits	SSE: 11.43 R-square: 0.9983 Adjusted R-square: 0.9958 RMSE: 2.391	SSE: 7.414 R-square: 0.9989 Adjusted R-square: 0.9972 RMSE: 1.925

4.4.2 Assessment of carbon emission and savings in DR programmes

4.4.2.1 Short Term Operating Reserve (STOR)

Each period of STOR operation is modelled as 50 hours with 60 runs of firing-up reserved BAU plants (CCGT and OCGT), diesel generators, CHP, as well as performing demand reduction.

In the case of standby diesel generation, it is presumed that an average diesel capacity of 500 MW is reserved for the aggregators. Using Eqs. (3.64) and (3.65) the capacity for reserved BAU plants can be determined. Three types of data (load factor, carbon emission level, and the resultant carbon emissions) are obtained in each warm-up and shutdown profiles for reserved BAU plants.

Fig. 4.49 shows the plot of carbon emissions of the reserved BAU plants (including warm-up and shutdown). It demonstrates the STOR operation as of two hours (per STOR event). The warm-up sequence is completed in approximately 30-35 minutes. This is when the reserved BAU plants are assumed to be ready to generate energy (short-term 6.7 % increase in fuel consumption) until the end of the STOR event. There is a slight increase of carbon emissions at the beginning of the STOR operation (from 0.5^{th} hour until 2.65^{th} hour). This happens due to the effect of TD losses.

During the shutdown phase, the duration is expected to be 10 minutes for OCGT plants (note the sharp drop of carbon emissions for OCGT plants at 2.5^{th} hour). In contrast, during the entire shutdown period, the CCGT plant instantly de-loads from the base-load. The shutdown initiation starts as soon as the load is smaller than the base-load, until the flame-off signal. For simplicity, the CCGT plants will be considered to shut down completely instead of 'parking' at certain load, and the plant would emit negligible emissions after the flame-off phase.

Due to the straightforward nature of operation of standby diesel generators, the carbon emissions can be determined as a single profile. Since carbon emissions for diesel generators $\mathscr{E}_I^k$ are defined as the product of the carbon factor and the energy generated, $\mathscr{E}_I^k$ is compared with the same scale generation by BAU plants (denoted by $\mathscr{E}_B^{ik'}$) using Eq. (3.65). The carbon savings are computed using Eq. (3.66).

Using Eq. (3.66), the carbon savings through the intervention by diesel generators in

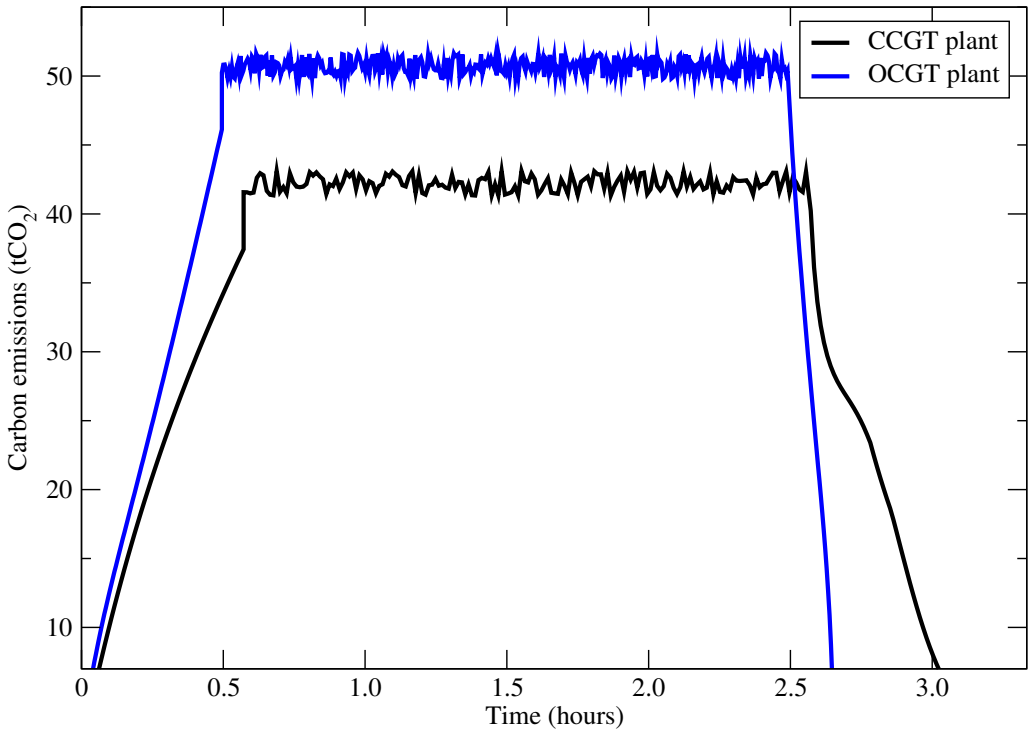

Figure 4.49: Carbon emissions of the 500 MW CCGT and OCGT plants in a single STOR event.

comparison with reserved BAU plants are shown in Tables 4.16 and 4.17, respectively. The total amount of 0.54±0.70 ktCO$_2$ is saved with 2.92±129.63 % reduction of using diesel generators in comparison with CCGT plants in the layout of the experiment. Similarly, 1.26±0.40 ktCO$_2$ is saved with 6.55±31.74 % reduced due to the substitution by diesel generators of the generation capacity in OCGT plants. The percentage uncertainty in this case is high due to randomised event and different operating policies of plants and generators. The carbon emissions are estimated assuming that the National Grid would call reserved BAU plants to contribute the total capacity of STOR, when an aggregator substitutes proportional part of the total STOR capacity. Because of the specific operational conditions, reserved BAU plants produce higher amount of carbon emissions than diesel generators.

Table 4.16: Carbon emissions and savings of diesel generators in comparison with CCGT plants, based on 60 STOR runs with 50 hours of operations.

	CCGT emissions (ktCO$_2$)	Diesel emissions (ktCO$_2$)	Carbon savings (ktCO$_2$)
Warm-up	4.45 ± 0.26	0.36 ± 0.02	4.09 ± 0.26
Operation	10.83 ± 0.60	17.62 ± 0.16	-6.79 ± 0.62
Shut-down	3.24 ± 0.18	0	3.24 ± 0.18
Total carbon savings (ktCO$_2$)			0.54 ± 0.70

Table 4.17: Carbon emissions and savings of diesel generators in comparison with OCGT plants, based on 60 STOR runs with 50 hours of operations.

	OCGT emissions ($ktCO_2$)	Diesel emissions ($ktCO_2$)	Carbon savings ($ktCO_2$)
Warm-up	4.04 ± 0.10	0.36 ± 0.02	3.68 ± 0.10
Operation	13.94 ± 0.36	17.62 ± 0.16	-3.68 ± 0.39
Shut-down	1.26 ± 0.02	0	1.26 ± 0.02
Total carbon savings ($ktCO_2$)			1.26 ± 0.40

For the case of demand reduction and CHP response, carbon savings can be determined through Eqs. (3.67) and (3.68) respectively. It is assumed that an average of 500 MW capacity of CHP and demand reduction during a STOR event. Table 4.18 shows the amount of carbon savings for CHP and demand reduction response. Total 9.44 ± 0.55 tCO_2 (50.97 ± 5.83 %) is saved using CHP and 11.44 ± 0.64 tCO_2 (61.77 ± 5.60 %) is saved with demand reduction. It should be noted that all the timeline and reserve capacity for the smart intervention in STOR programme are considered identical. In reality, such numbers vary significantly according to the capability in the scale of intervention by aggregators, and also the tendered volume and duration of the programme approved by National Grid.

Demand response types	Carbon savings (tCO_2)
CHP	9.44 ± 0.55
Demand reduction	11.14 ± 0.64
Overall Carbon savings (tCO_2)	20.58 ± 0.84

Table 4.18: Carbon savings of 500 MW CHP and demand reduction response based on 60 STOR runs with 50 hours of operations.

4.4.2.2 Triad

As indicated by Ward et al. (2012), the standard operation of a Triad event is one hour. It is likely to have up to 30 Triad warnings (30 hours of Triad operations) for a year at different times issued by the energy authorities before the event. Those Triad warnings are useful for Triad participants as they act as signals to trigger the intervention by diesel generators in providing back-up generation instead of buying the electricity from the UK energy grid. However, the actual reduction in TNUoS charges are only apparent as the result of hitting all the three Triad peaks as announced by National Grid. As Triad warnings are issued when there are high peak demands, the energy grid is presumably under 'stress' with high

amount of carbon intensity. Henceforth the Triad warnings may assist in lowering demand in the grid by having standby diesel generators operating independently.

The complete profiles of carbon emissions for reserved BAU plants are similar to STOR (see Fig. 4.49), but with different duration of operation due to different timeline projections of DR programmes. The reserved capacity for diesel generators is at the same scale as reserved BAU plants with total generating capacity of 1 GW. Using Eq. (3.69), the carbon savings of 30 Triad runs are shown in Tables 4.19 and 4.20 respectively.

Table 4.19: Carbon emissions and savings of diesel generators in comparison with CCGT plants, based on 30 Triad runs of one hour each.

	CCGT emissions ($ktCO_2$)	Diesel emissions ($ktCO_2$)	Carbon savings ($ktCO_2$)
Warm-up	5.06 ± 0.26	0.35 ± 0.02	4.71 ± 0.26
Operation	28.00 ± 1.47	21.15 ± 0.16	6.85 ± 1.48
Shut-down	3.69 ± 0.20	0	3.69 ± 0.20
Total carbon savings ($ktCO_2$)			15.25 ± 1.51

	OCGT emissions ($ktCO_2$)	Diesel emissions ($ktCO_2$)	Carbon savings ($ktCO_2$)
Warm-up	4.17 ± 0.10	0.35 ± 0.02	3.82 ± 0.10
Operation	17.13 ± 0.42	21.15 ± 0.16	-4.02 ± 0.45
Shut-down	1.29 ± 0.02	0	1.09 ± 0.02
Total carbon savings ($ktCO_2$)			0.89 ± 0.46

Table 4.20: Carbon emissions and savings of diesel generators in comparison with OCGT plants, based on 30 Triad runs of one hour each.

Through Triad programme, the total amount of 15.25 ± 1.51 $ktCO_2$ (41.49 ± 9.90 % reduction) are saved using diesel generators in comparison with CCGT plants. Carbon savings of 0.89 ± 0.46 $ktCO_2$ (3.93 ± 51.68 % reduction) can still be achieved compared with OCGT plants.

The sensitivity test to investigate how the extended duration of a Triad event may affect carbon savings in the DR programme (when they become negative) is performed. In this analysis, the emissions from diesel generators are compared with CCGT and OCGT plants running at longer hours. This result is shown in Figs. 4.50 and 4.51. The main aim of the sensitivity analysis performed in Figs. 4.50 and 4.51 is to show that continuous runs of diesel generators in a single Triad event do not guarantee carbon savings in case of longer programme duration. The result happens when diesel generators are operating at longer scale, beyond the current energy policies and programmes. This shows that diesel

generators are indeed beneficial in promoting carbon savings in short-term duration and unsuitable (in terms of carbon emissions) for long operation. In the normal mode of operation, BAU plants are most suitable for sustainable and reliable low-polluting energy generation. The emissions during the warm-up, standby and shutdown from BAU plants are counterbalanced by high amount of diesel-fuelled emissions.

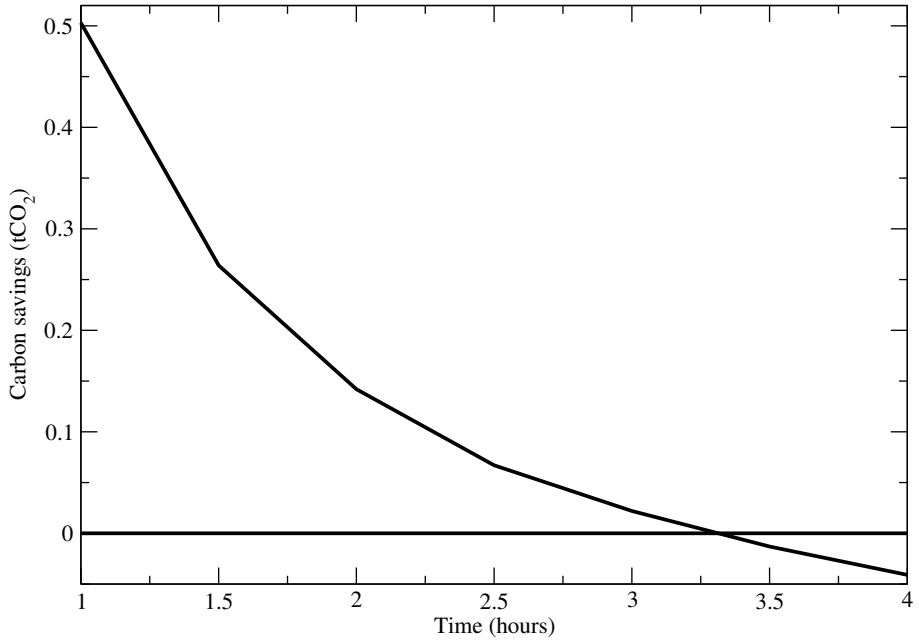

Figure 4.50: Carbon savings per Triad event as a function of the duration of the event.

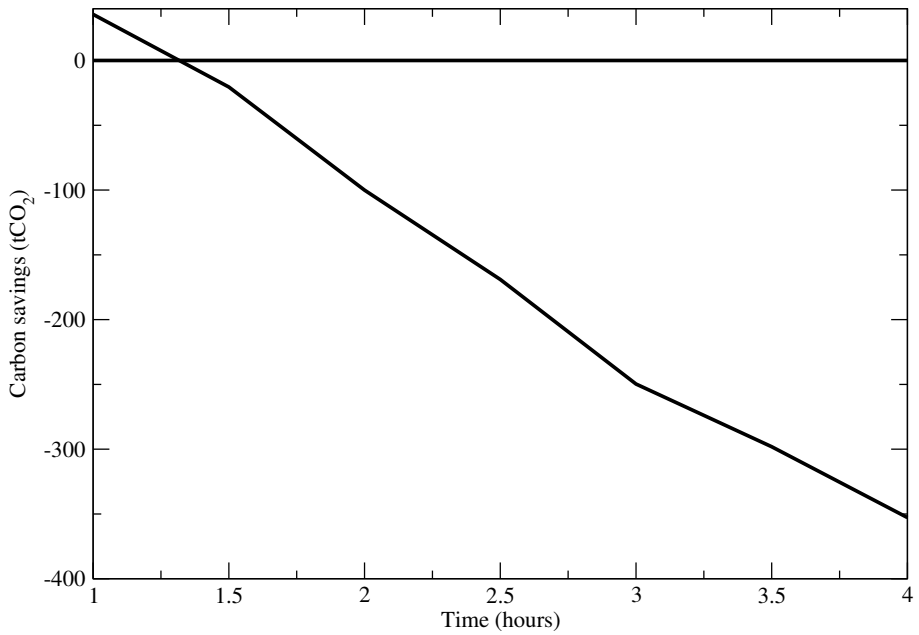

Figure 4.51: Carbon savings per Triad event as a function of the duration of the event.

4.4.2.3 Fast Reserve

The Fast Reserve operation is modelled as of total 365 days of the FFES-2 run. The tendered Fast Reserve period (01/04/13-31/03/14) from Table 3.9 is used to model Fast Reserve events within the timeline intervals. Fast Reserve events occur daily in mornings and evenings at various intervals. Duration of the Fast Reserve events varies. The operating profile of the FFES-2 is modelled based on the specifications provided in Table 3.7 with 90 MW generating size and 75 MW pumping capacity. The maximum energy utilisation for FFES-2 is limited to 250 MWh per operational day. The event duration is adjusted to be 15-30 minutes for a normal period (spring-summer) and 15-60 minutes for a critical period (autumn-winter). With the current 90 MW generating capacity, the FFES-2 is only allowed to operate for total duration of 2 hours and 47 minutes per operational day. Carbon emissions of FFES-2 ($\mathscr{E}_H$) are computed using Eq. (3.71). The $\mathscr{E}_H$ of the FFES-2 in the Fast Reserve programme is shown in Table 4.21. Based on Table 4.21, the simulation of FFES-2 estimates emissions $\mathscr{E}_H$ as 21.07$\pm$0.57 ktCO$_2$/year.

Table 4.21: Carbon emissions of the FFES-2 under Fast Reserve programme for one year period.

FFES-2 mode	Carbon emissions (ktCO$_2$/year)
Pump	20.89 ± 0.56
Generator	0.18 ± 0.08
Total carbon emissions (ktCO$_2$/year)	21.07 ± 0.57

Similar with STOR and Triad programmes, the operating profiles of reserved BAU plants are used to compare the carbon emissions against the Ffestiniog hydro plant. In some cases, when the remaining three fleets in the Ffestiniog plant are assumed operating with the same duration and reserved capacity of FFES-2, using Eq. (3.72) the emissions $\mathscr{E}'_H$ of the Ffestiniog plant are obtained as 84.28$\pm$2.28 ktCO$_2$/year. Additionally, the BAU emissions $\mathscr{E}^i_B$ are also computed considering the capacity of the BAU plants as the same as the Ffestiniog hydro plant during the mode of generating electricity. The carbon savings based on the intervention by the Ffestiniog plant are calculated using Eq. (3.73). Tables 4.22 and 4.23 demonstrate the carbon savings of the hydro-plant in comparison with reserved BAU plants.

Through the simulations of the Fast Reserve programme, total 61.75$\pm$5.70 ktCO$_2$ (42.29$\pm$9.23 % reduction) are saved using the hydro plant in comparison with CCGT

Table 4.22: Carbon emissions and savings of the Ffestiniog hyrdo-plant in comparison with CCGT plant for one year period.

Plant	Carbon emissions ($ktCO_2$/year)
CCGT	146.03 ± 5.22
Hydro-pump	84.28 ± 2.28
Carbon savings ($ktCO_2$/year)	61.75 ± 5.70

Plant	Carbon emissions ($ktCO_2$/year)
OCGT	146.37 ± 2.48
Hydro-pump	84.28 ± 2.28
Carbon savings ($ktCO_2$/year)	62.09 ± 3.37

Table 4.23: Carbon emissions and savings of the Ffestiniog hydro-plant in comparison with OCGT plant for one year period.

plants. Similarly, 62.09 ± 3.37 $ktCO_2$ are saved with 42.42 ± 5.42 % reduction achieved due to the substitution by the hydro plant of the generation capacity in OCGT plants. The carbon emissions and savings are estimated assuming that the National Grid would activate the reserved BAU plants to contribute the total capacity of Fast Reserve if the hydro-plant did not provide reserve at the mandatory event.

4.4.2.4 Frequency Control by Demand Management (FCDM)

The FCDM event is simulated for the programme duration of one year. Due to the unknown exact event frequency, the event frequency for FCDM is allocated randomly between the minimum 10 and maximum 40 annual frequency. The operational period of FCDM lies between 30 minutes and two hours. The required volume of demand reduction is pre-set within 3 MW (minimum) and 20 MW (maximum). All randomised parameters of FCDM can be simulated using random permutation in Matlab (permuted operation period and intended volume of reduction). A Monte Carlo simulation of N = 100 is performed to randomly sample the electricity grid carbon factor, FCDM periods and volume of reduction. Finally, Eq. (3.74) is applied to compute the amount of carbon savings due to the FCDM programme.

The carbon saving due to the FCDM programme is 184.72 ± 25.30 tCO_2. The results, however, not to be compared with the 'demand reduction' response in STOR and Irish smart metering programme due to different nature and purpose of each DR programmes.

4.4.2.5 Irish smart metering trial

The carbon emissions and savings resulting from the BAU and test group are compared in the smart meter installation. The BAU group acts as the baseline for the energy consumption and carbon emissions. As mentioned in Section 3.8.3.5, for feasibility purposes all ToU tariffs in combination with Demand Side Management (DSM) stimuli are compared for 132 days (01/01/2010-12/05/2010) of trial runs. The test group is compared with the BAU group for carbon savings assessment using Eq. (3.75). The result of the carbon savings based on all ToU tariffs in combination of DSM stimuli are shown in Table 4.24.

Table 4.24: Carbon savings of ToU tariffs in combination of DSM stimuli based on 132 days of trial runs (2010). IHEM - In-home electricity monitor; OLR - Overall load reduction incentive; BI - Bi-monthly detailed energy bill; MO - Monthly detailed energy bill. Negative values indicate additional emissions (no carbon savings) whereas positive values indicate saved emissions (carbon savings).

ToU Tariffs and DSM types	Overall carbon savings ($kgCO_2$)				
	Morning	Peak evening	Night	Midnight	Overall
Tariff A + IHEM	-38.82 ± 0.04	-12.26 ± 0.06	-21.18 ± 0.06	-32.24 ± 0.02	-96.87 ± 0.08
Tariff B + IHEM	-11.14 ± 0.08	-13.24 ± 0.08	-28.99 ± 0.08	-34.61 ± 0.04	-78.39 ± 0.14
Tariff C + IHEM	-13.10 ± 0.04	-14.83 ± 0.06	-19.07 ± 0.04	-24.33 ± 0.02	-62.63 ± 0.08
Tariff D + IHEM	$\mathbf{12.80 \pm 0.06}$	$\mathbf{0.16 \pm 0.08}$	$\mathbf{4.59 \pm 0.08}$	$\mathbf{11.65 \pm 0.04}$	$\mathbf{29.20 \pm 0.13}$
Tariff A + OLR	-21.41 ± 0.04	-11.76 ± 0.06	-14.83 ± 0.04	-21.05 ± 0.02	-62.03 ± 0.08
Tariff B + OLR	-67.88 ± 0.08	-49.69 ± 0.10	-58.15 ± 0.08	-56.61 ± 0.04	-204.21 ± 0.16
Tariff C + OLR	-46.19 ± 0.04	-13.92 ± 0.06	-30.30 ± 0.04	-27.10 ± 0.02	-105.22 ± 0.08
Tariff D + OLR	-12.69 ± 0.08	-8.24 ± 0.08	-16.80 ± 0.08	-19.21 ± 0.04	-52.17 ± 0.16
Tariff A + BI	-0.46 ± 0.04	-8.46 ± 0.06	-9.43 ± 0.04	-16.19 ± 0.02	-31.89 ± 0.08
Tariff B + BI	-31.53 ± 0.08	-9.17 ± 0.08	-16.66 ± 0.06	-11.13 ± 0.04	-64.71 ± 0.14
Tariff C + BI	-16.58 ± 0.04	-2.67 ± 0.06	-14.21 ± 0.06	-14.38 ± 0.02	-46.50 ± 0.10
Tariff D + BI	-37.95 ± 0.08	-19.25 ± 0.08	-20.47 ± 0.06	-17.55 ± 0.04	-86.19 ± 0.14
Tariff A + MO	-30.92 ± 0.04	-11.98 ± 0.06	-32.26 ± 0.04	-22.33 ± 0.02	-89.23 ± 0.08
Tariff B + MO	-28.48 ± 0.06	-24.49 ± 0.08	-16.27 ± 0.06	-23.05 ± 0.04	-82.62 ± 0.12
Tariff C + MO	-1.93 ± 0.04	-4.31 ± 0.02	-8.50 ± 0.02	-14.79 ± 0.01	-26.49 ± 0.08
Tariff D + MO	-20.88 ± 0.08	-3.85 ± 0.04	3.41 ± 0.04	-9.40 ± 0.02	-28.27 ± 0.14

Based on Table 4.24, the Tariff D in combination of In-home electricity monitor (IHEM) promotes reduction in energy usage and the resultant carbon emissions. The Tariff D incurs higher electricity price during the peak period, and lower price during the off-peak period than other tariffs. Moreover, with the aid of IHEM, consumers are aware of real time electrical usage and the tariff price. Therefore, maintaining the electrical usage is achievable in real time. Surprisingly, all other variable ToU rates and DSM stimuli do not promote carbon reductions but with additional emissions. This indicates that the test group is incapable of reducing their consumption at different variable rates and DSM stimuli.

The test group with the smart initiative of Tariff D in combination of IHEM is considered in further analysis. The diurnal trend of average carbon emissions for the BAU and test groups and their relative difference are shown in Fig. 4.52.

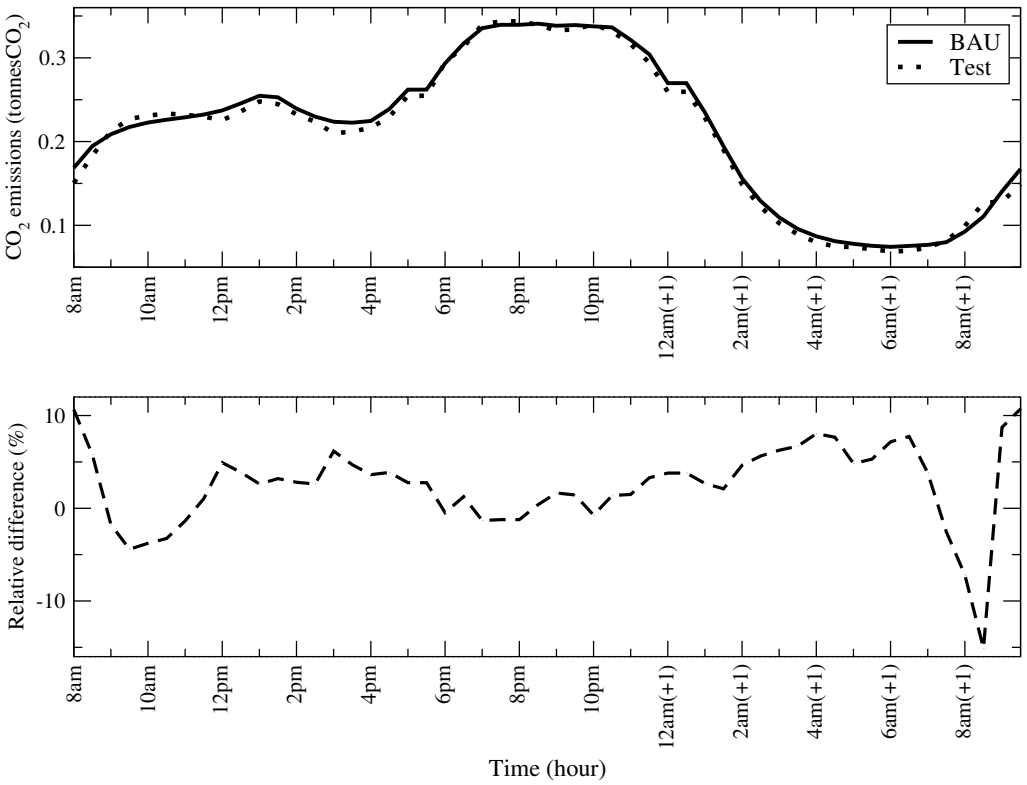

Figure 4.52: Irish smart metering trial. Top: carbon emissions of the BAU and test groups in a single day. Bottom: the relative difference of carbon emissions for the BAU and test group. Note that $(+1)$ indicates next day.

As can be seen in Fig. 4.52, at times of peak period 5 – 7pm (ToU rate of 38 cents/kWh) there is no distinct trend in reduction of carbon emissions and energy usage by the test group. However, emissions reduction by the test group are quite visible from 12 – 5pm. Additionally, there is a slight decrease of the carbon emissions by the test group from 10pm until the 6am next day. In contrast, there are higher energy consumption and emissions by the test group than the BAU group from 9am to 11am when morning-afternoon ToU rate is applied (12.5 cents/kWh). Overall, there is no clear trend in demand shift towards the cheapest tariff (midnight from 11pm to 8am next day). Additionally, there is only a small tendency of demand reduction during the peak period.

The carbon savings for Tariff D with the combination of IHEM are shown in Table 4.25.

Table 4.25 shows the overall $0.09 \pm 47.05\,\%$ reduction (0.16 ± 0.08 kgCO_2 saved) in

Table 4.25: Carbon savings for 132 days (01/01/2010-12/05/2010) of smart metering trial, based on different imposed Tariff D with the combination of In-home electricity monitor (IHEM) initiative.

	Morning-afternoon rate 8am-5pm	Peak rate 5pm-7pm	Night rate 7pm-11pm	Midnight-morning rate 11pm-8am
Carbon savings per consumer ($kgCO_2$)	12.80 ± 0.06	0.16 ± 0.08	4.59 ± 0.08	11.65 ± 0.04
Percentage reduction (%)	2.24 ± 0.46	0.09 ± 47.05	1.19 ± 1.74	3.79 ± 0.34

the peak period. The test group is not able to reduce the electricity usage during peak periods. Additionally, there is no definite demand shift of the test group as the test group still use lesser energy than the BAU group that contributes to carbon savings in other off-peak period. The average carbon savings achieved by the test group are estimated as 29.20 ± 0.13 $kgCO_2$ (1.83 ± 0.44 % reduction). Hence, the overall impact of the smart interventions (Tariff D + IHEM) is low. With the current 5000 participants in the trial, the carbon savings for 132 days would be 146 ± 0.65 tCO_2. It can be further estimated that if there are one million population in a metropolitan city, the overall carbon savings for 132 days would be 29.20 ± 0.13 $ktCO_2$.

4.4.3 Case study 1: Dynamic demand challenge

This case study is the part of the dynamic demand challenge prize competition in partnering with Nesta, National Grid, Climate KIC, Imperial College London and the Centre of Carbon Measurement at National Physical Laboratory. The case studies comprised five innovations from the team finalists. According to Nesta (2013), the competition was established to promote stimulations in technologies or services to promote carbon emission reductions. Types of solutions can be in the form of demand shifting to off peak times, or renewable generation with smart technologies. The detailed description of the scenarios can be found in Nesta (2013); The Centre for Carbon Measurement (2013). The test reports on carbon savings analysis based on five teams are permitted to be reported. The general description of the scenarios corresponding to each of the finalists are outlined below.

Team 1. Team 1 promoted reconciliation between the consumer and the smart heating control. A software product was developed that performed scheduled demand shifts based on the biased randomisation of the use of space and water heating

within households. Such innovation allowed reduction in costs for households and better demand management.

Team 2. Team 2 dealt with behavioural control of household consumers in using energy. A household community connected to one substation could use in-door indicators of high demand periods. Households responded to the high energy demand by varying their energy consumption (cancel or shift) manually. The success in achieving demand reduction or shifting would receive monetary rewards that would contribute to communal benefits.

Team 3. Team 3 developed a battery storage for households running PV panels. The battery storage was charged using the solar panels, and the control system then enabled the household to use the energy from the battery storage when they need it, thus achieving energy and carbon savings.

Team 4. Team 4 introduced a new thermal storage device that was used in conjunction with a heat pump for heat storage in domestic households and industrial estates. The thermal accumulator worked with heat pumps to provide heat when required, instead of drawing energy from the UK main energy grid.

Team 5. Team 5 developed a web-based solution that utilised the PV plus battery installations of the UK households in the National Grid Fast Reserve events.

4.4.3.1 Innovations

The technical description of all the innovations of the five team finalists is available in technical reports (Centre for Carbon Measurement, 2013a,b,c,d,e). Only general methodology is outlined in this section.

Team 1. The innovations are the algorithm and control system device that distribute demand for domestic heating over a longer time period. The algorithm and control system automatically switch domestic heating on and off at randomised intervals. The switching device was controlled using a web-based software interface. This software allowed the input data of a cloud calendar with requested heating periods. The switching device was connected using DC voltage, in series with

a resistor. Voltage across the resistor would provide an indication of the state of the relay. The relay would trigger switch on or off for appliances as controlled by the algorithm. The device was used in conjunction with a desired demand response curve to determine the relay switch periods daily. All relay switching were randomised depending on the user requirements and the desired demand response.

Team 2. Energy measurements were recorded with one minute interval from a substation. This dataset was used to generate predictions of daily usage profiles based on weather conditions. Each household in a considered community had a in-door indicator informing about active periods of high peak at the beginning of the day. The high peak period was assumed to be of random duration (1-2 hours) centred on the daily maximum peak. Based on the changes of energy use, the community might receive rewards. The reward earned per day day was based on the high-tide mark for the entire day besides the active period. The community might perform behavioural actions such as removing or reducing energy use, shift loads to previous day and delay loads for later day. As soon as the amount of reward was calculated, the earned reward was transmitted to all indicators. Every morning, the community would see the rewards gained yesterday and the active period for the present day.

The behavioural usage of energy was modelled as follows. During the active period, the household takes actions according to indicator a number of times as shown in Table 4.26. Such probabilities of the number of actions were provided by the team.

Table 4.26: Probabilities of the number of actions per day expected from customers.

Number of actions	Probability (%)
0	50
1	25
2	12.5
3	6.25
4	6.25

The household would perform: 1) the reduction of the current load by 3-10 %; 2)

delay 10-20 % of the current load to a better time where usage was significantly below the high-tide mark and the household will manually operate the energy usage (for instance, using a timer). Each single action was performed with equal probability: 1) reduce load by 3-10 %; 2) shift load to prior day; 3) delay 10-20 % of the load to later day.

Team 3. The self-battery storage for households was capable of storing energy from a PV array. The battery storage can be used as the main supply for domestic usage or exporting energy to the grid when electricity prices or carbon intensity were high. The battery storage was capable of converting the stored energy into the AC power. The battery had 4 kWh storage and charged only from PV panels. During the charging mode, a 900 W capability would take around 5 or 6 hours into 4 kWh batteries. During the discharging mode the 4 kWh would sustain around 6-7 hours of energy supply based on the discharging rate of 860 W/hour. Typically, approximately 8 hours of daytime exporting from the PV panels were required to reduce the main evening peak by up to 860 W.

It was assumed that the charging and discharging mode happened in around 250 sunny days annually in the UK. The annual energy displaced was approximated as 1000 kWh. For carbon modelling purposes, the battery was assumed to charge daily within 2-4 kWh. The battery was not allowed to drop below 50 % of the full capacity (2 kW).

Team 4. The prototype device was a thermal accumulator with a storage capacity of 2.5 kWh. The thermal accumulator coupled with a typical variable capacity heat pump provided space heating and hot water to households. It was expected to be mounted based in closed recirculating water flow in radiators and running hot water for kitchen and bathroom. The variable capacity heat pump would charge the thermal accumulator in the off peak period at part load (50 % to take advantage of the higher coefficient of performance). The thermal accumulator was discharged when it was needed. It was assumed that the heat pump would be switched off during the heat release by the thermal accumulator. The demand shift was achieved by charging the thermal accumulator at night period and using the heat energy from the thermal accumulator during evening peak hours

instead of using the heat pump.

The thermal accumulator would be charging for 4 hours of duration to achieve full thermal capacity. The team provided a simulated monthly variation in the Coefficient of Performance. The coefficient provided the amount of heat for each unit of energy consumed and the efficiency of the pump. The household was assumed to be a 3-bedroom semi-detached house with mean daily energy consumption of 22.5 kWh for space heating and 10 kWh for hot water. Heat exchanger losses were assumed to be 15 %.

The thermal accumulator produced carbon emissions through the charging periods in summer. This was due to the charging of the thermal accumulator from the main grid as the heat pump would not be required for operating in hot seasons. The emissions however were mitigated by carbon savings due to the demand shift. In contrast, during the winter the heat pump was assumed to operate at night that provided space heating and hot water for morning usage. Hence the charging of the thermal accumulator in winter was accomplished through the pump, without additional carbon emissions.

Team 5. Households with PV array and 8 kWh battery storage systems were assumed to participate in the Fast Reserve programme, which was a part of the 25,000-unit bid managed by the team. The system was implemented into the cloud service to distribute the Fast Reserve signal. The Fast Reserve requirements were the same as described in Section 2.5.2.3.

Total of 72 Fast Reserve events were anticipated per annum with the average of 6 events occurring per month. The battery charged only from PV panels and during the Fast Reserve event, the battery was assumed to be fully charged. The batteries should be able to provide electricity for at least 15 minutes energy supply without interruption.

4.4.3.2 Common scenario for assessment of carbon savings

The common scenario modelled for all five innovations, which allowed fair and comparable quantification of carbon emissions and savings. The scenario applied was as follows:

- Spatial scale of households/SMEs: 100 units;
- Temporal scale: 2013 year;
- Location based in London, with observed weather data provided (European Centre for Medium-Range Weather Forecasts (ECMWF) temperature);
- Energy usage of up to 50 kWh.

4.4.3.3 Quantification of carbon emissions and savings

Eq. (3.5) was used to calculate the amount of carbon emissions resulting from the interventions applied. For computation of carbon savings based on the BAU scenario and the interventions applied, the Eq. (3.6) is applied. Different BAU scenarios were assumed for five teams.

Team 1. The BAU layout was a household without implementation of switch relay, and the improved scenario layout included a water heater and storage heater by the algorithm and the switching device.

Team 2. The BAU layout was the same community without deployment of in-door indicator installed and therefore energy was used in normal pattern. The innovation scenario had in-door indicators, and carbon savings were determined due to behavioural changes of delay, shift or remove load.

Team 3. The BAU layout was a household without PV plus battery installation. In contrast, the innovation scenario included the PV plus battery installation. Such installation provided the household with stored energy during evening peak hours.

Team 4. The BAU layout was a household with an installed geothermal heat pump only. The improvement layout was the household with the heat pump combined with the thermal accumulator.

Team 5. In this case, the BAU layout was a household with PV plus battery installation. The innovation scenario includes the existing PV and battery and utilises the available stored energy for the Fast Reserve programme. Therefore, the assessment of carbon saving was when the household used in-house battery instead of using electricity from the UK grid during on the Fast Reserve events.

4.4.3.4 Results

Simulations of carbon emissions and savings for five innovations were performed with the common scenario as described in Section 4.4.3.2.

Team 1. The carbon savings due to the biased randomisation algorithm were estimated as 334±50 tCO_2/year for 100 households. There were no direct emissions as the energy demand was reduced. The uncertainty was due to different operational hours of electrical appliances as defined by households.

Team 2. The carbon savings were estimated as 155±15 tCO_2/year for 100 households. The savings were however estimated hypothetically due to assigned probabilities of households' actions. There were no direct emissions as the energy usage was reduced or maintained of the same level. The uncertainty was due to ranges of probabilities of behavioural actions.

Team 3. The carbon savings were estimated as 30.65±0.39 tCO_2/year for 100 households as the result of evening usage of energy from the battery storage which was charged using the PV panels in the daytime. There were no direct emissions as the battery storage was charged using the green energy (PV panels) instead from the main grid. The uncertainties were originated from amount of sunlight absorbed due to the weather and climate conditions, and also the different charging capacity of the battery storage.

Team 4. The carbon savings were estimated as 5.09±0.02 tCO_2/year for 100 households as the result of the use of the thermal accumulator. The carbon emissions approximated during summer due to night charging from the main grid were 41 tonnes. On the other hand, annual carbon savings from evening demand shift are about 46 tonnes. These brought the overall carbon savings about 5.09±0.02 tCO_2/year for 100 households. The uncertainty included the different efficiency of implemented heat pump as higher efficiency required shorter duration to deliver the same heat energy, thus impeding the carbon savings in the thermal accumulator, and also the heat loss in the pump and in the thermal accumulator.

Team 5. Simulations of 72 Fast Reserve randomised events per year were carried out

with 100 households instances in order to quantify uncertainties. The carbon savings were estimated as 1.64±0.01 tCO_2/year for 100 households as the result of the battery storage during the Fast Reserve events. There were no direct emissions as the battery storage was charged using the green energy (PV panels) instead from the main grid. The uncertainties were originated from the amount of sunlight absorbed due to the weather conditions, and also the different charging capacities of the battery storage. There were no direct emissions as the battery storage was charged using the green energy (PV panels) instead of the main grid. Sources of uncertainties included unknown Fast Reserve events, and also the difficulty in maintaining the 50 MW minimum delivery of Fast Reserve event due to the battery efficiency.

4.4.4 Case study 2: Carbon emissions and savings in the Transform model

The Transform model developed by EA Technology (2012, 2013) is a parametric representation of energy profiles based on various observational datasets, which allows one to forecast demand in the UK electricity market for mid and long-term horizons. The system parameters are superimposed with estimated forecasts of various Low Carbon Technologies (LCT). The earlier report by EA Technology (2012, 2013) considered two investment solutions: the BAU and incremental (INC). The BAU assumed only conventional solutions (installations of new cables and transformers). The INC strategy (also known as smart) assumed an optimal blend of conventional and smart interventions in the smart grid (for instance, energy storage, real-time thermal ratings and DR), with associated changes in demand profiles. The mentioned report considered four scenarios of uptake of LCT (SC1-SC4), using heat pumps, electrical vehicles, photovoltaics and generation based on scenarios from National Grid. The complete set of load profiles from the Transform model is available for the modelled years 2015-2060 for the three energy-wise important days (winter peak, winter average and summer average in each year), one for each LCT uptake scenarios in BAU and in INC investment strategies. The overview of the modelled scenario adapted from EA Technology (2013) is given in Table 4.27. The estimation of carbon emissions and savings based on the output projections of DR of

the Transform model are performed. Carbon emissions and savings for two investment strategies are taken into account, with four scenarios in each of the investment.

Table 4.27: Overview of the modelled scenarios of the Transform Model. Adapted from EA Technology (2013).

Scenario number	Scenario name	Heat pump uptake	Electric vehicle uptake	Solar Photovoltaic uptake	Generation mix uptake
1	High abatement in low carbon heat	High	Medium	Medium	Gone Green
2	High abatement in transport and bio-energy	Medium	High	Medium	Gone Green
3	Focus on high electrification	High	High	High	Gone Green
4	Purchase of international credits	Low	Low	Low	Slow Progression

4.4.4.1 National Grid's future generation mix

The UK's future energy development is based on two scenarios, Slow Progression and Gone Green, as reported by National Grid (2014b). In the Slow Progression scenario, the development of both renewable and LCT is relatively slow, which results in slower progress towards environmental goals (for instance, no planned carbon reduction target for 2020, and greenhouse gas reductions would not meet the 2050 carbon targets). In contrast, the Gone Green scenario is developed to meet the environmental targets (for instance, 15 % use of renewable energy by 2020, an overall of 80 % reduction of greenhouse gas emissions by 2050). The available Excel Spreadsheet published by National Grid (2014b) provided data for estimation of the future trends of carbon reduction targets. These data allowed the assessment of the transform model data with projection of carbon intensity in order to quantify the carbon emissions and the associated savings. Since National Grid predicted the future energy generation up to 2050, the method of least-square fitting was applied to further forecast the generation mixes up to 2060 in Fig. 4.53. The figure shows the estimated carbon intensity of Slow Progression and Gone Green scenarios.

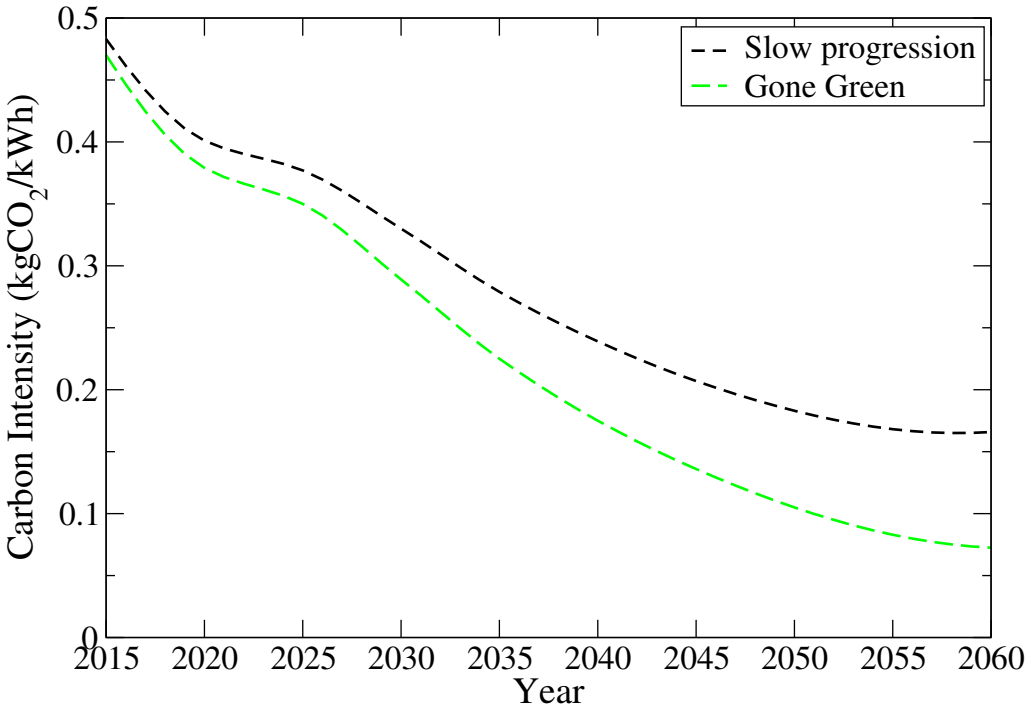

Figure 4.53: Carbon intensity of Slow Progression and Gone Green scenarios.

4.4.4.2 Carbon emissions and savings assessment

The carbon emissions resulting from the energy generated/consumed were derived from Eq. (3.5) and calculated as:

$$\mathscr{E}(t) = E(t) \cdot G(t), \tag{4.7}$$

where $\mathscr{E}(t)$ denotes carbon emissions (tCO_2), $E(t)$ is the amount of energy generated or consumed (kWh), and $G(t)$ is the dynamically changing electricity grid carbon factor (based on fuel mix) of the UK energy grid (tCO_2/kWh). The variable $G(t)$ is derived from the publicly available fuel mix data (BMRS and Elexon) following the Eq. (3.7).

Carbon savings S are generally derived from Eq. (3.6). In this context, the S is determined as the difference between carbon emissions of BAU ($\mathscr{E}_B$) and those in the INC ($\mathscr{E}_O$) energy profiles due to DR:

$$S^i(t) = \mathscr{E}_B^i(t) - \mathscr{E}_O^i(t), \tag{4.8}$$

where i indexes the scenarios (SC1-SC4).

4.4.4.3 The year 2013 real energy data

The real 2013 demand data from National Grid (2015) was considered and the average daily profiles for the three important days (winter peak, winter average, summer average) were analysed. Fig. 4.54 shows the 2013 average demand plots for the three important days based on the data provided by the EA Technology.

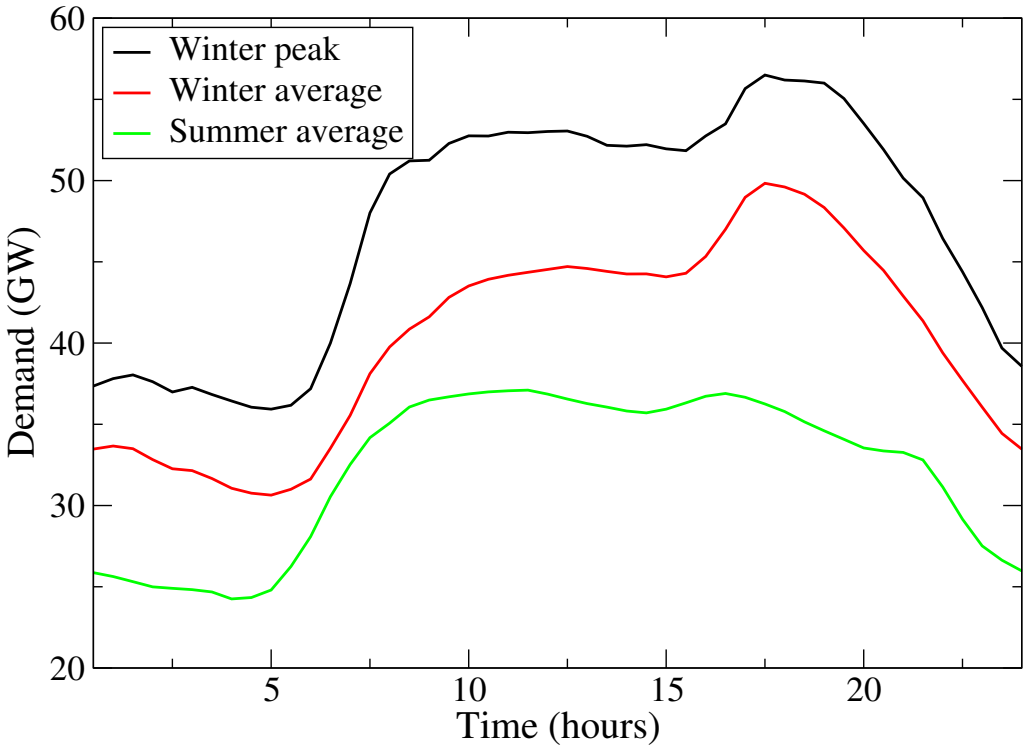

Figure 4.54: Average demand data for the three important days of 2013. Data courtesy of EA Technology.

The results from Fig. 4.54 are further compared with the Transform model results that comprise two main investment strategies with four scenarios each.

4.4.4.4 Evaluation of investment strategies

To evaluate the reduction of energy usage between the two investment strategies, BAU and INC, for each of the four scenarios the cumulative percentage energy reduction is calculated as

$$R = \sum_{t=1}^{N_t} \left(\frac{{}^{C}E_O^i(t) - {}^{C}E_B^i(t)}{{}^{C}E_B^i(t)} \right) \cdot 100\,\%, \tag{4.9}$$

where the superscript C indicates the cumulative summation of the energy reductions for BAU and INC solutions, i indexes the scenarios, t is the time step, $t = 1, 2, 3, \ldots, N_t$.

Total of the three important days were evaluated and the cumulative results were plotted in Figs. 4.55 to 4.57. This allowed the examination of the long-term energy reduction in various scenarios. As can be seen, in all three plots the least-optimised scenario SC4 demonstrates the lowest energy reduction.

Based on these results, the changes between BAU and INC were fairly small, which can be due to the projected low uptake of DR. The plots showed the difference of energy trends under four different scenario. However, the carbon emissions may vary significantly due to the energy target plan imposed by National Grid (due to the effect of Slow Progression and Gone Green Scenario). The carbon intensity (plotted in Fig. 4.53) was used to determine carbon emissions and savings.

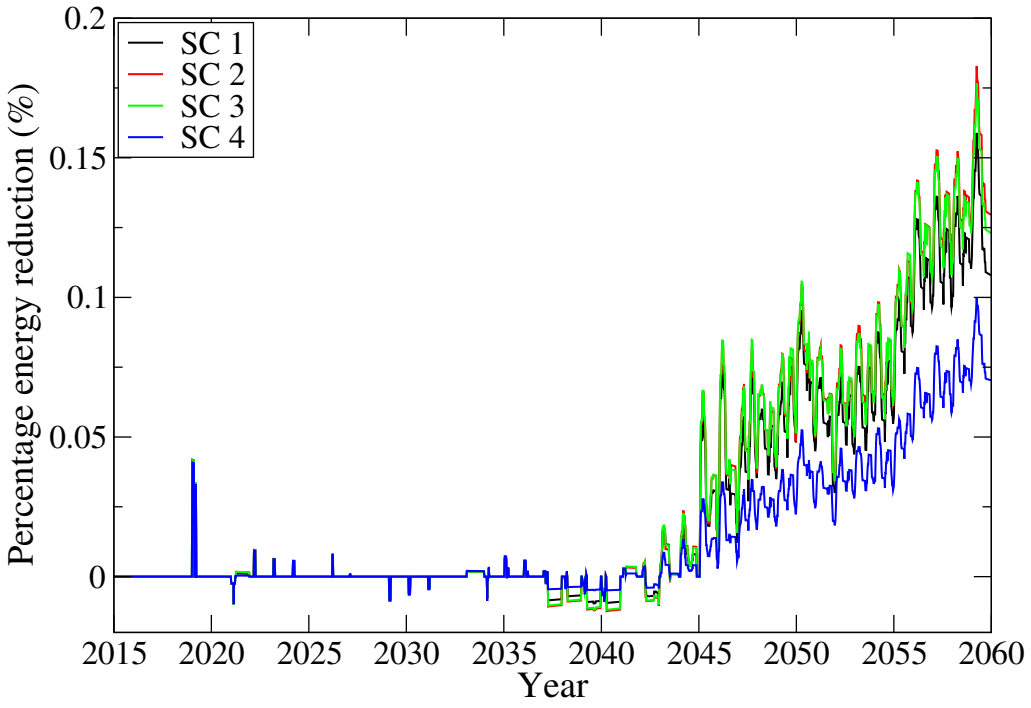

Figure 4.55: Cumulative percentage of energy reduction in peak winter days. SC – Scenario.

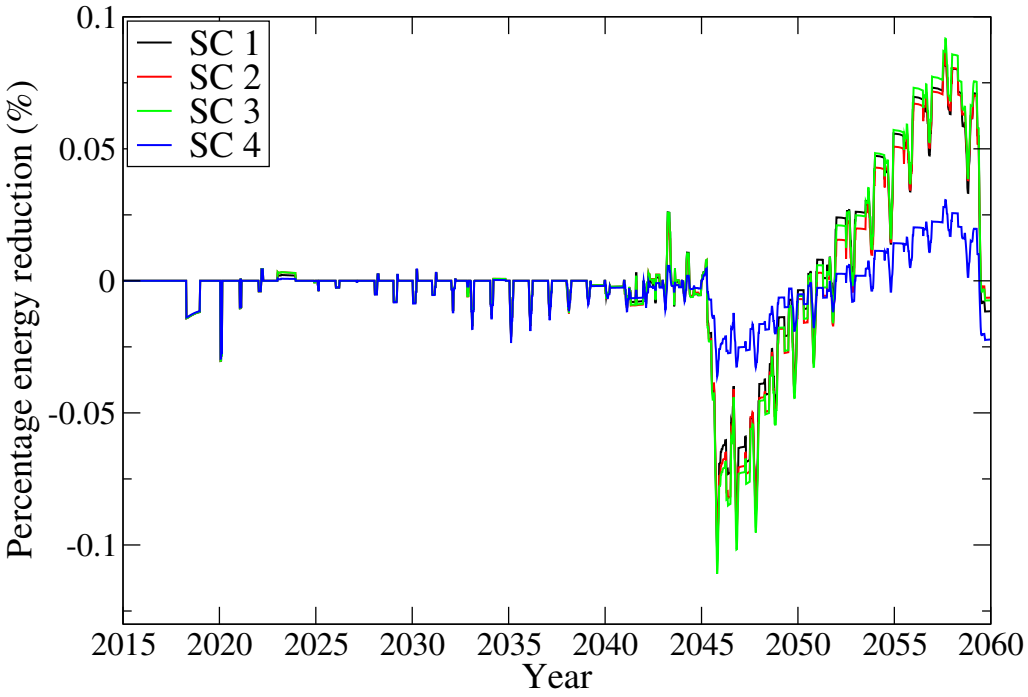

Figure 4.56: Cumulative percentage of energy reduction in average winter days. SC – Scenario.

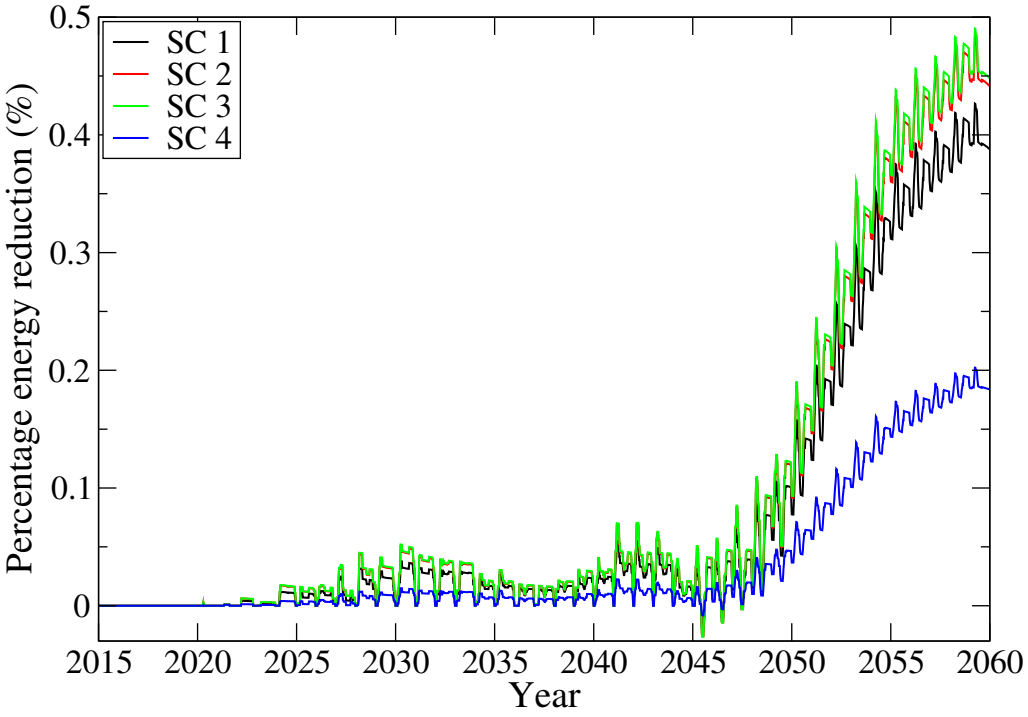

Figure 4.57: Cumulative percentage of energy reduction in summer average days. SC – Scenario.

4.4.4.5 Results

Carbon emission and savings for the three important days corresponding to each of the LCT uptake scenarios were computed. The mean of carbon savings is calculated from Eq. (4.8) and is denoted by $\mathbb{E}[S^i(t)]$. The corresponding standard deviations of carbon savings are also calculated ($\sqrt{\mathbb{E}[S^i(t)^2] - (\mathbb{E}[S^i(t)])^2}$). The results are summarised in the three tables (Table 4.28):

Table 4.28: Carbon savings in peak winter, average winter and summer days.

Scenario	Carbon savings ($ktCO_2$)		
	Peak winter	Average winter	Average summer
SC1	136.84 ± 7.98	-7.39 ± 15.30	212.68 ± 8.23
SC2	158.29 ± 8.16	-5.13 ± 15.35	258.47 ± 10.08
SC3	160.57 ± 8.75	-5.06 ± 16.93	258.47 ± 10.08
SC4	123.41 ± 6.49	-3.73 ± 10.76	184.52 ± 6.98

One can see that carbon savings in peak winter and average summer (Table 4.28) days were achieved. The employment of smart DR solutions (INC solution) following National Grid's Gone Green and Slow Progression scenario developed a greater potential towards carbon reduction targets. In addition, in the Slow Progression scenario the carbon intensity was higher than in the Gone Green scenario. The carbon savings based on SC4 were much lower than in other LCT uptake scenarios.

In contrast, the smart DR solutions introduced additional carbon emissions for the entire winter average period (Table 4.28). One of the possible barriers to the implementation of LCT was due to unavoidable circumstances (for instance, the constraints in infrastructure reinforcements).

Figs. 4.58 to 4.60 show the future trends of carbon savings from 2015 up to 2060. All plots demonstrate high fluctuations of carbon savings from 2045 onwards. One of the possible reasons for that maybe the projected LCT uptake (continued growth in onshore and offshore wind, new coal plants with carbon capture and storage technology, and increase in biomass use) forecast by National Grid (2014b). In addition, the increasing penetration of smart meters over time would also lead to an increased contribution of behavioural changes in energy use to the UK energy networks (EA Technology, 2012).

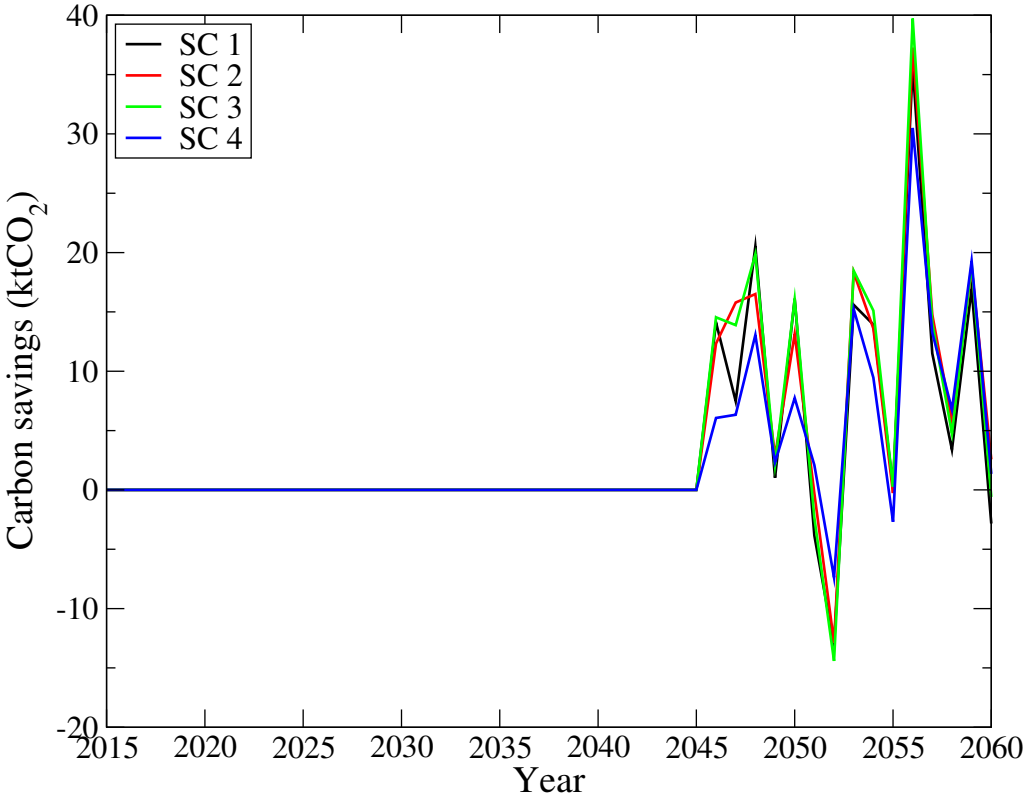

Figure 4.58: Projections of carbon savings for winter peak days.

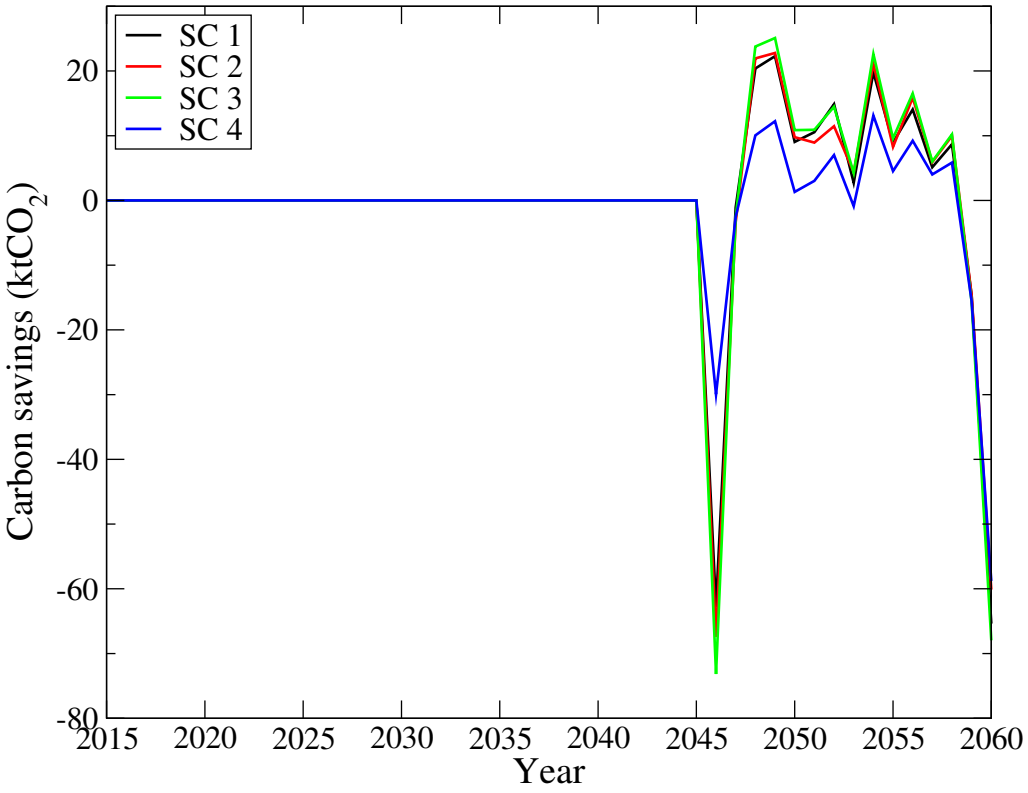

Figure 4.59: Projections of carbon savings for winter average days.

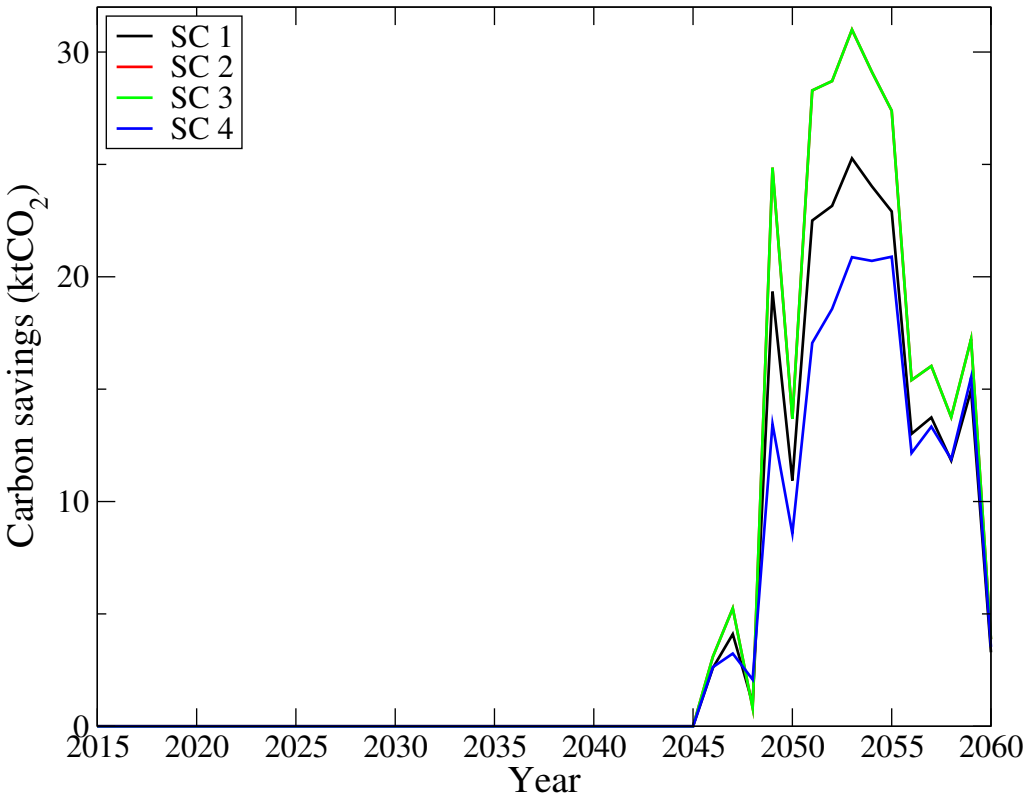

Figure 4.60: Projections of carbon savings for summer average days.

Chapter 5

Conclusions and future research

5.1 Research aim and objectives achievements

The section concludes how the established research aim and objectives have been met.

The research aim of the development of sound methodology for the quantification of carbon emissions and savings under smart grid has been successfully attained. Several scenarios based on real case studies are developed with necessary assumptions and control parameters. Whether or not a particular smart infrastructure or intervention produces carbon savings depends on the scale and operational policies.

The **first** research objective was to develop a stochastic model depending on the input sources. The input data is modelled developed initially using the HTF-based fitting with the real National Grid energy demand data for seasonal profiling of energy consumption based on groups of consumers. The real electrical data is obtained from the public sources (BMRS and Elexon).

The **second** research objective was to quantify carbon emissions and savings. The objective has been met by thorough reviews of GHG, carbon intensity (factor) across the power grid, the definition of carbon emissions and savings. The formulation of dynamic grid carbon factor with uncertainties, emissions and savings is performed analytically.

The **third** research objective requires quantification of uncertainties in the smart grid. General uncertainties include the changing dynamics of energy consumption and intermittency of green energy generation. Uncertainties are addressed by using EnKF forecast and assimilation. Additionally, uncertain carbon intensities were addressed by calculating

the resultant electricity grid carbon factor from from various fuels used in energy generation. The resultant calculation indicates the overall carbon intensity across the smart grid.

The **fourth** research objective requires numerical optimisation of the smart grid. This is formulated through the closed-loop optimal control, where the resultant assimilated energy data from the EnKF is combined with the optimisation procedure. The closed-loop optimal control is done using the EnOpt algorithm. Optimisation also requires formulation of objective functions along with operational constraints.

The **fifth** research objectives requires modelling and assessment of carbon emissions and savings under specific smart interventions in the UK. To address this the ancillary services such as the DR programmes that are currently exist in the UK are assessed. Several DR programmes such as STOR, Triad, Fast Reserve, FCDM and Irish smart grid project are considered in the research.

5.2 Conclusions

This section outlines the conclusions in four different sub-categories. Section 5.2.1 concludes on modelling of electricity consumption using HTFs. Section 5.2.2 concludes on quantification of carbon emissions based on several studies, and electricity grid carbon factor based on the fuel-mix in electricity generation. Section 5.2.3 concludes on the performance of EnKF in ensemble propagation and EnOpt algorithm, given two scenarios of the optimisation problem. Finally, Section 5.2.4 concludes the findings based on DR programmes.

5.2.1 Adaptive HTFs modelling

A novel approach in stochastic modelling of electricity consumption of various types of customers has been developed. Adaptive HTFs have demonstrated reliable results in reproducing dynamics of electricity data. HTFs also provide substantial advantages, such as great flexibility and simplicity of modelling with a few parameters. A comparative study of simulated and real data is performed using the HTF fitting. The results show that HTF is a useful function in providing estimates, fitting and forecast of electrical

consumption to various customers. The proposed HTF-based models correctly represent energy consumption and the resultant carbon emissions. The HTF model is compared with the PV data from Brunel University, various energy sources from Elexon, the Irish smart grid pilot project, and the UK's Distribution Network Operator pilot project.

The modelling results show that PV data exhibited a very similar seasonal trend with the seasonal dynamic model, although the HTF does not work well for data without a pronounced seasonal trend, In terms of the Elexon fuel data, the periodic cycles of oscillations in several power plants can be well fitted with HTF. In contrast, the wind energy generation data suggests that an exponential function better fits the distribution of wind data than the HTF. Additionally, as wind energy generation is highly intermittent, the HTF is therefore unsuitable to model and forecast the wind energy distribution. In the case of Irish smart grid project, the annual electricity consumption exhibits very similar trend to the dynamic HTF model. Finally, the real energy data from the UK's distribution network operator project also demonstrates periodical trends. Hence, HTF can be applied to model these data provided that there is no significant changes in the trend (due to regime change or maintenance).

5.2.2 Carbon emissions, electricity grid carbon factor and carbon intensity

Carbon emissions have been successfully calculated for the seasonal data (observed and modelled). The quantification of carbon emissions in the power grid is important for conservation of energy due to the environmental concerns.

Dynamical electricity grid carbon factor based on the fuel mix of generators reported by the Elexon and BMRS has been successfully derived. Evaluation of fuel mixes for the considered fuels are essential as they provide knowledge of the balancing of power plants across the network (for instance, the additional generation of non-green plants in balancing the low output of the green generation). Additionally, such balancing of power output may alter the overall emissions intensity across the network.

5.2.3 EnKF and EnOpt

The third conclusion mainly draws the attention of the resultant forecast/prediction and data assimilation technique by EnKF and the closed-loop optimal control using the EnOpt algorithm. The EnKF algorithm is used for data assimilation of both energy consumption and generation. Two separate EnKF simulations are performed for corresponding assimilation: 1) optimisations of carbon emissions for energy consumption of working family, pensioner, daytime office and one-day-shift industrial estate using the earlier developed dynamical HTF-based adaptive seasonal profile modelling; 2) optimisation of costs and carbon emissions in the ED problem of the smart grid incorporating thermal units and wind-based generation.

Overall, EnKF demonstrates high robustness in matching energy consumption and generation data, either in real-time or based on prior knowledge and historical records. Additionally, the numerical experimental of EnKF performs well in both short-term and long-term energy data forecast and assimilation. Generally, the EnKF allows minimisation of mismatches between the model predictions and the resultant ensemble updates. Still, as EnKF is a Monte Carlo type of data assimilation, the low number of ensemble sizes may produce a poor forecast. The ensemble of size $N_e = 100$ or 1000 provides sufficient convergence of the resultant EnKF propagations provided. For this reason, the EnKF simulation allows the convergence of data assimilations in the condition that the ensemble size is sufficiently large.

The EnKF'ed propagations of energy consumption and generation data are further applied for numerical optimisation of the smart grid through the closed-loop optimal control technique using the EnOpt algorithm. Two scenarios are applied using the EnOpt algorithm, where the first scenario considers optimisation of carbon savings. The second scenario considers optimisation of costs of generation accounting the emission and the wind generation representing the ED problem.

Overall, the EnOpt algorithm is robust in optimising carbon emissions for groups of consumers and costs of generation for energy plants. At every time step of the EnOpt simulation, the best control vector that optimises the objective function is selected. The optimal control vector represents the electrical variables that may be incorporated in operational strategies in the power grid that reduce costs and carbon emissions depending

on the current demand. The EnOpt algorithm applied in this study is instrumental in regulating energy consumption and generation.

5.2.4 DR programmes

Carbon emissions and savings under various DR programmes are assessed. The considered DR programmes include STOR, Triad, Fast Reserve, FCDM and the demand reduction in the Irish smart metering project. The Irish smart metering project is an example of behavioural DR based on different ToU rates. Types of the smart interventions considered in each of the DR programmes are as follows: 1) STOR – standby diesel generators, demand reduction and CHP; 2) Triad – standby diesel generators; 3) Fast Reserve – hydro-pumped storage; 4) FCDM – demand reduction; 5) Irish smart metering trial – ToU tariffs in combination with DSM stimuli. Each of DR programmes is modelled with required operational parameters and necessary assumptions. The profiles of BAU plants (CCGT and OCGT plants) and smart interventions are modelled with operational assumptions relating to firing up and shutdown efficiency, and corresponding energy level in DR programmes. The modelled profiles enabled the comparison of carbon emissions between the BAU and the smart solutions with quantification of uncertainties.

In general, due to the significantly lower value of carbon factor in CHP compared to diesel generators, and to the slightly lower value of the electricity grid carbon factor carbon savings in CHP scenario are achieved. The CHP fleets have excellent potential of achieving carbon savings due to substantial improvements in technology efficiency and may become conventional in the UK electricity market.

The high amount of carbon emissions during the Fast Reserve event is mainly due to the need to draw electricity from the main grid in order to pump high volume of water to the reservoir. In contrast, large volume of water from the reservoir is later released in order to provide high electricity volume instantly with minimal emissions. The intervention by the hydro-pumped plant still produce carbon savings in comparisons with BAU plants.

In the Irish smart metering trial, through the ToU tariffs in combination with DSM stimuli, electricity demand is shifted to other periods, when those ToU rates are notably lower than the peak rate. Consumers are expected to be aware of the high peak rate and therefore are expected to avoid using electricity. However, the results of analysis indicate

unclear trend of demand shift towards the cheapest tariff. One of the possible barriers to savings might be daily habitual activities such as breakfast, lunch and dinner.

The need for demand reduction or demand shifting at demand peak is very important, because it diminishes use of additional BAU plants which are to be in standby mode that may or may not be needed for generation. The firing of additional BAU plants increases the carbon intensity in the power grid. Hence, through demand reduction in FCDM and STOR, carbon savings are directly achievable.

The assessment of carbon savings in DR programmes is an important finding, as diesel generation is generally perceived as highly polluting. The analysis is based on the comparison between the fully allocated STOR/Triad capacity for both CCGT/OCGT plants and the substituted STOR/Triad volume using diesel generation. In both STOR and Triad programmes, by substituting diesel generators proportionate to energy generation from BAU plants, significant amount of carbon savings is achieved in this case. Through the intervention by diesel generators, the high amount of emissions is compensated by operating conditions of BAU plants. Reserved BAU plants produce higher amount of carbon emissions than diesel generators in this case.

It can be argued that for high demand periods the stable fuel plants are advisable to operate in order to balance the remaining amount of energy. However, some greener fuel plants such as nuclear plants have limited flexibility in response to sudden peak demand and operate at base load mode. The 'peaking' plant such as OCGT may provide reserve to mitigate the peak demand but may produce additional emissions. Therefore, the energy generation with diesel installations in this case provide security of supply and also mitigate carbon emissions problem.

Although diesel generators are highly polluting, in DR programmes by adhering to the opertaional policies the diesel generations still contribute substantial amount of carbon savings. However, carbon savings cannot be achieved if standard operating policies, such as the reserve volume, hours of operation and efficiencies, are violated. Therefore, diesel generators are efficient during the reserve or contingency periods with short runs and are not advisable to operate continuously. The uncontrolled operation of diesel generators would produce additional carbon emissions. Furthermore, diesel-fuel emissions of small particles may further contribute to air pollution. In the normal mode of operation with steady demand, BAU gas-fired plants, such as CCGT plants, are most efficient and least

polluting.

The present study has successfully demonstrated that the polluting technology has the ability to achieve carbon savings. If well-optimised, several types of interventions combined together may lead to both energy usage optimisation and carbon savings. This is where technology and control programmes may provide the best results for industry and customers.

5.3 Contribution to knowledge

(i) **The carbon savings model provides a conceptual framework on how the usage of energy is translated into carbon equivalent**. It allows consumers to be aware of the uncertainties in balancing the power output in addressing energy demand. Additionally, the information about carbon emissions and savings allows consumers to use energy wisely to reduce the network stress.

(ii) **The electricity consumption profiles are modelled using novel HTF-based approach**. The modelled profiles can be used for stochastic forecast of energy consumption data. Additionally, the parameters of the profiles based on the HTF are highly flexible and can be adjusted to fit various profiles. For instance, the tuning of the variables during the daylight saving mode can be done by shifting only time (forward or backward) without the need to adjust the other parameters.

(iii) **The derived electricity grid carbon factor with uncertainties provides a useful tool for the assessment of the carbon intensity across the network grid**. High carbon intensity may indicate high energy demand (demand stress), and more BAU non-renewable energy generation than renewables.

(iv) **In EnKF, the ensemble representation of uncertain energy consumption and generation provides a useful numerical tool in prediction and assimilation of energy data**. With the EnKF algorithm, the uncertain trends of energy generation and consumption can be predicted using the input data (historical or real time). With establishment of smart meters, high-resolution recordings of energy data can be used in the EnKF algorithm to predict the potential real-time energy usage.

(v) **In EnOpt, running and controlling complex smart grids allows to account emissions and renewable energy in a closed-loop optimal control.** The proposed approach combines estimation of energy consumption and generation through the EnKF algorithm and subsequent optimisation of carbon savings and costs of generation. It can be used by aggregators, distribution network operators, and National Grid, under the regulations of the UK Office of Gas and Electricity Markets (Ofgem) to quantify and minimise the trade-offs between costs and carbon emissions of the ED problem. The proposed model provides all economical and environmental solution for business decisions based on both costs and environmental benefits of optimised energy generation.

(vi) **Smart interventions in DR programmes allow the participants to understand the benefits of other smart interventions**. Nowadays, many participants perceive the use of green generation as the main and the best solution in reducing carbon emissions. However, due to the demand stress, DR programmes cope with intermittent green generation at high peak demands. With the DR interventions, a participating company will manage the limitations of the network infrastructure and have alternatives in mitigating the network shortages. Furthermore, the modelled profiles of BAU plants and generators will enable the participating companies to make the right investment with accurate utilisation of resources, while adhering to the emissions performance standards. In addition, the DR framework also allows the network operators develop an optimal operating strategy for greener control of generating fleets through ancillary services in order to ensure sustainability and minimal environmental impact of the power grid.

(vii) **A model has been developed for external companies based on the model of DR programmes**. The model allows one to forecast of the potential carbon savings based on self-generation by in comparison with BAU generation.

5.4 Limitations and suggestions for future research

As the proposed adaptive HTF model provides excellent approximation of the seasonal profiles of consumers, a future development of other adaptive models based on the same

approach is recommended. Non-linear adaptive models based on the Van Der Pol oscillator can be used. As the energy demand demonstrates periodical behaviour with oscillations, the Van Der Pol oscillator may be applicable in modelling the energy profiles across different types of consumers. As the current adaptive HTFs are used for four main groups (working family, pensioner, daytime office and one-day-shift industrial estate), the usage of Van Der Pol oscillator may extend the modelling capability for other groups of consumers.

As regards to EnKF and EnOpt, the proposed framework is very general and combines both short-term forecast using EnKF and a flexible optimisation routine. Currently, the public available information required for applying the proposed methodology in real-time systems and control rooms is insufficient. For instance, the control variables considered in this research are resultant optimised energy generation and consumption, used in the model simulator. In reality, such control variables are highly complex. There are several important requirements for providing more realistic modelling by EnKF simulation and optimisation by EnOpt: 1) network parameters under various balancing services of a transmission network operator; 2) reliability assumptions of the transmission systems; 3) controllable electric parameters (for instance, generalised frequency and voltage, substations properties, and generation output of the transmission network) involved in controlling system. The future opportunities to study these variables and conditions of a network operator will provide a realistic EnKF and EnOpt simulations of the smart grid.

Additionally, even though the steepest descent approach in EnOpt algorithm provides the optimised control with convergence, as the iterations get closer to a minimum, due to almost 'optimal' solution found, the steepest descent algorithm oscillates in a 'zig-zag' pattern for a long time before a real minimum is achieved. This makes the computations slow to converge. In order to compensate for this, the future work shall include a modification of the conventional steepest descent approach. One of the possible methods could be the conjugate-gradient method. It allows faster convergence of the control variables, as was proposed by Chaudhri et al. (2009).

As regards to DR programmes, one may argue that the demand reduction or shifting might increase the carbon intensity at other off-peak period. Therefore, averaging and smoothing techniques in profiling the energy usage pattern are needed. Such techniques already exist in the current electricity market with the potential of reducing carbon emis-

sions.

The current assessment of DR programmes compares only the carbon emissions; no further assessment has been made regarding respective levels of other GHG polluting compounds and gases. Currently, some installations by the transmission network operators prioritise balancing the costs and efficiency in supplying electrical energy to customers rather than the environmental impact. For instance, it is common to adjust the frequency deviations of the power grid without monitoring the amount of carbon emissions. Carbon emissions are therefore considered as secondary priority, especially in the current economic circumstances. Installation of new efficient and low carbon plants such as the thermal storage, CHP and the Carbon Capture and Storage technology may significantly improve carbon emissions of the power grid. Due to the rapid developments of technologies and efficiencies of power plants, the assessment of carbon emissions and savings should be revised frequently. This ensures that the DR programmes align with the carbon reduction targets (UK and EU) in the future.

Finally, the future work shall also include the thorough research and development of sophisticated methods (either in software or hardware implementation) in optimising the energy trilemma problem, as the current thesis mainly focuses on the quantification of carbon emissions and savings (Fig. 1.1). Other two elements such as the reduced energy costs and improved security of energy supply are only assessed through the optimisation problems. Therefore, with the improvement in the energy trilemma problem, this does not only to mitigate the carbon emissions problem, but also to reduce energy costs and enhance security of energy supply in the future.

References

Abrell, J. and Kunz, F. (2014). Integrating intermittent renewable wind generation - a stochastic multi-market electricity model for the european electricity market. *Network and Spatial Economics*, pages 117–147.

Albertos, P. and Sala, A. (1998). Fuzzy logic controllers, advantages and drawbacks. *IEEE Transactions on Control System Technology*.

Almendral-Vazquez, R. and Syversveen, A. R. (2006). The ensemble Kalman filter - theory and applications in oil industry. Technical report, Norsk Regnesentral. [Online]. Available: `https://www.nr.no/en/nrpublication?query=/file/4334/Almendral_Vazquez_-_Ensemble_Kalman_Filter_-_theory_and_applications_i.pdf`, [accessed 25.07.15].

Altaf, M. U., Butler, T., Mayo, T., Luo, X., Dawson, C., Heemink, A. W., and Hoteit, I. (2014). A comparison of ensemble kalman filters for storm surge assimilation. *Monthly Weather Review*, 142:2899–2914.

Asadolladi, A., Nævdal, G., Dadashpour, M., and Kleppe, J. (2014). Production optimization using derivative free methods applied to brugge field case. *Journal of Petroleum Science and Engineering*, 114:22–37.

Atzeni, I., Ordóñez, L., Scutari, G., Palomar, D. P., and Fonollosa, J. R. (2013). Demand-side management via distributed energy generation and storage optimization. *IEEE Transactions on Smart grid*, 4(2):866–876.

Azadeh, A., Ghaderi, S. F., and Sohrabkhani, S. (2008). Annual electricity consumption forecasting by neural network in high energy consuming electrical sectors. *Energy Conservation and Management*, 49(8):2272–2278.

Balabin, R. M., Safieva, R. Z., and Lomakina, E. I. (2008). Wavelet Neural Network (WNN) approach for calibration model building based on gasoline near infared (NIR) spectra. *Chemometrics and Intelligent Laboratory Systems*, 15(1):58–62.

Balancing and Settlement Code (2008). Bsc procedure: allocation of profile classes and sscs for non-half hourly sva metering systems registered in smrs (version 7.0). Technical report, Elexon ltd.

Baling, L. (2011). Fast cycling and rapid start-up: new generation of plants achieves impressive results. Technical report, Siemens.

Basam, A., Salgado-Tránsito, I., Oller, I., Santoyo, E., Jiménez, A. E., Hernández, J. A., Zapata, A., and Malato, S. (2012). Optimal performance assessment for a photo-fenton degradation pilot plant driven by solar energy using artifical neural networks. *International Journal of Energy Research*, 36(14):1314–1324.

Basokur, A. T. (1998). Digital filter design using the hyperbolic tangent functions. *Journal of The Balkan Geophysical Society*, 1:14–18.

Begum, N. (2009). Reservoir parameter estimation for reservoir simulation using ensemble kalman filter (EnKF). Master thesis, Department of Petroleum Engineering and Applied Geophysics, Norwegian University of Science and Technology, Trondheim.

Blickle, T., Lakatos, B. G., Mihálykó, C., and Ulbert, Z. (1998). The hyperbolic tangent distribution family. *Powder Technology*, 97(2):100–108.

BMRS (2015). BM reporting (updated daily). [Online]. Available: `http://www.bmreports.com`. [accessed 23.03.15].

Boait, P., Ardestani, B. M., and Snape, J. (2013). Accommodating renewable generation throughan aggregator-focused method for inducing demand side response from electricity consumers. *IET Renewable Power Generation*, 7(6):689–699.

Bowyer, C., Baldock, D., Kretschmer, B., and Polakova, J. (2012). The GHG emissions intensity of bioenergy: Does bioenergy have a role to play in reducing GHG emissions of europe's economy? Technical report, Institute for European Environmental Policy (IEEP), London.

Boyle, G., Everett, B., and Ramage, J. (2003). *Energy systems and sustainability*. United Kingdom: Oxford University Press.

Brewer, R. S. (2009). Literature review on carbon footprint collection and analysis. Technical report, Collaborative Software Development Lab, Department of Information and Computer Sciences, University of Hawai'i.

Brossat, X. (2013). A range of methods for electricity consumption forecasting. [Online]. Available: `http://www.newton.ac.uk/programmes/SCS/seminars/2013042214001.pdf`, [accessed 02.05.13]. Presentation at Energy Systems Week, Électricité de France, RD/Dpt/ OSIRIS, Isaac Newton Institute for Mathematical Sciences, Cambridge, 22-26 April 2013.

Capolei, A., Suwartadi, E., Foss, B., and Jørgensen, J. B. (2013). Waterflooding optimization in uncertain geological scenarios. *Computational Geosciences*, 17(6):991–1013.

Carbon Trust (2012). Carbon footprinting guide. [Online]. Available: `http://www.carbontrust.com/resources/guides/carbon-footprinting-and-reporting/carbon-footprinting`. [accessed 16.05.15].

Carbon Trust (2013). Conversion factors. [Online]. Available: `http://www.carbontrust.com/media/18223/ctl153_conversion_factors.pdf`. [accessed 16.05.15].

Catalão, J. P. S., Pousinho, H. M. I., and Mendes, V. M. F. (2011). Short-term wind power forecasting in portugal by neural networks and wavelet transform. *Renewable Energy*, 36(4):1245–1251.

Centre for Carbon Measurement (2013a). Test report for Nesta dynamic demand challenge prize finalist: Team 1. Technical report, National Physical Laboratory, Teddington, UK.

Centre for Carbon Measurement (2013b). Test report for Nesta dynamic demand challenge prize finalist: Team 2. Technical report, National Physical Laboratory, Teddington, UK.

Centre for Carbon Measurement (2013c). Test report for Nesta dynamic demand challenge prize finalist: Team 3. Technical report, National Physical Laboratory, Teddington, UK.

Centre for Carbon Measurement (2013d). Test report for Nesta dynamic demand challenge prize finalist: Team 4. Technical report, National Physical Laboratory, Teddington, UK.

Centre for Carbon Measurement (2013e). Test report for Nesta dynamic demand challenge prize finalist: Team 5. Technical report, National Physical Laboratory, Teddington, UK.

CER11080a (2011). Electricity smart metering customer behaviour trials (CBT) findings report. Technical report, Commision for Energy Regulation (CER).

Ceseña, E. A. M., Good, N., and Mancarella, P. (2015). Electrical network capacity support from demand side response: techno-economic assessment of potential business cases for small commercial and residential end-users. *Energy Policy*, 82:222–232.

Chaudhri, M. M., Phale, H. A., Liu, N., and Oliver, D. S. (2009). Fan improved approach for ensemble-based production optimization. *SPE Journal*.

Chen, C., Li, Y. P., and Huang, G. H. (2010a). Ensemble-based closed-loop optimization applied to Brugge field. *SPE Reservoir Evaluation and Engineering*, 13:72–81.

Chen, C., Li, Y. P., and Huang, G. H. (2013). An inexact robust optimization method for supporting carbon dioxide emissions management in regional-power systems. *Energy Economics*, 40:441–456.

Chen, W. T., Li, Y. P., Huang, G. H., Chen, X., and Li, Y. F. (2010b). A two-stage inexact-stochastic programming model for planning carbon dioxide emission trading under uncertainty. *Applied Energy*, 87(3):1033–1047.

Chen, Y., Oliver, D. S., and Zhang, D. (2009). Efficient ensemble-based close-loop production optimization. *SPE Journal*, 14(4):634–645.

Chen, Z., Wu, L., and Fu, Y. (2012). Real-time price-based demand response management for residential applicances via stochastic optimisation and robust optimisation. *IEEE Transactions on Smart Grid*, 3(4):1822–1831.

Christodoulos, C., Michalakelis, C., and Varoutas, D. (2010). Forecasting with limited data: Combining arima and diffusion models. *Technological Forecasting and Social Change*, 77(4):558–565.

Colorado, D., Hernández, J. A., El-Hamzaoui, Y., and Bassam, A. (2011). Error propagation on cop prediction by artificial neural network in a water purification system integrated to an absorption heat transformer. *Renewable Energy*, 36(5):1315–1322.

Contreras, J., Espínola, R., Nogales, F. J., and Conejo, A. J. (2003). ARIMA models to predict next-day electricity prices. *IEEE Transactions on Power Systems*, 18(3):1014–1020.

Convenant of Mayors (2010). Technical annex to the seap template instructions document: the emission factors. [Online]. Available: `http://www.eumayors.eu/IMG/pdf/technical_annex_en.pdf`. [accessed 08.07.13].

Cooper, S. J. G., Hammond, G. P., McManus, M. C., and Rogers, J. G. (2014). Impact on energy requirements and emissions of heat pumps and micro-cogenerators participating in demand side management. *[Special issue]. Applied Thermal Engineering*, 71(2):872–881.

Crow, M. L. (2009). *Computational methods for electric power systems*. CRC Press, New York, second edition edition. ISBN 9781420086607 - CAT# 8660X.

Cui, T., Goudarzi, H., Hatami, S., Nazarian, S., and Pedram, M. (2012). Concurrent optimization of consumer's electrical energy bill and producer's power generation cost under a dynamic pricing model. In *Proceedings of the Innovative Smart Grid Technologies (ISGT)*, pages 1–6, Washington, DC. IEEE PES.

Dai, P., Chen, G., Zhou, H., Su, M., and Bao, H. (2012). CO_2 mitigation measures of power sector and its integrated optimization in China. *The Scientific World Journal*, pages 1–8.

Dattoli, G. anf Del-Franco, M. (2010). Hyperbolic and circular trigonometry and application to special relativity. [Online]. Available: http://arxiv.org/ftp/arxiv/papers/1002/1002.4728.pdf, [accessed 17.05.15]. arXiv:1002.4728v1, February.

DECC (2013). Electricity generation costs 2013. Technical report, Department of Energy & Climate Change (DECC).

DEFRA (2015). Defra greenhouse gas conversion factor repository. [Online]. Available: http://www.ukconversionfactorscarbonsmart.co.uk. [accessed 17.05.15].

Dehdari, V. (2012). Sequential quadratic programming (SQP) for solving constrained production optimisation – case study from brugge field. Master thesis, Mewbourne School of Petroleum and Geological Engineering, University of Oklahoma, Norman, Oklahoma, U.S.

Dehdari, V., Oliver, D. S., and Deutsch, C. V. (2012). Comparison of optimization algorithms for reservoir management with constraints–A case study. *Journal of Petroleum Science and Engineering*, 100:41–49.

Depuru, S. S. S. R., Wang, L., and Devabhaktuni, V. (2011). Smart meters for power grid: Challenges, issues, advantages and status. *Renewable and Sustainable Energy Reviews*, 15(6):2736–2742.

DG Clima (2016). The 2050 low carbon economy. [Online]. Available: http://ec.europa.eu/clima/policies/strategies/2050/index_en.htm. [accessed 17.02.16].

Dong, D. and Petersen, I. R. (2010). Quantum control theory and applications: A survey. *IET Control Theory and Applications*, 4(12):2651–2671.

Dordonnat, V., Koopman, S. J., Ooms, M., Dessertaine, A., and Collet, J. (2008). An hourly periodic state space model for modelling french national electricity load. *International Journal of Forecasting*, 24(4):566–587.

Drysdale, B., Wu, J., and Jenkins, N. (2015). Flexible demand in the GB domestic electricity sector in 2030. *Applied Energy*, 139:281–290.

DUKES (2012). Chapter 7–combined heat and power. Technical Report ISBN 9780115155284, Department of Energy and Climate Change (DECC). Published with the permission of the DECC on behalf of the Controller of Her Majesty's Stationery Office.

DUKES (2013). Chapter 7–combined heat and power. Technical Report ISBN 9780115155284, Department of Energy and Climate Change (DECC). Published with the permission of the DECC on behalf of the Controller of Her Majesty's Stationery Office.

DUKES (2015). Digest of united kingdom energy statistics (dukes) 2015: printed content. Technical Report ISBN 9780115155314, Department of Energy and Climate Change (DECC). Published with the permission of the DECC on behalf of the Controller of Her Majesty's Stationery Office.

EA Technology (2012). Assessing the impact of low carbon technologies on Great Britain's power distribution networks. Technical Report Project no: 82530, Version: 3.1, EA Technology Ltd.

EA Technology (2013). Smart Grid Forum Work Stream 3 – phase 3.5. Technical Report Project no: 84170, Version: 3.5, EA Technology Ltd.

EDF Energy (2013). Triad charge reconciliation for large business. Technical report, EDF Energy.

ElDesouky, A. A. (2013). Security and stochastic economic dispatch of power system including wind and solar resources with environmental consideration. *International Journal of Renewable Energy Research*, 3(4):951–958.

Elexon (2014). Imbalance pricing guidance. Technical report, Elexon Ltd.

Elexon (2015). Elexon portal. Elexon Ltd., [Online]. Available: `https://www.elexonportal.co.uk/news/latest?cachebust=5tdys6qsn8`.

Environmental Agency (2011). Principles for determining start up and shut down criteria for gas turbines. Technical report, UK Technical Working Group 5.

E.ON UK (2016). The energy trilemma. [Online]. Available: https://www.eonenergy.com/for-your-business/large-energy-users/manage-energy/energy-efficiency/decentralised-energy-experts/The-energy-trilemma. [accessed 179.02.16].

Evensen, G. (1994). Sequential data assimilation with a nonlinear quasi-geostrophic model using Monte-Carlo methods to forecast error statistics. *Geophysical Research*, 99(5):10143–10162.

Evensen, G. (2003). The ensemble kalman filter: theoretical formulation and practical implementation. *Ocean Dynamics*, 53(4):343–367.

First Hydro Company (2005). First Hydro analysts conference. International Power Plc, [Online]. Available: http://www.iprplc-gdfsuez.com/~/media/Files/I/IPR-Plc/Attachments/presentations-pdfs/2005/hydrosite05.pdf.

First Hydro Company (2009). Welcome to First Hydro Company. [Online]. Available: http://www.iprplc-gdfsuez.com/~/media/Files/I/IPR-Plc/Attachments/presentations-pdfs/2009/hydro_09.pdf. [accessed 02.10.14].

Flexitricity (2010). Triad guidance notes. Technical report, Flexitricity Ltd. [accessed 29.09.14].

Flexitricity (2013). The carbon costs of system balancing. Technical report, Flexitricity Ltd.

Flexitricity (2015). Triad management. [Online]. Available: https://www.flexitricity.com/en-gb/solutions/triad/. [accessed 19.02.16].

Fonseca, R. (2011). Robust ensemble based multi-objective production optimization: application to smart wells. Master thesis, Department of Applied Earth Sciences, Delft University of Technology, Delft, Netherlands.

Forouzantar, F., Rossa, E. D., Russo, R., and Reynolds, A. C. (2013). Life-cycle production optimization of an oil field with an adjoint-based gradient approach. *Journal of Petroleum Science and Engineering*, 112:351–358.

Gast, N., Boudec, J-Y, L., and Tomozei, D. (2014). Impact of demand-response on the efficiency and prices in real-time electricity markets. In *Proceedings of The 5th International Conference on Future Energy Systems*, pages 171–182, New York, USA. ACM.

Geetha, K., Sharmila Deve, V., and Keerthivasan, K. (2015). Design of economic dispatch model for gencos with thermal and wind powered generators. *Electrical Power and Energy Systems*, 68:222–232.

Gharaie, M., Zhang, N., Jobson, M., Smith, R., and Panjeshahi, M. H. (2013). Simultaneous optimization of co_2 emissions reduction strategies for effective carbon control in the process industries. *Chemical Engineering Research and Design*, 91(8):1483–1498.

Gillijins, S., Barrero Mendoza, O. B., Chandrasekar, J., De Moor, B. L. R., Bernstein, D. S., and Ridley, A. (2006). What is the Ensemble Kalman Filter and how well does it work? In *Proceedings of the 2006 American Control Conference*, pages 4448–4453, Minneapolis, Minnesota, USA. IEEE.

Hall, B. (2014). An introduction to the GB generation market. Technical report, Cornwall Energy. [accessed 29.09.14].

Hasan, A., Foss, B., and Sagatun, S. (2013). Optimization of oil production under gas coning conditions. *Journal of Petroleum Science and Engineering*, 105:26–33.

Healy, D. P. (2012). Influence of the carbon intensity of electricity on carbon savings from CHP. *Building Research & Information*, 40(3):317–326.

Hedman, B. A. and Hampson, A. C. (2011). Fuel and CO_2 emissions savings calculation methodology for combined heat and power (CHP) systems. *ASHRAE Transactions*, 117:961–973.

Hetzer, J., Yu, D. C., and Bhattarai, K. (2008). An economic dispatch model incorporating wind power. *IEEE Transactions on Energy Conversion*, 23(2):603–611.

Hill, N., Dun, C., Watson, R., and James, K. (2014). 2014 government GHG conversion factors for company reporting: methodology paper for emission factors final. Technical report, Department of Energy and Climate Change (DECC).

Hill, N., Venfield, H., Dun, C., and James, K. (2013). Government GHG conversion factors for company reporting, methodology paper for emission factors. Technical report, Department for Environment Food and Rural Affairs (DEFRA).

Hippert, H. S., Pedreira, C. E., and Souza, R. C. (2001). Neural networks for short-term load forecasting: A review and evaluation. *IEEE Transactions on Power Systems*, 16:44–55.

Hou, J., Zhou, K., Zhang, X., Kang, X., and Xie, H. (2015). A review of closed-loop reservoir management. *Petroleum Science*, 12:114–128.

Houtemaker, P. L., He, B., and Mitchell, H. L. (2014). Parallel implementation of an ensemble kalman filter. *Monthly Weather Review*, 142(3):1163–1182.

Huang, C., Chen, S., Huang, Y., and Yang, H. (2012). Comparative study of evolutionary computation methods for active-reactive power dispatch. *IET Generation, Transmission & Distribution*, 6(7):636–645.

Hung, N. Q., Babel, M. S., and Weesakul, W. amd Tripathi, N. K. (2009). An artificial neural network model for rainfall forecasting in bangkok, thailand. *Hydrology and Earth System Sciences*, 13:1413–1425.

Independent Project Analysis Consulting, Econnect Ltd and Martin Energy (2006). Reducing the cost of system intermittency using demand side control measures. [Online]. Available: `http://www.ipaeconomics.com/publications/69441kel0003460000.pdf`. [accessed 30.09.14].

Investopedia Staff (2014). How to calculate the bid-ask spread. Investopedia, LLC.., [Online]. Available: `http://www.investopedia.com/articles/investing/082213/how-calculate-bidask-spread.asp`.

Jafroodi, G. and Zhang, D. (2011). New method for reservoir characterization and optimization using crm-enopt approach. *Journal of Petroleum Science and Engineering*, 77(2):155–171.

Jahangiri, H. R. (2012). *Optimization of coupled CO_2 sequestation and enhanced oil*

recovery. Phd thesis, Department of Petroleum Engineering, University of Southern California, Los Angeles.

Jammazi, R. and Aloui, C. (2012). Crude oil price forecasting: Experimental evidence from wavelet decomposition and neural network modeling. *Energy Economics*, 34(3):828–841.

JCGM_100:2008 (2008). Evaluation of measurement data - Guide to the expression of uncertainty in measurement (GUM). *Joint Committee for Guides in Metrology (JCGM)*, pages 1–116.

Jebaraj, S., Iniyan, S., and Goic, R. (2011). Forecasting of coal consumption using an artificial neural network and comparison with various forecasting technique. *Energy Source, Part A: Recovery, Utilization, and Environmental Effects*, 33(14):1305–1316.

Jenkins, D. P. (2008). Using dynamic simulation to quantify the effect of carbon-saving measures for a uk supermarket. *Journal of Building Performance Simulation*, 1(4):275–288.

Jenkins, D. P., Tucker, R., and Rawlings, R. (2009). Modelling the carbon-saving performance of domestic ground-source heat pumps. *Energy and Buildings*, 41(6):587–595.

Jensen, J. P. (2007). Ensemble kalman filtering for state and parameter estimation on a reservoir model. Master thesis, Department of Engineering Cybernetics, Norwegian University of Science and Technology, Trondheim.

Jia, J. S., Zhao, J. Z., Deng, H. B., and Duan, J. (2010). Ecological footprint simulation and prediction by arima model - a case study in henan province of china. *Ecologival Footprint*, 10(2):538–544.

John, C. J. and Mandel, J. (2008). A two-stage ensemble kalman filter for smooth data assimilation. *Environmental and Ecological Statistics*, 15:101–110.

Kalogirou, S. A. (2000). Applications of artificial neural-networks for energy systems. *Applied Energy*, 67(1–2):17–35.

Khan, N. A., Awan, A. B., Mahmood, A., Razzaq, S., Zafar, A., and Sidhu, G. A. S. (2015). Combined emission economic dispatch of power system including solar photo voltaic generation. *Energy Conversion and Management*, 92:82–91.

Killip, G. (2005). Emission factors and the future of fuel. Technical report, Environment Change Institute, University of Oxford, Oxford.

Korellis, S. (2014). Coal-fired power plant heat rate improvement options, part 1. [Online]. Available = `http://www.powermag.com/coal-fired-power-plant-heat-rate-improvement-options-part-1/`. [accessed 24.06.15].

Kourtis, G., Hadjipaschalis, I., and Poullikkas, A. (2011). An overview of load demand and price forecasting methodologies. *International Journal of Energy and Environment*, 2(1):123–150.

Kousksou, T., Bruel, P., Jamil, A., El Rhafiki, T., and Zeraouli, Y. (2014). Energy storage: applications and challenges. *Solar Energy Materials and Solar Cells*, 120(Part A):59–80.

Lau, E. T., Yang, Q., Taylor, G. A., Forbes, A. B., Wright, P., and Livina, V. N. (2014). Optimisation of carbon emissions in smart grids. In *Proceedings of the 49th International Universities' Power Engineering Conference, UPEC*, pages 1–4, Cluj-Napoca, Romania. IEEE.

Li, H., Tsotsis, T. T., Sahimi, M., and Qin, S. J. (2014a). Ensemble-based and ga-based optimization for landfill gas production. *AIChE Journal*, 60(6):2063–2071.

Li, Y. F., Huang, G. H., Li, Y. P., Xu, Y., and Chen, W. T. (2010). Regional-scale electric power system planning under uncertainty - a multistage interval-stochastic integer linear programming approach. *Energy Policy*, 38:475–490.

Li, Y. P., Huang, G. H., Nie, S. L., and Liu, L. (2008). In exact multistage stochastic integer programming for water resources management under uncertainty. *Journal of Environmental Management*, 88:93–107.

Li, Y. Z., Wu, Q. H., and Zhan, J. P. (2014b). Mean-variance model for power system economic dispatch with wind power integrated. *Energy*, 72:510–520.

Lin, Q. G., Huang, G. H., Bass, B., Huang, Y. F., and Zhang, X. D. (2011a). DESPU: Dynamic optimization for energy systems planning under uncertainty. *Energy Sources, Part B: Economics, Planning and Policy*, 6(4):321–338.

Lin, W., Wu, T., Zhang, C., and Yu, T. (2011b). Carbon savings resulting from the cooling effect of green areas: a case study in beijing. *Environmental Pollution*, 159(8-9):2148–2154.

Lindberg, C.-F., Zahedian, K., Solgi, M., and Lindkvist, R. (2014). Potential and limitations for industrial demand side management. *[Special issue]. Energy Procedia, International Conference on Applied Energy, ICAE 2014*, 61:415–418.

Liu, L. (2012). The forecast of qinhuangdao logistic based on bp neural network. *International Journal of Digital Content Technology and its Applications*, 6(8):8–16.

Logenthiran, T., Srinivasan, D., and Shun, T. Z. (2012). Demand side management in smart grid using heuristic optimization. *IEEE Transactions on Smart grid*, 3(3):1244–1252.

Logenthiran, T., Srinivasan, D., and Vanessa, K. W. M. (2014). Demand side management of smart grid: Load shifting and incentives. *Journal of Renewable and Sustainable Energy*, 6(033136):1–18.

Macak, J. J. (2001). Evaluation of gas turbine startup and shutdown emissions. In *Proceedings of the Air and Waste Management Association Annual and Exhibition*, pages 1–13, Orlando, FL. IEEE.

Magnago, F. H., Alemany, J., and Lin, J. (2015). Impact of demand response resources on unit commitment and dispatch in a day-ahead electricity market. *Electrical Power and Energy Systems*, 68:142–149.

Maier, H. R. and Dandy, G. C. (2000). Neural networks for the prediction and forecasting of water resources variables: A review of modelling issues and applications. *Environmental Modelling and Software*, 15:101–124.

Manchester Centre For Electrical Energy (2004). The future value of storage in the UK with generator intermittency. Technical report, DTI Technology Programme.

Mandel, J. (2009). A brief tutorial on the ensemble kalman filter. Technical report, Center for Computational Mathematics, University of Colorado Denver. [Online]. Available: `http://arxiv.org/abs/0901.3725`, [accessed 25.07.15].

Martin, A. (2013). Demand side electricity grid management. In *Presented as the 2013 Global Energy Systems Conference, Edinburgh, UK*, pages 1–9.

Marwan, M., Ledwich, G., and Ghosh, A. (2014). Demand-side response model to avoid spike of electricity price. *[Special issue]. Journal of Process Control*, 24(6):782–789.

Mazinani, M. S. and Zaeefi, N. (2013). Introduce a model of demand-side response load management comparison with electrical peak demands in mashhad city via smart grid approach. *International Journal of Innovation, Management and Technology*, 4(5):518–522.

McLoughlin, F., Duffy, A., and Conlon, M. (2013). Evaluation of time series techniques to characterise domestic electricity demand. *Energy*, 50:120–130.

McMenamin, J. S. and Monforte, F. A. (1998). Short term energy forecasting with neural networks. *The Energy Journal*, 19(4):43–61.

Mečiarová, Z. (2007). Modelling and forecasting seasonal time series. *Journal of Information, Control and Management Systems*, 5:73–80.

Michael, R., Mildred, H., Alissa, C., and Antonio, B. (2013). Thermal energy storage. *ASHRAE Journal*, 55(6):62–66.

Mohan, S. and Vedula, S. (1995). Multiplicative seasonal arima model for longerm forecasting of inflows. *Water Resource Management*, 9(2):115–126.

Mohanta, S. and Mishra, B. K. (2009). On the adequacy of distribution curves used in coal cleaning - a statistical analysis. *Fuel*, 88(11):2262–2268.

Moomaw, W., Burgherr, P., Heath, G., Lenzen, M., Nyboer, J., and Vbruggen, A. (2012). Annex ii: Methodology. In IPCC Special Report on Renewable Energy Sources and

Climate Change Mitigation [Edenhofer O., R. Pichs-Madruga, Y. Sokona, K. Seyboth, P. Matschoss, S. Kadner, T. Zwickel, P. Eickemeier, G. Hansen, S. Schlömer, C. Stechow(eds)]. Cambridge, United Kingdom and New York, NY, USA: Cambridge University Press.

Nævdal, G., Brouwer, D. R., and Jansen, J.-D. (2006). Waterflooding using closed-loop control. *Computational Geosciences*, 10:37–60.

Nævdal, G., Johnsen, L. M., Aanonsen, S. I., and Vefring, E. H. (2003). Reservoir monitoring and continuous model updating using ensemble kalman filter. In *SPE Annual Technical Conference and Exhibition*, pages 1–12, Denver, Colorado, USA. SPE.

National Grid (2011). Appendix i–chapter specific terminology, used within chapter 5 (plant margin) under 2011 nets seven year statements. [Online]. Available: `http://www.nationalgrid.com/NR/rdonlyres/0580EB05-E883-4A72-8417-E199B84F1799/46997/NETSSYS2011AppendixI.pdf`. [accessed 30.09.14].

National Grid (2013a). Fast reserve service description. [Online]. Available: `http://www2.nationalgrid.com/WorkArea/DownloadAsset.aspx?id=11757`. [accessed 30.09.14].

National Grid (2013b). Removing the barriers to demand side response. [Online]. Available: `http://www.nationalgridconnecting.com/removing-the-barriers-to-demand-side-response/`. [accessed 29.09.14].

National Grid (2013c). Short term operating reserve, fuel type analysis –Season 8.5 (27/10/14–02/02/15). Technical report, National Grid PLC.

National Grid (2014a). Fast reserve - FR market information (January 2014). [Online]. Available: `http://www2.nationalgrid.com/WorkArea/DownloadAsset.aspx?id=32172`. [accessed 30.09.14].

National Grid (2014b). Future energy scenarios. Technical report, National Grid PLC.

National Grid (2014c). Short term operating reserve, fuel type analysis –Season 8.3 (18/08/14–22/09/14). Technical report, National Grid PLC.

National Grid (2015). Data explorer – historical demand data. [Online]. Available: http://www2.nationalgrid.com/UK/Industry-information/Electricity-transmission-operational-data/Data-Explorer/. [accessed 03.09.15].

National Grid (2015a). Demand data historic (updated daily). [Online]. Available: http://www2.nationalgrid.com/WorkArea/DownloadAsset.aspx?id=33385. [accessed 01.10.15].

National Grid (2015b). Frequency control by demand management. [Online]. Available: http://www2.nationalgrid.com/uk/services/balancing-services/frequency-response/frequency-control-by-demand-management/. [accessed 28.05.15].

National Grid (2015c). Market information and tender round results. [Online]. Available: http://www2.nationalgrid.com/UK/Services/Balancing-services/Reserve-services/Short-Term-Operating-Reserve/Short-Term-Operating-Reserve-Information/. [accessed 27.02.15].

National Grid (2015d). STOR market information for TR_24. Technical report, National Grid PLC.

Nemirovski, A., Juditsky, A., Lan, G., and Shapiro, A. (2009). Robust stochastic approximation approach to stochastic programming. *SIAM Journal on Optimization*, 19(4):1574–1609.

Nesta (2013). Dynamic demand challenge prize. [Online]. Available: http://www.nesta.org.uk/project/dynamic-demand-challenge-prize. [accessed 11.08.15].

Neves, D., Pina, A., and Silva, C. A. (2015). Demand response modelling: a comparison between tools. *Applied Energy*, 146:288–297.

Niu, D. and Wei, Y. (2013). A novel social-environmental-economic dispatch model for thermal/wind power generation and application. *International Journal of Innovative Computing, Information and Control*, 9(7):3005–3014.

Nolan, S. and O'Malley, M. (2015). Challenges and barriers to demand response deployment and evaluation. *Applied Energy*, 152:1–10.

Nwaozo, J. (2006). Dynamic optimization of a water flood reservoir. Master thesis, Mewbourne school of Petroleum and Geological Engineering, University of Oklahoma, Norman.

ODPM (2006). Low or zero carbon energy sources: strategic guide. [Online]. Available: `http://www.planningportal.gov.uk/uploads/br/BR_PDF_PTL_ZEROCARBONfinal.pdf`. [accessed 17.05.15].

Palensky, P. and Dietrich, D. (2011). Demand side management: demand response, intelligent energy systems, and smart loads. *IEEE Transactions on Industrial Informatics*, 7(3):381–388.

Petvipusit, R. (2011). Dynamic well scheduling and well type optimization using ensemble-based method (enopt). Master thesis, Mewbourne school of Petroleum and Geological Engineering, University of Oklahoma, Norman.

Petzer, G. and Burger, L. (2007). Air quality assessment for the open cyclc gas turbine (OCGT) power plant's additional units in Mossel Bay. Technical Report APP/07/SHA-01 Rev 1.0, Airshed Planning Professionals (Pty) .Ltd, South Africa.

POSTnote 268 (2006). Carbon factor of electricity generation. Technical report, Parliamentary Office of Science and Technology. [Online]. Available: `http://www.parliament.uk/documents/post/postpn268.pdf`, [accessed 01.10.14].

POSTnote 383 (2011). Carbon factor of electricity generation. Technical report, Parliamentary Office of Science and Technology. [Online]. Available: `http://www.parliament.uk/documents/post/postpn_383-carbon-footprint-electricity-generation-references.pdf`, [accessed 01.10.14].

Rahmani, A. H. and Jamshidnezhad, Z. (2013). Global green energy consumption forecasting using an integrated simulated annealing and artificial neural network. *Bulletin of Environment, Pharmacology and Life Sciences*, 2(8):48–53.

Rajasomashekar, S. and Aravindhababu, P. (2012). Biogeography based optimization technique for best compromise solution of economic emission dispatch. *Swarm and Evolutionary Computation*, 8:47–57.

Ramanathan, R. (1994). Emission constrained economic dispatch. *IEEE Transactions on Power Systems*, 9(4):1994–2000.

Rau, N. S. (2009). *Optimization principles - practical applications to the operation and markets of the electric power industry*. John Wiley & Sons, Hoboken, New Jersey. ISBN: 978-0-471-45130-4.

Realtimecarbon (2013). Carbon intensity. [Online]. Available: `http://www.realtimecarbon.org/`. [accessed 27.07.14].

Reichle, R. H., McLaughlin, D. B., and Entekhabi, D. (2002). Hydrologic data assimilation with the ensemble kalman filter. *Americal Meteorological Society*, 130:103–114.

Ricardo-AEA (2015). Ricardo-AEA: Home. [Online]. Available: `http://www.ricardo-aea.com/cms/`. [accessed 03.10.15].

Riihimaki, V. (2012). Wärtsilä smart power generation. Technical report, Wärtsilä.

Robin, L. (2011). Energy : efficiency gains alone won't reduce emissions. *Nature*, 455(7212):460.

Roth, E., Sponberg, S., and Cowan, N. J. (2014). A comparative approach to closed-loop computation. *Theoretical and Computational Neuroscience*, 25:54–62.

Schellong, W. (2011). Energy demand analysis and forecast, Energy management systems, Dr. Giridhar Kini (Ed.). [Online]. Available: `http://www.intechopen.com/books/energy-management-systems/energy-demand-analysis-and-forecast`, [accessed 02.05.13]. ISBN: 978-953-307-579-2, InTech, DOI: 10.5772/21022.

Scottish Power (2010). Cruachan power station: site information. [Online]. Available: `http://www.spenergywholesale.com/userfiles/file/CruachanSite.pdf`. [accessed 30.09.14].

Senthil, K. and Manikandan, K. (2010). Economic thermal power dispatch with emission constraint and valve point effect loading using improved tabu search algorithm. *International Journal of Computer Applications*, 3(9):6–11.

Shang, H. L. (2012). Functional time series approach for forecasting very short-term electricity demand. *Journal of Applied Statistics*, 40:152–168.

Shen, B., Ghatikar, G., Lei, Z., Li, J. Wikler, G., and Martin, P. (2014). The role of regulatory reforms, market changes, and technology development to make demand response a viable sources in meeting energy challenges. *Applied Energy*, 130:814–823.

Smith, K. W. (2007). Cluster ensemble kalman filter. *Tellus A*, 59(5):749–757.

Stözer, M., Hauer, I., Richter, M., and Styczynski, Z. A. (2015). Potential of demand side integration to maximize use of renewable energy sources in germany. *Applied Energy*, 146:344–352.

Strachan, N. and Kannan, R. (2008). Hybrid modelling of long-term carbon reduction scenarios for the uk. *Energy Economics*, 30(6):2947–2963.

Strbac, G. (2008). Demand side management: benefits and challenges. *Energy policy*, 36(12):4419–4426.

Subramanian, S. and Ganesan, P. (2010). A simple approach for emission constrained economic dispatch problems. *International Journal of Computer Applications*, 8(11):39–45.

Sumer, K. K., Goktas, O., and Hepsag, A. (2009). The application of seasonal latent variable in forecasting electricity demand as an alternative method. *Energy Policy*, 37(4):1317–1322.

Svoboda, P. and Brčák, J. (2013). Electricity consumption demand model in Czech households. *International Advances in Economic Research*, 19:63–64.

The Centre for Carbon Measurement (2013). New challenge prize set to tackle uk's power struggle. [Online]. Available: `http://www.npl.co.uk/news/new-challenge-prize-set-to-tackle-uks-power-struggle`. [accessed 11.08.15].

Tu, J. V. (1996). Advantages and disadvantages of using artificial neural networks versus logistic regression for predicting medical outcomes. *Journal of Clinical Epidemiology*, 49(11):1225–1231.

Tzimas, E., Mercier, A., Cormos, C., and Peteves, S. D. (2007). Trade-off in emissions of acid gas pollutants and of carbon dioxide in fossil fuel power plants with carbon capture. *Energy Policy*, 35(8):3991–3998.

U.S. DoE (2006). Benefits of demand response in electricity market and recommendations for achieving them, report to the United States Congress pursuant to Section 1252 of the energy policy Act of 2005. Technical report, U.S. Department of Energy.

Wang, C. C., Hsu, Y. S., and Liou, C. H. (2011). A comparison of arima forecasting and heuristic modelling. *Applied Financial Economies*, 21(15):1095–1102.

Wang, J., Bloyd, C. N., Hu, Z., and Tan, Z. (2010). Demand response in china. *Energy*, 35(4):1592–1597.

Ward, J., Pooley, M., and Owen, G. (2012). Paper 4–what demand-side services can provide value to the electricity sector? Technical report, Sustainability First.

Warren, P. (2014). A review of demand-side management policy in the uk. *Renewable and Sustainable Energy Reviews*, 29:941–951.

Wärtsilä (2012). Ofgem's electricity SCR initial consultation - a response from Wa*rtsila* corporation: supporting modellingy. Technical report, Wärtsilä.

Wei, W., Liang, Y., Liu, F., Mei, S., and Tian, F. (2014). Taxing strategies for carbon emissions: a bilevel optimization approach. *Energies*, 7(4):2228–2245.

Wiedmann, T. and Minx, J. (2008). *A definition of ćarbon footprint. In: Pertsova, C.C., ecological economics research trends: chapter 1, pp. 1-11.* Nova Science Publishers, Hauppauge NY, USA.

Wright, L. A., Simon, K., and Williams, I. (2011). Carbon footprinting: towards a universally accepted definition. *Carbon management*, 2:61–72.

Young, J. (2013). Electricity demand forecasting and the problem of embedded generation. [Online]. Available: http://mcs.open.ac.uk/energymeeting/energymeeting2013/slides/Electricity%20demand%20forecasting%20and%20the%20problem%20of%20embedded%20generation%20V2.0.pdf. [accessed 01.04.15].

Zabalza-Mezghani, I., Manceau, E., Feraille, M., and Jourdan, A. (2004). Uncertainty management: From geological scenarios to production scheme optimization. *Journal of Petroleum Science and Engineering*, 44(1-2):11–25.

Zarenezhad, B. and Aminian, A. (2011). Accurate prediction of the dew points of acidic combustion gases by using an artificial neural network model. *Renewable Energy*, 52(2):911–916.

Zhang, G. P. and Qi, M. (2005). Neural network forecasting for seasonal and trend time series. *European Journal of Operational Research*, 160(2):501–504.

Zhu, J. (2009). *Optimization of power system operation*. John Wiley & Sons, Hoboken, New Jersey. ISBN: 978-0-470-29888-6.

Zhu, Y., Li, Y. P., and Huang, G. H. (2013). Planning carbon emission trading for beijing's electric power systems under dual uncertainties. *Renewable and Sustainable Energy Reviews*, 41:113–128.

Zhu, Y., Li, Y. P., and Huang, G. H. (2015). An optimization decision support approach for risk analysis of carbon emission trading in electric power systems. *Environmental Modelling and Software*, 67:43–56.

Appendix A

Excel spreadsheet result on the performance of substations

Substation ID	P = (Annual load/(NHH_EAC + total_HH)	P lies within ± 15% ?
#1	0.095923677	'Yes'
#2	0.095234758	'Yes'
#3	0.085138541	'Yes'
#4	0.08953081	'Yes'
#5	0.112443983	'Yes'
#6	0.112742048	'Yes'
#7	0.109928465	'Yes'
#8	0.243661175	**'No'**
#9	0.096113223	'Yes'
#10	51.53840395	**'No'**
#11	0.090691176	'Yes'
#12	0.129236227	'Yes'
#13	0.083115044	'Yes'
#14	0.089350969	'Yes'
#15	0.103575932	'Yes'
#16	0.148066776	'Yes'
#17	0.063096698	'Yes'
#18	0.087506123	'Yes'
#19	0.071972424	'Yes'
#20	0.086480424	'Yes'
#21	0.092833512	'Yes'
#22	0.113414381	'Yes'
#23	0.089591644	'Yes'
#24	0.099053275	'Yes'
#25	0.090423704	'Yes'
#26	0.07933005	'Yes'
#27	0.500354754	**'No'**
#28	0.10538886	'Yes'
#29	0.188087113	**'No'**
#30	0.111515347	'Yes'
#31	0.08514821	'Yes'
#32	0.099775364	'Yes'
#33	0.093626944	'Yes'
#34	0.094437176	'Yes'
#35	8.795136393	**'No'**
#36	0.108948055	'Yes'
#37	0.08092526	'Yes'
#38	0.099439104	'Yes'
#39	0.10033407	'Yes'
#40	0.093944635	'Yes'
#41	0.185243125	**'No'**
#42	0.118248872	'Yes'
#43	0.118254609	'Yes'
#44	0.127623664	'Yes'

#45	0.089793179	'Yes'
#46	0.088581629	'Yes'
#47	0.114069323	'Yes'
#48	0.081563127	'Yes'
#49	0.093891562	'Yes'
#50	0.094714481	'Yes'
#51	0.084004385	'Yes'
#52	0.08304288	'Yes'
#53	0.126207261	'Yes'
#54	0.086823484	'Yes'
#55	0.089403468	'Yes'
#56	0.068311795	'Yes'
#57	0.091685798	'Yes'
#58	0.124521888	'Yes'
#59	0.066917489	'Yes'
#60	0.077421769	'Yes'
#61	0.101645257	'Yes'
#62	0.112685587	'Yes'
#63	0.100998087	'Yes'
#64	0.128617508	'Yes'
#65	0.087702734	'Yes'
#66	0.093902425	'Yes'
#67	0.285402719	**'No'**
#68	0.30407959	**'No'**
#69	0.124486014	'Yes'
#70	0.188884922	**'No'**
#71	0.207167514	**'No'**
#72	0.134340414	'Yes'
#73	0.127563487	'Yes'
#74	0.122675144	'Yes'
#75	0.150027516	**'No'**
#76	0.125200183	'Yes'
#77	0.126327225	'Yes'
#78	0.093407288	'Yes'
#79	0.109897778	'Yes'
#80	0.043765715	'Yes'
#81	0.076268339	'Yes'
#82	0.093874978	'Yes'
#83	0.06941807	'Yes'
#84	0.101522674	'Yes'
#85	0.088507076	'Yes'
#86	0.086074239	'Yes'
#87	0.087105563	'Yes'
#88	0.107902097	'Yes'

Carbon emissions according to energy generated, EAC and HH within type ('Type 1 – Type_HH' consumers)

Highest amount of carbon emissions (kgCO2/kWh) based on **energy generated** according to each type:

Table 1

	Type1	Type2	Type3	Type4	Type5	Type6	Type7	TypeHH
Substation ID	**#1**	**#2**	**#3**	**#4**	**#5**	**#6**	**#7**	**#8**
ECERP	439044	225712	495807	604921	227587	638553	**760046**	508850
EACC	385642	53689	5212	1025565	183777	62556	873288	0
EHHCE	0	336855	845509	0	232604	935871	533690	783226

ECERP = Estimated carbon emission from real energy generated ($kgCO_2$)
EACC = Estimated Non Half-Hourly (NHH) annual carbon emission from consumers ($kgCO_2$)
EHHCE = Estimated Half-hourly metered (HH) carbon emission from consumers ($kgCO_2$)

The highest carbon emission is in substation ID: **#7**, with emissions of 760.05 tonnesCO_2

##########

Highest amount of carbon emissions (kgCO2/kWh) based on **EAC** from consumers according to each type:

Table 2

	Type1	Type2	Type3	Type4	Type5	Type6	Type7
Substation ID	**#9**	**#10**	**#11**	**#12**	**#13**	**#14**	**#15**
EACC	445164	54897	156397	1025565	247685	794358	**1397746**
ECERP	178326	32980	199602	604921	113447	589967	378409
EHHCE	0	0	179969	0	0	487132	160503

EACC = Estimated NHH annual carbon emission from consumers ($kgCO_2$)
ECERP = Estimated carbon emission from real energy generated ($kgCO_2$)
EHHCE = Estimated HH metered carbon emission from consumers ($kgCO_2$)

The highest carbon emission is in substation ID: **#15**, with emissions of 1397.75 tonnesCO_2.

##

Highest amount of carbon emissions (kgCO2) based on **HH** metered consumers according to each type:

Table 3

	Type1	Type2	Type3	Type4	Type5	Type6	Type7	TypeHH
Substation ID	**#16**	**#17**	**#18**	**#19**	**#20**	**#21**	**#22**	**#23**
EHHCE	374457	503831	845509	694804	232604	**14731048**	533690	1099775
ECERP	373669	221715	495807	86960	227587	87937	760046	419669
EACC	238741	12969	5212	163311	183777	124473	873288	0

EHHCE = Estimated HH metered carbon emission from consumers ($kgCO_2$)

ECERP = Estimated carbon emission from real energy generated ($kgCO_2$)

EACC = Estimated NHH annual carbon emission from consumers ($kgCO_2$)

The highest carbon emission is in substation ID: **#21**, with emissions of 14731.05 tonnesCO_2.

Appendix B

CCGT OPERATIONAL PROFILE

The warm up profile for CCGT plant

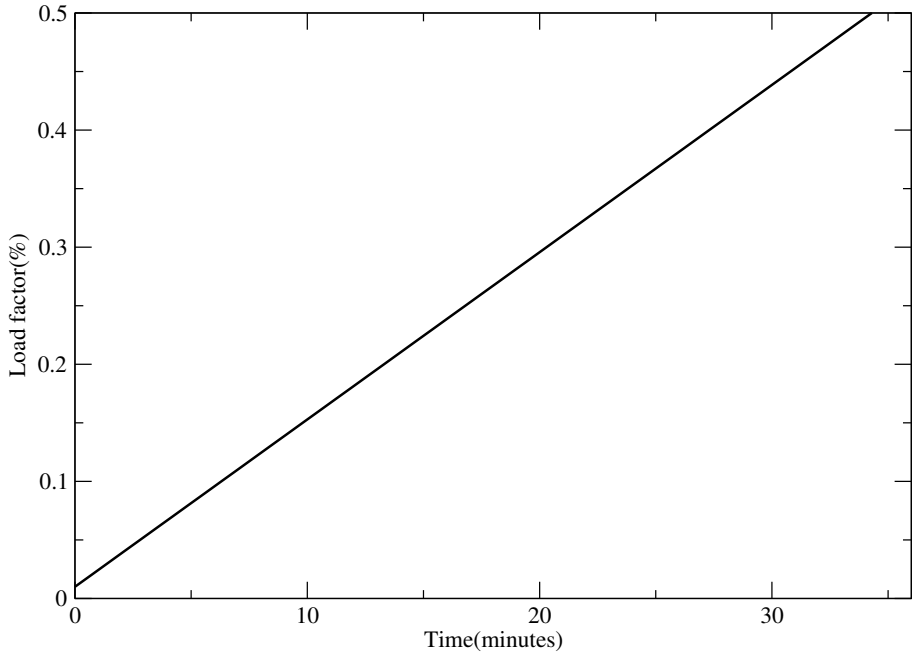

Figure 1: The load factor for CCGT

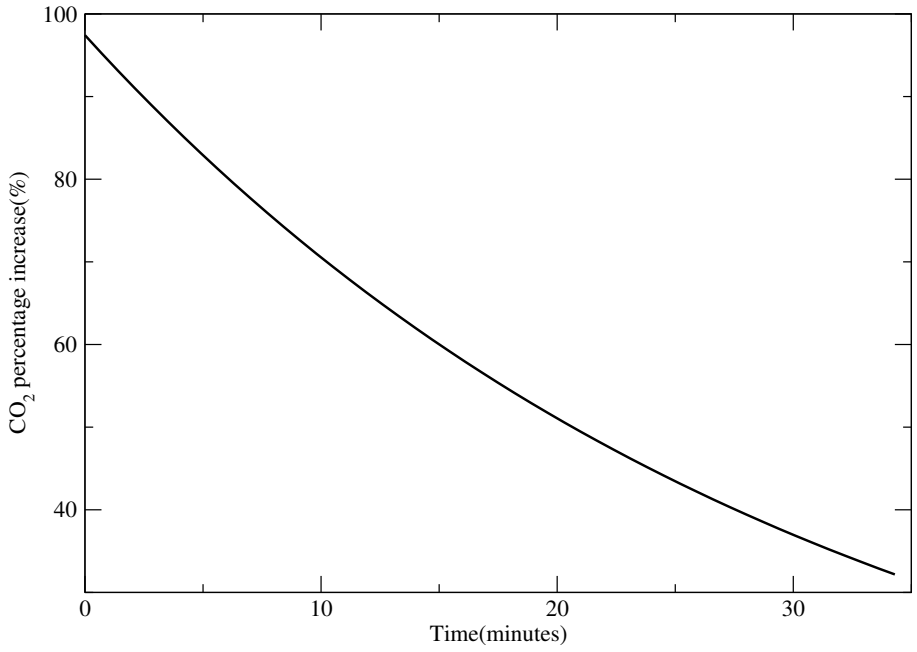

Figure 2: Percentage increase of carbon emissions of CCGT plants during the warm-up period.

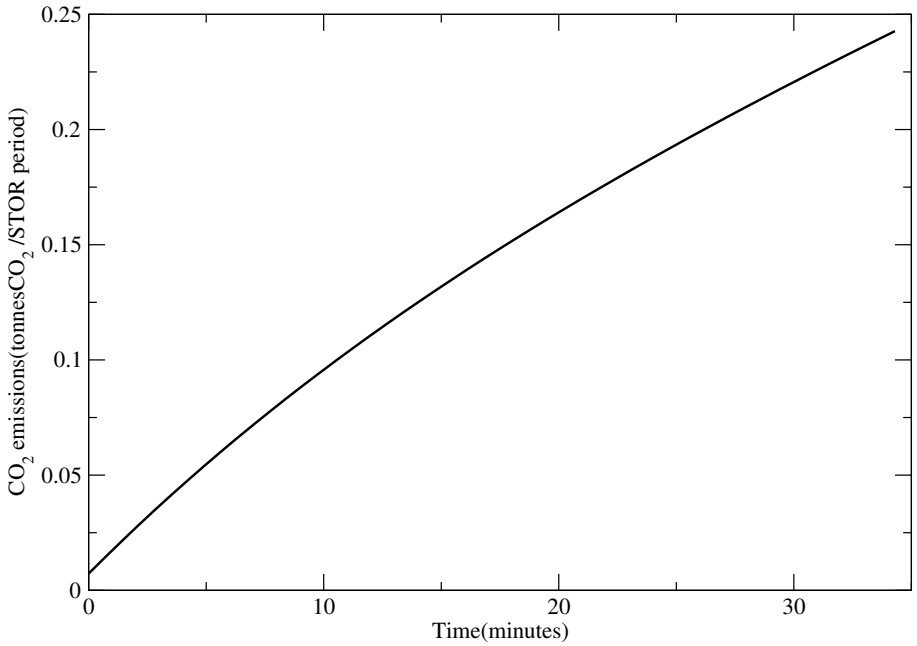

Figure 3: Carbon emissions of CCGT plants for the entire warm-up period.

The shutdown profile for CCGT plant.

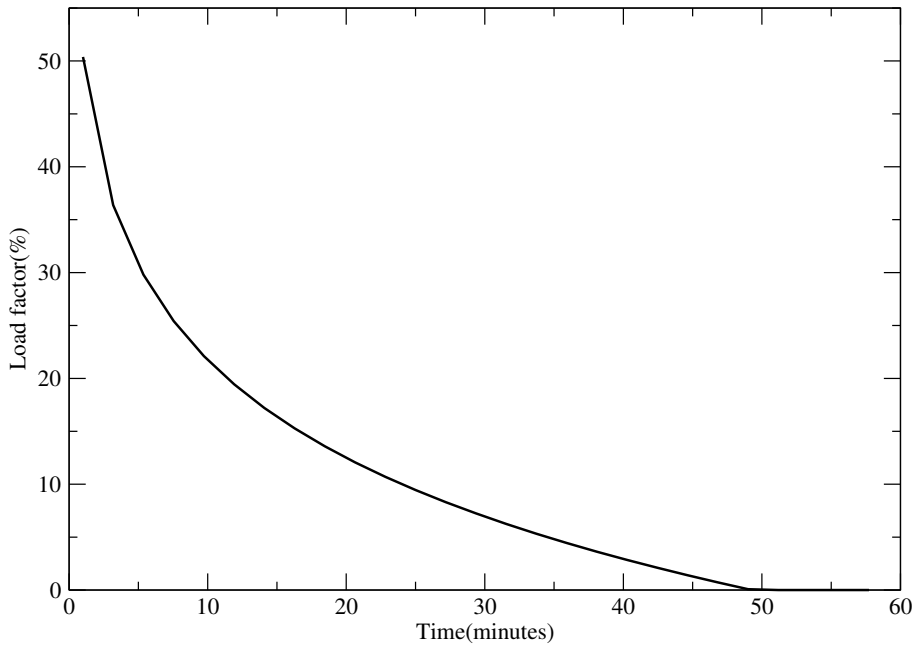

Figure 4: Load factor of CCGT plants for the shutdown period.

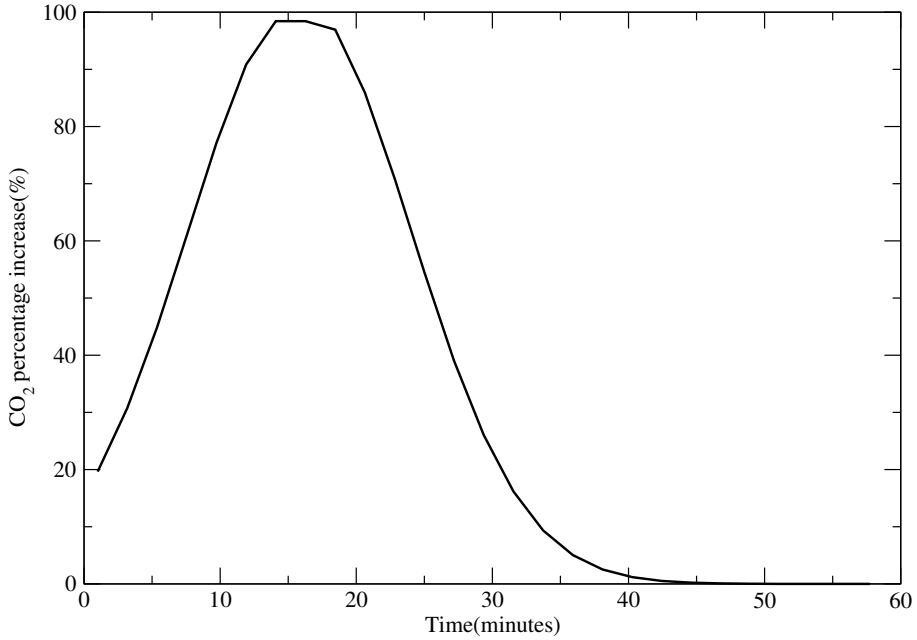

Figure 5: Percentage increase of carbon emissions of CCGT plants for the shutdown period.

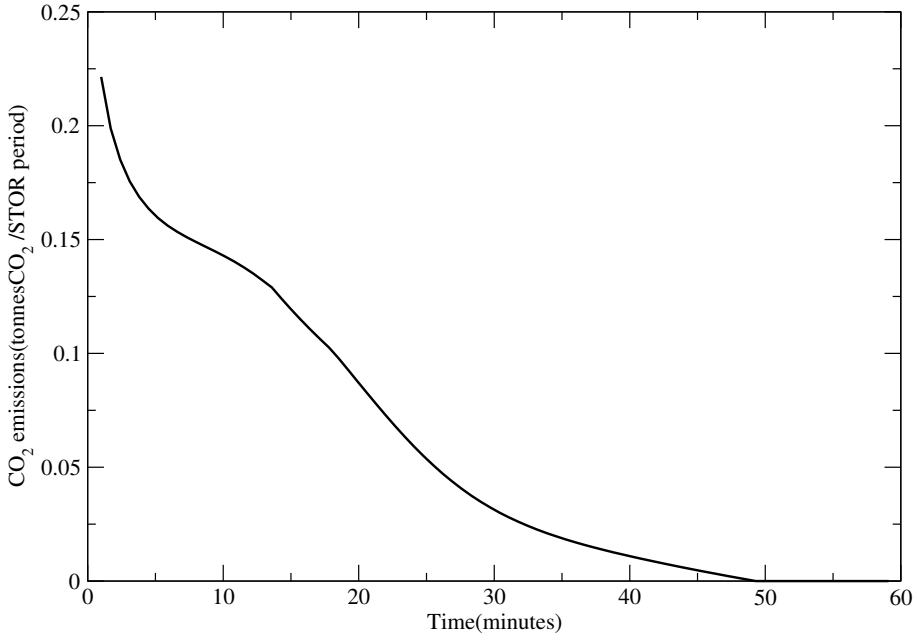

Figure 6: Carbon emissions of CCGT plants for the shutdown period.

OCGT OPERATIONAL PROFILE

The warm up profile for OCGT plant

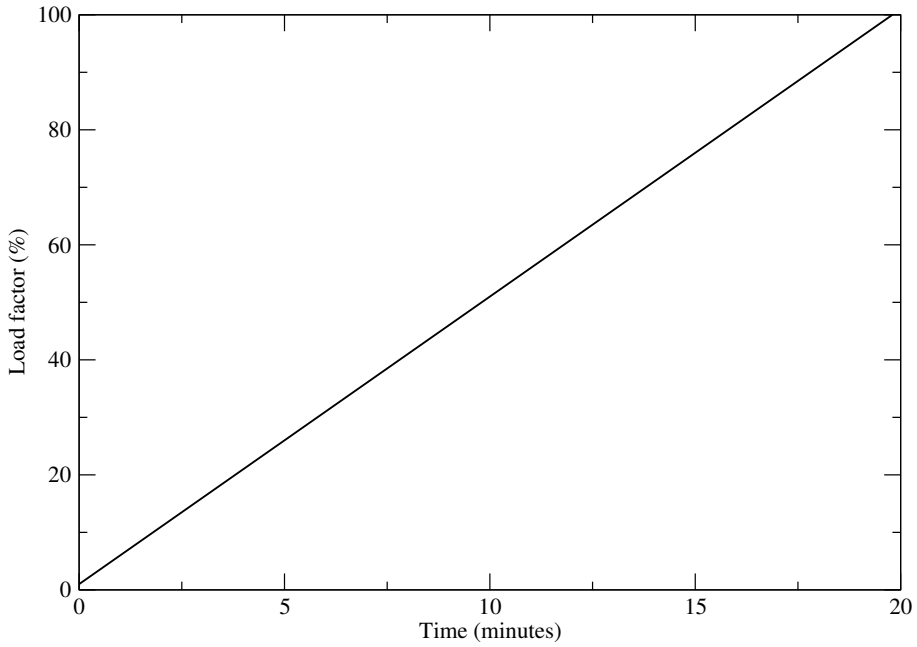

Figure 7: Load factor of OCGT plants for the warm-up period.

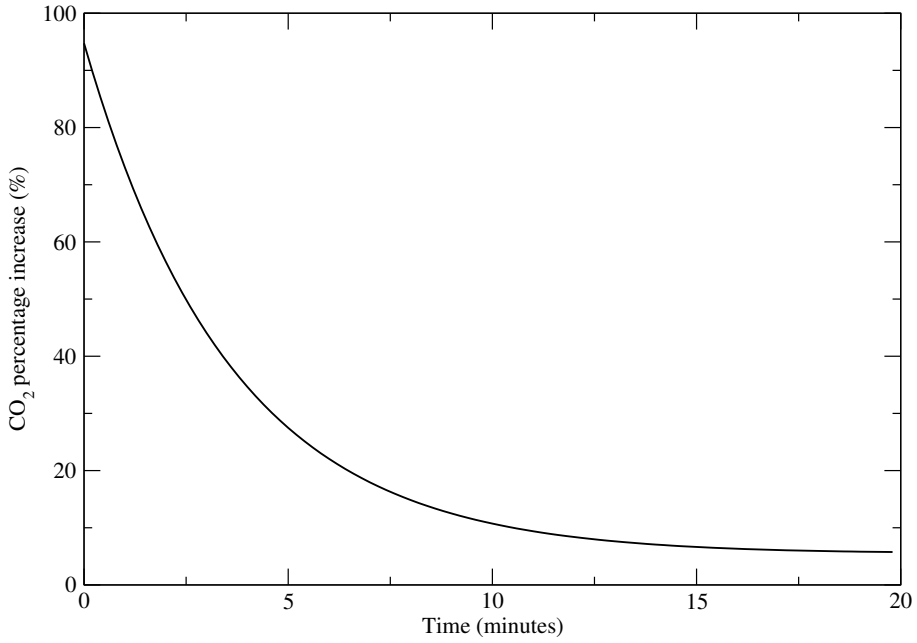

Figure 8: Percentage increase of carbon emissions of OCGT plants during the warm-up period.

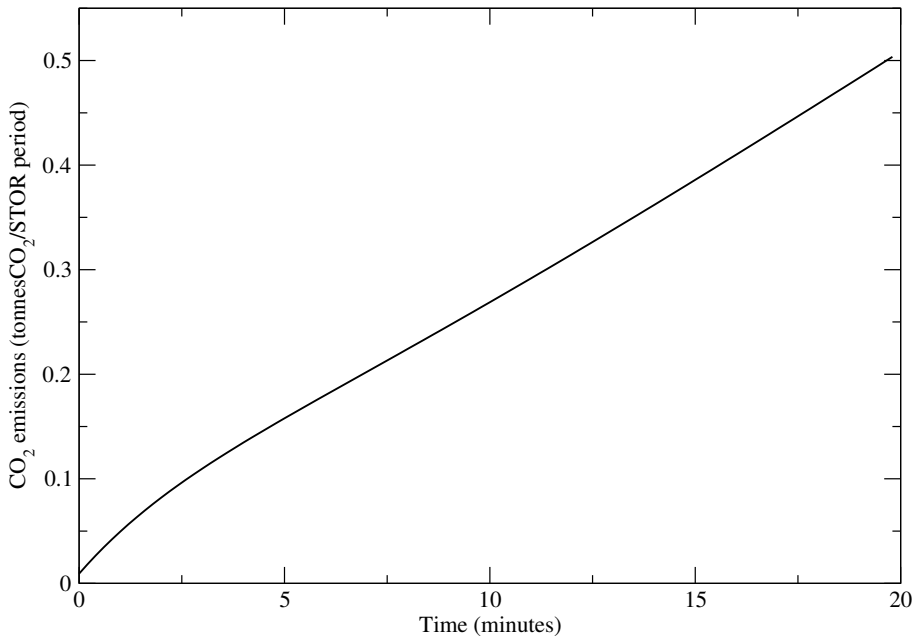

Figure 9: Carbon emissions of OCGT plants for the entire warm-up period.

The shutdown profile for OCGT plant.

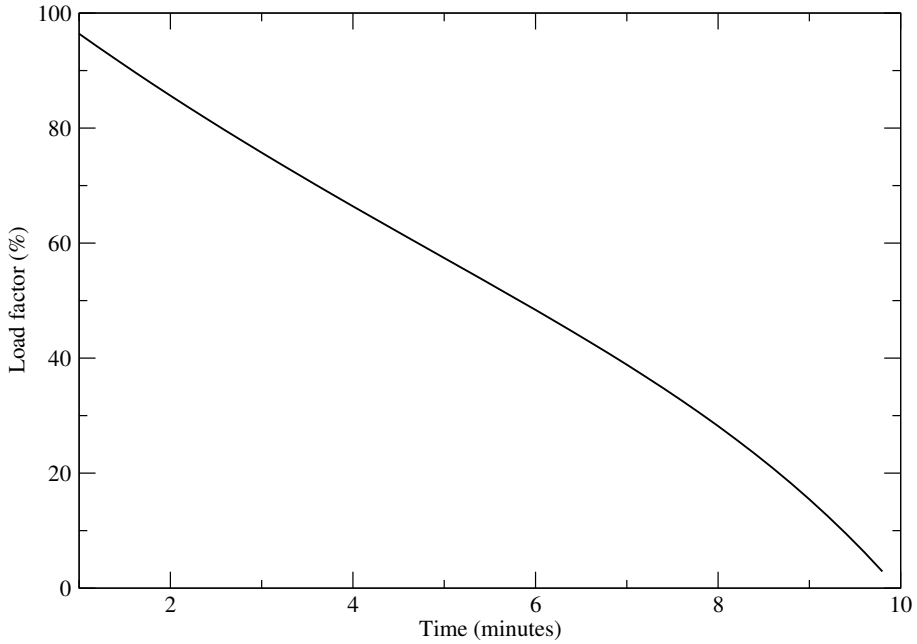

Figure 10: Load factor of OCGT plants for the shutdown period.

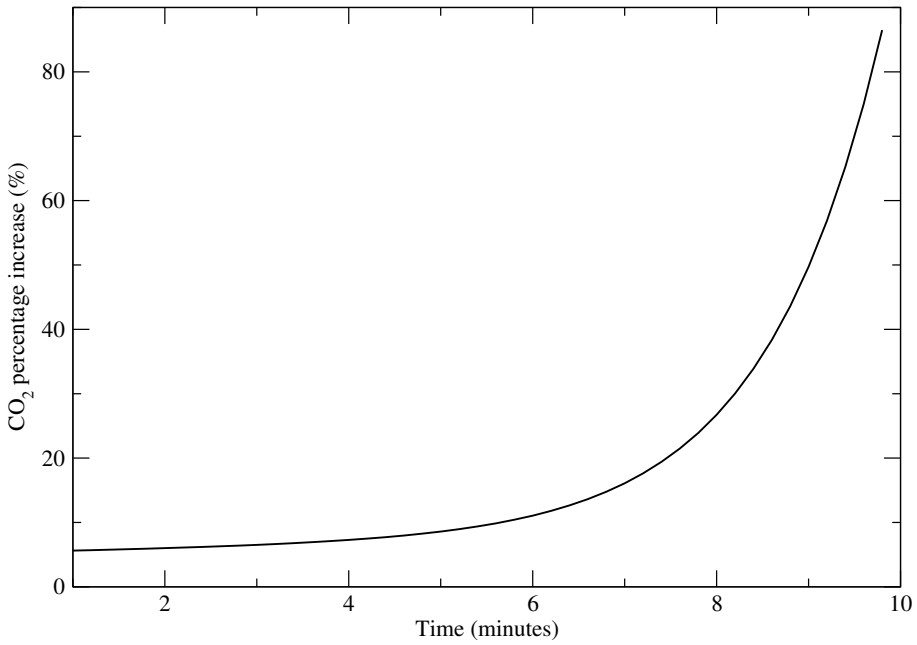

Figure 11: Percentage increase of carbon emissions of OCGT plants for the shutdown period.

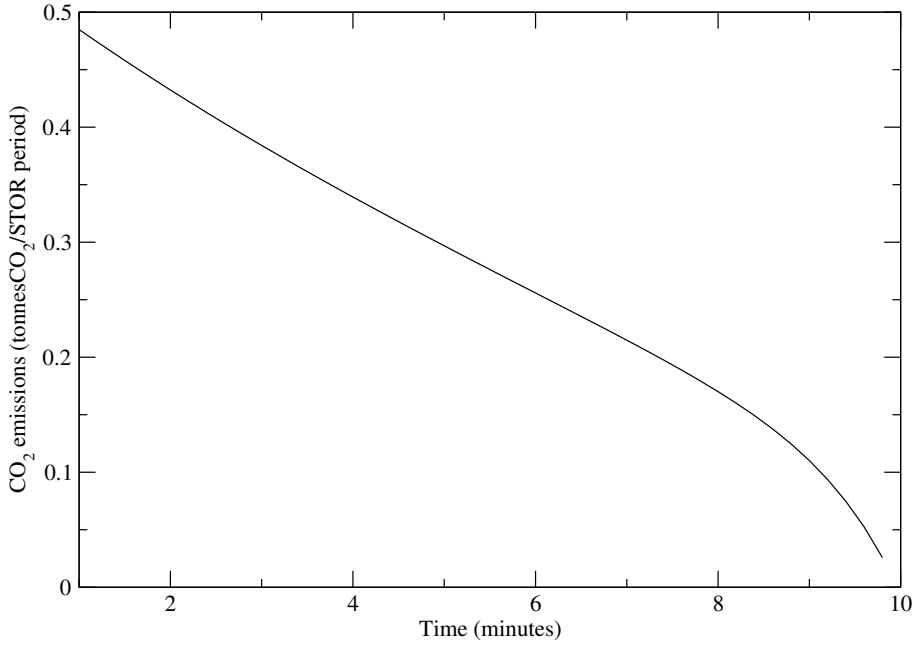

Figure 12: Carbon emissions of OCGT plants for the shutdown period.